Model-Based Therapeutics for Type 1 Diabetes Mellitus

by Xing-Wei Wong

A thesis presented for the degree of
Doctor of Philosophy
in
Mechanical Engineering
at the
University of Canterbury,
Christchurch, New Zealand.

23 June 2008

Acknowledgements

In this research and in the time I have worked on it, I have depended on certain people. If it were not for this special and diverse entourage, I would not have succeeded or have had such a worthwhile and rewarding experience in this time.

To Irene, you taught and continue to teach me what life is truly about, keeping me on an even keel, and to be the best I can be.

To my parents, you have always given me your unwavering love, support and encouragement (as well as the best Malaysian food outside of Malaysia).

To Prof. Geoff Chase, my supervisor, for his constant support in every sense of the word and uncanny vision for opportunities and possibilities where I have thought were exhausted.

To Drs. Chris Hann and Geoff Shaw, my co supervisors, for their mathematical and medical know-how, as well as Dr. Dominic Lee for his statistical insight.

To Kerri Morrone, the staff of the Christchurch Diabetes Centre and Christchurch Hospital Cardiothoracic Ward, and all the individuals who helped organise, collect and/or donated their personal data for this research.

Lastly, to my fellow friends and colleagues of the Centre for Bioengineering, past and present, you have without a doubt, proven to me the heights to which you have brought this fine profession.

I thank you all for the privilege.

Contents

List of Figures

List of Tables

Nomenclature

ACRONYMS and ABBREVIATIONS	
AACE	American Association of Clinical Endocrinologists
Ac.f	Autocorrelation function
Acv.f	Autocovariance function
ADA	American Diabetes Association
AEP	Artificial endocrine pancreas
AIDA	Automated Insulin Dosage Advisor
AR	Autoregressive
AUC	Area under curve
BMI	Body mass index
CDF	Cumulative distribution function
CGM	Continuous glucose measurement
CIR	Carbohydrate insulin ratio
CNS	Central nervous system
CGMS	Continuous glucose measurement system
CSII	Continuous subcutaneous insulin infusion
CTW	Cardiothoracic Ward
CV	Coefficient of variation
CV_{inter}	CV between different patients
CV_{intra}	CV within the same patient
DFT	Discrete Fourier transform
DKA	Diabetic ketoacidosis
EGP	Endogenous glucose production
FFA	Free fatty acid
FFT	Fast Fourier transform
FPG	Fasting plasma glucose
GDM	Gestational diabetes mellitus
GEC	Glucose equivalent carbohydrate

GFR	Glomerular filtration rate
GH	Growth hormone
GI	Glycaemic index
GLUT	Glucose transporter
HbA_{1C}	Glycosylated haemoglobin
HGP	Hepatic glucose production
HLA	Human leukocyte antigen
ICU	Intensive Care Unit
IDDM	Insulin dependent diabetes mellitus
IFG	Impaired fasting glucose
IGT	Impaired glucose tolerance
IIT	Intensive insulin therapy
IR	Insulin resistance
ISF	Insulin sensitivity factor
ITT	Insulin Tolerance Test
IV	Intravenous
IVGTT	Intravenous Glucose Tolerance Test
MC	Monte Carlo
MCR	Metabolic clearance rate
MDI	Multiple daily injection
MI	Monomeric insulin
MM	Minimal Model of glucose kinetics
MSD	Multiplicative standard deviation
NGT	Normal glucose tolerance
NLS	Non linear least squares
NPH	Neutral Protamine Hagedorn
NRLS	Non recursive least squares
OGTT	Oral Glucose Tolerance Test
OGIS	Oral Glucose Insulin Sensitivity
OMM	Oral Minimal Model
PD	Pharmacodynamic
PDF	Probability distribution function
PK	Pharmacokinetic
PID	Proportional-integral-derivative
RGT	Renal glucose threshold
RGC	Renal glucose clearance
Ra	Rate of appearance

RI	Regular insulin
RMSE	Root Mean Square Error
SD	Standard Deviation
Sc	Subcutaneous
SSE	Sum Squared Error
SMBG	Self monitoring blood glucose
TBGU	Total body glucose uptake
TDV	Total distribution volume
T1DM	Type 1 diabetes mellitus

MATHEMATICAL VARIABLES

$x_h(t)$	Mass in the hexameric compartment [mU]
$x_{h,ulen}(t)$	Mass in the ultralente hexameric compartment [mU]
$x_{h,gla}(t)$	Mass in the glargine hexameric compartment [mU]
$c_{NPH}(t)$	Mass in the NPH crystalline protamine compartment [mU]
$c_{len}(t)$	Mass in the lente crystalline zinc compartment [mU]
$c_{ulen}(t)$	Mass in the ultralente crystalline zinc compartment [mU]
$p_{gla}(t)$	Mass in the glargine precipitate compartment [mU]
$x_{dm}(t)$	Mass in the dimer/monomer compartment [mU]
$u_{total,mono}(t)$	MI input [mU/min]
$u_{total,RH}(t)$	RI input [mU/min]
$u_{total,NPH}(t)$	NPH insulin input [mU/min]
$u_{total,len}(t)$	Lente insulin input [mU/min]
$u_{total,ulen}(t)$	Ultralente insulin input [mU/min]
$u_{total,gla}(t)$	Insulin glargine input [mU/min]
α_{NPH}	Proportion of $u_{total,NPH}(t)$ in protamine crystalline state at injection
α_{len}	Proportion of $u_{total,len}(t)$ in zinc crystalline state at injection
α_{ulen}	Proportion of $u_{total,ulen}(t)$ in zinc crystalline state at injection
α_{gla}	Proportion of $u_{total,gla}(t)$ in precipitate state at injection
$u_{c,NPH}(t)$	NPH crystalline state insulin input [mU/min]
$u_{c,len}(t)$	Lente crystalline state insulin input [mU/min]

$u_{c,ulen}(t)$	Ultralente crystalline insulin input [mU/min]
$u_{c,gla}(t)$	Glargine precipitate state insulin input [mU/min]
$u_h(t)$	RI hexamer state insulin input [mU/min]
$u_{h,NPH}(t)$	NPH hexamer state insulin input [mU/min]
$u_{h,len}(t)$	Lente hexamer state insulin input [mU/min]
$u_{h,ulen}(t)$	Ultralente hexamer state insulin input [mU/min]
$u_{h,gla}(t)$	Glargine hexamer state insulin input [mU/min]
$u_{mono}(t)$	MI dimer/monomer state insulin input [mU/min]
$u_{m,RH}(t)$	RI dimer/monomer state insulin input [mU/min]
$u_{m,NPH}(t)$	NPH dimer/monomer state insulin input [mU/min]
$u_{m,len}(t)$	Lente dimer/monomer state insulin input [mU/min]
$u_{m,ulen}(t)$	Ultralente dimer/monomer state insulin input [mU/min]
$u_{m,gla}(t)$	Glargine dimer/monomer state insulin input [mU/min]
$k_{crys,NPH}$	NPH protamine crystalline dissolution rate [1/min]
$k_{crys,len}$	Lente zinc crystalline dissolution rate [1/min]
$k_{crys,ulen}$	Ultralente zinc crystalline dissolution rate [1/min]
$k_{prep,gla}$	Glargine precipitate dissolution rate [1/min]
V_{inj}	Insulin dose injection volume [ml] or [cm^3]
$r_{dis,max}$	Maximum glargine precipitate dissolution rate [mU/min]
k_1	Hexamer dissociation rate [1/min]
$k_{1,ulen}$	Ultralente hexamer dissociation rate [1/min]
$k_{1,gla}$	Glargine hexamer dissociation rate [1/min]
k_2	Dimeric/monomeric insulin transport rate into interstitium [1/min]
k_3	Interstitium insulin transport rate into plasma [1/min]
$k_{d,i}$	Rate of loss from interstitium [1/min]
k_d	Rate of diffusive loss from hexameric and dimeric/monomeric state compartments [1/min]
C_h	Concentration of hexameric insulin [$(l/mU)^2$]
C_D	Concentration of dimeric insulin [$(l/mU)^2$]
Q_D	Hexameric-dimeric equilibrium constant [$(l/mU)^2$]

D	Diffusion constant of hexameric and dimeric/monomeric insulin [cm^2/min]
r	Radius of the sc depot [cm]
$x_i(t)$	Mass in the interstitium compartment [mU]
$I(t)$	Plasma insulin concentration [mU/l]
$Q(t)$	Interstitial (effective) insulin concentration [mU/l]
k	Rate of absorption and clearance of insulin into and out of interstitial fluid [1/min]
n	Plasma insulin rate of clearance [1/min]
V_i	Insulin plasma distribution volume [l/kg]
m_b	Body mass [kg]
$G(t)$	Plasma glucose concentration [mmol/l]
CNS	Central nervous system glucose uptake [mmol/l.min]
EGP_{0-G}	Endogenous glucose production extrapolated to zero plasma glucose concentration [mmol/l.min]
p_G	Glucose effectiveness [1/min]
S_I	Insulin sensitivity [l/(min.mU)]
$RGC(t)$	Renal glucose clearance [mmol/l.min]
$P(t)$	Meal plasma glucose rate of appearance [mmol/l.min]
GFR	Glomerular filtration rate [l/min]
RGT	Renal glucose threshold [mmol/l]
V_p	Glucose distribution volume [l/kg]
$STO(t)$	Mass of carbohydrate/glucose in the stomach [g]
$GUT(t)$	Mass of carbohydrate/glucose in the gut [g]
$GABS(t)$	Gut carbohydrate/glucose absorption rate [g/min]
$GABS_{max}$	Maximum gut carbohydrate/glucose absorption rate [g/min]
k_6	Carbohydrate/glucose gastric emptying rate [1/min]
k_7	Carbohydrate/glucose gut-absorption rate [1/min]
$u_{CHO}(t)$	Meal carbohydrate/glucose input [g/min]

Abstract

The incidence of Type 1 diabetes is growing yearly. Worryingly, the aetiology of the disease is inconclusive. What is known is that the total number of affected individuals, as well as the severity and number of associated complications are growing for this chronic disease. With increasing complications due to severity, length of exposure, and poor control, the disease is beginning to consume an increasingly major portion of healthcare costs to the extent that it poses major economic risks in several nations.

Research has shown that intensive insulin therapy aimed at certain minimum glycosylated haemoglobin threshold levels reduces the incidence of complications by up to 76% compared to conventional insulin therapy. Moreover, the effects of such intensive therapy regimes over a 6.5y duration persists for at least 10y after, a so called *metabolic memory*. Thus, early intervention can slow the momentum of complications far more easily than later intervention. Early, safe, intensive therapy protocols offer potential solutions to the growing social and economic effects of diabetes.

Since the 1970s, the artificial endocrine pancreas has been heralded as just this type of solution. However, no commercial product currently exists, and ongoing limitations in sensors and pumps have resulted in, at best, modest clinical advantages over conventional methods of insulin administration or multiple daily injection. With high upfront costs, high costs of consumables, significant complexity, and the extensive infrastructure and support required, these systems and devices are only used by 2-15% of individuals with Type 1 diabetes. Clearly, there is an urgent need to address the large majority of the Type 1 diabetes population using conventional glucose measurement and insulin administration. For these individuals, current conventional or intensive therapies are failing to deliver recommended levels of glycaemic control.

This research develops an understanding of clinical glycaemic control using conventional insulin administration and glucose measurement techniques in Type 1 diabetes based on a clinically validated *in silico* virtual patient simulation. Based on this understanding, a control protocol for Type 1 diabetes that is relatively simple and clinically practical is developed. The protocol design incorporates physiological modelling and engineering techniques to adapt to individual patient clinical requirements. By doing so, it produces accurate, patient-specific recommendations for insulin interventions.

Initially, a simple, physiological compartmental model for the pharmacokinetics of subcutaneously injected insulin is developed. While the absorption process itself is subject to significant potential variability, such models enable a real-time *estimation* of plasma insulin concentration. This information would otherwise be lacking in the clinical environment of outpatient Type 1 diabetes treatment due to the inconvenience, cost, and laboratory turnaround for plasma insulin measurements. Hence, this validated model offers significant opportunity to optimise therapy selection.

An *in silico* virtual patient simulation tool is also developed. A virtual patient cohort is developed on patient data from a representative cohort of the broad diabetes population. The simulation tool is used to develop a robust, adaptive protocol for prandial insulin dosing against a conventional intensive insulin therapy, as well as a controls group representative of the general diabetes population. The effect on glycaemic control of suboptimal and optimal, prandial and basal insulin therapies is also investigated, with results matching clinical expectations. To gauge the robustness of the developed adaptive protocol, a Monte Carlo analysis is performed, incorporating realistic and physiological errors and variability.

Due to the relatively infrequent glucose measurement in outpatient Type 1 diabetes, a method for identifying the diurnal cycle in effective insulin sensitivity and modelling it in retrospective patient data is also presented. The method consists of identifying deterministic and stochastic components in the patient effective insulin sensitivity profile. Circadian rhythmicity and sleep-wake phases have profound effects on effective insulin sensitivity. Identification and prediction of this rhythm is of utmost clinical relevance, with the potential for safer and more effective glycaemic control, *with* less frequent measurement. It is thus a means

of further enhancing any robust protocol and making it more clinically practical to implement.

Finally, this research presents an entire framework for the realistic, and rapid development and testing of clinical glycaemic control protocols for outpatient Type 1 diabetes. The models and methods developed within this framework allow rapid and physiological identification of time-variant, patient-specific, effective insulin sensitivity profiles. These profiles form the responses of the virtual patient and can be used to develop and robustly test clinical glycaemic control protocols in a broad range of patients. These effective insulin sensitivity profiles are also rich in dynamics, specifically those circadian in nature which can be identified, and used to provide more accurate glycaemic prediction with the potential for safer and more effective control.

Chapter 1

Introduction

The number of people with diabetes is increasing rapidly due to modern living environments and lifestyles, aging populations, and increasing levels of obesity. The resulting exponential increase that is occurring in diabetes related complications has cataclysmic implications on healthcare systems and on entire economies across all countries. Existing tools and methods for glycaemic control are often blamed, but in reality, could also be better utilised. Across populations, even moderate improvement in control, and its subsequent reduction in complications, would lead to measurable reduction in the associated burden on the society and the individual. This chapter discusses the overall prevalence of diabetes, its development and underlying problems, and its clinical classification and diagnosis.

1.1 The Diabetes Epidemic

Diabetes is a disease that has reached epidemic proportions. An estimated 171 million people were diagnosed worldwide with Type 2 diabetes in the year 2000. This number is expected to rise to 366 million by 2030 [Wild et al., 2004]. About the same numbers are estimated to have undiagnosed diabetes or pre-diabetes [Hossain et al., 2007; Wild et al., 2004], effectively doubling those numbers. In New Zealand, current figures are 157,000 with diabetes of all types, with 11,000-15,000 having Type 1 diabetes according to NZ Ministry of Health figures. It is estimated that by 2021, 250,000 people will have diabetes and 500,000 more will have pre-diabetes, directly affecting about 15% of the population [PriceWaterhouseCoopers, 2001].

The total diabetes related health expenditure in the USA in 2002 was US$132 billion, second only to all cancer types combined [Kleinfield, 2006]. This figure is predicted to increase to US$192 billion in 2020 [Hogan et al., 2003]. These costs are incurred primarily by treatment of chronic long-term complications, such as retinopathy leading to blindness, nephropathy resulting in renal failure, neuropathy and limb amputation, and hypertension and cardiovascular disease [ADA, 2006a]. As a result, diabetes is the third leading cause of death in the USA, and may be much higher due to under-reporting or diabetes being only a contributing factor in death.

One of the underlying causes of this epidemic is a worldwide obesity epidemic and an increasingly sedentary lifestyle [Hossain et al., 2007]. It is estimated that worldwide 1.1 billion people are overweight, 312 million of whom are clinically obese (Body mass index or BMI > 30), a number that has tripled in the past 20 years [Hossain et al., 2007]. An estimated 155 million children are overweight or obese.

The greatest threat of obesity is from the populations of China, the Middle East, Southeast Asia and the Pacific Islands, as is shown in Figure 1.1. This threat is mainly due to changing dietary habits from long-term diets of the past [ADA, 2006a; Hossain et al., 2007]. Thus, where the disease was seen as a problem almost exclusively of developed countries in the past, it is the developing countries that now exhibit the most rapid increases in incidence [Hossain et al., 2007; Wild et al., 2004].

At a smaller level, Type 1 diabetes has also been increasing by a rate of around 3.0% per annum globally since the 1950s [Onkamo et al., 1999]. Statistically significant increases have been recorded for all geographic regions except in Central America and the West Indies [Karvonen, 2006]. Like Type 2 diabetes, there is a wide geographical variation in the incidence of Type 1 diabetes (up to 350-fold), with the highest incidence in the Caucasoid populations of Northern Europe and the lowest in China and South America [Karvonen et al., 1993]. Referring to Figure 1.2, the incidence rate is 40.9 per 100,000/year in Finland and 0.1 per 100,000/year in China in the 10 year period from 1990 to 1999 [Karvonen, 2006].

Conservative predictions show that in 2010, the incidence rate will be 50.2

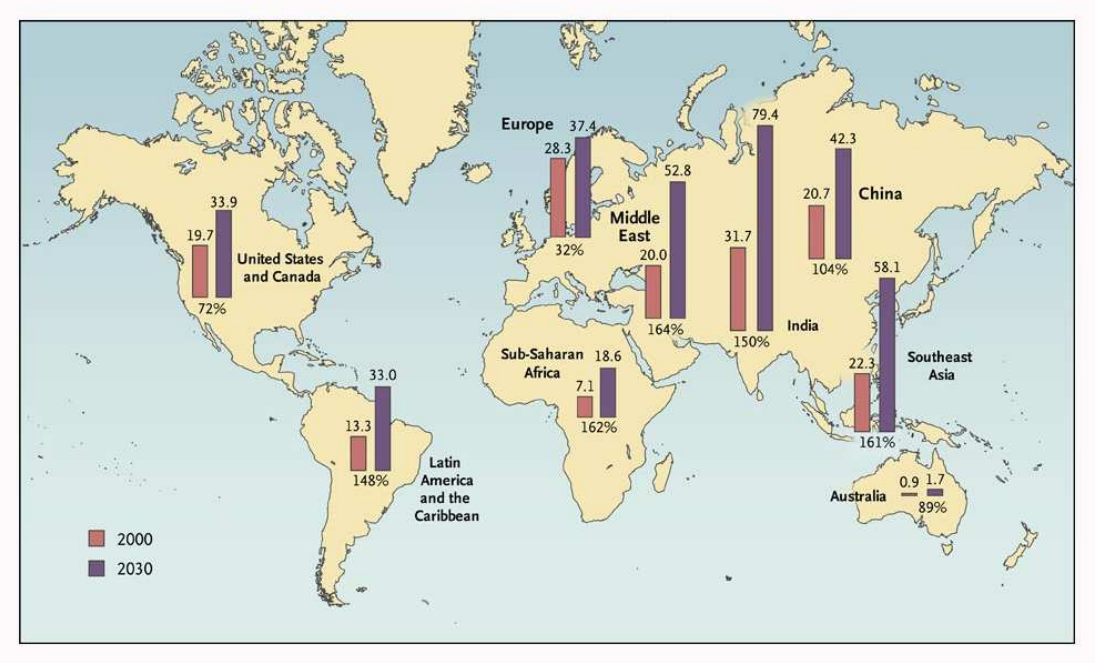

Figure 1.1 Cases of diabetes in 2000 and estimated numbers for 2030 with the projected percentile increases [Hossain et al., 2007; Wild et al., 2004]. Largest increases are seen in developing countries.

per 100,000/year in Finland and will exceed 30 per 100,000/year in many other countries [Onkamo et al., 1999]. As in Type 2 diabetes, the countries with the lowest incidence are predicted to have the highest relative increases. New Zealand has the 9th highest incidence rate of Type 1 diabetes in the world, above that of USA and Australia [Karvonen, 2006], and is predicted to exceed an incidence of 25 per 100,000/year in 2010 [Onkamo et al., 1999].

Overall, it should be noted that Type 1 diabetes offers the greater long-term exposure and risk of complications. However, with the onset of Type 2 diabetes occurring earlier, this gap is closing rapidly. Hence, over time, both types will result in expensive and difficult complications. Thus, their continued growth in number and severity poses serious questions for managing this chronic disease.

1.2 Development of Diabetes

The complete name of the disease is *Diabetes mellitus*. *Diabetes* is derived from the Greek word for "passing through", and *mellitus* from the Latin word "honey",

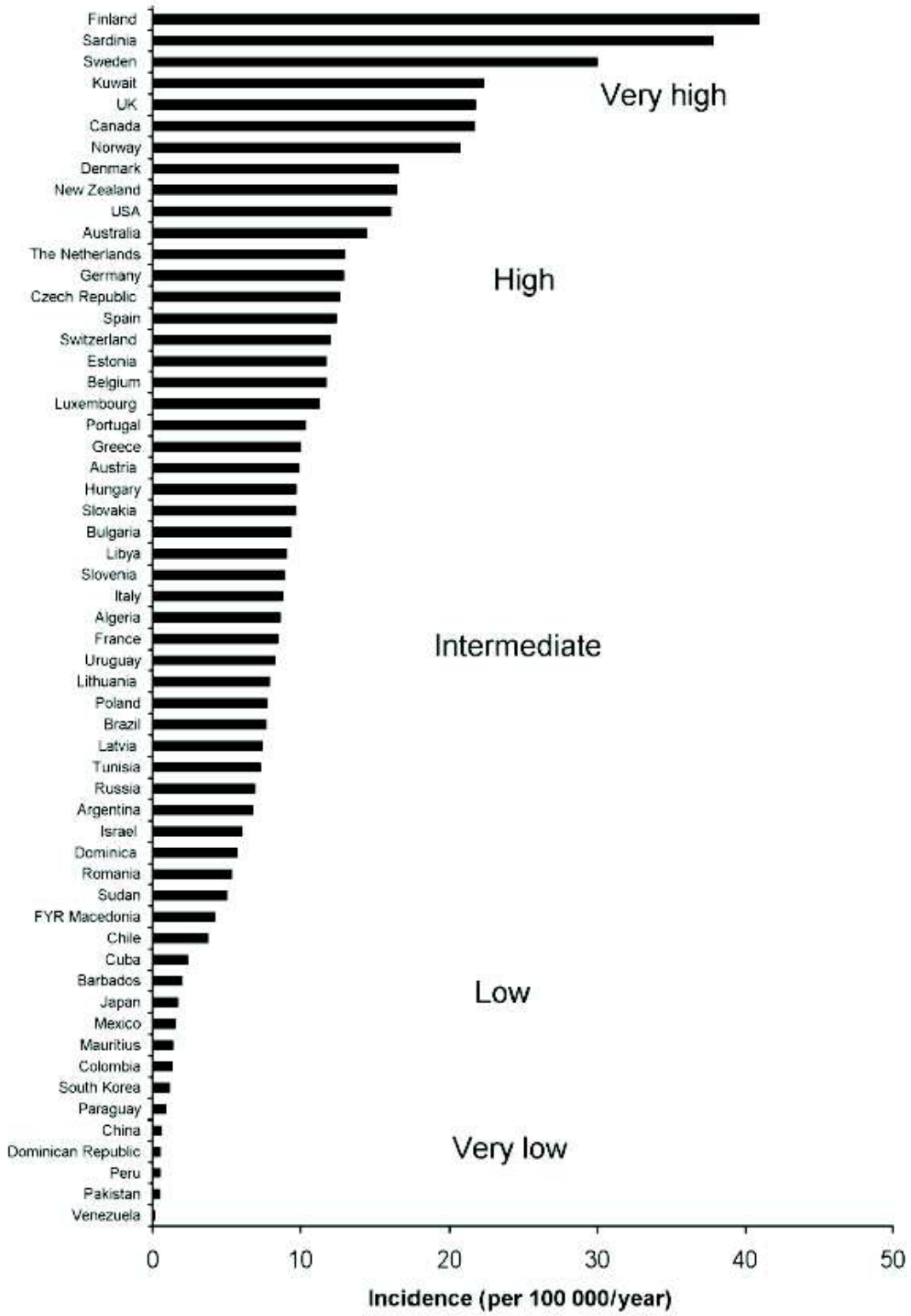

Figure 1.2 Age-standardized incidence of Type 1 diabetes in children under 14 years of age (per 100,000/year). Countries are arranged in descending order of incidence. Reproduced from [Karvonen, 2006].

referring to the glucose excreted in the urine of patients with excessive blood sugar or glucose levels [Dobson, 1776]. Diabetes combines a group of different metabolic disorders, which have different origins, but all resulting in hyperglycaemia or high blood glucose levels [ADA, 2006a]. Glucose uptake by the cells is facilitated only by insulin. High blood glucose levels are mainly caused by a deficiency or a resistance to the insulin available and/or a lack of ability to produce enough insulin.

The three main recognised types of diabetes are Type 1, Type 2 and gestational diabetes mellitus (GDM). The last occurs only temporarily during pregnancy. As only the first two are lasting chronic disease states, and a persisting GDM after pregnancy is classified as Type 2 diabetes, GDM will not be described in detail. Type 1 and Type 2 diabetes represent significantly different metabolic conditions with different pathologies.

1.2.1 Type 2 Diabetes

Type 2 diabetes is characterised by a *resistance* to insulin along with eventual loss of insulin production. The development of Type 2 diabetes is a more gradual process than in Type 1. It starts with the pre-diabetes stages of impaired glucose tolerance (IGT) and impaired fasting glucose (IFG), before a clinical classification of diabetes is made [ADA, 2006a]. The progression of the disease is often undiagnosed and untreated for many years, until health complications start to appear.

The risk of developing Type 2 diabetes has a partial genetic component, but is strongly affected by obesity, which significantly increases insulin resistance [Ferrannini et al., 1997; Hossain et al., 2007; Kahn et al., 2006b; Petersen and Shulman, 2006]. Weight reduction and lifestyle intervention to a healthier diet and increased exercise has been shown to greatly decrease insulin resistance and the prevalence of developing or worsening Type 2 diabetes [Camastra et al., 2005; McAuley et al., 2002; Tuomilehto et al., 2001]. However, these interventions are difficult to implement and/or maintain in some patients, necessitating other forms of treatment.

The development of insulin resistance and eventual reduced β-cell function

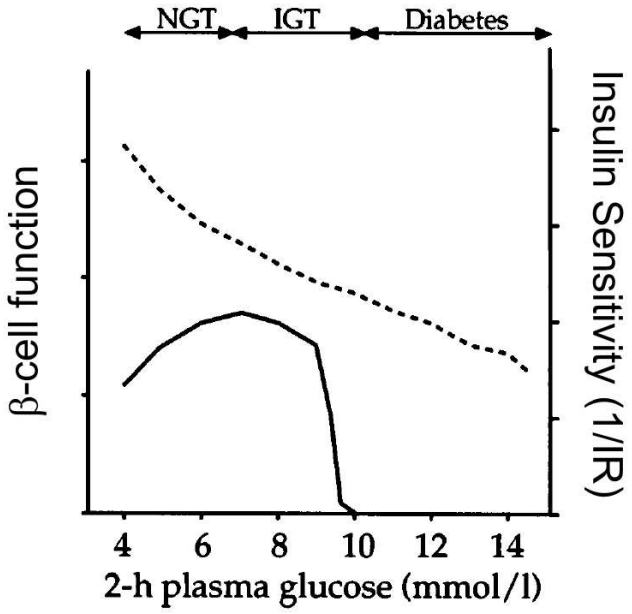

Figure 1.3 Progression of β-cell function (solid) and insulin sensitivity (dashed), opposite of insulin resistance, in the development from normal glucose tolerance (NGT) to impaired glucose tolerance (IGT), resulting in Type 2 diabetes [Ferrannini, 1997]. The x-axis indicates blood glucose concentration 2h post oral glucose challenge, a diagnostic criteria of diabetes.

in the progression to Type 2 diabetes is shown in Figure 1.3. A gradual decrease of insulin sensitivity (increase of insulin resistance) is seen. This decrease is initially accompanied by a compensatory increase in pancreatic insulin secretion to maintain normal glucose levels. When the pancreas cannot meet the increased demand, it begins to exhaust itself. The result is a further increase in basal plasma glucose levels due to the decrease in insulin available. It is not fully understood if the primary underlying problem is insulin resistance or a defect in β-cell function [Ferrannini and Mari, 2004]. However, it is well accepted that both factors play an important role to maintain glucose balance [ADA, 2006a; Schinner et al., 2005].

Treatment of Type 2 diabetes consists first of lifestyle changes to increase insulin sensitivity, followed by, or combined with, oral hypoglycaemic medication to enhance insulin sensitivity or stimulate the pancreas. In later, or more extreme stages, insulin therapy, as in Type 1 diabetes, is required to maintain normoglycaemia.

1.2.2 Type 1 Diabetes

Type 1 diabetes is the least understood of the diabetes types and is characterised by a significant, often sudden, *deficiency* of insulin. It is caused by an auto-immune disorder that destroys the pancreatic β-cells that produce insulin. Type 1 diabetes is typically diagnosed at a young age, but can also strike younger adults. It is not linked to obesity [ADA, 2006a]. About 10% of people with diabetes have Type 1 diabetes [ADA, 2006a]. Unlike Type 2, the aetiology of Type 1 is not well understood, but studies indicate it is multifactorial on human leukocyte antigen (HLA) genetics and environmental factors [Cudworth et al., 1979; Dahlquist and Mustonen, 1994]. Due to its typical onset at a young age, it is sometimes referred to as juvenile onset diabetes.

The destruction of insulin producing β-cells resulting in Type 1 diabetes can occur very rapidly over weeks or months, or take several years. Generally, little insulin secretory function remains. Treatment is mainly by regular insulin injections, taken 3-4 times per day to replace this function. If glucose levels are not controlled within a tight range, long-term complications, diabetic ketoacidosis (DKA), and/or hypoglycaemic coma can occur with the latter two very possibly fatal. Long-term exposure to very high blood sugar levels results in complications like retinopathy and neuropathy, which can lead to blindness and limb amputation.

Unlike Type 2 diabetes, glucose counterregulation is severely impaired in Type 1 diabetes [Cryer et al., 2003]. More specifically, a signalling defect causes glucagon secretion to cease responding to hypoglycaemia with increasing endogenous insulin deficiency. Epinephrine secretion is also shifted to a lower plasma glucose concentration with increased iatrogenic hypoglycaemia.

The attenuated epinephrine response results in *hypoglycaemia unawareness*, a reduced sympathoadrenal response resulting in a loss of warning neurogenic symptoms. This forms a vicious cycle, perpetuating more hypoglycaemia with increasing *hypoglycaemia unawareness*. As a result, rates of severe hypoglycaemia in Type 2 diabetes are only around 10% that in Type 1 diabetes [Cryer et al., 2003]. Despite the difficulties, many patients with Type 1 diabetes can live long and healthy lives through tight glycaemic control.

1.2.3 Insulin Sensitivity

Insulin sensitivity quantifies the ability of the body to reduce blood glucose levels with insulin. This definition is very broad and includes many underlying physiological effects that contribute to the whole body response. Insulin sensitivity is not a well defined metric or directly measurable with a simple test. Reduced insulin sensitivity is the main underlying problem in the pathogenesis of Type 2 diabetes as well as the effective management of blood glucose levels in Type 1 diabetes.

The main effects contributing to insulin-dependent glucose uptake are shown schematically in Figure 1.4. The three primary effects are the sensitivity of tissue cells to bind insulin (peripheral sensitivity), the effect of insulin on the liver to suppress glucose production (hepatic sensitivity), and the ability of the pancreas to respond with insulin secretion to an increase in glucose concentration (β-cell or pancreatic function). Hence, many researchers define and try to test for all three specific tissue sensitivities to insulin. Depending on the design of the chosen method to assess insulin sensitivity and its assumptions, one or more of these effects can be lumped together yielding varying results requiring different interpretations [Radziuk, 2000]. However it is measured, insulin sensitivity remains the driving factor in diagnosis and therapy.

1.2.4 Insulin Sensitivity Variation over Time

Circadian rhythmicity and sleep-wake phases have profound and independent effects on insulin sensitivity, as reviewed by Van Cauter et al. [1997]. In normal man, insulin secretion maintains the delicate balance between hepatic glucose production and glucose uptake to achieve plasma glucose homeostasis with little variation across the day. Diurnal patterns in effective insulin sensitivity exist in normal, healthy humans but are more apparent in patients with Type 1 diabetes.

Diurnal effective insulin sensitivity time-variation is now thought to be caused by sleep-associated growth hormone (GH) secretion. The exact mechanism is still being debated, but has been attributed to impaired suppression of hepatic glucose production and peripheral glucose clearance. Diurnal cycles are well documented

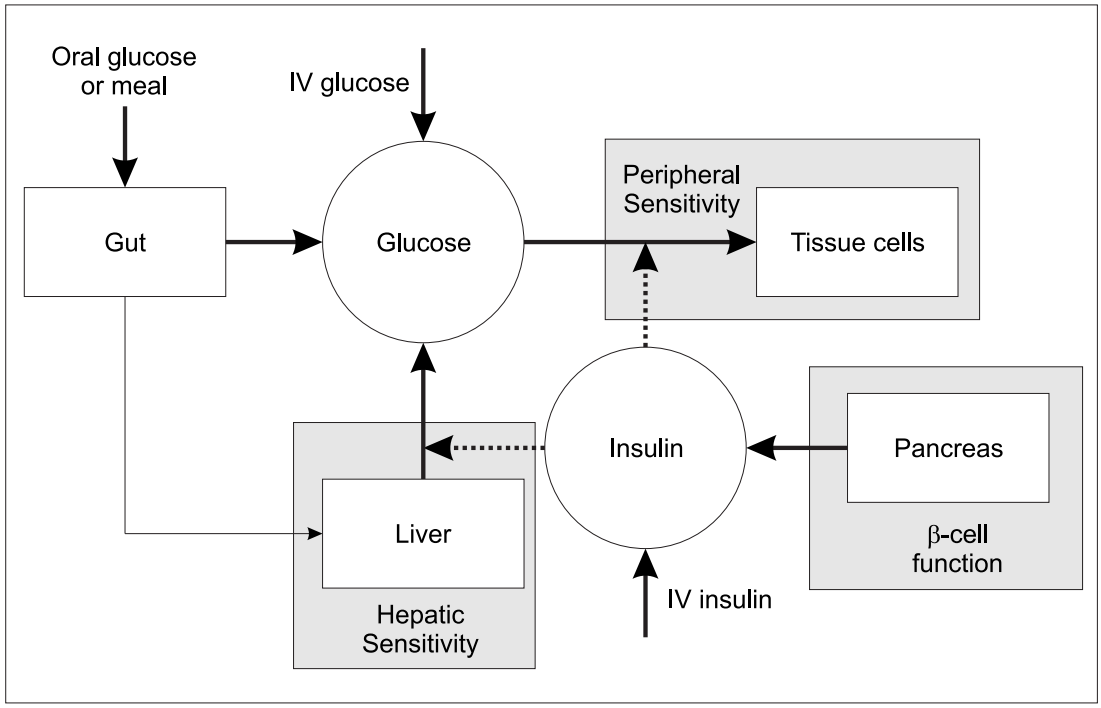

Figure 1.4 Overview of the physiological effects measured by insulin sensitivity tests. Depending on the design of the method, it can measure either one, a lumped effect of two, or of all three. The dashed lines indicate a mediated or enhanced effect.

in Type 1 diabetes and are consistent and reproducible intra-subject [Bolli et al., 1993].

On a larger scale, insulin sensitivity is also affected by exercise and diet [Duncan et al., 2003; McAuley et al., 2002; Nishida et al., 2002; O'Gorman D et al., 2006; Tuomilehto et al., 2001], as well as body weight [Camastra et al., 2005; Ferrannini et al., 2005, 1997]. These factors are usually associated with the development of Type 2 diabetes. However, they have similar effects on insulin sensitivity in Type 1 diabetes as well. Other treatments include sensitivity enhancing medication, such as thiazolidinediones (Rosiglitazone), biguanides (Metformin) or sulfonylureas (Glyburide) [Kahn et al., 2006a].

1.3 Diagnostic Criteria

The general diagnosis of diabetes in general, as recommended by the American Diabetes Association or ADA [ADA, 2006a] is by any of three criteria:

1. **Symptoms of diabetes** (polyuria, polydipsia, unexplained weight loss) plus plasma glucose concentration any time of the day ≥200mg/dl (11.1mmol/l).
2. **Fasting plasma glucose (FPG)** ≥126mg/dl (7.0mmol/l).
3. **2h post OGTT glucose** ≥200mg/dl (11.1mmol/l) during an oral glucose tolerance test (OGTT) (75g glucose content diluted in water).

People with elevated glucose levels that do not meet the criteria for Type 2 diabetes are classified with impaired glucose tolerance (IGT) or impaired fasting glucose (IFG). These conditions are defined as follows:

- **IFG**: Fasting glucose between 100-125mg/dl (5.6-6.9mmol/l).
- **IGT**: 2h postload OGTT glucose between 140-199mg/dl (7.8-11.1mmol/l).

1.4 Preface

Control of Type 1 diabetes and insulin-dependent Type 2 diabetes is a widely studied research field. Published control methods are diverse, with different routes of insulin administration and glucose measurement. Since the 1970s, the closed-loop artificial endocrine pancreas (AEP) has been heralded as the solution (as reviewed by Bequette [2005]). While no commercial product currently exists, the systems in current clinical use that are likely to constitute the components of an AEP are the continuous subcutaneous insulin infusion (CSII) pump and a continuous glucose measurement (CGM) device. In fact, current CGM devices are still not able to be used clinically without conventional self-monitoring blood glucose or SMBG devices [Guerci et al., 2003].

Advanced control algorithms and methods to 'close the loop' have also been widely studied (as reviewed by Bellazzi et al. [2001] and Steil et al. [2004, 2006]) in spite of early and ongoing limitations in sensors and pumps. Currently, the use of open-loop CGM and/or CSII has resulted in at best, a modest clinical advantage over conventional methods of insulin administration or multiple daily injection (MDI) as reviewed by Klonoff [2005] and NICE [2003]. None of the advanced or closed-loop algorithms are yet in clinical use.

Additionally, the advanced sensors and pumps in these envisaged systems are only used by a small population of patients with Type 1 diabetes due to high upfront costs, the high costs of consumables, significant complexity, and the extensive healthcare infrastructure and support required. Prevalence of CSII use is as low as 2% of the Type 1 diabetes population in the UK and up to 15-20% elsewhere and in the US [DiabetesUK, 2007]. As a result, many patients with diabetes do not want to use, or have access to the equipment that might be used in such a closed-loop system.

Hence, there is a more practical and urgent need to address the large majority of the Type 1 diabetes population using conventional glucose measurement, i.e., SMBG, and insulin administration, i.e., MDI, and for whom current conventional or intensive therapies are failing to deliver recommended levels of glycaemic control [ADA, 2006b]. In the US, over 50% of diagnosed patients aged 20-64 are deemed 'out of control' [Mainous et al., 2006]. The higher accuracy of bedside capillary blood glucose meters [Cohen et al., 2006; Guerci et al., 2003], and the latest insulin analogues for MDI therapy [Bolli et al., 1999; Gerich, 2002], coupled with better control methods have the potential to provide better care to the majority of outpatient or ambulatory Type 1 diabetes patients than is currently observed. Such techniques must necessarily be simple to implement to ensure broad clinical uptake by the diabetes population.

The goal of this research is to develop an understanding of clinical glycaemic control using conventional insulin administration and glucose measurement techniques in Type 1 diabetes. Based on this understanding, a control protocol for Type 1 diabetes that is relatively simple and practical has been developed. To develop this protocol, *in silico* simulation on a virtual patient cohort is utilised.

Overall, this treatment and outcome focussed goal has largely been ignored by researchers for several decades since the AEP was first postulated. Instead, efforts have concentrated in developing the enabling technologies. These technologies also remain elusive to all but a few sufferers of the disease. Unsurprisingly, effective solutions are thus yet to be found.

This goal is pursued in this thesis by developing physiological models of the entire system, from subcutaneous insulin pharmacokinetics to meal glucose appearance. Current methods of glycaemic control are tested using an *in silico*

simulation tool with Monte Carlo analysis to uncover its limitations. Design restrictions are that the control protocol must operate within today's environment of Type 1 diabetes control using current tools for insulin administration and glucose measurement with little extra burden on resources.

Once developed and tested *in silico*, the method must prove robust *and* safe in the presence of all quantifiable errors. More specifically, knowledge of metabolic behaviour is combined with modelling and algorithms to achieve this goal. A brief overview of the thesis includes:

Chapter 2 reviews the models of subcutaneous insulin pharmacokinetics from literature and develops the subcutaneous insulin pharmacokinetic model of this research in the context of the prior work in the field. A model is developed that is suitable for application in this research of *in silico* simulation and real-time clinical decision support, identified and validated on clinical pharmacokinetic studies.

Chapter 3 presents the plasma modelling and identification method required for application in this study. It addresses the physiology and modelling of insulin, endogenous glucose production and the insulin-independent clearance or uptake by various tissues. The result is a new glucose-insulin pharmacodynamic system model and fitting method for specific application in outpatient Type 1 diabetes with sparsely measured glucose.

Chapter 4 presents the *in silico* simulation of the developed adaptive protocol for glycaemic control in Type 1 diabetes, and compares it to a conventional intensive insulin therapy and a controls group as a function of self-monitoring blood glucose frequency. The result obtained for the conventional intensive insulin therapy and controls match clinical expectations for control which supports the *in silico* simulation as an accurate technique for determining the performance of the adaptive protocol.

Chapter 5 further assesses the adaptive protocol developed in Chapter 4 by performing a Monte Carlo analysis. The errors and variability incorporated into the analysis are physiological and realistic, with the intention of simulating *in silico* the potential for errors and variability to affect the performance of the protocol. The protocol is shown to be acceptably robust in effectiveness and safety in this analysis.

Chapter 6 introduces the concept of modelling the diurnal cycle in the main, driving parameter of the model, i.e., effective insulin sensitivity. Physiologically, diurnal cycles are widely accepted, and the modelling and prediction of the cycles can be of significant advantage in glycaemic control where reduced glucose measurement is desirable.

Chapters 7 and 8 summarise the key aspects of the thesis and present possible future improvements and applications for this research.

Chapter 2

Subcutaneous Insulin Pharmacokinetic Modelling

For more than 80 years, administration of insulin via the subcutaneous (sc) route into the peripheral circulation has been the most widely used therapy in ambulatory or outpatient diabetes. Since Binder [1969], the absorption kinetics of subcutaneously injected insulin has emerged as a mature research field [Berger et al., 1982; Binder et al., 1984; Galloway et al., 1981].

Sc insulin absorption kinetics are complex and can be influenced in many ways. Insulin-independent factors include sc blood flow which is affected by temperature [Berger et al., 1982; Koivisto et al., 1981], exercise [Koivisto and Felig, 1978; Kolendorf et al., 1979], smoking [Klemp et al., 1982a,b], depth of injection [Demeijer et al., 1990; Hildebrandt et al., 1983], and site of injection [Galloway et al., 1981]. There are also insulin-dependent factors which include the species of insulin [Hildebrandt, 1991], and the concentration and volume of injected insulin [Binder, 1969; Galloway et al., 1981; Hildebrandt et al., 1983; Mosekilde et al., 1989]. As a result, sc insulin pharmacokinetics (PK) are variable enough to offer significant practical difficulties in providing consistent therapy for diabetes. Most studies report inter-individual variation in key pharmacokinetic summary measures from 15% [Heinemann et al., 1998] to 107% [Galloway et al., 1981] depending on insulin type.

Some diabetes decision support and control methods, e.g., Andreassen et al. [1994]; Hovorka et al. [2004]; Lehmann and Deutsch [1992b]; Shimoda et al. [1997] rely on sc absorption models to deterministically predict plasma insulin appearance from sc injection, thus tracking onboard insulin from multiple doses over extended periods. Some would argue the clinical value of such models given the

inherent and significant intra- and inter-patient variability in absorption [Guerci and Sauvanet, 2005; Heinemann, 2002; Heinemann et al., 1998; Heise et al., 2004; Lepore et al., 2000; Scholtz et al., 2005]

Nevertheless, given the often limited data available for glycaemic control in diabetes [Evans et al., 1999; Schutt et al., 2006], an estimation of plasma insulin time-course may be the *only* means for efficient dosing. Given the impaired glucose counterregulation in Type 1 diabetes, iatrogenic hypoglycaemia is best avoided by preventing overinsulinisation. Deterministic models of absorption can also form the basis of stochastic methods, as hinted by Andreassen et al. [1994] with significant potential. These models have also proven useful for glycaemic control simulation [Andreassen et al., 1994; Berger and Rodbard, 1989; Lehmann and Deutsch, 1992b] and diabetes education [Lehmann, 1998]. This chapter gives an overview of the state of the art in the fields explored in this research. A variety of subcutaneous insulin PK models are included, differing by application and complexity.

2.1 Subcutaneous Insulin: A Brief History

Following the discovery of insulin in 1921 by Banting et al. [1922], it was quickly found that adding certain *protraction agents* could alter insulin absorption and prolong its duration of action. This had the useful purpose of reducing the number of insulin injections required daily. The first breakthrough came in 1946, when Hagedorn and associates developed an insulin preparation containing zinc ions and protamine which crystallises at neutral pH. This intermediate-acting insulin is called Neutral Protamine Hagedorn (NPH) or isophane [Home and Alberti, 1992] and has a 8-14h duration. Other developments include lente (10-24h) and ultralente (12-28h) which form amorphous or crystalline zinc precipitates to lower the absorption rate *in subcutis*. In contrast, the shortest acting insulin available at the time was soluble or regular insulin (RI) with a duration of 2-6h and a peak at 2-4h. RI is not sufficiently absorbed for injection at meals, requiring an injection half hour or so prior to the start of the meal to prevent postprandial hyperglycaemia and late postprandial hypoglycaemia.

Up until the 80s, advancements in insulin were restricted to purification and

production of bovine or porcine insulin. In 1982, recombinant DNA technology made possible the commercial production of proteins molecularly identical to human insulin. Synthetic human insulin became commonplace, replacing most animal insulin in the various insulin preparations. Today, RI is more accurately described as regular human insulin or RHI but the RI nomenclature will be maintained throughout this study. While molecular and, hence, physicochemical differences exist between animal RI and synthetic human RI [Heinemann and Richter, 1993], the PK issues with RI as a prandial bolus insulin remained.

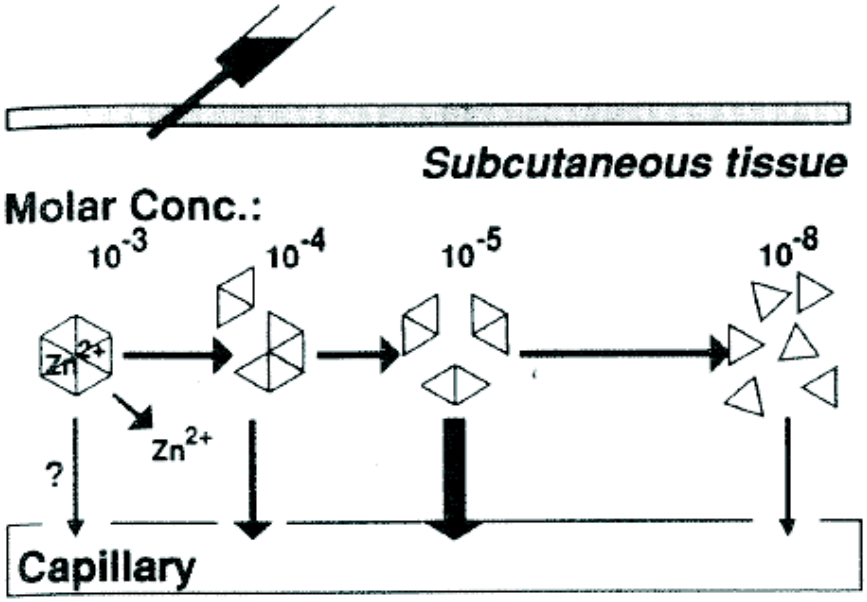

Figure 2.1 Concentration of hexameric Zn^{2+} insulin, predominant association state of soluble insulin in U-40 and U-100 concentrations. Dissociation into dimeric insulin requires 50- to 100-fold dilution, and dissociation into monomeric insulin requires 1000-fold dilution. Reproduced from Brange et al. [1990].

As shown in Figure 2.1, RI in solution is a dynamic equilibrium of monomeric, dimeric, and zinc-containing hexameric states [Brange et al., 1990]. The issue lies in the tendency of insulin in neutral solution to aggregate and form these polymers with increasing molar concentrations. The self-association of insulin ensures stable storage in the β-cell granule. As insulin binds to its receptor in monomeric form only, this behaviour does not affect its pharmacological activity. The shift of equilibrium from hexameric to more readily absorbed monomeric and dimeric state delays the absorption of injected RI *in subcutis*. This property is thought to be responsible for the inverse relationship between absorption rate, and the volume and concentration of the injected RI solution [Binder, 1969; Brange et al., 1990; Kang et al., 1991a].

The next revolution came in the 1996 with commercial availability of the first rapid-acting, synthetic *designer* insulin analogue (insulin lispro or Lys^{B28}, Pro^{B29} human insulin) produced via rDNA technology. By substitution of a single amino acid from human insulin, this class of insulin (now extended to insulin aspart and insulin glulisine) resists aggregation into hexamers, resulting in dissociation of the zinc-MI complex into monomeric form at concentrations of 10^{-4}M vs 10^{-8}M for RI, a 1000-fold difference in dilution [Brange and Volund, 1999]. Clinically, MI sc administration is less affected by sc blood flow due to more rapid absorption, and is unaffected by volume and concentration of injection [Kaku et al., 2000; Woodworth et al., 1993], resulting in less variable absorption than RI. This and the ability to inject MI *at* meals (5mins before to 15mins after meals), rather than 30-45mins before with RI, allows a significantly more flexible, consistent and convenient style of therapy.

Recently, advances in insulin analogues have extended to basal-acting insulin. The first of these is insulin glargine which was approved by the US Federal Drug Administration in 2000 for use in diabetes [Gerich, 2004]. Unlike NPH, lente or ultralente insulin, insulin glargine provides a peakless 24h duration of action. This PK profile is achieved via a shift in isoelectric point, effectively shifting solubility to a higher pH. Once injected into the neutral environment *in subcutis*, insulin glargine forms a stable microprecipitate which slowly dissolves giving the prolonged action. Insulin glargine is injected as an acidic, clear solution requiring no mixing before injection. This greatly reduces variability in absorption over that of NPH [Heinemann et al., 2000] in day to day use.

With its duration of action, only a single injection per day of insulin glargine is required which offers significant convenience for the patient with diabetes. Insulin determir, approved by the European Medical Agency in 2004, is the latest basal-acting insulin analogue but with an entirely different mechanism of protraction to insulin glargine [Chapman and Perry, 2004; Hordern and Russell-Jones, 2005]. Studies on insulin determir (approved for diabetes since 2004) are few as clinical experience with the insulin matures but has been shown to be even more consistent in PK profile than insulin glargine [Heise et al., 2004].

The developments in sc administered insulin analogues over the last 11 years promises the tools with which diabetes can be now more effectively managed. The PK profile of the latest rapid and basal-acting analogues now mimic pancreatic

insulin secretion better than any insulin previously. To the majority of diabetes patients, these tools have the potential for greater control, greater convenience, greater flexibility and greater safety from hypoglycaemia than previously possible.

2.2 Review of Subcutaneous Insulin Pharmacokinetic Modelling

2.2.1 Compartmental Models

Previous work in insulin PK modelling is voluminous. Kobayashi et al. [1983] experimented with a single-compartment and pure time delay model for regular insulin (RI) absorption. Later, Kraegen and colleagues [Furler and Kraegen, 1989; Kraegen and Chisholm, 1984] developed a two-compartment model, which was refined with a more minimal approach by Puckett and Lightfoot [1995], modelling the long-acting ultralente insulin as an unlikely continuous flow in addition to RI.

As the use of monomeric insulin (MI) types matured clinically, more models concentrated on its absorption kinetics. In this research, the term 'monomeric insulin' or MI is a convenient misnomer used for rapid-acting insulin analogues whose hexamers dissociate very rapidly into dimers/monomers in subcutaneous tissue, resulting in a monoexponential decay curve [Kang et al., 1991a]. With a similar three-compartment model, Shimoda et al. [1997] modelled both RI and MI absorption. More recently, Wilinska et al. [2005] demonstrated a three-compartment model of MI absorption with fast/slow absorption channels and local insulin degradation. Brief descriptions of the history of sc insulin PK studies are provided below.

Kobayashi et al. [1983]

Referring to Figure 2.2 and Equation 2.1, the model by Kobayashi et al. [1983] consists of one compartment with first-order absorption and decay rates.

$$C(t) = \begin{cases} \frac{K_a \cdot D}{V_d \cdot (K_a - K_e)} \cdot (e^{K_e \cdot t} - e^{K_a \cdot t}) & \text{if } t \geq \tau \\ 0 & \text{if } t < \tau \end{cases} \tag{2.1}$$

where K_a and K_e are the first-order rate constants for absorption and elimination respectively, V_d is the distribution volume, D is the sc injection dose of RI insulin and τ is the pure time delay before sc administered insulin appears in the compartment.

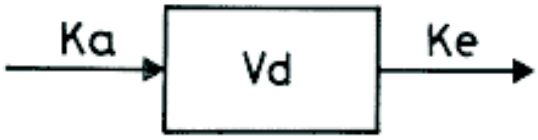

Figure 2.2 Schematic representation of a one-compartment model: where K_a is the apparent first-order absorption rate constant and K_e is the first-order elimination rate constant. V_d is the distribution volume. Reproduced from Kobayashi et al. [1983].

The Kobayashi et al. model is identified using both RI bolus sc injection (0.15U/kg) and RI continuous sc infusion (0.15U/kg infused over 1h period).

Kraegen and Chisholm [1984]

Kraegen and Chisholm [1984] studied two models, Model 1 and Model 2 shown in Figure 2.3. Model 1 is a single compartment model in Equation 2.2 to 2.3 and Model 2 is a dual compartment model (see Equations 2.4 to 2.6).

$$\frac{\mathrm{d}x}{\mathrm{d}t} = S(t) - k_{sp} \cdot x - k_d \cdot x \tag{2.2}$$

$$\frac{\mathrm{d}y}{\mathrm{d}t} = k_{sp} \cdot x - \frac{\mathrm{MCR}}{\mathrm{TDV}} \cdot y + I(t) \tag{2.3}$$

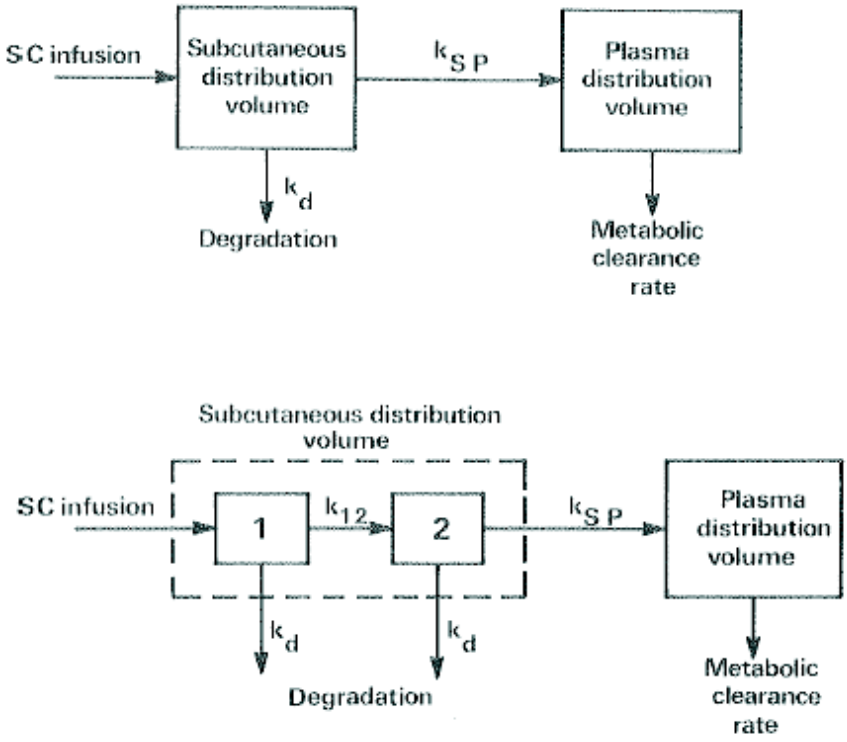

Figure 2.3 Top panel: Model 1 is a single pool model. Bottom panel: Model 2 is a split-pool model of subcutaneous space for insulin. Reproduced from Kraegen and Chisholm [1984].

$$\frac{\mathrm{d}x_1}{\mathrm{d}t} = S(t) - (k_d + k_{12}) \cdot x_1 \tag{2.4}$$

$$\frac{\mathrm{d}x_2}{\mathrm{d}t} = (k_{12} + k_{sp}) \cdot x_1 \tag{2.5}$$

$$\frac{\mathrm{d}y}{\mathrm{d}t} = k_{sp} \cdot x_2 - \frac{\mathrm{MCR}}{\mathrm{TDV}} \cdot y + I(t) \tag{2.6}$$

where x is the mass of sc insulin in the single pool (Model 1), x_1 and x_2 are the masses of sc insulin in the 1st and 2nd pools (Model 2), k_{12}, k_d and k_{sp} are the rate constants as shown in Figure 2.3, $S(t)$ and $I(t)$ are the sc and IV insulin infusion rates respectively, y is the mass of insulin in the plasma compartment which has volume TDV (total distribution volume) and decay rate MCR (metabolic clearance rate). The Kraegen and Chisholm models are identified using a combination of IV insulin infusion (to obtain quantitative estimates of MCR and TDV) and two RI sc infusion studies, a short 10U infusion over 5mins and prolonged 2.4U/hr infusion over 4h. The authors concluded that the single

pool Model 1 fitted poorly relative to Model 2.

Puckett and Lightfoot [1995]

The Puckett and Lightfoot [1995] model is structurally similar to the Kraegen and Chisholm [1984] model with the difference lying in the removal of insulin degradation, k_d, from the subcutaneous distribution pools and the implementation of an *effectiveness* parameter, α, at injection. While the model also accounts for ultralente insulin injection, the approach using a constant insulin absorption rate is oversimplified and questionable physiologically. Model equations are shown in Equation 2.7 to Equation 2.9.

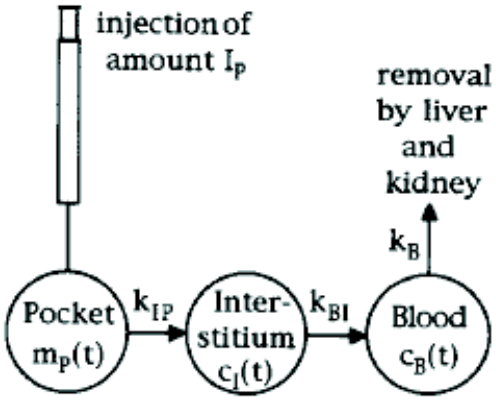

Figure 2.4 Model structure of subcutaneous insulin by Puckett and Lightfoot [1995]. Model consists of 2 pools for subcutaneous insulin distribution and 1 for blood plasma. Total mass in the injection *pocket* is $m_p(t)$ with initial concentration at injection of $\alpha.I_p$. Concentrations of insulin in interstitium and plasma are $c_I(t)$ and $c_B(t)$ respectively with volumes V_I and V_B. First-order transport rates are k_{IP} and k_{BI}, with k_b the first-order clearance rate by the liver and kidneys. Reproduced from Puckett and Lightfoot [1995].

$$\frac{\mathrm{d}m_p(t)}{\mathrm{d}t} = -k_{IP} \cdot m_p(t) \tag{2.7}$$
$$m_P(0) = \alpha \cdot I_P$$
$$V_I \frac{\mathrm{d}c_I(t)}{\mathrm{d}t} = k_{IP} \cdot m_P(t) - k_{BI} \cdot c_I(t) \tag{2.8}$$
$$c_I(0) = 0$$
$$V_B \frac{\mathrm{d}c_B(t)}{\mathrm{d}t} = k_{BI} \cdot c_I(t) - k_B \cdot c_B(t) + k_B \cdot I_B \cdot u(t) \tag{2.9}$$
$$c_B(0) = I_B$$

where $m_p(t)$ is the insulin mass in the *pocket*, k_{IP} and k_{BI} are the first-order transport rates from the *pocket* to interstitium, and from interstitium to plasma respectively. Concentrations of insulin in interstitium and plasma are $c_I(t)$ and $c_B(t)$ respectively with volumes V_I and V_B. α is the *effectiveness* factor which accounts for insulin degradation at injection. The Puckett and Lightfoot model is identified using a combined multiple injection regime of ultralente insulin and RI.

Shimoda et al. [1997]

In Shimoda et al. [1997], sc insulin PK is studied for application in an AEP. Like Kraegen and Chisholm [1984] and Puckett and Lightfoot [1995], the model structure consists of 2 pools for sc insulin distribution and 1 for plasma insulin as shown in Figure 2.5 and Equation 2.10 to Equation 2.13. Unlike the rest of the models reviewed so far, the Shimoda et al. [1997] model is used for MI in addition to RI with the same model structure identified using a 0.12U/kg dose of U-40 RI and U-40 MI diluted to 4U/ml and injected sc.

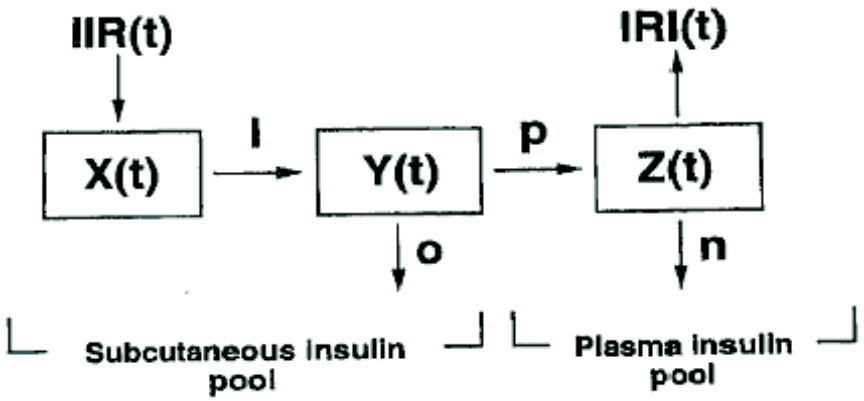

Figure 2.5 Shimoda et al. [1997] model for sc insulin PK. $X(t)$ and $Y(t)$ are insulin masses in the sc insulin pools, $IIR(t)$ is the sc insulin infusion rate, $IRI(t)$ is the plasma insulin concentration and $Z(t)$ is the plasma insulin mass. l, n, o and p are the first-order transport rate constants and r is the plasma volume of distribution. Reproduced from Shimoda et al. [1997].

$$\frac{\mathrm{d}X(t)}{\mathrm{d}t} = IIR(t) - l \cdot X(t) \tag{2.10}$$

$$\frac{\mathrm{d}Y(t)}{\mathrm{d}t} = l \cdot X(t) - (p + o) \cdot Y(t) \tag{2.11}$$

$$\frac{\mathrm{d}Z(t)}{\mathrm{d}t} = p \cdot Y(t) - n \cdot Z(t) \tag{2.12}$$

$$IRI(t) = \frac{Z(t)}{r} \tag{2.13}$$

where $X(t)$ and $Y(t)$ are insulin masses in the sc insulin pools, $IIR(t)$ is the sc insulin infusion rate, $IRI(t)$ is the plasma insulin concentration and $Z(t)$ is the plasma insulin mass. l, n, o and p are the first-order transport rate constants and r is the plasma volume of distribution. The Shimoda et al. model is identified using a 0.12U/kg dose of sc injected MI and RI insulin. Controversially, the identified plasma distribution volumes, r, are different for MI and RI (0.08ml vs. 0.125ml respectively), which is improbable physiologically.

Wilinska et al. [2005]

Like Shimoda et al. [1997], the aim of the Wilinska et al. [2005] MI model is to model insulin pump sc bolus and continuous infusion for implementation in

an AEP. The model consists of local degradation at injection, with two pathways of insulin absorption (slow and fast). The degradation is saturable with Michaelis-Menten dynamics. The model is shown in Figure 2.6 and Equation 2.14 to Equation 2.19. The developed model is chosen from 11 hypothesized models based on model fit error, precision of parameter estimates, randomness of residuals, and parsimony. The two absorption channels in the model have admittedly no physiological basis currently. The model is identified using prandial MI insulin injections of unspecified size and concentration.

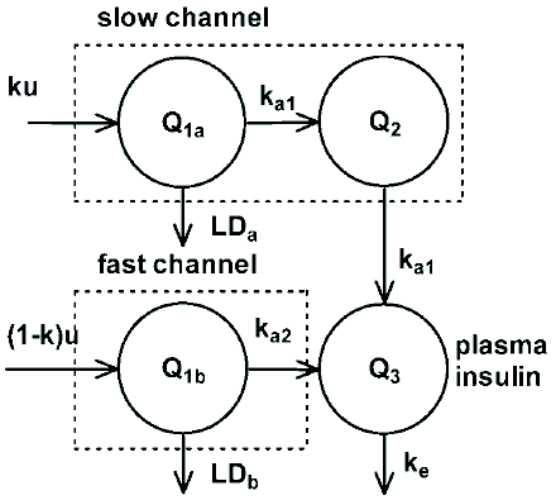

Figure 2.6 Model structure by Wilinska et al. [2005]. Q_{1a}, Q_{1b} and Q_2 are the masses of insulin in the channels, k is the proportion of u, the insulin input, that passes through the slower channel, k_{a1} and k_{a2} are the transport rates between compartments, k_e is the rate of clearance of insulin from plasma by the liver and kidneys, and LD_a and LD_b are the Michaelis-Menten degradation terms from Q_{1a} and Q_{1b} respectively. Note that both slow and fast channels have identical Michaelis-Menten saturation levels for degradation.

$$\frac{\mathrm{d}Q_{1a}}{\mathrm{d}t} = k \cdot u - k_{a1}Q_{1a} - LD_a \tag{2.14}$$

$$\frac{\mathrm{d}Q_{1b}}{\mathrm{d}t} = (1-k) \cdot u - k_{a2} \cdot Q_{1b} - LD_b \tag{2.15}$$

$$\frac{\mathrm{d}Q_2}{\mathrm{d}t} = k_{a1} \cdot Q_{1a} - k_{a1} \cdot Q_2 \tag{2.16}$$

$$\frac{\mathrm{d}Q_3}{\mathrm{d}t} = k_{a1} \cdot Q_2 + k_{a2} \cdot Q_{1b} - k_e \cdot Q_3 \tag{2.17}$$

$$LD_a = \frac{V_{max,LD} \cdot Q_{1a}}{k_{M,LD} + Q_{1a}} \tag{2.18}$$

$$LD_b = \frac{V_{max,LD} \cdot Q_{1b}}{k_{M,LD} + Q_{1b}} \tag{2.19}$$

2.2.2 Non-Compartmental Models

So far, the reviewed compartmental models apply to prandial insulin only. Basal-acting insulin is required in ∼90% of all cases of insulin-dependent diabetes excluding those on insulin pump therapy (calculated based on estimated insulin pump use [Pham, 2005] and prevalence of diabetes [CDC, 2005], 2003 and 2005 statistics, US figures only) which is limiting. The accepted RI absorption dependency on dose, concentration, and volume of injection is also not addressed by the simpler compartmental models above. One of the earliest non-compartmental modelling approaches include Berger and Rodbard [1989] whose simulation model has been adopted by the AIDA decision support system [Lehmann and Deutsch, 1993].

Berger and Rodbard [1989]

The Berger and Rodbard [1989] model was developed for computer simulation of glucose as a function of insulin dose, timing, regimen and diet. Being a simulation tool, this model has been population identified using clinical sc PK studies. It remains a landmark model because, for a long time, it was the only model capable of simulating the sc insulin PK of NPH intermediate-acting insulin as well as a wide range of older insulin types including RH, lente and ultralente (until Tarin et al. [2005]). A three-parameter logistic equation with linear dose dependency is used to describe sc insulin plasma rate of appearance as shown in Equation 2.20 to Equation 2.21, while a two-compartment model describes plasma insulin kinetics and action. This model accounts for general dose dependency of absorption but does not account for the underlying volume or concentration effects.

$$A\%(t) = 100 - \frac{100 \cdot t^2}{(T_{50}^s) + t^2} \tag{2.20}$$

$$T_{50}(D) = a \cdot D + b \tag{2.21}$$

$$\frac{\mathrm{d}A}{\mathrm{d}t} = \frac{s \cdot t^s \cdot (T_{50})^s \cdot D}{t \cdot [(T_{50})^s + t^s]^2} - k_e \cdot A \tag{2.22}$$

$$I(t) = \frac{A(t)}{V_I} \tag{2.23}$$

where A is the normalised plasma insulin concentration, the dependency of T_{50} on dose is defined by Equation 2.21, a, b, s are insulin specific population parameters identified from clinical sc PK studies [Berger and Rodbard, 1989], D is the insulin dose, k_e is the plasma insulin elimination constant, and V_I is the plasma insulin distribution volume.

Mosekilde et al. [1989]

The model by Mosekilde et al. [1989] describes the absorption kinetics of RI with three coupled partial differential equations of detailed physicochemical properties of insulin. Insulin at injection is modelled as a dynamic equilibrium of low molecular weight (dimeric), high molecular weight (hexameric) and a reversible bound state as shown in Figure 2.7.

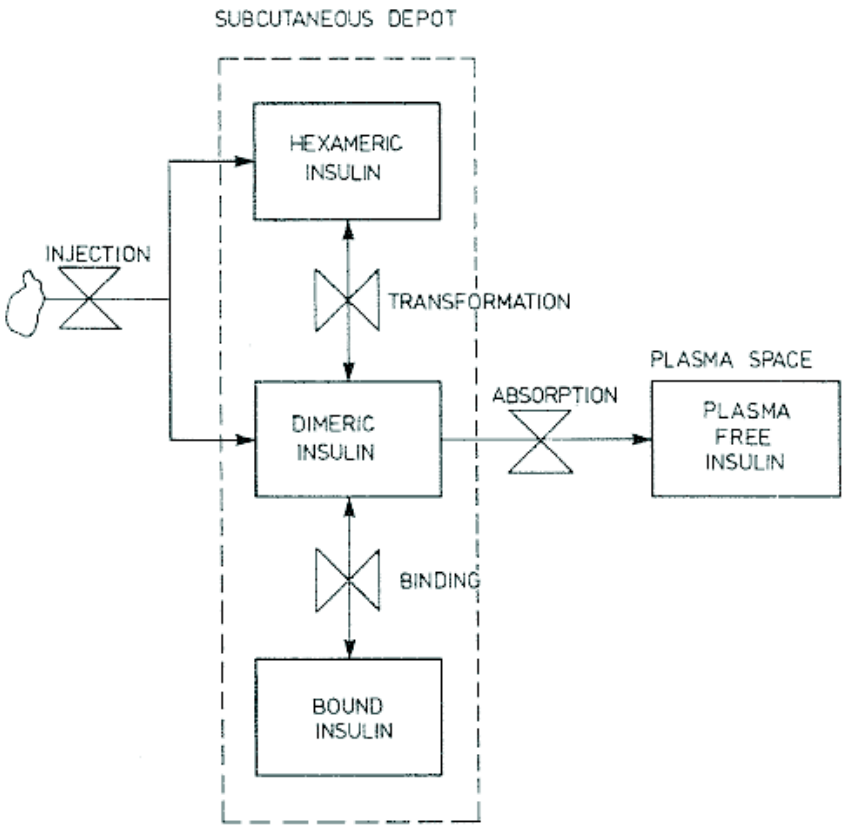

Figure 2.7 Model of sc absorption of soluble RI insulin. Three different forms of insulin are assumed present *in subcutis* with dimeric insulin being the only absorbable form of insulin. Reproduced from Mosekilde et al. [1989]

Only the dimeric state can be absorbed into plasma. While accounting for

dose, volume and concentration dependency, solving the non-linear coupled differential equations it employs is computationally burdensome, and only RI is modelled. Due to the number of parameters, model parameters are *a priori* identified from literature and the model response simulated against published clinical data for comparison. The model is theoretically unidentifiable. As a real-time clinical tool, this model is too limited and computationally burdensome to implement.

Trajanoski et al. [1993]

The Mosekilde et al. [1989] model was subsequently simplified by Trajanoski et al. [1993]. Trajanoski et al. estimates the parameters of the Mosekilde et al. model using plasma insulin profiles from sc injection and adapts the model to MI to widen its clinical appeal. To do this, simplifications and assumptions were introduced. The most significant of these is the assumption of a spherical depot and the removal of bound insulin (which was found to be significant only at extremely low concentrations by Mosekilde et al.). The diffusion equation is spatially discretised into 15 shells. Despite the efforts, the model cannot be made identifiable. The model parameters are still identified *a priori* from *in vivo* and *in vitro* studies and are adjusted to match clinical PK studies.

Tarin et al. [2005]

The Tarin et al. [2005] model is based on the Trajanoski et al. [1993] and Mosekilde et al. [1989] models. Physiologically, this class of models are the most justified and the Tarin et al. model is the most complete of the reviewed models. The Tarin et al. model introduces a bound state for insulin glargine. The injected insulin glargine is assumed to be completely in the bound state. The bound to hexameric state conversion is proportional to the concentration of bound insulin and a proportionality factor, and is saturable.

Using an iterative identification method, 6 parameters are identified for insulin glargine. Three parameters each for MI, RI, NPH and semilente are not identified but obtained *a priori* from literature, mainly from Trajanoski et al. [1993]. There are several minor discrepancies with the Tarin et al. model. The

bound state is not applied to NPH and semilente even though a crystalline or amorphous precipitate is clearly present in these insulin types. The bound state exists only for insulin glargine. Also, the diffusion constant parameter D is the same for all insulin types except MI which is not the case. The insulin glargine hexamer has an increased number of inter-hexamer interactions compared to human insulin which should be recognised in a reduced value for D [Home and Ashwell, 2002].

2.2.3 Review Summary

From this review, the complex non-compartmental models are more accurate physiologically and better capture published insulin absorption kinetics than the compartmental models. However, the associated computational cost is prohibitive compared to the simpler compartmental methods, especially if the intended or potential end use is a real-time diabetes decision support system or an *in silico* simulation tool. The class of models by Tarin et al. [2005], Trajanoski et al. [1993] and Mosekilde et al. [1989] make the strongest attempt to model the diffusion *in subcutis* and the dynamic equilibrium between hexameric and dimeric/monomeric states. The binding within a precipitate is also modelled by Tarin et al. for insulin glargine and this model remains the only model for this basal-acting insulin analogue.

However, the more complicated kinetics of RI have not been modelled using compartment models, nor have insulin glargine or older intermediate and long-acting insulin types such as lente and ultralente. Most existing models also describe only one insulin type or a limited number with no commonality [Shimoda et al., 1997]. For additional reference, critical reviews of some of these models are available from Nucci and Cobelli [2000]. Compartmental modelling methods are also well reviewed in Carson and Cobelli [2001].

2.3 Subcutaneous Insulin Pharmacokinetic Model

This section develops a physiological compartment model for a wide range of insulin types. Specifically, the fast- and short-acting prandial insulins (MI and RI),

and the intermediate- and long-acting basal insulins (NPH, lente, ultralente, and insulin glargine) are modelled. The main principle is to more accurately capture the main dynamics of the absorption kinetics with a compartmental model using first-order kinetics. The secondary goal is to provide a computationally-minimal, yet consistent, and physiologically unified framework for all insulin types. The model also accounts for volume and concentration dependency on sc absorption of human insulin. The intended end use is as an *in silico* simulation model for a real-time diabetes decision support system.

2.3.1 Method

A simple diagram of the structure of the sc insulin absorption kinetic model is shown in Figure 2.8. The model equations are then listed, followed by a description of the individual sections of the model for each insulin type. After this description, the full model diagram is illustrated in Figure 2.9 with a summary of the model.

Hexameric state: common to RI, NPH and lente insulin types

$$\begin{aligned}\dot{x_h}(t) = &-(k_1 + k_d) \cdot x_h(t) + k_{crys,NPH} \cdot c_{NPH}(t) + k_{crys,len} \cdot c_{len}(t) + \\ &u_{h,RH}(t) + u_{h,NPH}(t) + u_{h,len}(t)\end{aligned} \tag{2.24}$$

Dimeric/monomeric state: common to all insulin types

$$\begin{aligned}\dot{x_{dm}}(t) = &-(k_2 + k_d) \cdot x_{dm}(t) + k_1 \cdot x_h(t) + \\ &k_{1,ulen} \cdot x_{h,ulen}(t) + k_{1,gla} \cdot x_{h,gla}(t) + \\ &u_{mono}(t) + u_{m,RH}(t) + u_{m,NPH}(t) + \\ &u_{m,len}(t) + u_{m,ulen}(t) + u_{m,gla}(t)\end{aligned} \tag{2.25}$$

NPH and lente insulin compartments

$$\dot{c_{NPH}}(t) = -k_{crys,NPH} \cdot c_{NPH}(t) + u_{c,NPH}(t) \tag{2.26}$$

$$\dot{c_{len}}(t) = -k_{crys,len} \cdot c_{len}(t) + u_{c,len}(t) \tag{2.27}$$

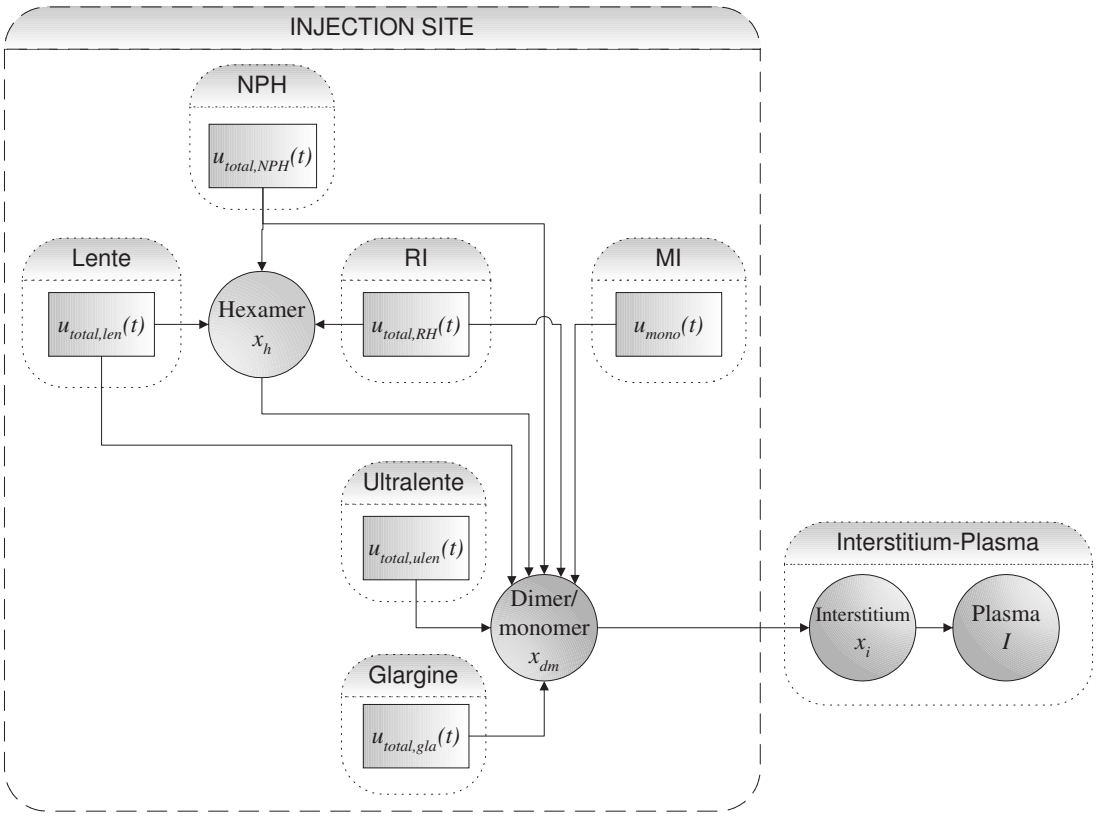

Figure 2.8 Basic structure of the overall sc insulin pharmacokinetic model. Six injected insulin types (MI, RI, NPH, lente, ultralente and glargine) are modelled. The model is characterised by a common hexameric state compartment (x_h) for the RI ($u_{total,RI}(t)$), NPH ($u_{total,NPH}(t)$) and lente ($u_{total,len}(t)$) insulin inputs. All insulin types flow into common dimeric-monomeric state (x_{dm}), interstitium (x_i), and plasma (I) compartments.

Ultralente insulin compartments

$$\dot{x_{h,ulen}}(t) = -(k_{1,ulen} + k_d) \cdot x_{h,ulen}(t) + k_{crys,ulen} \cdot c_{ulen}(t) + u_{h,ulen}(t) \tag{2.28}$$

$$\dot{c_{ulen}}(t) = -k_{crys,len} \cdot c_{ulen}(t) + u_{c,ulen}(t) \tag{2.29}$$

Insulin glargine compartments

$$\dot{x_{h,gla}}(t) = -(k_{1,gla} + k_d) \cdot x_{h,gla}(t) + \min(k_{prep,gla} \cdot p_{gla}(t), r_{dis,max}) + u_{h,gla}(t) \tag{2.30}$$

$$\dot{p_{gla}}(t) = -\min(k_{prep,gla} \cdot p_{gla}(t), r_{dis,max}) + u_{p,gla}(t) \tag{2.31}$$

Mass balance insulin inputs

$$u_{total,mono}(t) = u_{mono}(t) \tag{2.32}$$
$$u_{total,RH}(t) = u_{h,RH}(t) + u_{m,RH}(t) \tag{2.33}$$
$$u_{total,NPH}(t) = u_{c,NPH}(t) + u_{h,NPH}(t) + u_{m,NPH}(t) \tag{2.34}$$
$$u_{total,len}(t) = u_{c,len}(t) + u_{h,len}(t) + u_{m,len}(t) \tag{2.35}$$
$$u_{total,ulen}(t) = u_{c,len}(t) + u_{h,ulen}(t) + u_{m,ulen}(t) \tag{2.36}$$
$$u_{total,gla}(t) = u_{p,gla}(t) + u_{h,gla}(t) + u_{m,gla}(t) \tag{2.37}$$

Mass input fractions and components

$$u_{c,NPH}(t) = \alpha_{NPH} \cdot u_{total,NPH}(t) \tag{2.38}$$
$$u_{c,len}(t) = \alpha_{len} \cdot u_{total,len}(t) \tag{2.39}$$
$$u_{c,ulen}(t) = \alpha_{ulen} \cdot u_{total,ulen}(t) \tag{2.40}$$

$$u_{p,gla}(t) = \alpha_{gla} \cdot u_{total,gla}(t) \tag{2.41}$$

$$u_{h,NPH}(t) + u_{m,NPH} = (1 - \alpha_{NPH}) \cdot u_{total,NPH}(t) \tag{2.42}$$
$$u_{h,len}(t) + u_{m,len} = (1 - \alpha_{len}) \cdot u_{total,len}(t) \tag{2.43}$$
$$u_{h,ulen}(t) + u_{m,ulen} = (1 - \alpha_{ulen}) \cdot u_{total,ulen}(t) \tag{2.44}$$
$$u_{h,gla}(t) + u_{m,gla} = (1 - \alpha_{gla}) \cdot u_{total,gla}(t) \tag{2.45}$$

where all variables in Equation 2.24 to Equation 2.45 are defined:

$x_h(t)$	Mass in the hexameric compartment [mU]
$x_{h,ulen}(t)$	Mass in the ultralente hexameric compartment [mU]
$x_{h,gla}(t)$	Mass in the glargine hexameric compartment [mU]
$c_{NPH}(t)$	Mass in the NPH crystalline protamine compartment [mU]
$c_{len}(t)$	Mass in the lente crystalline zinc compartment [mU]
$c_{ulen}(t)$	Mass in the ultralente crystalline zinc compartment [mU]
$p_{gla}(t)$	Mass in the glargine precipitate compartment [mU]
$x_{dm}(t)$	Mass in the dimer/monomer compartment [mU]

$u_{total,mono}(t)$	MI input [mU/min]
$u_{total,RH}(t)$	RI input [mU/min]
$u_{total,NPH}(t)$	NPH insulin input [mU/min]
$u_{total,len}(t)$	Lente insulin input [mU/min]
$u_{total,ulen}(t)$	Ultralente insulin input [mU/min]
$u_{total,gla}(t)$	Insulin glargine input [mU/min]
α_{NPH}	Proportion of $u_{total,NPH}(t)$ in protamine crystalline state at injection
α_{len}	Proportion of $u_{total,len}(t)$ in zinc crystalline state at injection
α_{ulen}	Proportion of $u_{total,ulen}(t)$ in zinc crystalline state at injection
α_{gla}	Proportion of $u_{total,gla}(t)$ in precipitate state at injection
$u_{c,NPH}(t)$	NPH crystalline state insulin input [mU/min]
$u_{c,len}(t)$	Lente crystalline state insulin input [mU/min]
$u_{c,ulen}(t)$	Ultralente crystalline insulin input [mU/min]
$u_{c,gla}(t)$	Glargine precipitate state insulin input [mU/min]
$u_{h,NPH}(t)$	NPH hexamer state insulin input [mU/min]
$u_{h,len}(t)$	Lente hexamer state insulin input [mU/min]
$u_{h,ulen}(t)$	Ultralente hexamer state insulin input [mU/min]
$u_{h,gla}(t)$	Glargine hexamer state insulin input [mU/min]
$u_{mono}(t)$	MI dimer/monomer state insulin input [mU/min]
$u_{m,RH}(t)$	RI dimer/monomer state insulin input [mU/min]
$u_{m,NPH}(t)$	NPH dimer/monomer state insulin input [mU/min]
$u_{m,len}(t)$	Lente dimer/monomer state insulin input [mU/min]
$u_{m,ulen}(t)$	Ultralente dimer/monomer state insulin input [mU/min]
$u_{m,gla}(t)$	Glargine dimer/monomer state insulin input [mU/min]
$k_{crys,NPH}$	NPH protamine crystalline dissolution rate [1/min]
$k_{crys,len}$	Lente zinc crystalline dissolution rate [1/min]
$k_{crys,ulen}$	Ultralente zinc crystalline dissolution rate [1/min]
$k_{prep,gla}$	Glargine precipitate dissolution rate [1/min]
V_{inj}	Insulin dose injection volume [ml] or [cm^3]

n	Plasma insulin rate of clearance [1/min]
$r_{dis,max}$	Maximum glargine precipitate dissolution rate [mU/min]
k_1	Hexamer dissociation rate [1/min]
$k_{1,ulen}$	Ultralente hexamer dissociation rate [1/min]
$k_{1,gla}$	Glargine hexamer dissociation rate [1/min]
k_2	Dimeric/monomeric insulin transport rate into interstitium [1/min]
k_3	Interstitium insulin transport rate into plasma [1/min]
$k_{d,i}$	Rate of loss from interstitium [1/min]
k_d	Rate of diffusive loss from hexameric and dimeric/monomeric state compartments [1/min]

RI sub-model structure

The RI model (Equations 2.24 to 2.25) is based on insulin physicochemical properties [Mosekilde et al., 1989]. For soluble human insulins, it is generally accepted that the dynamic equilibrium of the hexameric, dimeric, and bound states characterises absorption kinetics [Brange et al., 1988, 1990; Kang et al., 1991a]. The equilibrium is concentration dependent and is destabilised by dilution and diffusion in the sc depot [Emdin et al., 1980; Mosekilde et al., 1989]. Qualitatively, the monomeric state has the highest absorption rate into plasma [Kang et al., 1991a], and becomes increasingly stable towards the end of the absorption process when insulin concentration at the site decreases.

For simplicity, the dimeric and monomeric states are lumped in $x_{dm}(t)$ (see Equation 2.25). Both states have higher relative absorption rates into plasma than the hexameric state, although the dimer is absorbed discernibly slower than the monomer [Kang et al., 1991a]. There is no provision for a reversible, bound state [Mosekilde et al., 1989]. However, for many common concentrations of insulin preparation, insulin binding has been shown to be negligible [Trajanoski et al., 1993]. Reversible binding also becomes apparent only at low doses and concentrations [Mosekilde et al., 1989]. This result implies that the effect of insulin binding is relatively small, especially when large prandial injections are administered, and might be ignored for decision support.

Thus, the RI input (Equation 2.33) is assumed to consist of hexameric, $x_h(t)$ and dimeric/monomeric, $x_{dm}(t)$ states according to the equilibrium of Equation 2.46 [Mosekilde et al., 1989], but only at the injection at $t = 0$ (see Equation 2.47).

$$C_h = Q_D \cdot {C_D}^3 \tag{2.46}$$

$$\frac{u_h(t=0)}{V_{inj}} = Q_D \cdot \left(\frac{u_m(t=0)}{V_{inj}}\right)^3 \tag{2.47}$$

where

C_h	Concentration of hexameric insulin [(mU/l)]
C_D	Concentration of dimeric insulin [(mU/l)]
Q_D	Hexameric-dimeric equilibrium constant [(l/mU)^2]
V_{inj}	Insulin dose injection volume [l]
$u_m(t)$	Dimer/monomer state insulin input [mU]
$u_h(t)$	Hexamer state insulin input [mU]

This equation is an acknowledged simplification of the hexameric-dimeric state dynamic equilibrium, while still accounting for dose and concentration effect. Assuming a spherical depot, volume effect is modelled by a rate of diffusive loss, k_d, from both $x_h(t)$ and $x_{dm}(t)$ compartments in the sc depot (Equations 2.48 and 2.49).

$$k_d = \frac{3 \cdot D}{r^2} \tag{2.48}$$

$$r = \left(\frac{3 \cdot V_{inj}}{4 \cdot \pi}\right)^{\frac{1}{3}} \tag{2.49}$$

where

k_d	Rate of diffusive loss from hexameric and dimeric/monomeric state compartments [1/min]

D	Diffusion constant of hexameric and dimeric/monomeric insulin [cm^2/min]
r	Radius of the sc depot [cm]
V_{inj}	Insulin dose injection volume [ml] or [cm^3]

Both hexameric and dimeric/monomeric states are assumed to have the same diffusion constant, a further simplification of the absorption process that was also made by Mosekilde et al. [1989].

NPH, lente and ultralente insulin sub-model structures

The NPH, lente and ultralente insulin sub-model structures are similar to the RI model with an additional crystalline state compartment (Equations 2.24 to 2.29). The crystalline state accounts for the protraction mechanism. Specifically, the formation of protamine (NPH, $x_{c,NPH}(t)$) or zinc crystals (lente, $x_{c,len}(t)$ and ultralente, $x_{c,ulen}(t)$) to delay the dissolution process [Gin and Hanaire-Broutin, 2005; Guerci and Sauvanet, 2005] (Equations 2.26 and 2.27). These states then *flow* into the hexameric state after dissolution.

Unlike RI injection (Equation 2.33), a large proportion of the injected dose is crystalline ($u_{c,NPH}(t)$, $u_{c,len}(t)$ and $u_{c,ulen}(t)$), while the rest consists of hexameric ($u_{h,NPH}(t)$, $u_{h,len}(t)$ and $u_{h,ulen}(t)$) and dimeric/monomeric states ($u_{m,NPH}(t)$, $u_{m,len}(t)$ and $u_{m,ulen}(t)$) (Equation 2.38 to 2.40 and Equation 2.42 to 2.44). Both the NPH and lente insulin models incorporate the common hexameric state compartment as RI, $x_h(t)$ (Equation 2.24), while a separate, slower hexameric state is introduced for ultralente insulin, $x_{h,ulen}(t)$ (Equation 2.28).

Insulin glargine sub-model structure

The insulin glargine model structure has several key differences to the NPH, lente and ultralente models (Equations 2.30 and 2.31). The model structure consists of a precipitate compartment, $p_{gla}(t)$ (Equation 2.31), similar in purpose to the crystalline state compartment for NPH and zinc-based insulins. Like the formation of crystals, the formation of an amorphous micro-precipitate in neutral

sc tissue is the primary protraction mechanism of insulin glargine, which has an acidic isoelectric point [Brange and Volund, 1999]. An empirical approximation is used to model the maximum dissolution rate, $r_{dis,max}$, of the precipitate, $p_{gla}(t)$, into a hexameric form unique to glargine, $x_{h,gla}(t)$ (Equation 2.50).

$$r_{dis,max}(t) = \sum_{i=1}^{N} r_{dis,max_i}\big(H(t - t_{i-1} - H(t - t_i))\big) \tag{2.50}$$

$$r_{dis,max_i} = r_{dis,max}(t_i < t < t_{i+1}) = \begin{cases} 15 & \text{if } u_{p,gla}(t_i) < 30000 \\ 15\big(\frac{u_{p,gla}(t_i)}{30000}\big) & \text{if } u_{p,gla}(t_i) \geq 30000 \end{cases}$$

where

$H(t - t_i)$ Heaviside function defined as $H(t - t_i) = 0$ when t is less than t_i, and $H(t - t_i) = 1$ when t is greater than or equal to t_i.

Thus, $r_{dis,max}$ is a function of dose size for doses ≥30U, and is a constant 15 mU/min for doses <30U. This function has been selected based on the following model identification of the model parameters in this research. The glargine insulin hexamer is also strengthened to reduce dissociation [Brange and Volund, 1999; Campbell et al., 2001; Gerich, 2004], resulting in greater stability in this state. This behaviour is modelled using a separate hexameric state compartment, $x_{h,gla}(t)$, with a different hexameric dissociation rate ($k_{prep,gla}$) to that used for intermediate ($k_{crys,len}$, $k_{crys,NPH}$) and zinc-based, long-acting ($k_{crys,ulen}$) insulin (see Equation 2.30). Thus, insulin glargine is injected in a mixture of precipitate ($u_{p,gla}(t)$), glargine hexameric ($u_{h,gla}(t)$), and dimeric/monomeric states ($u_{m,gla}(t)$) (Equations 2.37, 2.41 and 2.45). The rate of diffusive loss from hexameric and dimeric/monomeric states, k_d, remains the same as for RI.

MI sub-model structure

The MI model structure follows from the RI model structure in that the MI dose is assumed to be injected ($u_{mono}(t)$) entirely into the dimeric/monomeric, $x_{dm}(t)$ compartment as 100% dimers/monomers (Equation 2.32) and is immedi-

ately available for absorption into the interstitium after injection (Equation 2.25). Thus, the absorption kinetics of MI injection is concentration independent, unlike RI [Kaku et al., 2000; Woodworth et al., 1993], and is effectively a three-pool model identical to the model of Shimoda et al. [1997] (Equations 2.25, 2.51 and 2.52).

Interstitium and plasma insulin model structure

From the dimeric/monomeric state, insulin diffuses into interstitium, $x_i(t)$ (Equation 2.51) and subsequently into plasma, $I(t)$ (Equation 2.52). Plasma insulin is represented by the widely accepted one-pool model [Chase et al., 2005b; Furler and Kraegen, 1989; Kobayashi et al., 1983; Puckett and Lightfoot, 1995; Shimoda et al., 1997] in Equation 2.52. The plasma insulin kinetics model will be further discussed in Chapter 3.

$$\dot{x_i}(t) = -(k_3 + k_{d,i}) \cdot x_i(t) + k_2 \cdot x_{dm}(t) \tag{2.51}$$

$$\dot{I}(t) = -n \cdot I(t) + k_3 \cdot \left(\frac{x_i(t)}{V_i \cdot m_b} \right) \tag{2.52}$$

where

$x_i(t)$	Mass in the interstitium compartment [mU]
$I(t)$	Plasma insulin concentration [mU/l]
V_i	Insulin plasma distribution volume [l/kg]
m_b	Body mass [kg]
n	Rate of hepatic clearance of insulin [1/min]
$k_{d,i}$	Rate of diffusive loss from interstitium [1/min]

Summary of model structure

The total model structure consists of 10 compartments with 16 parameters for 6 sc injected insulin types. Each insulin sub-model involves no more than 2-3 exclusive compartments and parameters, and each individual sub-model is computationally

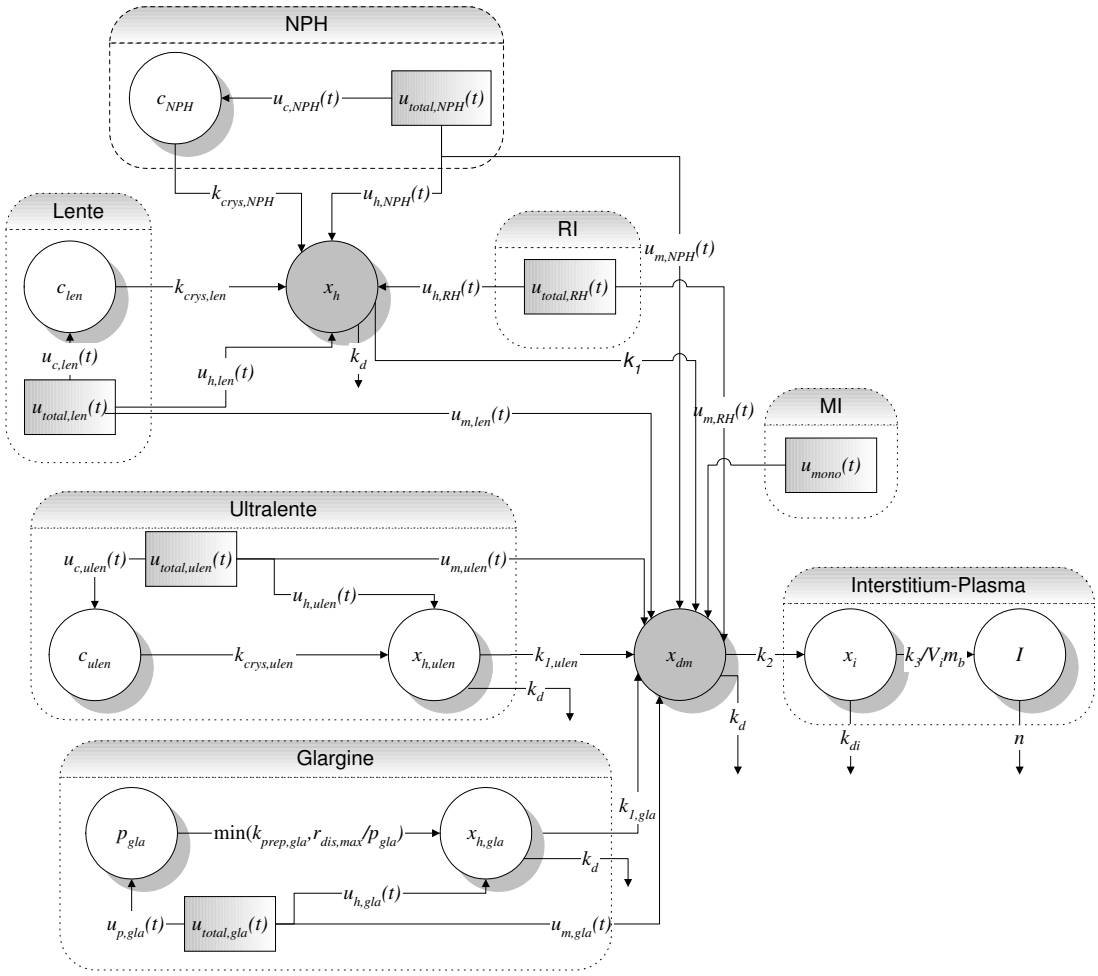

Figure 2.9 Full structure of the overall sc insulin absorption kinetic model. The model is characterised by a common hexameric state compartment for RI, NPH and lente insulins (x_h) while those for insulin glargine and ultralente ($x_{h,ulen}$ and $x_{h,gla}$) are separate. A crystalline state compartment for NPH (c_{NPH}), lente (c_{len}) and ultralente (c_{ulen}) insulins, and a precipitate compartment for insulin glargine (p_{gla}) model these insulin specific protraction mechanisms. All insulin types flow into common dimeric-monomeric state (x_{dm}), interstitium (x_i), and plasma (I) compartments.

modest as a result. The model structure is integrated in that all insulin types eventually emerge in the common, physiologically expected dimeric/monomeric state prior to transport into interstitium and plasma (Equations 2.25, 2.51 and 2.52). Except for the specific insulin glargine and ultralente insulin cases, the RI, NPH and lente insulin types similarly share one hexameric state compartment with the same transport rates (Equation 2.24).

Increased NPH and lente duration of action are described by the formation of the crystalline state only (Equations 2.26 and 2.27). Increased action dura-

tion of ultralente insulin and insulin glargine are modelled by both formation of the crystalline/precipitate state and a more stable, slower dissociating hexamer (Equation 2.28 to 2.30). The use of the crystalline and precipitate compartments is physiological, but highly simplified compared to non-linear non-compartmental approaches [Mosekilde et al., 1989; Tarin et al., 2005; Trajanoski et al., 1993].

First-order transport rates are used except where *in vivo* knowledge is unpublished or unknown. In this case, empirical assumptions are made as in the case of the dose response of insulin glargine (Equation 2.50). In this particular case, the empirical approximation is based on observations during model identification, as presented in this study.

While the absorption processes, i.e., dissolution, dissociation and diffusion are two-way, only the net flow into plasma is modelled. This approach is another acknowledged simplification from other more complex models. It is similar to the recent compartment model of Clausen et al. [2006] for a biphasic protamine-retarded MI-MI preparation. This particular model also has a similar crystalline state compartment and models only net flows, but with no hexameric state due to the modelling of MI only.

2.3.2 Model Parameter Identification

Certain model parameters are identified *a priori* from results in the literature and used as patient-independent population values (Table 2.6). All remaining parameters for all insulin types are patient-specific and identified with non-linear least squares (NLS) and unconstrained non-linear optimisation methods. The data utilised is taken from 37 sets of plasma insulin time-course absorption curves (Tables 2.7 and 2.8).

Table 2.6 *A priori* identified parameters from literature

Parameter	Value	Reference
V_i	0.1421 [l/kg]	Lehmann and Deutsch [1992b]
n	0.16 [1/min]	Chase et al. [2005b]
$k_{d,i}$	0.0029 [1/min]	Shimoda et al. [1997]
D	$0.9e^{-4}$ [cm^2/min]	Mosekilde et al. [1989]
Q_d	$1.5e^{-12}$ [l/(mU)^2]	Mosekilde et al. [1989]

The data was collected via a literature review of relevant insulin PK studies searched in the MEDLINE and Science Citation Index Expanded (SCI - EXPANDED) databases. Only studies using direct measurement methods were considered [Heinemann and Anderson, 2004] with data generally in the form of mean plasma insulin time-course measurements. These studies differ widely in cohort studied, methods and protocol. However, the data suffices for this study where the goal is to develop a mean PK simulation model for a diabetes decision support system. Rather than limiting the parameter identification to a specific cohort, experimental method and/or protocol, a parameter fit across a broad range of studies is felt to be more likely to result in an averaged PK response suitable for clinical use over the similarly wide population encountered in the general diabetes control problem.

There are several major factors that may affect the data used for parameter identification. First, insulin antibodies may not be quantified and/or cannot be presumed negligible. This problem is an issue with Type 1 or insulin-dependent Type 2 study cohorts with an extended history of diabetes and have been or are being treated using older, highly immunogenic insulin types, e.g., porcine or bovine insulin. If the cohort is not naïve to the specific insulin used, insulin antibodies can significantly affect the plasma insulin concentration measurement.

Insulin antibodies generally affect plasma insulin appearance proportionately, leading to inaccurate insulin distribution volume assumptions [Kobayashi et al., 1983]. However, in a model-based diabetes decision support system where effective insulin sensitivity is optimised in real-time [Chase et al., 2005b; Wong et al., 2006b], a trade-off between effective insulin sensitivity and insulin distribution volume can occur [Chase et al., 2004; Hann et al., 2005b]. In this case, the shape of the plasma insulin curve is more critical within reasonable bounds, than its exact magnitude [Chase et al., 2004].

Second, endogenous insulin production may not be corrected or be presumed negligible. This determination is typically performed using C-peptide measurements for NIDDM or normal study cohorts. In most cases however, administered doses are sufficient to suppress endogenous insulin production, and its effect may largely be disregarded when using a large number of studies for an average identification.

Finally, in the case of insulin analogues, especially insulin glargine (and also insulin detemir), or animal-based insulins, insufficient cross-reactivity with a non-specific insulin assay may result in underestimated plasma insulin concentrations. With respect to these concerns, all studies are specifically identified in Table 2.7 and 2.8 where insulin antibodies and endogenous insulin production are accounted for, and if cross-reactivity with the insulin assay of the study insulin is sufficient. If concentration of the insulin preparation is not quoted, a typical concentration of 100U/ml is assumed. If the insulin dose is quoted in U/kg, a bodyweight of 80kg is assumed if no other information is provided. All of these assumptions are indicated where made, and illustrate the lack of full data reporting that can often occur.

Table 2.7 Published PK studies used for model parameter identification

Insulin type	Dose	Concentration [U/ml]	Cohort studied	Reference
MI	7.1±1.3 U	100	T1DM	Plank et al. [2002]*†‡
MI	0.12 U/kg	4	IDDM	Shimoda et al. [1997]*†‡
MI	10 U	100	T1DM	Hedman et al. [2001]*‡
MI	0.05 U/kg	100	Normals	von Mach et al. [2002]‡
RI (porcine)	0.15 U/kg (6-9 U)	40	IDDM/NIDDM	Kobayashi et al. [1983]*†
RI	0.1 U/kg	-	Normals	Cernea et al. [2004]
RI (porcine)	10 U (rapid sc delivery)	3.3	Normals	Kraegen and Chisholm [1984]*
RI (porcine)	10 U (rapid sc delivery)	40	Normals	Kraegen and Chisholm [1984]*
RI	0.12 U/kg	4	IDDM	Shimoda et al. [1997]*†
RI	12 U	100	IDDM	Kang et al. [1991b]*
RI	10 U	-	Normals	Berger et al. [1982]
RI	15 U	40	Normals	Hubinger et al. [1992]*
RI	15 U	100	Normals	Hubinger et al. [1992]*
RI	6 U	99	Normals	Davis et al. [1991]
RI (porcine)	0.25 U/kg	-	Normals	Galloway et al. [1981]†‡ (NPH study)
RI (porcine)	0.25 U/kg	-	Normals	Galloway et al. [1981]†‡ (Lente study)
NPH	0.15 U/kg	100	Normals	Owens et al. [2000]*
NPH	0.3 U/kg	100	T1DM	Lepore et al. [2000]*
NPH	0.4 U/kg	-	Normals	Scholtz et al. [2005]* (Clamp 1)
NPH	0.4 U/kg	-	Normals	Scholtz et al. [2005]* (Clamp 2)
NPH	15 U	40	Normals	Hubinger et al. [1992]*
NPH	15 U	100	Normals	Hubinger et al. [1992]*
NPH	0.4 U/kg	40	Normals	Bottermann et al. [1982]
NPH	14 U	95	Normals	Davis et al. [1991]
NPH	0.25 U/kg	-	Normals	Galloway et al. [1981]†‡
NPH	0.4 U/kg	86.4	Normals	Heinemann et al. [2000]†

Table 2.8 Published PK studies used for model parameter identification (continued)

Insulin type	Dose	Concentration [U/ml]	Cohort studied	Reference
Lente	0.25 U/kg	-	Normals	Galloway et al. [1981][†‡]
Ultralente	0.4 U/kg	-	Normals	Scholtz et al. [2005][*] (Clamp 1)
Ultralente	0.4 U/kg	-	Normals	Scholtz et al. [2005][*] (Clamp 2)
Ultralente	0.3 U/kg	40	T1DM	Lepore et al. [2000][*]
Ultralente	0.3 U/kg	100.5	Normals	Owens et al. [1986][*]
Glargine	0.3 U/kg	100	T1DM	Lepore et al. [2000][*‡]
Glargine	0.15 U/kg	100	Normals	Owens et al. [2000][*‡] (15μg/ml zinc)
Glargine	0.15 U/kg	100	Normals	Owens et al. [2000][*‡] (80μg/ml zinc)
Glargine	0.4 U/kg	86.4	Normals	Heinemann et al. [2000][†]
Glargine	0.4 U/kg	-	Normals	Scholtz et al. [2005][*] (Clamp 1)
Glargine	0.4 U/kg	-	Normals	Scholtz et al. [2005][*] (Clamp 2)

[*] Corrected for endogenous glucose production, suppressed by protocol or justified negligible by baseline C-peptide measurements (usually for NIDDM and normal cohorts only)

[†] Corrected for insulin antibodies or justified negligible by measurement (usually for IDDM cohorts only)

[‡] Corrected for cross-reactivity of study insulin with insulin assay (usually insulin analogue or animal insulin studies only)

Table 2.9 Fitted k_2 and k_3 to published MI PK data

Parameter	Reference				Median	Mean (SD)	CV [%]
	1	2	3	4			
k_2 [1/min]	0.0106	0.0085	0.0119	0.0106	0.106	0.0104 (0.0014)	14
k_3 [1/min]	0.0473	0.0752	0.0355	0.0876	0.0613	0.0614 (0.0241)	39

1-Plank et al. [2002]
2-Shimoda et al. [1997]
3-Hedman et al. [2001]
4-von Mach et al. [2002]

Table 2.10 Fitted k_1, k_2 and k_3 to published RI PK data

Parameter	Reference									
	1	2	3		4	5	6	7		8
k_1 [1/min]	0.0565	0.0217	0.0348	0.0264	0.0275	0.0266	0.0365	0.0229	0.0148	0.0870
k_2 [1/min]	0.0089	0.0148	0.0201	0.0205	0.0027	0.0088	0.0057	0.0086	0.0083	0.0067
k_3 [1/min]	0.0681	0.0619	0.0581	0.0621	0.0631	0.0615	0.0744	0.0613	0.0612	0.0839

1-Kobayashi et al. [1983]
2-Cernea et al. [2004]
3-Kraegen and Chisholm [1984]
4-Shimoda et al. [1997]
5-Kang et al. [1991b]
6-Berger et al. [1982]
7-Hubinger et al. [1992]
8-Davis et al. [1991]

Table 2.11 Fitted k_1, k_2 and k_3 to published RI PK data (continued)

Parameter	Reference	Median	Mean (SD)	CV [%]
	9			
	NPH study	Lente study		
k_1 [1/min]	0.0235	0.0233	0.0250	0.0331 (0.0200)	60
k_2 [1/min]	0.0113	0.0104	0.0089	0.0106 (0.0054)	51
k_3 [1/min]	0.0616	0.0614	0.0618	0.0649 (0.0073)	11
9-Galloway et al. [1981]					

Table 2.12 Fitted $k_{crys,NPH}$ and α_{NPH} to published NPH PK data

Parameter	Reference								
	1	2	3		4		5	6	7
$k_{crys,NPH}$ [1/min]	0.0018	0.0029	0.0017	0.0013	0.0015	0.0010	0.0038	0.0002	0.0004
α_{NPH} [unitless]	0.9945	0.9471	0.9393	0.9501	0.9061	0.9018	1.0000	0.9386	0.9234

1-Owens et al. [2000]
2-Lepore et al. [2000]
3-Scholtz et al. [2005]
4-Hubinger et al. [1992]
5-Bottermann et al. [1982]
6-Davis et al. [1991]
7-Galloway et al. [1981]

Table 2.13 Fitted $k_{crys,NPH}$ and α_{NPH} to published NPH PK data (continued)

Parameter	Reference	Median	Mean (SD)	CV [%]
8				
$k_{crys,NPH}$ [1/min]	0.0010	0.0014	0.0016 (0.0011)	70
α_{NPH} [unitless]	0.9737	0.9432	0.9475 (0.0336)	4
8-Heinemann et al. [2000]				

Table 2.14 Fitted $k_{crys,len}$ and α_{len} to published lente PK data

Parameter	Reference
	Galloway et al. [1981]
$k_{crys,len}$ [1/min]	0.0037
α_{len} [unitless]	0.9447

Table 2.15 Fitted $k_{crys,ulen}$, $k_{1,ulen}$ and α_{ulen} to published ultralente PK data

Parameter	Reference				Median	Mean (SD)	CV [%]
	1		2	3			
	Clamp 1	Clamp 2					
$k_{crys,ulen}$ [1/min]	0.0048	0.0012	0.0013	0.0012	0.0013	0.0021 (0.0018)	84
$k_{1,ulen}$ [1/min]	0.0015	0.0014	0.0044	0.0020	0.0018	0.0023 (0.0014)	61
α_{ulen} [unitless]	1.0000	1.0000	0.8897	1.0000	1.0000	0.9724 (0.0552)	6

1-Scholtz et al. [2005]
2-Lepore et al. [2000]
3-Owens et al. [1986]

Table 2.16 Fitted $k_{prep,gla}$, $k_{1,gla}$ and α_{gla} to published glargine PK data

Parameter	Reference					Median	Mean (SD)	CV [%]
	1	2	3	4				
	80 μg/ml	15 μg/ml	Clamp 1	Clamp 2				
$k_{prep,gla}$ [1/min]	0.0007	0.0016	0.0005	0.0008	0.0008	0.0008	0.0011 (0.0006)	53
$k_{1,gla}$ [1/min]	0.0143	0.0018	0.0062	0.0105	0.0124	0.0084	0.0078 (0.0054)	69
α_{gla} [unitless]	0.9578	0.7694	0.9570	0.9426	0.9388	0.9498	0.9462	0.9192 (0.0738)	8

1-Lepore et al. [2000]
2-Owens et al. [2000]
3-Heinemann et al. [2000]
4-Scholtz et al. [2005]

The model is essentially identified by extension from the MI model structure (Figures 2.8 and 2.9), which is identical to Shimoda et al. [1997], and similar to Kraegen and Chisholm [1984] and Furler and Kraegen [1989]. Equivalent parameter values from Shimoda et al. [1997] are thus able to be used as starting points for the NLS optimisation of k_2 and k_3 to the MI data (Table 2.9).

With fixed population values of k_2 and k_3 identified from MI data, a two-stage NLS optimisation is used optimise k_1, k_2 and k_3 using RI data (Table 2.10 and 2.11). Note that the overall fitted k_2 and k_3 values to RI data are very close to the fitted k_2 and k_3 values to MI data (Table 2.9), and all fitted parameters display a low coefficient of variation (CV) as summarised in Table 2.18. Hence, the k_2 and k_3 parameters are consistent in describing these common physiological states during the sc insulin absorption process even among different insulin types.

Referring to Figure 2.9, there are 2 parameters that each must be identified for the NPH ($k_{crys,NPH}$ and α_{NPH}) and lente insulin ($k_{crys,len}$ and α_{len}) data set, where fixed population k_1, k_2 and k_3 values from the RI and MI data parameter identification are used. Likewise, 3 parameters must each be fitted for the ultra-lente ($k_{crys,ulen}$, $k_{1,ulen}$ and α_{ulen}) and insulin glargine ($k_{prep,gla}$, $k_{1,gla}$ and α_{gla}) data sets using the same fixed k_1, k_2 and k_3 population values.

Due to the larger number of data sets, parameters for the NPH, lente, ultralente and insulin glargine sub-models are fitted via unconstrained non-linear optimisation using a simplex search method for multiple variables which is a quicker method. The objective function is the plasma insulin concentration sum squared error (SSE), defined in Equation 2.53 for the jth data set. As only mean insulin time-course data is used in this study, the variability of the mean value is neglected. Depending on the number of measurements in the calculation of the mean, the sum of the percentage measurement error would result in a wide error band around each mean value which is of little value for model fit validation.

$$SSE_j = \sum_{i=1}^{N_j} \left(\bar{I}_{j,i} - I_j\big(t_{j,i}\big) \right) \tag{2.53}$$

where

N_j	Number of plasma insulin data points in the jth data set
$\bar{I}_{j,i}$	ith plasma insulin concentration data point in the jth data set
$I_j(t_{j,i})$	Modelled plasma insulin concentration for the jth data set at $t_{j,i}$, the time at the ith plasma insulin concentration data point

There are 37 data sets in total for all insulin types (4 MI, 12 RI, 10 NPH insulin, 1 lente insulin, 4 ultralente insulin and 6 insulin glargine). Results for the NPH, lente, ultralente and insulin glargine parameter identifications are shown in Tables 2.12 to 2.16. Note that even with fixed population values for k_1, k_2 and k_3, the CV of all fitted NPH, lente, ultralente and insulin glargine model parameters are <100%. Specifically, a median CV of 57% and a CV 95th percentile of 3.6-69.1% were achieved (results not shown). Referring to Table 2.18, the median CV *across all parameters and insulin sub-models* was 51.3% (95th percentile of 3.6-60.6%). This precision of fitted parameters is adequate given the data, and the parameters can be considered *a posteriori* identifiable following the definition of Wilinska et al. [2005].

Table 2.18 Summary of parameter identification to published PK data

Insulin Type	Parameter [units]	Median	Mean (SD)	CV [%]
MI	k_2 [1/min]	0.0106	0.0104 (0.0014)	14
MI	k_3 [1/min]	0.0613	0.0614 (0.0241)	39
RI	k_1 [1/min]	0.0250	0.0331 (0.0200)	60
RI	k_2 [1/min]	0.0089	0.0106 (0.0054)	51
RI	k_3 [1/min]	0.0618	0.0649 (0.0073)	11
NPH	$k_{crys,NPH}$ [1/min]	0.0014	0.0016 (0.0011)	70
NPH	α_{NPH} [1/min]	0.9432	0.9475 (0.0336)	4
Lente	$k_{crys,len}$ [1/min]	0.0037	-	-
Lente	α_{len} [1/min]	0.9447	-	-
Ultralente	$k_{crys,ulen}$ [1/min]	0.0013	0.0021 (0.0018)	84
Ultralente	$k_{1,ulen}$ [1/min]	0.0018	0.0023 (0.0014)	61
Ultralente	α_{ulen} [1/min]	1.0000	0.9724 (0.0552)	6
Glargine	$k_{prep,gla}$ [1/min]	0.0008	0.0011 (0.0006)	53
Glargine	$k_{1,gla}$ [1/min]	0.0084	0.0078 (0.0054)	69
Glargine	α_{gla} [1/min]	0.9462	0.9192 (0.0738)	8
			Median	51.3
			(95th percentile)	(3.6-60.6)
			Range	(3.6-80.4)

2.4 Model fit and prediction errors

In Table 2.19, model fit error (both absolute and absolute percentage errors) and model prediction errors using population parameters (both absolute and absolute percentage errors) are shown. Across all insulin types, median absolute model fit errors range from 0.62mU/l to 3.20mU/l, and median absolute percentage model fit errors range from 10.96% for glargine to 21.42% for lente of which there was only one data set. This figure is hence unaffected by the averaging effect of multiple studies and may not be accurate.

Table 2.19 Model fit and model prediction errors

Insulin type	Error type [units]	Model fit [Median (90% range)]	Model prediction using population parameters [Median (90% range)]
MI	Absolute [mU/l]	1.54 (0.84-3.25)	1.85 (0.78-3.69)
	Absolute percentage [%]	13.30 (5.18-32.45)	15.56 (5.69-41.00)
RI	Absolute [mU/l]	2.65 (0.65-7.96)	6.49 (1.48-13.13)
	Absolute percentage [%]	18.35 (5.94-43.37)	38.95 (15.38-72.77)
NPH	Absolute [mU/l]	1.10 (0.33-2.42)	1.57 (0.57-4.79)
	Absolute percentage [%]	16.25 (4.90-36.05)	22.70 (9.51-46.17)
Lente	Absolute [mU/l]	3.20 (1.68-6.11)	3.20 (1.68-6.11)
	Absolute percentage [%]	21.42 (13.10-58.18)	21.42 (13.10-58.18)
Ultralente	Absolute [mU/l]	0.80 (0.36-2.19)	1.81 (0.42-4.06)
	Absolute percentage [%]	14.32 (4.75-27.99)	31.05 (7.43-49.00)
Glargine	Absolute [mU/l]	0.62 (0.26-0.93)	0.84 (0.38-1.31)
	Absolute percentage [%]	10.96 (5.61-19.85)	14.88 (8.43-28.68)

To calculate the model prediction errors, the plasma insulin concentration is

generated using the model and the population parameters identified. As expected, the more stable insulin analogues, e.g., MI and glargine have much lower model prediction errors (13.30% and 10.96% respectively) whereas the more variable insulin, e.g., RI (18.35%) and NPH (16.25%) have considerably higher prediction errors. The more stable insulin analogues are hence better predicted using fixed population parameter values than less stable insulin types.

2.5 Subcutaneous Insulin Model Validation

This section reports the validation of an identified physiological compartment model of subcutaneous insulin pharmacokinetics presented in Section 2.3. A range of clinically current insulin types are modelled, specifically, the prandial insulins monomeric insulin and regular insulin, and the intermediate- and long-acting basal insulins NPH and insulin glargine. The older insulin types lente and ultralente insulins are also modelled. This facility enables retrospective data of patients treated with these insulin types to be used for model identification and validation. The model has been previously identified with good precision in all identified parameters using a wide range of clinical data and this validation study aims to gauge the accuracy of the parameter identification and model dynamics using published pharmacokinetic summary measures.

2.5.1 Method

The data used for model identification and now validation was collected via a literature review of relevant insulin PK studies searched in the MEDLINE and Science Citation Index Expanded (SCI - EXPANDED) databases. Only studies using direct measurement methods were considered [Heinemann and Anderson, 2004]. These studies differ widely in cohort studied, methods and protocol. However, the data suffices for this study where the goal is to develop a mean PK simulation model for a diabetes decision support system. A parameter fit and validation across a broad range of studies is likelier to result in an averaged PK response suitable for clinical use over a wide population. However, there are potentially three factors that may affect the accuracy of the data:

1. **Insulin antibodies (IDDM cohort only)**

2. **Endogenous insulin production (NIDDM and normal cohorts only)**

3. **Insufficient cross-reactivity of test insulin with insulin assay (insulin analogue and animal insulin studies only)**

Due to an almost universal lack of availability of spread data for each time point in the majority of these studies, a simpler validation criterion is proposed. Referring to Figure 2.10, two common PK summary measures, t_{max} (time to maximal plasma insulin concentration) and C_{max} (maximal plasma insulin concentration) for each fitted model curve ($t_{max,model}$ and $C_{max,model}$) can be compared to reported clinical values for each data set ($t_{max,data}$ and $C_{max,data}$). For these measures, a reported spread over the study for these two parameters ($\text{SD}_{t_{max,data}}$ and $\text{SD}_{C_{max,data}}$) is used to validate the equivalent identified model and results. Other well-accepted measures including t_{50} (half-time to and decrease from peak) and AUC (area under curve) are not always uniformly reported by all studies and were thus not used here.

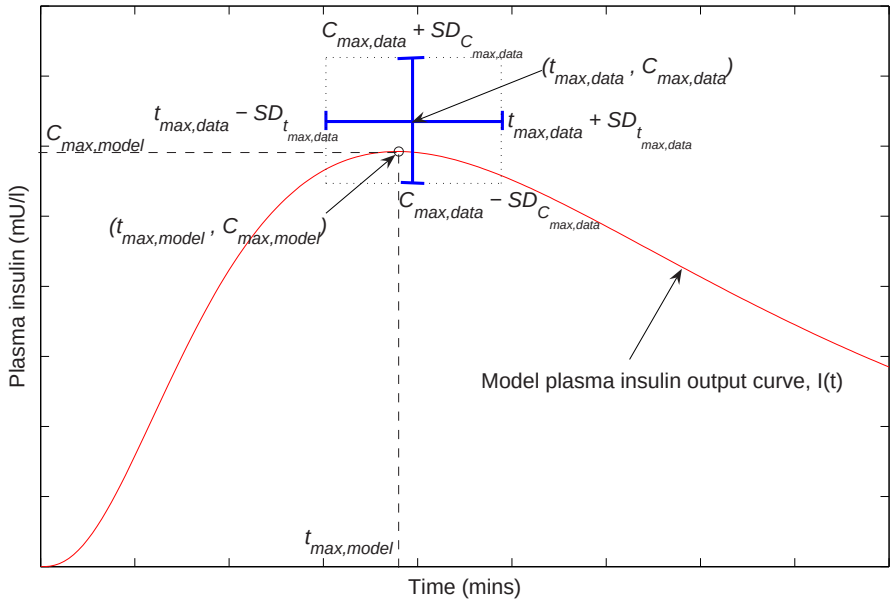

Figure 2.10 Schematic diagram of a plasma insulin model output curve with $t_{max,model}$ and $C_{max,model}$, and corresponding data set reported $t_{max,data}$ and $C_{max,data}$ (with standard deviation $\text{SD}_{t_{max,data}}$ and $\text{SD}_{C_{max,data}}$ respectively)

While this validation criterion may not be fully rigorous, it is the only method to assess the model fit to the data in the absence of other complete data over several studies. Summary measures like these are also very commonly used for describing insulin PKs and were thus readily available for most studies allowing validation criteria comparison across studies. Finally, t_{max} and C_{max} describe the basic and fundamental clinical features of insulin action.

The result of this comparison is shown in Tables 2.20 to 2.27 and a summary is shown in Tables 2.28 to 2.30. Where t_{max} or C_{max} values are not reported in the study, they are calculated from the mean PK curves used for the parameter identification. All reported measures are unit standardised and expressed as mean±SD if reported differently. Some values are baseline corrected to match the data used for parameter identification. If a summary measure is not reported and bounds cannot be estimated from the reported data, or if only a mean value is reported with no variation or spread, then the model fit cannot be validated on that particular measure for that particular study.

Possible validation outcomes are therefore limited to the following cases for each study:

1. **The model fit is fully validated if both model curve t_{max} and C_{max} ($t_{max,model}$ or $C_{max,model}$) are within $t_{max,data} \pm \mathbf{SD}_{t_{max,data}}$ and $C_{max,data} \pm \mathbf{SD}_{C_{max,data}}$**

2. **The model fit is considered partially validated if only $C_{max,model}$ lies outside $C_{max,data} \pm \mathbf{SD}_{C_{max,data}}$**

3. **If $t_{max,model}$ lies outside $t_{max,data} \pm \mathbf{SD}_{t_{max,data}}$, the model fit is invalidated regardless of $C_{max,model}$. This case choice slightly emphasises the qualitative shape of the model curve rather than the quantitative plasma insulin concentration**

4. **Clearly, the model fit is also invalidated if both model curve t_{max} and C_{max} ($t_{max,model}$ or $C_{max,model}$) lie outside $t_{max,data} \pm \mathbf{SD}_{t_{max,data}}$ and $C_{max,data} \pm \mathbf{SD}_{C_{max,data}}$ respectively**

5. **If $C_{max,model}$ cannot be validated but $t_{max,model}$ lies within $t_{max,data} \pm \mathbf{SD}_{t_{max,data}}$ or vice versa, the model fit is partially validated**

6. **If both $t_{max,model}$ and $C_{max,model}$ cannot be validated, the model fit cannot be validated overall**

In case of outcomes 5 and 6, a percentage error is still calculated and shown in Tables 2.28 to 2.30 to provide an estimate of reliability.

2.5.2 MI sub-model validation summary

Referring to Table 2.20 and Tables 2.28 to 2.30, all MI model curve t_{max} and C_{max} values are fully validated (outcome 1) except for the study by Shimoda et al. [1997] which cannot be validated (outcome 6).

Table 2.20 Summary measures for fitted MI model curve compared to published values. Units are standardised from original reported units in literature and values are transformed into mean±SD if reported differently. Some values have been baseline corrected where necessary

Parameter		Reference			
		1	2	3	4
t_{max} [mins]	Modelled	47	41	52	36
	Literature	46.7±23.0	31.8	49.0±11.2	33.3±11.6
C_{max} [mU/l]	Modelled	26.8	32.3	39.0	22.0
	Literature	24.3±14.5*	35.0	42.5±14.5	24.6±5.8

1-Plank et al. [2002]
2-Shimoda et al. [1997]
3-Hedman et al. [2001]
4-von Mach et al. [2002]
* Baseline corrected to match plotted data used for model parameter fit

2.5.3 RI sub-model validation summary

With reference to Tables 2.21 and 2.22 for RI data and Tables 2.28 to 2.30, the study by Davis et al. [1991] is invalidated (outcome 3) with a very short t_{max} of 30.0±7.9 min (for RI) resulting in 90±26% error. This study underestimates t_{max} as it is not corrected for endogenous production, leading to overestimation of plasma insulin appearance in the early part of the trial where insulin production has not been fully suppressed. The 6U RI dose is also insufficient to fully suppress insulin production, which is confirmed by the reported C-peptide measurements [Davis et al., 1991]. Another study by Kang et al. [1991b] is partially

validated (outcome 2) with 11.8% C_{max} error considering that insulin antibodies were unaccounted for in the IDDM cohort. Finally, as for MI, the RI model fit to Shimoda et al. [1997] cannot be validated due to lack of fully reported data (outcome 6).

2.5.4 NPH sub-model validation summary

For NPH data in Tables 2.23, 2.24 and Tables 2.28 to 2.30, poor model curve t_{max} values are also obtained for Davis et al. [1991] in addition to Galloway et al. [1981] compared to reported values. While the model fit to Davis et al. [1991] is invalidated (outcome 3), Galloway et al. [1981] is still fully validated due to use of incorrect normal descriptive statistics for non-normal data distribution.

Similar to the RI study by Davis et al. [1991], these two study protocols are both uncorrected for endogenous insulin production and prescribe a relatively low dose (14U and 0.25U/kg respectively) compared to other studies uncorrected for insulin production (0.4U/kg for Bottermann et al. [1982] and Heinemann et al. [2000]). The studies by Heinemann [2002] and Bottermann et al. [1982] use higher comparative insulin doses, and Bottermann et al. [1982] reports a negligible serum C-peptide concentration for most of the study duration.

Table 2.21 Summary measures for fitted RI model curve compared to published values. Units are standardised from original reported units in literature and values are transformed into mean±SD if reported differently. Some values have been baseline corrected where necessary

Parameter		Reference								
		1	2	3		4	5	6	7	
		3.3 U/ml		40 U/ml					40 U/ml	100 U/ml
t_{max} [mins]	Modelled	65	80	53	66	107	93	84	83	112
	Literature	50-88*	83.3±42.2	45-75**	45-90**	84.0	111.0±58.8	92.0±55.0	78.0±24.0	144.0±60.0
C_{max} [mU/l]	Modelled	59.2	43.9	73.2	63.0	10.5	37.0	20.8	39.1	30.6
	Literature	50-65**	51.4±13.4*	65-90**	54-82**	8.8	27.4-33.1**	22.2±6.0	38.1±14.6	31.6±12.0

1-Kobayashi et al. [1983]
2-Cernea et al. [2004]
3-Kraegen and Chisholm [1984]
4-Shimoda et al. [1997]
5-Kang et al. [1991b]
6-Berger et al. [1982]
7-Hubinger et al. [1992]
* Baseline corrected to match plotted data used for model parameter fit
** Estimated from plotted data as value is not quoted in study

Table 2.22 Summary measures for fitted RI model curve compared to published values. Units are standardised from original reported units in literature and values are transformed into mean±SD if reported differently. Some values have been baseline corrected where necessary (continued)

Parameter		Reference		
		8	9	
			NPH study	Lente study
t_{max} [mins]	Modelled	57	83	86
	Literature	30.0±7.9	108.0±66.0	156.0±198.0
C_{max} [mU/l]	Modelled	26.1	87.1	75.7
	Literature	24.5**	70.5±21.7	72.8±15.6

8-Davis et al. [1991]

9-Galloway et al. [1981]

* Baseline corrected to match plotted data used for model parameter fit

** Estimated from plotted data as value is not quoted in study

Table 2.23 Summary measures for fitted NPH model curve compared to published values. Units are standardised from original reported units in literature and values are transformed into mean±SD if reported differently. Some values have been baseline corrected where necessary

Parameter		Reference								
		1	2	3		4		5	6	7
				Clamp 1	Clamp 2	40 U/ml	100 U/ml			
t_{max} [mins]	Modelled	260	211	228	250	197	133	211	69	82
	Literature	180-300**	240	234±84	282±180	288±174	318±276	240**	240±56	276±192
C_{max} [mU/l]	Modelled	7.8	21.9	19.9	16.1	11.5	9.1	52.4	12.0	7.2
	Literature	7.5**	22.8±9.8	23.2±5.0	18.4±2.3	16.2±7.8	13.2±4.4	63.2**	12.0**	21.8±38.8

1-Owens et al. [2000]
2-Lepore et al. [2000]
3-Scholtz et al. [2005]
4-Hubinger et al. [1992]
5-Bottermann et al. [1982]
6-Davis et al. [1991]
7-Galloway et al. [1981]
** Estimated from plotted data as value is not quoted in study
† Summary measures quoted by study not identical to plotted values due to differences in calculation method

Table 2.24 Summary measures for fitted NPH model curve compared to published values. Units are standardised from original reported units in literature and values are transformed into mean±SD if reported differently. Some values have been baseline corrected where necessary (continued)

Parameter		Reference
		8
t_{max} [mins]	Modelled	282
	Literature	396±264†
C_{max} [mU/l]	Modelled	13.6
	Literature	20.3±5.0†

8-Heinemann et al. [2000]

** Estimated from plotted data as value is not quoted in study

† Summary measures quoted by study not identical to plotted values due to differences in calculation method

2.5.5 Lente and ultralente sub-model validation summary

All lente model fits are fully validated (see Table 2.25 and Tables 2.28 to 2.30) as are all but two ultralente model fits (see Table 2.26 and Tables 2.28 to 2.30), where Lepore et al. [2000] and Owens et al. [1986] are partially validated (outcome 5) with 20.5% and 8.2% C_{max} error respectively.

Table 2.25 Summary measures for fitted lente model curve compared to published values. Units are standardised from original reported units in literature and values are transformed into mean±SD if reported differently. Some values have been baseline corrected where necessary

Parameter		Reference
		Galloway et al. [1981]
t_{max} [mins]	Modelled	200
	Literature	210±174
C_{max} [mU/l]	Modelled	25.6
	Literature	31.0±15.8

Table 2.26 Summary measures for fitted ultralente model curve compared to published values. Units are standardised from original reported units in literature and values are transformed into mean±SD if reported differently. Some values have been baseline corrected where necessary

Parameter		Reference			
		1		2	3
		Clamp 1	Clamp 2		
t_{max} [mins]	Modelled	495	900	477	771
	Literature	648±300	816±360	600	840
C_{max} [mU/l]	Modelled	14.3	7.9	21.0	7.0
	Literature	16.4±8.3	14.3±8.4	25.9±9.4	7.8±6.0

1-Scholtz et al. [2005]
2-Lepore et al. [2000]
3-Owens et al. [1986]

2.5.6 Insulin glargine sub-model validation summary

For insulin glargine (see Table 2.27 and Tables 2.28 to 2.30), Heinemann et al. [2000] reported measures calculated using a different method to the plotted data and cannot be validated. Using the isoglycaemic clamp method, another study by Lepore et al. [2000] corrects the plasma insulin concentration for insulin glargine (measured via non-specific insulin assay) only from 3 hours onward, after the IV insulin infusion rate had decreased to near nil. The origin of the insulin in plasma is thus indeterminate with IV insulin infusion in this time period. Unlike

the reported C_{max} (measured between 3-24h), all insulin measurements were used in the model parameter fit to data, which may have contributed to the C_{max} error of 8.5±6.9% (outcome 5).

Table 2.27 Summary measures for fitted glargine model curve compared to published values. Units are standardised from original reported units in literature and values are transformed into mean±SD if reported differently. Some values have been baseline corrected where necessary

Parameter		Reference					
		1	2		3	4	
			80 μg/ml zinc	15 μg/ml zinc		Clamp 1	Clamp 2
t_{max} [mins]	Modelled	356	554	724	520	780	777
	Literature	180-1440‡‡	600**	840**	822±522†	744±270	660±321
C_{max} [mU/l]	Modelled	20.5	4.1	3.8	7.0	7.9	8.0
	Literature	18.9±1.3‡	5.5**	4.8**	13.1±4.3†	12.1±5.7	10.0±2.5

1-Lepore et al. [2000]
2-Owens et al. [2000]
3-Heinemann et al. [2000]
4-Scholtz et al. [2005]
** Estimated from plotted data as value is not quoted in study
† Summary measures quoted by study not identical to plotted values due to differences in calculation method
‡ Plateau concentration measured from 3-24h
‡‡ Plateau time (3-24h)

Table 2.28 Summary of model validation to reported t_{max} and C_{max} summary measures

Insulin Type	Study	Within t_{max} bounds			Within C_{max} bounds			Fully Validated	Partially Validated	Validation cannot be Performed	Validation Failed
		Yes	No	N/A	Yes	No	N/A				
MI	1	✓			✓			✓			
MI	2			✓(29%)			✓(8%)			✓	
MI	3	✓			✓			✓			
MI	4	✓			✓			✓			
RI	5	✓			✓			✓			
RI	6	✓			✓			✓			
RI	7	✓			✓			✓			
RI	7	✓			✓			✓			
RI	2			✓(27%)			✓(19%)			✓	
RI	8	✓				✓(11.8%)			✓[2]		
RI	9	✓			✓				✓		
RI	10	✓			✓				✓		
RI	10	✓			✓				✓		
RI	11		✓(90±26%)				✓(7%)				✓[3]
RI	12	✓			✓				✓		
RI	12	✓			✓				✓		

Table 2.29 Summary of model validation to reported t_{max} and C_{max} summary measures (continued)

Insulin Type	Study	Within t_{max} bounds			Within C_{max} bounds			Fully Validated	Partially Validated	Validation cannot be Performed	Validation Failed
		Yes	No	N/A	Yes	No	N/A				
NPH	13	✓					✓(4%)		✓[2]		
NPH	14			✓(12%)	✓				✓[5]		
NPH	15	✓			✓			✓			
NPH	15	✓			✓			✓			
NPH	10	✓			✓			✓			
NPH	10	✓			✓			✓			
NPH	16			✓(12%)			✓(17%)			✓	
NPH	11		✓(71±23%)		✓						✓[3]
NPH	12	✓			✓			✓			
NPH	17			✓			✓			✓	
Lente	12	✓			✓			✓			
Ultralente	15	✓			✓			✓			
Ultralente	15	✓			✓			✓			
Ultralente	14			✓(21%)	✓				✓[5]		
Ultralente	18			✓(8%)	✓				✓[5]		

Table 2.30 Summary of model validation to reported t_{max} and C_{max} summary measures (continued)

Insulin Type	Study	Within t_{max} bounds			Within C_{max} bounds			Fully Validated	Partially Validated	Validation cannot be Performed	Validation Failed
		Yes	No	N/A	Yes	No	N/A				
Glargine	14	✓				✓(8.5±6.9%)			✓[5]		
Glargine	13			✓(8%)			✓(26%)			✓	
Glargine	13			✓(14%)			✓(21%)			✓	
Glargine	17			✓			✓			✓	
Glargine	15	✓			✓			✓			
Glargine	15	✓			✓			✓			

1-Plank et al. [2002]
2-Shimoda et al. [1997]
3-Hedman et al. [2001]
4-von Mach et al. [2002]
5-Kobayashi et al. [1983]
6-Cernea et al. [2004]
7-Kraegen and Chisholm [1984]
8-Kang et al. [1991b]
9-Berger et al. [1982]
10-Hubinger et al. [1992]
11-Davis et al. [1991]
12-Galloway et al. [1981]
13-Owens et al. [2000]
14-Lepore et al. [2000]
15-Scholtz et al. [2005]
16-Bottermann et al. [1982]
17-Heinemann et al. [2000]
18-Owens et al. [1986]

[2,3,5] Refer to Subsection 2.5.1 for list of partial and failed validation outcomes

In summary, it can be seen that 22 model fits are fully validated using both reported t_{max} and C_{max} summary measures, or estimated values from plotted data where not reported (see Tables 2.28 to 2.30). A further 6 model fits are partially validated on t_{max} only (outcome 2), or on C_{max} only if t_{max} cannot be validated (outcome 5). All partially validated model fits have errors not exceeding 12% of reported or estimated t_{max} or C_{max} ranges. Validation cannot be performed for 7 model fits. This occurred due to incompletely reported summary measures, only a mean value reported, and/or if a range of t_{max} and C_{max} cannot be estimated from plotted data (outcome 6). Even then, this error is <30%. Only 2 model fits failed the validation with 90±26% and 71±23% error on t_{max} only. In both cases, significant protocol-based reasons were identified and these errors are still <100%. The data in both cases also came from the same study (Davis et al. [1991] for RI and NPH). No model fit was invalidated on both t_{max} and C_{max} measures.

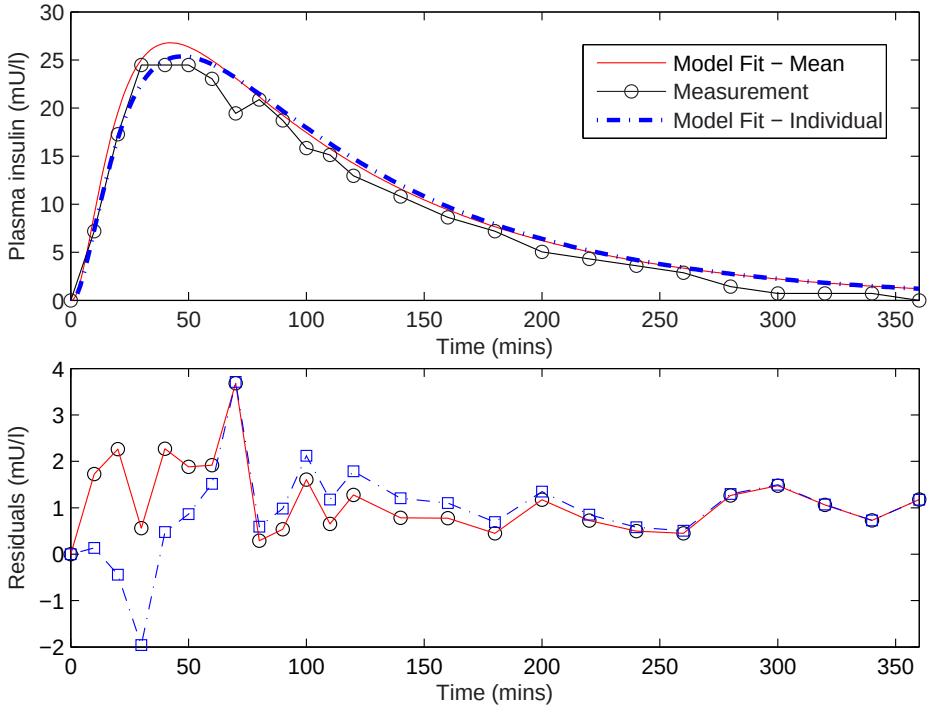

Figure 2.11 MI model fit to data of Plank et al. [2002].

As an additional validation, sample model fits to MI [Plank et al., 2002] and insulin glargine [Lepore et al., 2000] data are shown in Figures 2.11 to 2.13. The model generated curve using median or mean parameter values as an overall

population value is shown in addition to the individual model fit curve. In both cases the results are excellent matches for the data reported in these cases.

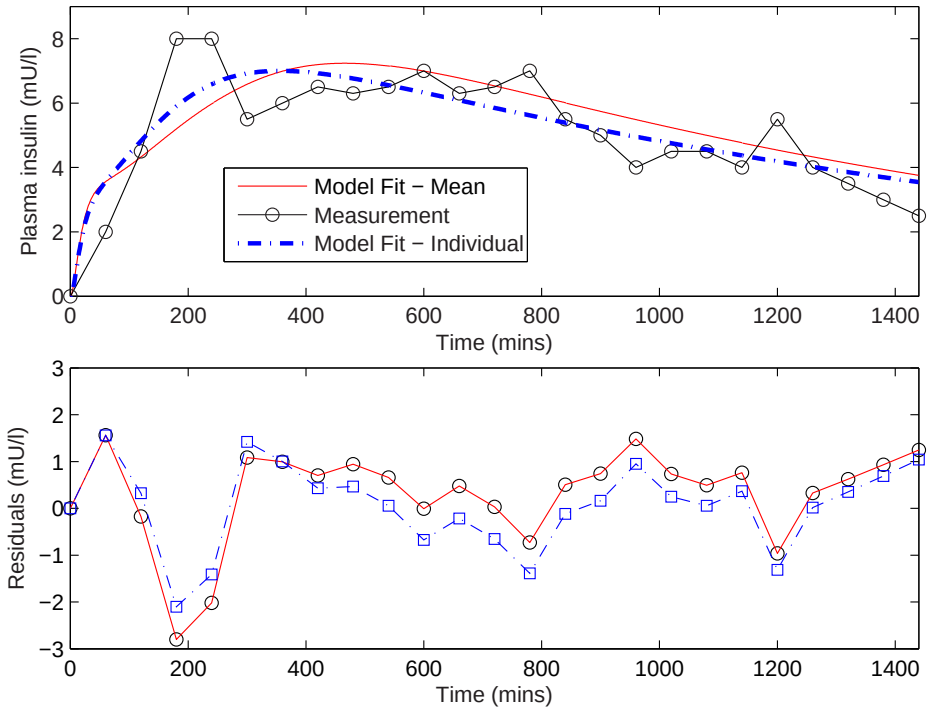

Figure 2.12 Insulin glargine model fit to data of Lepore et al. [2000]. Note that the plasma insulin concentration is corrected for cross-reactivity with insulin glargine only between 3-24h, i.e., the first three data points are inaccurate in respect to the exogenous insulin glargine concentration in plasma due to the presence of a not insignificant IV insulin infusion.

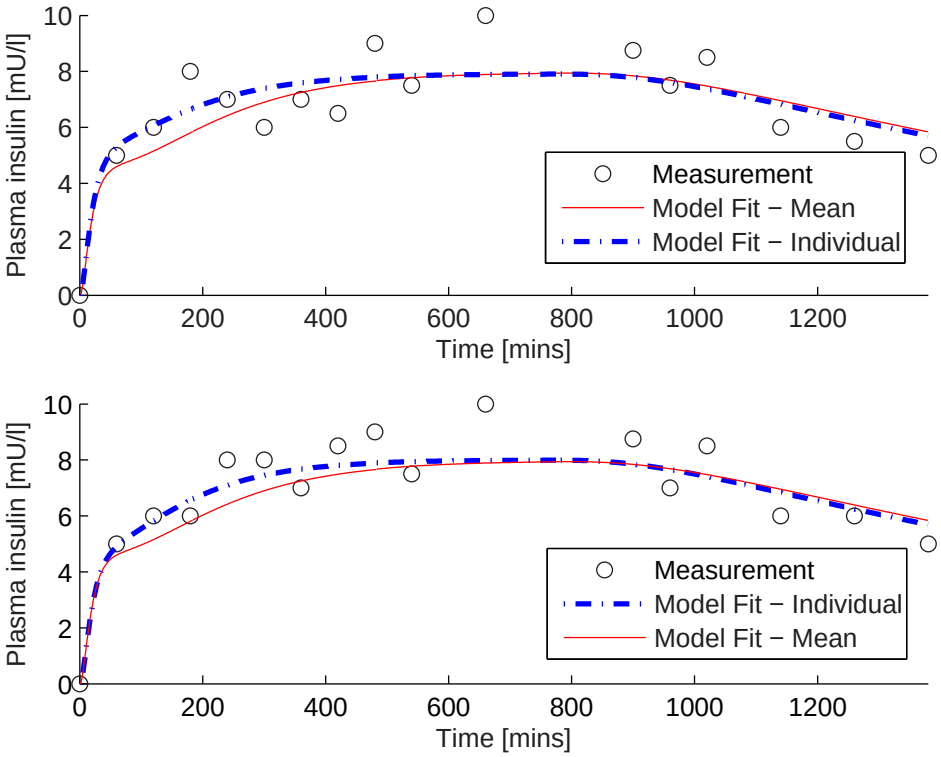

Figure 2.13 Insulin glargine model fit to data of Scholtz et al. [2005]. Top panel shows the results of the model fit to Clamp 1 and bottom panel shows the fit to Clamp 2. Study is corrected for endogenous glucose production only. Note the relatively small difference between mean model parameter *simulation* and the individual model *fit* to the data using non-linear least squares.

2.6 Model Simulation and Output

A comparison of model outputs using the population model parameters for an injection of 10U for all insulin types is shown in Figure 2.14. Results are compared to output from the AIDA insulin PK model [Lehmann and Deutsch, 1992b] by Berger and Rodbard [1989] which uses a non-linear, non-compartmental model. This model is one of the foremost sc insulin PK models developed for computer simulation of multiple insulin types and was subsequently applied in the AIDA diabetes education and decision support system. While the most complete of insulin models, it does not model MI or insulin glargine absorption as it was first published in 1989 before these types were developed. As shown in Figure 2.14, the dynamics of each modelled insulin type are visually similar between the two models, providing an additional measure of validation.

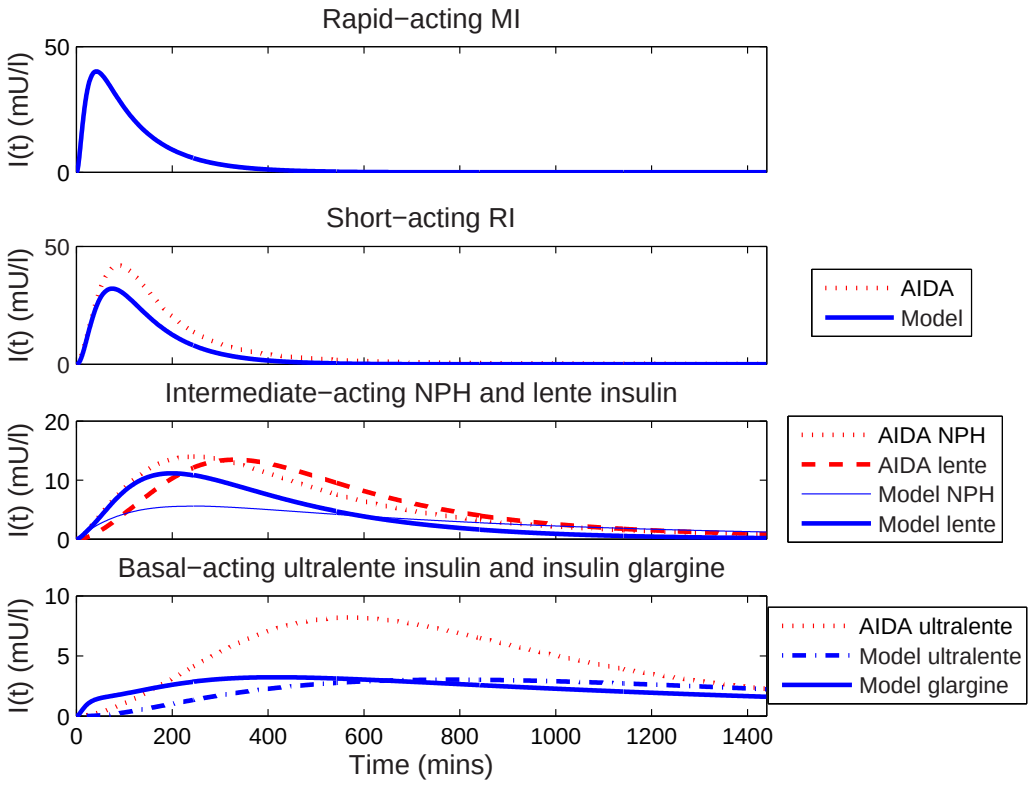

Figure 2.14 Comparison of model output and the AIDA insulin sc PK model for a 10U injection of all insulin types [Berger and Rodbard, 1989; Lehmann and Deutsch, 1992b]. Published in 1989, the AIDA model does not model MI or insulin glargine absorption

The model dynamics are also demonstrated for RI concentration dependency and insulin glargine dose dependency in Figure 2.15. For a given RI dose, the

rate of absorption decreases with increasing insulin concentrations until 500 U/ml, where it begins to increase slightly. This latter phenomenon has not been reported in any study, although such high concentrations are rarely, if ever, clinically used. For a given dose, absorption rate usually decreases with increasing concentration of insulin preparation. However, while the mass in the hexameric state increases, the rate of diffusive loss, k_d, from the dimeric/monomeric compartment, drops markedly with decreasing injection volume, which ultimately results in an increasing net rate of absorption at very high concentrations of injected insulin solution.

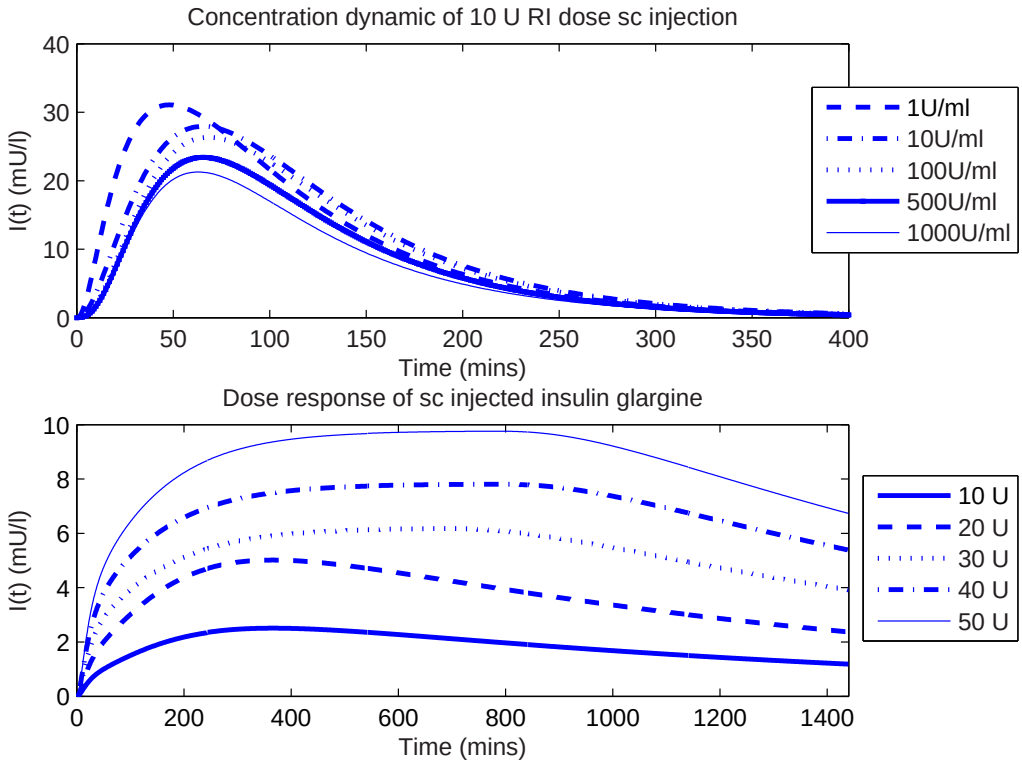

Figure 2.15 Dynamics of RI concentration dependency and insulin glargine dose response demonstrated by the model

2.7 Conclusions

A simple, physiological compartmental model is developed for computer simulation of sc injected insulin PKs for a diabetes decision support system. Most clinically current insulin types including MI, RI, NPH and insulin glargine are modelled. The model accounts for concentration dependency of sc RI injec-

tion and models the dose dependency of insulin glargine absorption. In total, 13 patient-specific model parameters are fitted to 37 sets of plasma insulin mean time course data over all insulin types from reported clinical studies. The remaining model parameters are assumed patient-independent constants and *a priori* identified from literature. All fitted parameters have a coefficient of variation <100% (median 57%, 95th percentile 3.6-60.6%) and can be considered *a posteriori* identifiable. Hence, a model has been created based on known sc absorption kinetics and identified on a broad range of clinically reported studies. The precision in identified parameters is acceptable, and all the main clinically current insulin types are modelled.

The identified model is validated using the simple criterion of t_{max} and C_{max} PK summary measures, reported the most widely in these studies. Of 37 model fits, 22 are validated on both summary measures reported by each study, or estimated from plotted data used for parameter fit where not reported. An additional 6 model fits are partially validated on t_{max} only or on C_{max} if, and only if, t_{max} cannot be validated. All partially validated model fits have errors not exceeding 12% of reported or estimated t_{max} or C_{max} ranges. Another 7 studies cannot be validated due to unreported data or reporting of only the mean values of t_{max} and C_{max}, and/or because a range of t_{max} and C_{max} could not be estimated from the data reported in the study. Finally, 2 model fits from the same study failed the validation with 90% and 71% error on t_{max} only, which is likely to be protocol-based. No model fit failed the validation for *both* reported t_{max} and C_{max} values.

Overall, the model is reasonably validated in whole or in part across 35 of 37 studies with low errors. The model demonstrates the ability to capture the fundamental dynamics of insulin action for several insulin types. Model development and identification is based on data from a wide range of studies and cohorts and is characterised by a unified and consistent, computationally-minimal compartmental structure. With this model, this research is now equipped with one of the tools for *in silico* simulation of glycaemic control protocols. In the next chapter, plasma glucose and insulin modelling is explored.

Chapter 3

Plasma Glucose and Insulin Modelling

To perform a model-based *in silico* simulation and for clinical diabetes decision support, a pharmacodynamic model of the interaction of glucose and insulin is required. The modelling goal is to combine the subcutaneous insulin pharmacokinetic model developed in Chapter 2 with other dynamics categorised as the plasma kinetics of insulin, glucose and their pharmacodynamic interaction, as well as the glucose rate of appearance in plasma from meal carbohydrates.

The models must be physiologically justified, and be simple enough to be uniquely identifiable in the context of clinical decision support with the only the available data that is implied. Previous model-based approaches are discussed to improve overall method performance and robustness, and reduce possible sources of methodological error.

This chapter reports the development of a system model of the Type 1 diabetes insulin-glucose regulatory system. The model developed has several novel and unique features. This study is the basis for a novel, model-based application to develop a simple and practical adaptive method for clinical glycaemic control of Type 1 diabetes using multiple daily injection and self-monitoring blood glucose measurements in Chapter 4. In addition, the modelling of long-term clinical outcomes of glycaemic control and their corroboration against clinical expectations and studies will be further explored in a subsequent *in silico* simulation on a virtual patient cohort which is also reported in Chapter 4. Later, the complex interaction of all quantifiable errors in protocol application is investigated in a Monte Carlo study to test the robustness of the developed protocol in effectiveness and safety.

3.1 Physiology

3.1.1 Plasma Insulin

Insulin is a hormone secreted by the pancreas which regulates glucose uptake by muscle and the liver, prevents protein catabolism and promotes fat synthesis and storage [Guyton and Hall, 2000; Jefferson and Cherrington, 2001]. It also has other, anti-inflammatory effects that are not the focus of this thesis and are well discussed in the relevant literature [Dandona et al., 2006; Hansen et al., 2003].

The insulin hormone is a polypeptide, composed of 51 amino acids, with a molecular weight of 5808Da. It is produced by the β-cells within the islets of Langerhans of the pancreas [Guyton and Hall, 2000]. The pancreas secretes insulin into the portal vein, where it first passes through the liver and subsequently enters circulation. From there, it is distributed to interstitial fluid, where it binds to cell-membrane receptors to assist glucose uptake [Jefferson and Cherrington, 2001], as shown in Figure 3.1.

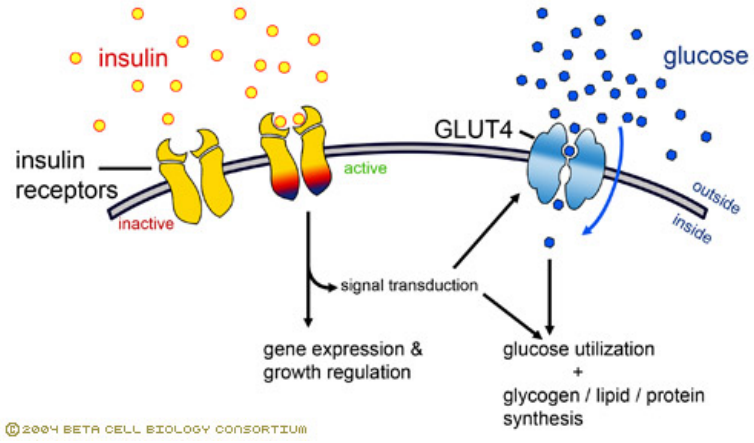

Figure 3.1 Schematic of insulin binding to receptors on tissue cells to activate glucose uptake (taken from www.betacell.org [2004]).

Secretion of insulin by the pancreas is biphasic in healthy individuals [Guyton and Hall, 2000; Jefferson and Cherrington, 2001]. The first phase consists of a pulse or bolus of stored insulin as plasma glucose concentrations rise significantly. After approximately 10 minutes, a second phase begins, which is a steady rise in insulin secretion rate to meet the metabolic needs of the body [Guyton and Hall, 2000; Jefferson and Cherrington, 2001]. This response is not unlike a PID

controller, which has been used in closed-loop control of diabetes [Chase et al., 2006; Chee et al., 2003; Steil et al., 2006].

Clearance of insulin by the body is mainly accomplished by the liver, accounting for up to 80% of total clearance [Duckworth et al., 1988; Ferrannini and Cobelli, 1987b]. After portal vein secretion, insulin passes through the liver, where approximately 50% is extracted and stored, or degraded (first-pass extraction) before reaching systemic circulation [Duckworth et al., 1988; Ferrannini and Cobelli, 1987b]. Mechanically, this allows for a fast response and control of circulating insulin but in reality, hepatic insulinisation is much higher than in the periphery, a gradient that does not exist with exogenous insulin administration in diabetes (whether intravenously or subcutaneously). This fundamental difference in insulinisation between normal and diseased states results in a difference in the relative contributions of glucose uptake by the liver and periphery as a function of plasma insulin concentration [Cherrington, 1999].

Further clearance performed by the kidneys, as a function of glomerular filtration rate (GFR) and renal glucose threshold (RGT) [Duckworth et al., 1998], and through cellular degradation after receptor binding to enable glucose uptake in the periphery [Guyton and Hall, 2000; Jefferson and Cherrington, 2001].

First isolated from dogs [Banting et al., 1922], the first commercial insulins were extracted from pigs, cattle, and even fish [Jefferson and Cherrington, 2001]. The first commercial rDNA engineered human insulin appeared in 1982. Presently, there are about 180 branded insulin preparations available. 2001 UK figures show that most insulins sold are rDNA engineered human insulins (85%), analogues (8% but doubling every year since 1997) and animal insulins (7%) [Owens et al., 2001]. Worldwide insulin consumption is split 26% soluble insulin (including RI and MI), 35% basal insulin and 39% premixed insulin. From Chapter 2, these different insulins are absorbed from subcutaneous tissue at different rates into plasma, providing a range of duration to better mimic first (bolus) or second (basal) phase pancreatic insulin response.

In this chapter, once insulin diffuses into plasma, the remaining kinetics can be modelled physiologically. To summarise the physiology to be modelled: Insulin diffuses into plasma from subcutaneous tissue from sc injection or infusion. It is cleared by the liver, and to a lesser extent, the kidneys. Through transcapillary

transport, insulin is diluted into interstitial fluid, reaching tissue cells where it binds to the cell membrane to activate glucose uptake. In this final process, insulin is internalised and degraded by the cell.

3.1.2 Plasma Glucose

Glucose is a monosaccharide and is the most important source of energy in the body. It is oxidised in the cells to provide ATP with energy, which in turn provides energy to the cell [Guyton and Hall, 2000]. The intake of glucose is through carbohydrates in food, which are digested and absorbed in the alimentary tract and released into plasma mainly in the form of glucose. Glucose in plasma is transported to the cells for use as energy, and if available in abundance, stored by the liver and the cells for future use.

The molecular weight of glucose is 180Da, which is small enough to diffuse rapidly within plasma and body fluids, its main site of action [Guyton and Hall, 2000]. The uptake by cells in the brain and the central nervous system is by diffusion alone, as they are highly permeable to glucose. In contrast, muscle and adipose cells control a majority of the total uptake and require insulin binding to cell receptors to activate or mediate glucose uptake [Despopoulos and Silbernagl, 2003; Guyton and Hall, 2000]. Hence, glucose uptake in this form is referred to as 'insulin-mediated' versus 'non-insulin-mediated' uptake in other organs.

Excess circulating glucose is stored in the liver and cells in the form of *glycogen*, a large polymer of glucose, which is created by a process called *glycogenesis* [Guyton and Hall, 2000; Zierler, 1999]. If glycogen stores are saturated, further glucose is converted into fat and stored in the liver and in fat cells in the adipose tissue. These processes can be reversed in times of energy demand. Glucose can be rapidly released from glycogen by a process called *glycogenolysis*, and if the glycogen stores are depleted, free fatty acids (FFA) are metabolised with amino acids to form glucose in a process called *gluconeogenesis* [Guyton and Hall, 2000; Zierler, 1999].

The body also has another energy source in ketone bodies. *Ketogenesis* occurs when FFAs are converted into ketone bodies by the liver. In Type 1 diabetes, *ketosis* commonly occurs as a result of acute and prolonged lack of insulin result-

ing in cell starvation even when plasma glucose levels are high. Excessive ketone bodies can accumulate in plasma, lowering blood pH resulting in *ketoacidosis* which has a high mortality rate if untreated. Occurrence of *diabetic ketoacidosis* or DKA is much more common in Type 1 diabetes than Type 2 diabetes due to a complete lack of endogenously produced insulin. *Ketosis* can also occur in severe starvation.

Commonly, the combined processes of *glycogenolysis* and *gluconeogenesis* are described as endogenous glucose production (EGP) [Zierler, 1999]. EGP is tightly regulated by the body to keep plasma glucose levels as constant as possible. External appearance or input of glucose, through meals or intravenous injection, immediately results in a rapid inhibition of EGP [Caumo and Cobelli, 1993; Jefferson and Cherrington, 2001]. Low plasma glucose has the contrary effect, stimulating glucagon secretion by the pancreatic α-cells, which activates *glycogenolysis* and thus rapidly increases glucose concentrations in plasma. Overall, these processes operate in a balance with insulin-mediated glucose removal to maintain normal blood glucose levels or glucose homeostasis.

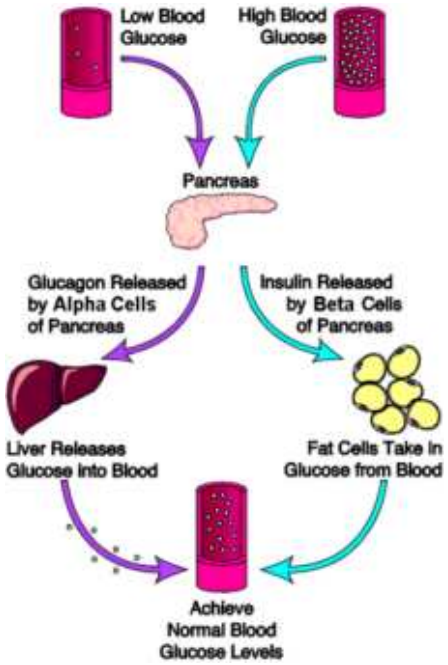

Figure 3.2 Hormonal control of glucose metabolism to store or release glucose on demand (taken from www.endocrine.com).

3.1.3 Meal Glucose Appearance in Plasma

Carbohydrates are the only source of meal glucose. Carbohydrates exist in the normal human diet in three forms [Guyton and Hall, 2000].

1. **Sucrose (cane sugar)**
2. **Lactose (milk sugar)**
3. **Starches**

Both sucrose and lactose are disaccharides while starches are polysaccharides. These forms of carbohydrate are readily digestible and subsequently absorbed as glucose into plasma. Other forms of carbohydrate, e.g., insoluble fibre like cellulose are not digestible as the human body lacks the necessary enzymes for hydrolysis. On average, once the food becomes completely mixed with the gastric secretions, ∼30-40% of consumed starches have been hydrolysed to mainly maltose from the action of salivary amylase.

In the small intestine, pancreatic amylase which is several times more powerful than salivary amylase is mixed in with the *chyme*. Within 15-30mins of gastric emptying into the duodenum and mixing with the pancreatic juice, all starches will be digested and converted into maltose and smaller glucose polymers.

Hydrolysis of the disaccharide into monosaccharides occurs in the intestinal epithelium as shown in Figure 3.3. Referring to Figure 3.4, lactose, sucrose, and maltose are split into combinations of glucose, galactose and fructose by the enzymes contained within the enterocytes lining the intestinal *villi*. This represents the end point of carbohydrate digestion and the beginning of carbohydrate absorption.

Glucose is absorbed mainly by *active transport* in tandem with sodium active transport. Transport proteins for sodium facilitated diffusion combine with glucose for transport across the brush border of the enterocyte to its interior. The active transport of Na therefore provides the *motivation* for glucose transport. Galactose is similarly absorbed. Fructose is not co-transported with sodium and its overall rate of transport is approximately half that of glucose or galactose

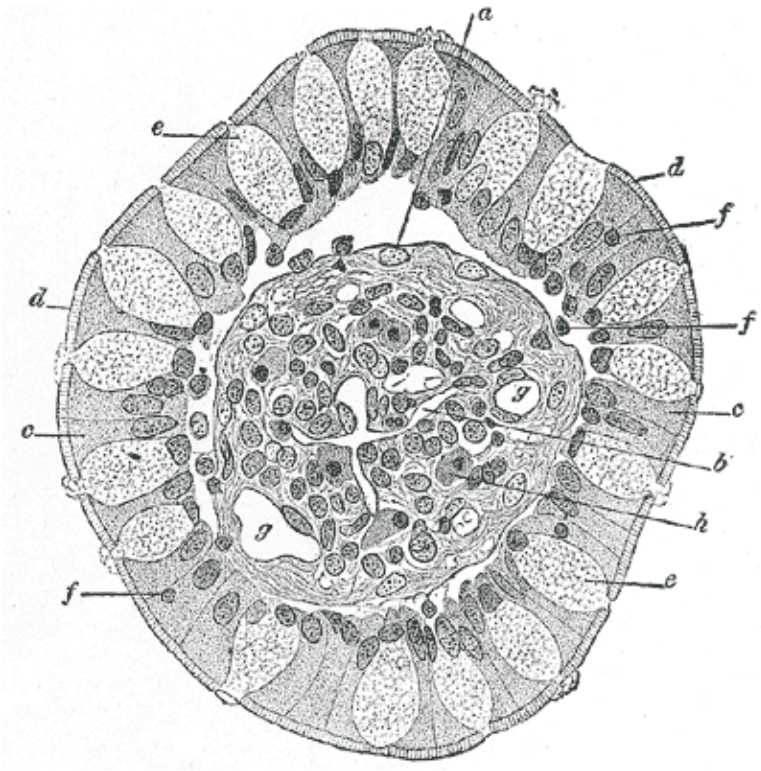

Figure 3.3 Transverse section of a *villus* of the human intestine. *a.* Basement membrane. *d.* Brush border. *e.* Epithelial cells. Reproduced from Gray and Lewis [1918]

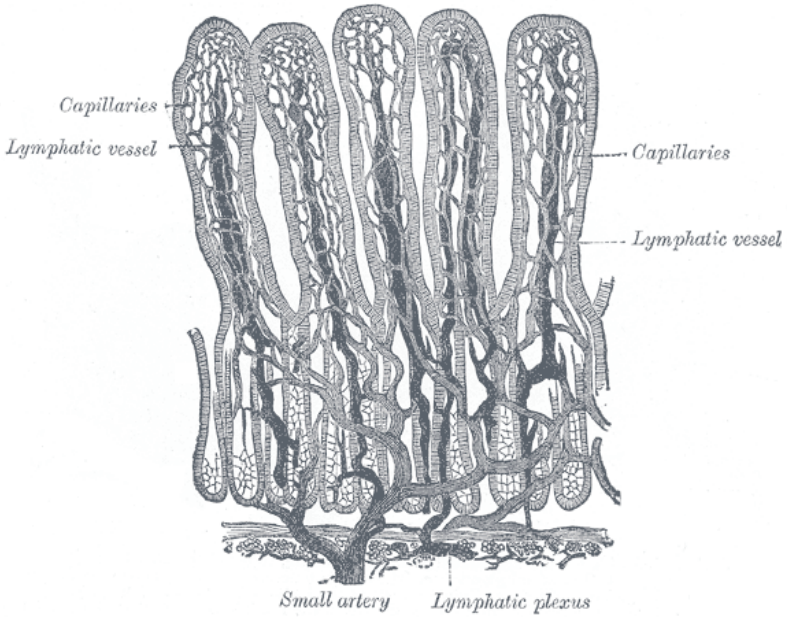

Figure 3.4 *Villi* of small intestine, showing blood vessels and lymphatic vessels. Reproduced from Gray and Lewis [1918].

[Guyton and Hall, 2000]. Fructose is also phosphorylated in the enterocyte and converted to glucose before facilitated diffusion into paracellular space, further slowing down its effective absorption into plasma.

3.2 Background

3.2.1 Plasma Insulin

Many different insulin modelling approaches have been pursued since the late 1960s, analysing insulin kinetics with one- to three-compartment models with different losses and physiological explanations [Frost et al., 1973; Hovorka et al., 1993; Jones et al., 1984; McGuire et al., 1979; Sherwin et al., 1974; Silvers et al., 1969; Tranberg and Dencker, 1978]. Physiological explanations for the compartments and their parameters differed depending on the parameter values identified using clinical data.

In the pioneering work in this field by Sherwin et al. [1974], an IV bolus of insulin and a constant infusion was fitted with different models ranging from one to four compartments as shown in Figure 3.5. The authors concluded that a three-compartment model is necessary to accurately reflect the kinetics of the decay curve, and propose a model with compartments representing plasma, hepatic plasma and extravascular fluids. The Sherwin et al. [1974] model also contains inputs to the hepatic and plasma compartments, and irreversible losses from the plasma compartment. Due to the large number of parameters and the limited sampling resolution available, this model is difficult to identify uniquely.

Other studies have examined simplifying this model to two compartments as two exponentials can describe the observed plasma insulin decay sufficiently well within measurement error [Ferrannini and Cobelli, 1987a; Turnheim and Waldhausl, 1988]. These studies typically unify the plasma and hepatic compartments, as shown in Figure 3.6, approximating them as fast exchanging relative to other dynamics [Frost et al., 1973; Polonsky et al., 1986; Tranberg and Dencker, 1978]. These simplifications allow easier identification, but the assumed transport paths are not always physiologically accurate and thus do not give an accurate representation of the observed kinetics. Ferrannini and Cobelli [1987a] concluded, after a

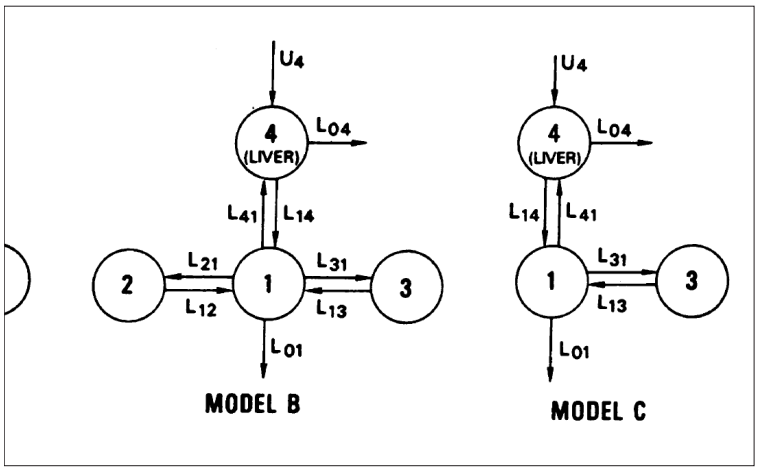

Figure 3.5 The three models analysed in the pioneering work by Sherwin et al. [1974].

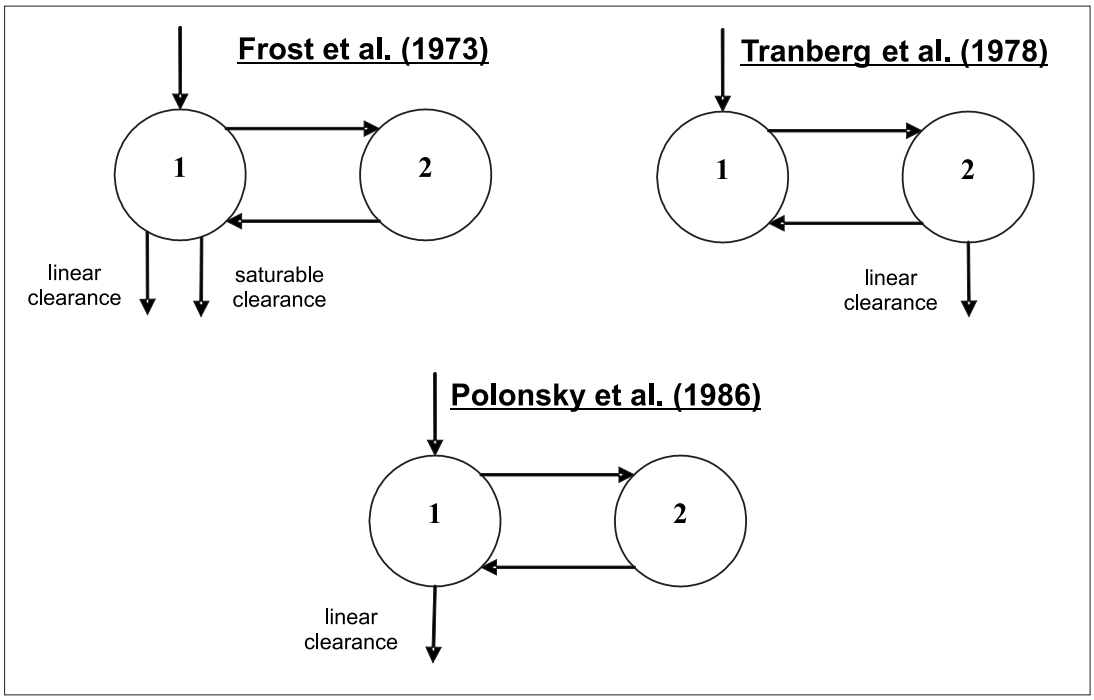

Figure 3.6 Three two compartment models with varying locations and interpretations of irreversible losses [Frost et al., 1973; Polonsky et al., 1986; Tranberg and Dencker, 1978].

detailed review of modelling efforts to that date, that a two-compartment model with irreversible losses to both compartments would provide the best compromise in physiological accuracy and identifiability. However, unique model identification remains a challenge [Ferrannini and Cobelli, 1987a].

Due to these identification problems, most recent studies have employed a

mono-compartmental description, with a single linear loss and an input term [Bergman et al., 1985; Carson and Cobelli, 2001; Toffolo et al., 2006, 1995]. Combined with the physiology of a delayed, remote site of insulin action results in a two compartment description for insulin action, modelling only the forward net flow into the remote site where the pharmacodynamic action of insulin on the receptor occurs [Furler and Kraegen, 1989; Kobayashi et al., 1983; Lehmann and Deutsch, 1992b; Puckett and Lightfoot, 1995; Shimoda et al., 1997]. A form of this simplified kinetics model has been successfully used in glycaemic control studies in the ICU [Chase et al., 2006, 2005b; Wong et al., 2006a].

$$\dot{I(t)} = \frac{-n \cdot I(t)}{1 + \alpha_I \cdot I(t)} + \frac{u(t)}{V_P} \tag{3.1}$$

$$\dot{Q(t)} = -k \cdot Q(t) + k \cdot I(t) \tag{3.2}$$

This model is a reasonably accurate representation of insulin kinetics. It has been particularly useful in control applications using *a priori* simulation of plasma insulin concentration with no or limited knowledge of the actual insulin concentration. Limitations are that it does not necessarily adhere to mass conservation laws.

In this study, plasma insulin kinetics are modelled as follows. From the dimeric/monomeric state in Chapter 2, insulin diffuses into interstitium, $x_i(t)$ (Equation 3.3) and subsequently into plasma, $I(t)$ (Equation 3.4) before it exerts its pharmacodynamic effect at the cell-membrane at interstitium concentrations (Equation 3.5). Plasma insulin is represented by the widely accepted one-pool model in Equation 3.4.

$$\dot{x_i}(t) = -(k_3 + k_{d,i}) \cdot x_i(t) + k_2 \cdot x_{dm}(t) \tag{3.3}$$

$$\dot{I}(t) = -n \cdot I(t) + k_3 \cdot \left(\frac{x_i(t)}{V_i \cdot m_b} \right) \tag{3.4}$$

$$\dot{Q(t)} = -k \cdot Q(t) + k \cdot I(t) \tag{3.5}$$

where

$x_i(t)$	Mass in the interstitium compartment [mU]
$I(t)$	Plasma insulin concentration [mU/l]
$Q(t)$	Interstitial insulin concentration [mU/l]
V_i	Insulin plasma distribution volume [l/kg]
m_b	Body mass [kg]
n	Rate of hepatic clearance of insulin [1/min]
k	Rate of absorption and clearance of insulin into and out of interstitial fluid [1/min]
$k_{d,i}$	Rate of diffusive loss from interstitium [1/min]

3.2.2 Plasma Glucose

The kinetics of glucose have been described in similar ways as insulin, with one- to three-compartment models [Bergman et al., 1979; Carson and Cobelli, 2001; Cobelli et al., 1984; Insel et al., 1974]. As glucose is a smaller molecule than insulin, with a molecular weight of 180Da (compared to insulin with 5808Da), it distributes more rapidly in the body. Well perfused organs in the splanchnic area, primarily the liver, are known to take up or store glucose very rapidly, further adding to the difficulty in measuring these kinetics to create accurate models.

A three-compartment model was used to fit glucose kinetics in an early study by Insel et al. [1974]. The model incorporated insulin-dependent and insulin-independent glucose losses, and was identified using data from various dose-response and glycaemic clamp tests with the help of glucose tracers. They concluded that the fast compartment was impossible to identify from sampled data, as equilibration between this compartment and plasma was too fast. The losses were assumed to occur from the fast and medium exchanging compartments, not accounting for peripheral losses, thus limiting its validity.

Later attempts by Cobelli et al. [1984], Jacquez [1992] and Overkamp et al. [1997] resulted in more physiological losses and explanations for the model parameters. However, unique identification of these models required complicated and costly multi-tracer experiments and imposed parameter constraints. These aspects limit their use to very specialised research studies and render them im-

practical for control or clinical use. Some of these modelling attempts are shown schematically in Figure 3.7.

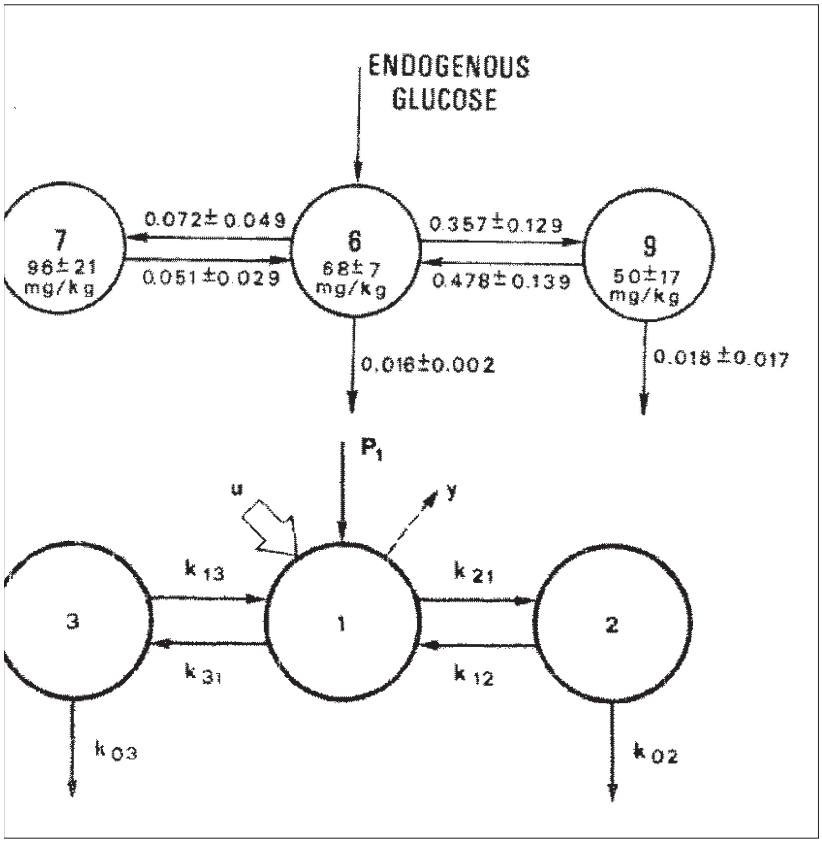

Figure 3.7 Two three compartment glucose kinetics models developed by Insel et al. [1974] (above) and Cobelli et al. [1984] (below).

As the fast equilibrating compartment was found to be too fast to identify accurately (time constant 0.6mins), it was proposed that the fast and the medium compartment be combined [Cobelli et al., 1984]. This merger is similar to the assumption made in modelling insulin, resulting in an accessible compartment representing plasma and fast exchanging tissues, and a slow compartment representing interstitial fluid. Similar two compartment models had been proposed earlier by Radziuk et al. [1978], in which the losses from both compartments were made equal to enable unique identifiability, and later by Caumo and Cobelli [1993] and Hovorka et al. [2002]. These latter models contain constant, as well as glucose-dependent and insulin-dependent losses, and more complicated dynamics, allowing an estimation of EGP by deconvolution [Carson and Cobelli, 2001; Caumo and Cobelli, 1993]. Again, these models require the use of glucose tracers to be uniquely identifiable and are thus impractical for widespread clinical

use. For reference, the model presented by Caumo and Cobelli [1993] is shown in Figure 3.8.

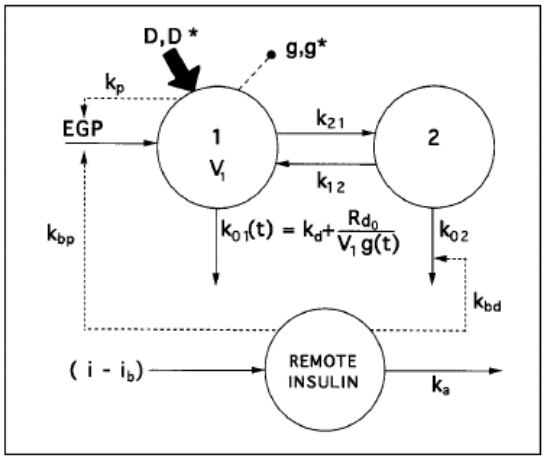

Figure 3.8 Two compartment model of glucose kinetics proposed by Caumo and Cobelli [1993].

The simplest description of glucose kinetics is by using only one compartment, with the best known model being the Minimal Model of glucose kinetics proposed by Bergman et al. [1979]. The model is described by the following equations:

$$\frac{dG(t)}{dt} = -S_G^{MM}(G(t) - G_b) - G(t)X(t) \qquad G(0) = \frac{D}{V_G} \tag{3.6}$$

$$\frac{dX(t)}{dt} = -p_2 X(t) + p_3(I(t) - I_b) \qquad S_I^{MM} = \frac{p_3}{p_2} \tag{3.7}$$

where

$G(t)$	Plasma glucose concentration
G_b	Fasting glucose
D	Glucose dose
V_G	Volume of distribution
$X(t)$	Remote insulin effectiveness
$I(t)$	Plasma insulin concentration
I_b	Fasting insulin
S_G^{MM}	Glucose effectiveness at basal insulin
S_I^{MM}	Insulin sensitivity
p_2, p_3	Transport rates defining delay in insulin effect

This approach assumes fast equilibration between the compartments and thus equivalent concentrations throughout the body. Losses are possible by insulin-independent pathways (brain, liver, kidneys) via the parameter S_G^{MM} (1/min), denoted as *glucose effectiveness* at basal insulin, and by insulin-dependent (mainly muscle and adipose tissue cells), as mediated by remote *insulin effectiveness* $X(t)$ (1/min). The variable $X(t)$ in this model accounts for the combined delay in insulin transport to the periphery, as well as the insulin sensitivity of the cells, thus combining transport kinetics and action dynamics.

The Minimal Model is widely used, mostly combined with an IVGTT to assess insulin sensitivity in research studies [Bergman et al., 1985, 1981]. Its main advantages are simplicity and thus practicality. However, numerous studies have questioned the validity of its derived parameters, and the question was postulated as to whether it is 'too minimal' [Caumo and Cobelli, 1993; Caumo et al., 1996, 1999; Quon et al., 1994; Regittnig et al., 1999]. In particular, studies have shown that the estimation of S_G^{MM} is imprecise and usually results in a significant overestimation of its contribution, with the consequent result being a significant underestimation of S_I^{MM} [Caumo et al., 1999].

The reason identified for this problem by Caumo et al. [1999] is that glucose kinetics should be described by two compartments to describe the fast decay during the initial 30mins after a glucose dose and the slower decay thereafter. When fitting the Minimal Model to IVGTT data using accepted methods, the model tries to match the initial fast decay with a single exponential, resulting in an overestimation of the slow decay that follows [Caumo et al., 1999; Quon et al., 1994]. Despite this problem, the model is able to capture the dominant dynamics and has been somewhat successfully used in a slightly modified form for glycaemic control trials in the critically ill [Chase et al., 2005a; Wong et al., 2006a].

Further models of glucose kinetics usually combine more complex kinetics, such as a circulatory model by Mari [1998], accounting for mixing of injected glucose in the circulation. More complex simulation models include those presented by Lehmann and Deutsch [1992a] or Arleth et al. [2000]. These models include many more physiological effects, such as glucose appearance from meals, liver feedback, and renal clearance thresholds. In particular, the glucose balance surface by Arleth et al. [2000] is built on knowledge and assumptions on the be-

haviour of glucose transporters (GLUT) [Guyton and Hall, 2000], incorporating saturation of glucose clearance. Its parameters are identified by fitting the model to values gathered from a wide range of clinical studies of glucose and insulin metabolism, resulting in a three-dimensional surface that allows prediction of metabolic behaviour in a population sense.

To summarise, modelling approaches exist to capture most metabolic characteristics of glucose. However, they are usually limited to experimental environments, overly simplified, or both. For a model to be useful in an *in silico* simulation and/or clinical real-time decision support setting, it should be readily identifiable with limited data, but compromising only slightly on physiological accuracy to ensure the relevance of the results.

3.2.3 Meal Glucose Rate of Appearance

Modelling of meal glucose rate of appearance (Ra) in plasma is a complex process not widely studied [Yates and Fletcher, 2000] unlike plasma glucose and insulin. The process can be divided into several main processes which include digestion in the stomach and gut, gastric emptying into the gut, absorption from the gut and subsequent transport into plasma.

The kinetics of meal glucose appearance in plasma, like both insulin and glucose, have been described with one- to three-compartment models [Worthington, 1997] and even a five compartment model [Boroujerdi et al., 1987]. Worthington [1997] found the one-compartment model with time delay had the smallest fitting error. This result was obtained with a model fit to plasma glucose data and, hence, is not model-independent.

There are also approaches which are non-compartmental. Berger and Rodbard [1989] and Lehmann and Deutsch [1992b] use complex functions to describe gastric emptying. Gastric emptying is assumed to follow (depending on the quantity of carbohydrate/glucose load consumed) a triangular or trapezoidal function while intestinal absorption is modelled as a first-order linear process. No fractional losses occur between intestinal absorption and glucose appearance in plasma via the portal vein. Model equations are:

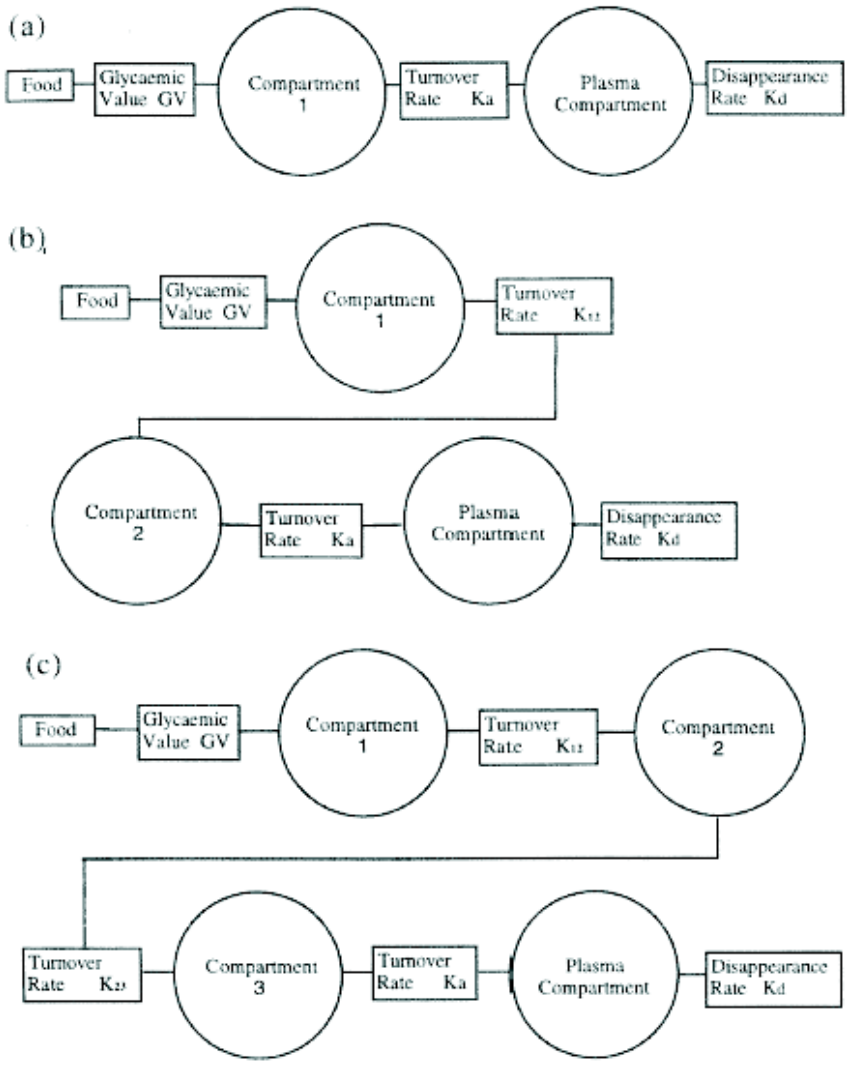

Figure 3.9 Gut model structure for (a) one compartment model, (b) two compartment model and (c) three compartment model by Worthington [1997].

$$\dot{G_{gut}} = G_{empt} - k_{gabs} \cdot G_{gut} \tag{3.8}$$

$$G_{empt}(t) = \begin{cases} \frac{Vmax_{ge}}{Tasc_{ge}} \cdot t & t < Tasc_{ge} \\ Vmax_{ge} & Tasc_{ge} < t \leq Tasc_{ge} + Tmax_{ge} \\ Vmax_{ge} & Tasc_{ge} + Tmax_{ge} \leq t \\ -\frac{Vmax_{ge}}{Tdes_{ge}} \cdot (t - Tasc_{ge} - Tmax_{ge}) & < Tasc_{ge} + Tmax_{ge} + Tdes_{ge} \\ 0 & \text{otherwise} \end{cases} \tag{3.9}$$

$$Vmax_{ge} = \frac{2 \cdot D}{Tasc_{ge} + 2 \cdot Tmax_{ge} + Tdes_{ge}} \tag{3.10}$$

$$G_{in} = k_{gabs} \cdot G_{gut} \tag{3.11}$$

where

$G_{empt}(t)$	Rate of gastric emptying
$Vmax_{ge}$	Maximal rate of gastric emptying
$Tmax_{ge}$	Length of time at maximum and constant rate of gastric emptying
$Tasc_{ge}$	Length of time of the ascending branch of the gastric emptying trapezoidal function
$Tdes_{ge}$	Length of time of the descending branch of the gastric emptying trapezoidal function
k_{gabs}	Rate of glucose absorption from the gut into systemic circulation

$Tmax_{ge}$ is a function of the carbohydrate content of the meal and, hence, determines the shape of the complex function of gastric emptying. The Lehmann et al. model was never formally identified on tracer glucose Ra data or on plasma glucose data. However, a model-based (and, hence, model-dependent) deconvolution study was performed by Yates and Fletcher [2000] with results of acceptable accuracy reported. The Lehmann et al. model has been used in a robust diabetes control study by Parker et al. [2000] with the same maximal gastric emptying rate, $Vmax_{ge}$ of 0.36g/min.

The Elashoff et al. [1982] model utilises the same linear gut absorption model but implements a power exponential for the description of G_{empt} as shown in Equation 3.12. Both Lehmann et al. and Elashoff et al. models are effectively mono-compartment models of the gut with *complex* functions describing gastric emptying *into* the gut.

$$G_{empt}(t) = D \cdot \beta \cdot k^{\beta} \cdot t^{\beta-1} \cdot e^{\{-(kt)^{\beta}\}} \tag{3.12}$$

where

k	Rate of gastric emptying
β	Shape factor

A different approach by Hovorka et al. [2004] uses a complex equation in Equation 3.13 (effectively a two-compartment chain of identical transfer rates) to describe digestion, gastric emptying, and the gut absorption rate, $U_G(t)$ directly into plasma.

$$U_g(t) = \frac{D_G A_G t e^{-t/t_{max,G}}}{t_{max,G}^2} \tag{3.13}$$

where

$t_{max,G}$	Time to maximum appearance rate of glucose in the accessible glucose compartment
D_G	Amount of carbohydrates/glucose digested
A_G	Carbohydrate biovailability

The gut absorption term is assumed to enter plasma directly into the accessible compartment (in this study, plasma consists of two compartments, an accessible and non-accessible compartment) with a suitable clearance from first-pass splanchnic sequestration or degradation in the carbohydrate bioavailability term, A_G. A similar approach was taken by Fisher [1991]. Glucose Ra in plasma, $P(t)$, from intestinal absorption is described with effectively a mono-compartment model in Equation 3.14 where B and k are chosen to match plasma glucose data after oral glucose tests.

$$P(t) = B \cdot e^{(-kt)} \tag{3.14}$$

Thus far, most models reviewed have not been validated on tracer data, but rather, only on model-dependent plasma glucose data or not validated at all in simulation-only applications. This reflects the main difficulty with all models of meal glucose Ra, that is the data required to identify all parameters uniquely. Such data of meal glucose Ra can only be sourced via expensive and complicated tracer experiments. To determine the relationship between meal glucose Ra and glucose load accurately also requires a large number of experiments over a range

of meal glucose loads. In a clinical role, meal glucose Ra models are limited to a simulation role only with population *a priori* parameters. Tracer data is not readily available clinically, being invasive and time consuming, which prohibits the identification of patient-specific, real-time parameters.

In a study by Dalla Man et al. [2006], the Lehmann and Deutsch [1992b] and Elashoff et al. [1982] models were evaluated against a linear and non-linear three-compartment model using gold standard tracer data. The Dalla Man et al. model in Equations 3.15 to 3.18 consists of dual stomach compartments with a non-linear gastric emptying rate with 4 identified parameters. In the linear model, the gastric emptying term, k_{empt}, is a constant, and in the non-linear model, it is replaced by Equation 3.16. Non-linear gastric emptying is described by a hyperbolic tangent function of the proportion of the consumed carbohydrate remaining in the stomach in Equation 3.16. There is no saturation term for gastric emptying or gut absorption for large meals.

$$\begin{cases} \dot{q_{sto1}}(t) = -k_{21} \cdot q_{sto1}(t) + D\delta(t) \\ \dot{q_{sto2}}(t) = -k_{empt} \cdot q_{sto2}(t) + k_{21} \cdot q_{sto1}(t) \\ \dot{q_{gut}}(t) = -k_{abs} \cdot q_{gut}(t) + k_{empt} \cdot q_{sto2}(t) \\ Ra(t) = f \cdot k_{abs} \cdot q_{gut}(t) \end{cases} \tag{3.15}$$

$$\begin{aligned} k_{empt}(q_{sto}) =& k_{min} + \frac{k_{max} - k_{min}}{2} \cdot \{\tanh[\alpha(q_{sto} - b \cdot D)] - \\ & \tanh[\beta(q_{sto} - c \cdot D)] + 2\} \end{aligned} \tag{3.16}$$

$$\alpha = \frac{5}{2 \cdot D \cdot (1 - b)} \tag{3.17}$$

$$\beta = \frac{5}{2 \cdot D \cdot c} \tag{3.18}$$

where

q_{sto1}(t)	Amount of glucose in the stomach (solid phase)
q_{sto2}(t)	Amount of glucose in the stomach (liquid phase)
$\delta(t)$	Impulse function
D	Amount of ingested glucose
$q_{gut}(t)$	Glucose mass in the intestine

k_{21}	Rate of grinding
k_{empt}	Rate of gastric emptying
k_{abs}	Rate of intestinal absorption
f	Fraction of intestinal absorption which appears in plasma
k_{min}	Minimum gastric emptying rate
k_{max}	Maximum gastric emptying rate

In this study, it is concluded that the Lehmann et al. and Elashoff et al. models fail to fit the data adequately due to their simplistic model structures, as the tracer data seemed to possess two or even three phases which were not captured by the less complex models in the comparison. The Ra data is shown in Figure 3.10. From Figure 3.10, the grey area of variability is far wider than the errors in any of the four model fits to any one particular set of data. In a clinical environment, where there is no tracer data, there would be little difference overall if either of the four models were used for *a priori* simulation of meal glucose Ra in plasma.

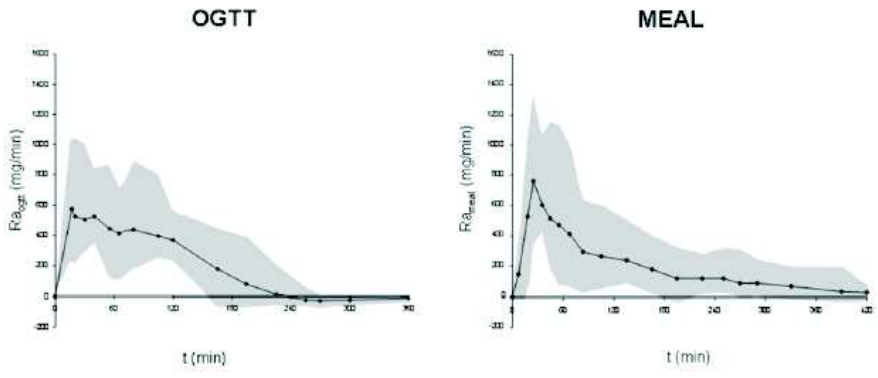

Figure 3.10 Rate of appearance (Ra) measured with the multiple tracer tracer-to-tracee clamp technique during OGTT (left) and meal (right); grey area represents range of variability. Reproduced from Dalla Man et al. [2006]

3.3 Modelling

3.3.1 Plasma Insulin Model Structure

The insulin kinetics model used in this study is shown in Figure 3.11. It is derived from the Sherwin et al. [1974] three compartment model but reduced to two compartments by integrating the hepatic and plasma compartments, as the transport between these compartments is very fast [Ferrannini and Cobelli, 1987a; Sherwin et al., 1974]. The decay of an IV injection of insulin has been shown to follow a double exponential decay curve sufficiently well in several studies [Carson and Cobelli, 2001; Ferrannini and Cobelli, 1987a; Turnheim and Waldhausl, 1988], further justifying this reduction.

The model in Figure 3.11 consists of a central or accessible compartment representing the plasma space and fast exchanging tissues, such as the splanchnic bed, and a peripheral compartment representing the interstitial fluid which is where the pharmacodynamic action of insulin is performed on the glucose receptor. These compartments are further described as plasma and interstitial spaces. Referring to Chapter 2, insulin diffuses into interstitium, $x_i(t)$, from the dimeric/monomeric state at the injection site, and subsequently into plasma, $I(t)$ (Equation 3.19).

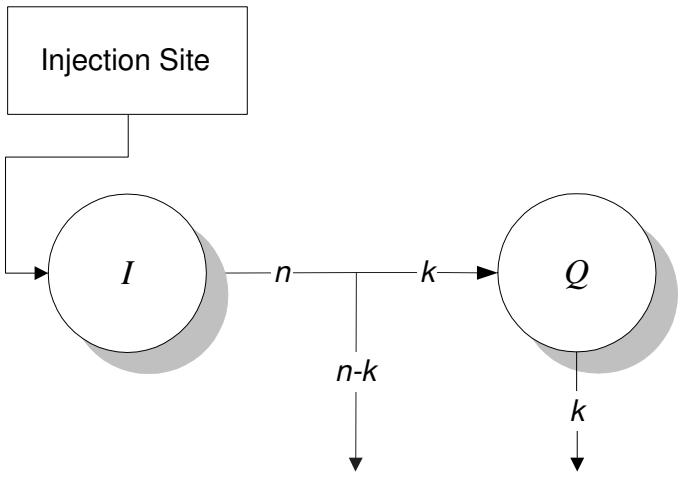

Figure 3.11 Structure of the two compartment plasma insulin kinetics model which is shown here with the interstitium compartment receiving input from the sc injection site.

$$\dot{I}(t) = -n \cdot I(t) + k_3 \cdot \left(\frac{x_i(t)}{V_i \cdot m_b} \right) \tag{3.19}$$

where

$x_i(t)$	Mass in the interstitium compartment [mU]
$I(t)$	Plasma insulin concentration [mU/l]
V_i	Insulin plasma distribution volume [l/kg]
m_b	Body mass [kg]
n	Rate of hepatic clearance of insulin [1/min]
k_3	Interstitium insulin transport rate into plasma [1/min]

Plasma insulin, as represented by a one-pool model in Equation 3.19, is also widely accepted in literature [Furler and Kraegen, 1989; Kobayashi et al., 1983; Puckett and Lightfoot, 1995; Shimoda et al., 1997] and in this current form has been used by Chase et al. [2005b] and Wong et al. [2006b]. While diffusion is bi-directional, only the mono-directional net transport between the two compartments is modelled from plasma, $I(t)$, into interstitial fluid, $Q(t)$. Each compartment has a clearance pathway. Intravenous injection or infusion is also modelled (if required) as an input into the $I(t)$ compartment.

The differential equation describing the amount of insulin in the $Q(t)$ compartment is dependent on the hepatic clearance rate from plasma, n (which inevitably lumps the combined insulin clearances by both the liver and kidneys, as well as the rate of diffusion, k, into interstitial fluid where insulin acts upon the glucose receptor), the amount of insulin in the compartment, $Q(t)$, and the rate constant, k, of the internalisation and degradation of insulin after pharmacodynamic action.

$$\dot{Q}(t) = -k \cdot Q(t) + k \cdot I(t) \tag{3.20}$$

where

$Q(t)$	Interstitial fluid insulin concentration [mU/l]

$I(t)$	Plasma insulin concentration [mU/l]
k	Rate of absorption and clearance of insulin into and out of interstitial fluid [1/min]

This formulation includes the main pathways of insulin, but inevitably lumps some separate physiological processes into single processes. This minimises the number of parameters to be identified *a priori* from literature, as well as reduces computational burden in the scenario of a clinical decision support system or as an *in silico* simulation tool.

The irreversible clearance of insulin from plasma is mainly performed by the liver and the kidneys. The liver accounts for as much as 80% of total losses [Ferrannini and Cobelli, 1987b], a figure which varies widely depending on the individual. Studies have also shown a saturation of liver clearance at higher concentrations [Ferrannini et al., 1983; Thorsteinsson, 1990], due to the mechanism by which insulin is cleared, namely binding to liver cells and its resulting degradation. While other studies have included a Michaelis-Menten saturation term [Chase et al., 2005b; Lotz et al., 2006b; Thorsteinsson, 1990], it was deemed unnecessary in this study as hyperinsulinaemia is not common in Type 1 diabetes. Chase et al. [2005b] modelled a highly dynamic and insulin resistant critically ill cohort while Lotz et al. [2006b] developed the model as a diagnostic tool for Type 2 diabetes, both conditions of elevated insulin resistance and commonly supraphysiological plasma insulin concentrations.

Transcapillary transport from plasma to interstitium has been studied by others and found to occur mainly via diffusion *in vivo* in dogs and humans [Castillo et al., 1994; Gudbjornsdottir et al., 2003; Rasio et al., 1967; Sjostrand et al., 1999; Steil et al., 1996; Yang et al., 1989]. In this model, a passive transport by diffusion alone is assumed, due to a large amount of evidence that it is the primary and/or dominant mechanism. While transcapillary diffusion is concentration driven and bi-directional, it is described in this model by the *net* diffusion transport constant k.

The irreversible loss from the peripheral interstitial compartment is believed to occur mainly due to binding of insulin to the cells and its subsequent degradation [Conn and Goodman, 1998; Jefferson and Cherrington, 2001]. The rate

constant at which insulin is degraded at the cells is similarly described by k.

Being a Type 1 diabetes model, all insulin input into the plasma compartment is assumed exogenous in origin and only from sc insulin injection or infusion from the injection site. If required, intravenous injection or infusion of insulin can be modelled as inputs into the plasma compartment, I, if necessary. No endogenous secretion is accounted for. The three plasma insulin kinetics model parameters are identified physiologically *a priori* from literature. As the model in this same basic form has been used prior to this research by Chase and colleagues [Chase et al., 2004, 2005b; Wong et al., 2006b], the model parameters are identified from the sources referenced in these studies.

3.3.2 Plasma Glucose Model Structure

The model structure chosen for this application is a mono-compartmental description, similar to the Minimal Model and the model used in previous glycaemic control research at the University of Canterbury [Chase et al., 2005b]. The system model shown in Equation 3.21 is an evolution of the model of Chase et al. [2005b] and Wong et al. [2006b].

$$\dot{G}(t) = EGP_{0-G} - p_G \cdot G(t) - S_I \cdot G(t) \cdot Q(t) - RGC(t) - CNS + P(t) \quad (3.21)$$

where

$G(t)$	Plasma glucose concentration [mmol/l]
CNS	Central nervous system glucose uptake [mmol/l.min]
EGP_{0-G}	Endogenous glucose production extrapolated to zero plasma glucose concentration [mmol/l.min]
p_G	Glucose effectiveness [1/min]
S_I	Insulin sensitivity [l/(min.mU)]
$Q(t)$	Interstitial (effective) insulin concentration [mU/l]
$RGC(t)$	Renal glucose clearance [mmol/l.min]
$P(t)$	Meal plasma glucose rate of appearance [mmol/l.min]

This glucose model differs mathematically from the model developed by Chase et al. [2005b] and Wong et al. [2006b] in the removal of insulin effect saturation, and the addition of renal glucose clearance rate, $RGC(t)$. These two studies were on highly dynamic, critically-ill patients with high effective insulin resistance and treated with intravenous insulin doses. The removal of the insulin effect saturation was deemed suitable for modelling more compliant, insulin sensitive, and stable Type 1 diabetes patients treated with subcutaneously administered insulin.

$$RGC(t) = \begin{cases} \frac{GFR}{V_p \cdot m_b}\big(G(t) - RGT\big) & \text{if } G(t) > RGT \\ 0 & \text{if } G(t) \leq RGT \end{cases} \tag{3.22}$$

where

$RGC(t)$	Renal glucose clearance [mmol/l.min]
GFR	Glomerular filtration rate [l/min]
$G(t)$	Plasma glucose concentration [mmol/l]
RGT	Renal glucose threshold [mmol/l]
V_p	Glucose distribution volume [l/kg]
m_b	Body mass [kg]

Referring to Equation 3.22, the renal glucose clearance rate, $RGC(t)$, models glucose removal by the kidney above the renal glucose threshold, RGT, using a linear relationship proportional to the glucose concentration above RGT and the glomerular filtration rate, GFR. From the study by Johansen et al. [1984], this linear approximation is acceptable. Linear models have also been used in AIDA [Lehmann, 1998] by Lehmann and Deutsch [1992b] and Arleth et al. [2000].

The main advantage over a multi-compartmental description is its identifiability using limited glucose samples, while still accounting for the dominant dynamics. This model has also performed well in a variety of insulin and nutrition based glycaemic control trials, as well as in retrospective data fitting of critically ill patients [Chase et al., 2005b; Hann et al., 2005b]. As the intended use of the model is in a situation less dynamic, and less frequently sampled, errors due to undermodelling from assuming a mono-compartmental structure should

be minimal.

Recent studies sampling interstitial fluid concentrations of glucose directly from the muscle tissue using a microperfusion technique [Regittnig et al., 2003, 1999], found a mean delay of 22mins (SD 3mins) between a bolus injection of 20g glucose and the equilibration of concentrations in plasma and ISF. This delay explains the fast decay seen in IVGTT plasma glucose data during the first 30mins, which causes an overestimation of Minimal Model S_G^{MM} when it is used to fit a single exponential, as discussed in Subsection 3.2.2. An additional loss at these high glucose concentrations ($\sim$14mmol/l), not identified by the researchers, could be renal glucose clearance.

The saturation of insulin-dependent glucose clearance, evident in long-term hyperglycaemic, hyperinsulinaemic, critically ill individuals [Chase et al., 2004], is likely not evident in typical Type 1 diabetes which is the target cohort of the models and methods in this study. In the late postprandial and fasting states in Type 1 diabetes, this assumption is likely to hold true [Prigeon et al., 1996]. However, in conditions of hyperinsulinaemia (most typically prandial periods), it is very likely that the glucose clearance by insulin is sufficiently rapid that periods of insulin effect saturation has minimal influence on the identification of the model. Note that at higher insulin dosing, saturation effects could affect the estimation of S_I, as both parameters trade off [Chase et al., 2004; Prigeon et al., 1996].

Further enhancements made include a more physiological and complete description of the uptake and production mechanisms of glucose. The developed model schematic is shown in Figure 3.12. The additions to the model and their physiological justification are explained in more detail in the following sections.

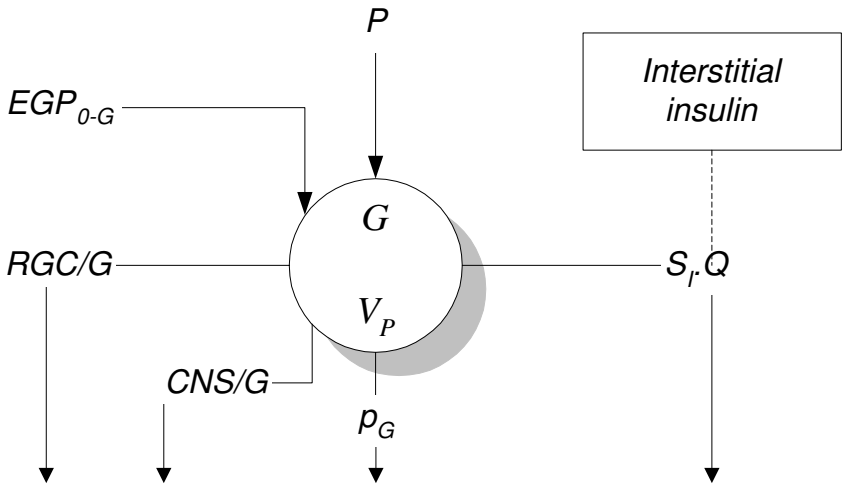

Figure 3.12 Schematic of the developed full glucose PK and PD model. Shown are all exogenous (P) and endogenous (EGP_{0-G}) inputs, the constant loss CNS, the insulin-independent losses p_G and RGC, and the insulin-dependent loss mediated by S_I.

3.3.2.1 Insulin-Dependent Uptake

Insulin-dependent glucose uptake, mostly by muscle and adipose cells, is dependent on the product of peripheral or interstitial insulin, Q, total glucose concentration, G, and insulin sensitivity, S_I, as seen in the third term of Equation 3.21. This assumption is physiologically valid and widely accepted, having been identified and observed in many studies [Bergman et al., 1979; Jefferson and Cherrington, 2001; Yang et al., 1989].

As the modelled insulin concentrations are absolute values and not those above basal, as in the Minimal Model, the parameter S_I now includes a dynamic that is included in S_G^{MM} in the Minimal Model, namely glucose uptake at basal insulin, I_b. The effect of this glucose uptake, which has now been removed from the insulin-independent portion of the model, will now tend to increase S_I and consequently reduce p_G.

3.3.2.2 Insulin-Independent Uptake

Insulin-independent uptake in a basal state is primarily due to the brain and central nervous system [Zierler, 1999], and to a lesser extent by some splanchnic,

well perfused organs. Most of this uptake is independent of glucose concentration and can thus be seen as a constant loss that is compensated by endogenous production to keep steady state levels. This uptake accounts for about 75% of basal glucose uptake and is in the magnitude of ∼1mg/kg/min [Best et al., 1981; Zierler, 1999].

In addition to insulin-independent glucose uptake in the fasting basal state, glucose can enhance its own uptake at hyperglycaemic levels and inhibit EGP [Ader et al., 1997; Best et al., 1996; Jefferson and Cherrington, 2001]. These two effects, uptake and suppression are lumped into the parameter p_G of Equation 3.21 and in the Minimal Model parameter S_G^{MM} [Bergman et al., 1979].

Like the Minimal Model, the model is unable to differentiate non-insulin mediated glucose uptake from production, which are lumped in a linear relationship with glucose. Referring to Figures 3.13 and 3.14, total body glucose uptake (TBGU) and hepatic glucose production (HGP) data from Del Prato et al. [1997, 1995] are used to identify CNS, EGP_{0-G} and p_G. Data at glucose exceeding the approximate RGT of 10mmol/l are ignored to eliminate the need to evaluate renal glucose clearance, RGC, and associated errors. Under fasting and insulinopenic conditions, the $P(t)$ and $S_I G(t)Q(t)$ terms of Equation 3.21 can be further eliminated.

By the linear definition of the effect of hyperglycaemia on TBGU, CNS can then be derived as the 'virtual' y-intercept of the linear TBGU curve. The term 'virtual' is used as no glucose uptake is theoretically possible at zero glucose. The central nervous system glucose uptake, CNS, is saturated at 3.3mmol/l and is relatively insensitive to insulin and glucose [Best et al., 1981; Siesjo, 1988]. At euglycaemia, CNS accounts for ∼70% of all non-insulin mediated glucose uptake [Baron et al., 1988] and this proportion is likely to increase with hypoglycaemia. Hence, the use of the term CNS for the virtual y-intercept of the linear TBGU curve is justified.

Similarly, by the linear definition of the effect of hyperglycaemia on HGP, EGP_{0-G} is the y-intercept of the linear HGP curve, and p_G, the slope of the combined TBGU and HGP curve. Hence, p_G is similar to the Minimal Model glucose effectiveness, S_G, but defined under conditions of insulinopenia or sub-basal insulin, rather than basal insulin [Best et al., 1996].

Unlike the Minimal Model, the insulin model in this study models the absolute insulin concentration, not insulin concentration above basal. In Type 1 diabetes, insulinopenia is not uncommon and the assumption of basal insulin may not be met all the time. Using data from Del Prato et al. [1995] for an insulinopenic normal cohort (Figure 3.13), values of CNS=1.4mg/kg.min, EGP_{0-G}=2.6mg/kg.min and p_G=0.006min^{-1} are obtained compared CNS = 1.3mg/kg.min, EGP_{0-G} of 3.0mg/kg.min and p_G=0.009min^{-1} under basal insulin conditions (figure not shown). Compared to insulinopenia, the presence of basal insulin results in overestimation of p_G, although this value is still approximately half that of published values of the Minimal Model S_G for a normal cohort ∼0.024min^{-1} [Best et al., 1996].

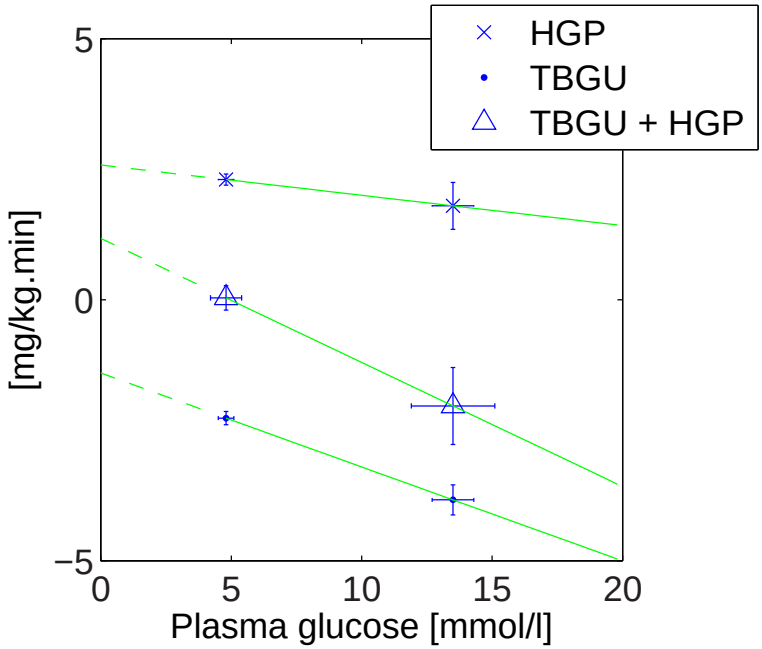

Figure 3.13 Using HGP and TBGU data from Del Prato et al. [1995] for an insulinopenic normal cohort, values of CNS=1.4mg/kg.min, EGP_{0-G}=2.6mg/kg.min and p_G=0.006min^{-1} can be calculated by linear regression

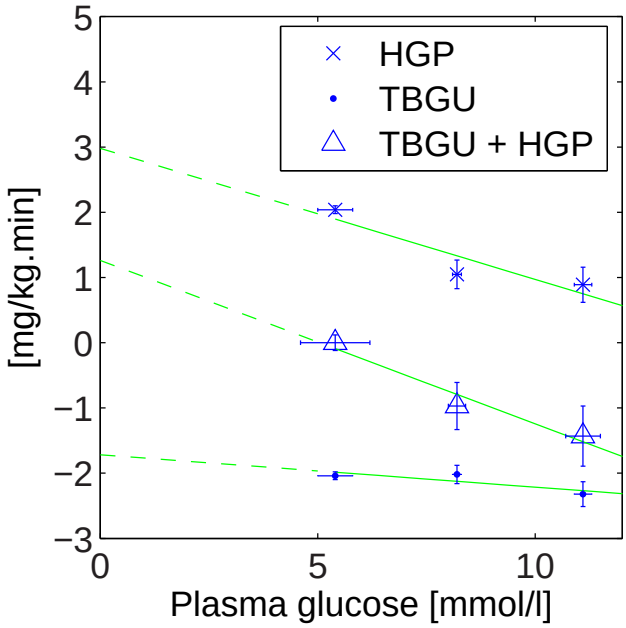

Figure 3.14 Using HGP and TBGU data of Del Prato et al. [1997] for an IDDM cohort under basal insulin, values of CNS=1.7mg/kg.min, EGP_{0-G}=3.0mg/kg.min and p_G=0.006min^{-1} can be calculated by linear regression

Using the data of Del Prato et al. [1997] for an IDDM cohort under basal insulin (Figure 3.14), values of CNS=1.7mg/kg.min, EGP_{0-G}=3.0mg/kg.min and p_G=0.006min^{-1} are obtained. Hence, p_G of the normal, insulinopenic cohort [Del Prato et al., 1995] is similar to the IDDM cohort under basal insulin [Del Prato et al., 1997]. This result is logical since S_G is decreased in IDDM [Best et al., 1981] while basal insulin increases S_G, either by increased glucose uptake [Best et al., 1981] or suppression of endogenous glucose production [Del Prato et al., 1995]. In IDDM, the p_G obtained is also approximately half that of published S_G values of ∼0.013min^{-1} [Best et al., 1996]. One explanation is the elimination of the data at high glucose concentrations from the p_G analysis, which if unaccounted for, would include the effect of urinary glucose excretion, thereby increasing the 'effective' glucose uptake. From this investigation, it can be deduced that for an IDDM cohort under conditions of insulinopenia, p_G must have an upper bound of 0.006min^{-1}, which is assumed in this study. The values of CNS obtained are in agreement with Baron et al. [1988]; Scheinberg [1965] and Boyle et al. [1994], and the assumption that CNS is approximately equal to the virtual y-intercept of the linear TBGU curve is valid.

3.3.2.3 Meal Glucose Rate of Appearance

The minimal models of meal glucose Ra by Worthington [1997] and Lehmann and colleagues [Lehmann, 1998; Lehmann and Deutsch, 1992b] form the basis of the model used in this study. Referring to Figure 3.15 and Equations 3.23 to 3.26, the model consists of two compartments for the stomach and gut, with linear gastric emptying and gut-absorption rates to describe the plasma glucose Ra, $P(t)$, in Equation 3.21.

Meal carbohydrate amount and type have been shown to be the main factors affecting meal glucose Ra [Wolever and Bolognesi, 1996a,b; Yates and Fletcher, 2000]. However, clinical models of glucose Ra almost universally accept input of meal glucose amount only. An additional simplification is the expression of meal carbohydrate content (in grams) as equivalent to the same mass of glucose monosaccharide regardless of the meal carbohydrate type. Such meal data is again typically unavailable in a clinical setting. Glucose equivalent carbohydrate (GEC) introduced by Yates and Fletcher [2000] to express carbohydrate values as monosaccharide equivalents necessarily depends on an *a priori* knowledge of the carbohydrate type within the meal to be consumed, which is unrealistic in the clinical environment of ambulatory Type 1 diabetes.

Carbohydrate counting is a technique commonly taught by diabetes care providers to improve glycaemic management [Bruttomesso et al., 2001; Gregory and Davis, 1994; Warshaw and Kulkarni, 2004]. Glycaemic index (GI), a measure of the *effect* of carbohydrate type, is not easily calculable for mixed meals [Flint et al., 2004] nor readily available like carbohydrate content.

$$\dot{STO}(t) = -k_6 \cdot STO(t) + u_{CHO}(t) \tag{3.23}$$

$$\dot{GUT}(t) = -GABS(t) + k_6 \cdot STO(t) \tag{3.24}$$

$$GABS(t) = \min\big(k_7 \cdot GUT(t), GABS_{max}\big) \tag{3.25}$$

$$P(t) = \frac{GABS(t)}{0.18 \cdot (V_p \cdot m_b)} \tag{3.26}$$

where

$STO(t)$	Mass of carbohydrate/glucose in the stomach [g]
$GUT(t)$	Mass of carbohydrate/glucose in the gut [g]
$GABS(t)$	Gut carbohydrate/glucose absorption rate [g/min]
$GABS_{max}$	Maximum gut carbohydrate/glucose absorption rate [g/min]
k_6	Carbohydrate/glucose gastric emptying rate [1/min]
k_7	Carbohydrate/glucose gut-absorption rate [1/min]
$u_{CHO}(t)$	Meal carbohydrate/glucose input [g/min]
$P(t)$	Meal plasma glucose rate of appearance [mmol/l.min]
V_p	Glucose plasma distribution volume [l/kg]
m_b	Body mass [kg]

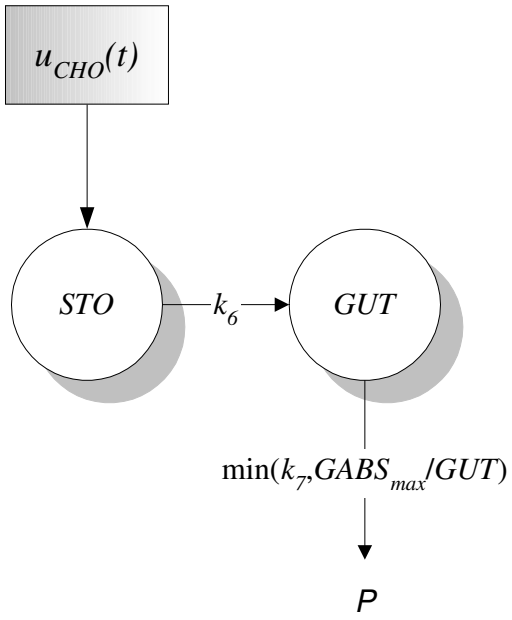

$$P = GABS/0.18(V_p m_b) \text{ where}$$

$$GABS = \min(k_7 GUT, GABS_{max})$$

Figure 3.15 Structure of the meal glucose rate of appearance model. The model is characterised by a delta function to describe meal glucose input ($u_{CHO}(t)$), linear gastric emptying (k_6) and gut absorption (k_7) rates, and saturable gut absorption ($GABS_{max}$)

In this study, the complex digestion process including the hydrolysis of polysaccharides, are assumed linear and lumped into the simplified linear transport rates. This study uses a linear gastric emptying with rate constant, k_6, while the glucose input into the stomach compartment, $u_{CHO}(t)$, is described by a delta function.

Similar to the saturable gastric emptying rate of Lehmann and Deutsch [1992b], this study incorporates a saturable gut-absorption rate, $GABS_{max}$. Saturable gut-absorption has been postulated by Korach-Andre et al. [2004] in experiments using very large starch meals. However, this difference is likely to be small considering the minimal nature of both models.

Referring to Figure 3.16, the effective gut absorption rate is shown as a function of the mass of carbohydrate/glucose in the GUT compartment. The addition of the saturable term $GABS_{max}$ effectively makes the gut absorption rate non-linear as a function of the amount of carbohydrate in the gut. This dynamic is similar to that of the non-linear three-compartment model of Dalla Man et al. [2006] as shown in Figure 3.17. Unlike the model in this study however, the Dalla Man et al. model does not account for saturation of transport with increasing *size* of carbohydrate/glucose meal load but rather models the rate constant of gastric emptying as a fixed non-linear function of the proportion of glucose in the stomach compartment.

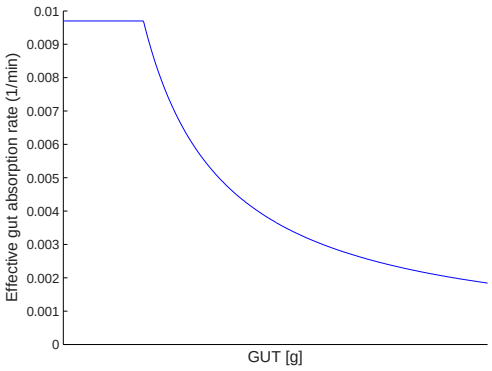

Figure 3.16 Qualitative plot of the effective gut absorption rate as a function of the mass of carbohydrate/glucose in the GUT compartment. While the processes of gastric emptying is linear, the addition of the saturable gut absorption term, $GABS_{max}$ of 1.1g/min effectively makes the process of gut absorption and, hence, meal glucose Ra, non-linear. At low glucose levels in the gut, the effective gut absorption rate is 0.0097min^{-1}.

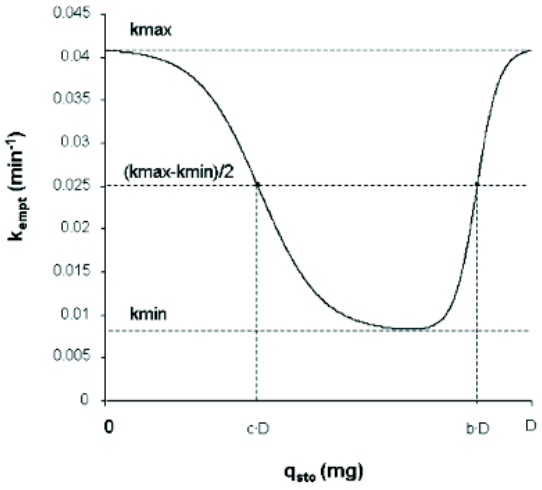

Figure 3.17 Qualitative plot of gastric emptying rate (k_{empt}) as a function of the amount of glucose in the stomach, q_{sto}: it equals k_{max} when the stomach contains the amount of the ingested glucose, D, then it decreases to a minimum (k_{min}). b is the percentage of the dose for which k_{empt} decreases at (k_{max}-k_{min})/2; c is the percentage of the dose for which k_{empt} is back to (k_{max}-k_{min})/2. Reproduced from Dalla Man et al. [2006].

3.4 Model Parameter Identification

The complete model derived in this study is shown in Figure 3.18. Unique identification of all model parameters in Figure 3.18 is difficult. Commonly used non-linear recursive least squares (NRLS) approaches are starting point dependent and computationally intense [Carson and Cobelli, 2001]. Used correctly, a wide range of starting values should be employed to enable identification of a global minimum [Thorsteinsson et al., 1987]. To overcome this problem, other methods have been proposed, such as Bayesian approaches employing *a priori* known parameter distributions to force parameter estimates into a physiological range [Carson and Cobelli, 2001; Pillonetto et al., 2002]. Nonetheless, with a rising number of parameters, unique identification becomes difficult, and often, several permutations of physiological parameters can result in a comparable fit to clinical data.

To overcome this limitation,the number of identified parameters must be reduced by exploiting known *a priori* physiological information to fix parameters to constant values or introduce relationships between them [Carson and Cobelli, 2001; Hann et al., 2005b; Hovorka et al., 1993].

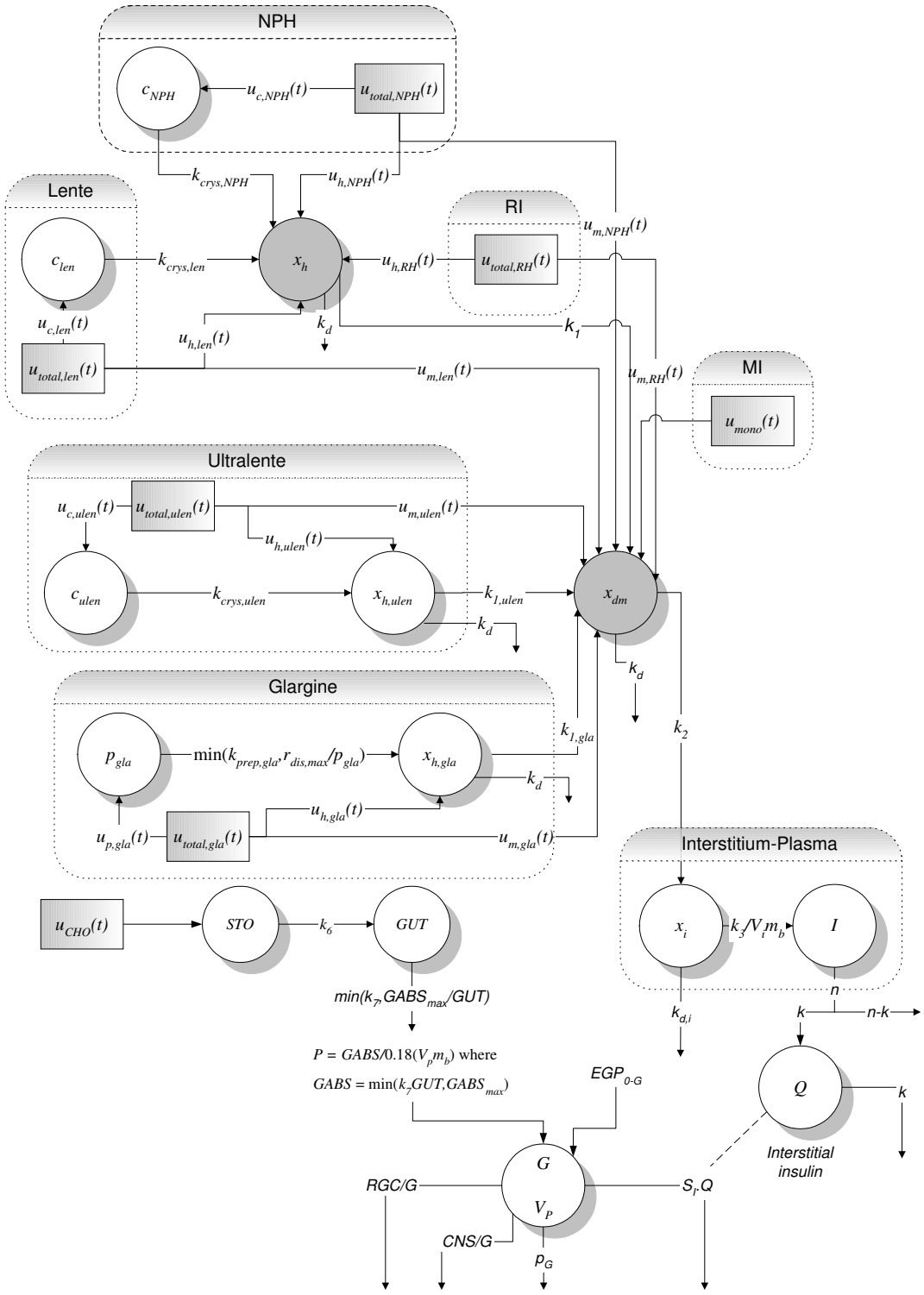

Figure 3.18 Complete glucose insulin pharmacodynamic system model and accompanying sc insulin pharmacokinetic and meal glucose rate of appearance models.

Referring to Table 3.12, the values of patient-independent model population

constants are *a priori* identified from literature. The renal glucose threshold, RGT, has been shown to vary considerably in Type 1 diabetes [Johansen et al., 1984; Rave et al., 2006] but a median value of 10mmol/l has been reported by Windhager [1992]. The glucose distribution volume, V_p, is taken to be 0.22l/kg, the same value used by Lehmann and Deutsch [1992b]. The glomerular filtration rate, GFR is taken as 0.12l/min or 120ml/min which reflects the average adult GFR of 125ml/min [Guyton and Hall, 2000].

Table 3.12 *A priori* identified model constants obtained from literature except the linear gastric emptying and gut absorption rates (k_6 and k_7 respectively) which are optimised using non-linear least squares to model-independent, mixed-meal tracer glucose Ra data [Dalla Man et al., 2004]

Model constants	Values [units]	References
$GABS_{max}$	1.1 [g/min]	Noah et al. [2000]
p_G	0.0060 [1/min]	Del Prato et al. [1997, 1995]
CNS	1.7 [mg/(kg.min)]	Del Prato et al. [1997, 1995]
EGP_{0-G}	3.0 [mg/(kg.min)]	Del Prato et al. [1997, 1995]
GFR	0.12 [l/min]	Guyton and Hall [2000]
RGT	10 [mmol/l]	Windhager [1992]
V_P	0.22 [l/kg]	Lehmann and Deutsch [1992b]
k_6	0.0388 [1/min]	Dalla Man et al. [2004]
k_7	0.0097 [1/min]	Dalla Man et al. [2004]

In a study by Dalla Man et al. [2004], the maximum meal Ra (Ra_{meal}) was ∼8-9mg/kg.min after an oral dose of 1g/kg glucose. In the study by Korach-Andre et al. [2004], the exogenous meal Ra (Ra_{exo}) was approximately 7-9mg/kg.min for a meal of 4g/kg of starch (∼4.4g/kg glucose). Despite a fourfold increase in glucose load, the maximum Ra remains at ∼9mg/kg.min or ∼0.72g/min for an average adult. In a study by Noah et al. [2000], a higher figure still of ∼11mg/kg.min is reported in a porcine model. The *maximum* value for the rate of gut absorption is hence taken as 1.1g/min using the Noah et al. study as a basis, assuming a 100kg body weight.

The proportion of glucose lost to first-pass splanchic uptake is still being debated with proportions from negligible [Ferrannini et al., 1985; Mari et al., 1994] to as high as 30% reported in some studies [Capaldo et al., 1999]. As there will be no tracer data in the application of the model in this study, negligible losses from first-pass splanchnic sequestration and complete absorption is assumed through necessity [Livesey et al., 1998].

The values of k_6 and k_7 are optimised using non-linear least squares to model-independent, mixed-meal, mean tracer glucose Ra data [Dalla Man et al., 2004] (results not shown).

Identification of S_I and EGP_{0-G} is performed using a linear and convex, integral-based parameter identification [Hann et al., 2005a]. This fitting method uses the integrals of the differential equations to reduce the non-linear estimation problem to a set of linear equations that can be easily solved by minimising the L_2-norm between the measured and estimated values. This method has the advantages of being convex and independent of starting point. Equally important, parameters can be defined as stepwise constants for different time segments to enable identification of time varying parameters if required [Hann et al., 2005b; Lotz et al., 2006a].

The method is demonstrated on Equation 3.21 to identify the parameters S_I and EGP_{0-G}, which is first integrated in the interval $[t_{i-1}, t_i]$.

$$\begin{aligned}
\int_{t_{i-1}}^{t_i} \dot{G}(t)\mathrm{d}t &= \int_{t_{i-1}}^{t_i} \big[EGP_{0-G} - p_G \cdot G(t) - \bar{S}_{I,i} \cdot G(t) \cdot Q(t) \\
&\quad - RGC(t) - CNS + P(t)\big]\mathrm{d}t \\
G(t_i) - G(t_{i-1}) &= \int_{t_{i-1}}^{t_i} \big[- RGC(t) - CNS + P(t)\big]\mathrm{d}t \\
&\quad + EGP_{0-G} \int_{t_{i-1}}^{t_i} \mathrm{d}t \\
&\quad - p_G \int_{t_{i-1}}^{t_i} G(t)\mathrm{d}t \\
&\quad - \bar{S}_{I,i} \int_{t_{i-1}}^{t_i} G(t) \cdot Q(t)\mathrm{d}t
\end{aligned} \tag{3.27}$$

Rearranging

$$\begin{aligned}
\bar{S}_{I,i} \int_{t_{i-1}}^{t_i} G(t) \cdot Q(t)\mathrm{d}t - EGP_{0-G}(t_i - t_{i-1}) &= \int_{t_{i-1}}^{t_i} \big[- RGC(t) - CNS + P(t)\big]\mathrm{d}t \\
&\quad - p_G \int_{t_{i-1}}^{t_i} G(t)\mathrm{d}t \\
&\quad - \big[G(t_i) - G(t_{i-1})\big]
\end{aligned} \tag{3.28}$$

All quantities on the RHS are known except $G(t)$, which is approximated as piecewise linear between discrete glucose measurement data, $\bar{G}$. Linear interpolation is sufficient in longer term data [Hann et al., 2005b] or control trials [Wong et al., 2005].

$$G(t) = \sum_{i=1}^{N} \left[\bar{G}_{i-1} + (\bar{G}_i - \bar{G}_{i-1}) \left(\frac{t - t_{i-1}}{t_i - t_{i-1}} \right) \right] \big(H(t - t_{i-1}) - H(t - t_i) \big) \quad (3.29)$$

The resulting errors of any reasonable approximation to the true curve can be shown to be very small due to the integrations over several time intervals [Hann et al., 2005b]. In addition, integral functions are robust to noise in measured $G(t)$ data, effectively applying low-pass filtration in the summations involved in numerical integration. Hence, the dominant sources of bias will be due to model, rather than computational or methodological error.

This integral-based approach effectively matches the area under the measured response curves for each interval considered. This approach is in contrast to standard, well accepted methods, that typically use gradients to directly match the response trajectory. Given the multiplication and summation operations used in the numerical integration, there are several analogies to a digital filtering identification process that could possibly be made. More importantly, this approach converts a computationally intense, non-convex problem into a much simpler convex problem, offering several advantages in speed and the quality of the results [Hann et al., 2006, 2005b].

Simplifying

$$\bar{A} \left\{ \begin{array}{c} \bar{S}_{I,i} \\ EGP_{0-G} \end{array} \right\} = \bar{b} \quad (3.30)$$

where

$$\begin{aligned}\bar{A} &= \left[\int_{t_{i-1}}^{t_i} G(t)\cdot Q(t)\mathrm{d}t \qquad (t_i - t_{i-1})\right] \\ \bar{b} &= \int_{t_{i-1}}^{t_i} \big[-RGC(t) - CNS + P(t)\big]\mathrm{d}t \\ &\quad - p_G \int_{t_{i-1}}^{t_i} G(t)\mathrm{d}t \\ &\quad - \big[G(t_i) - G(t_{i-1})\big]\end{aligned} \tag{3.31}$$

The $[t_{i-1}, t_i]$ time interval for the identification of $S_I(t)$ and EGP_{0-G} can be chosen arbitrarily but should reflect the resolution of $G(t)$ data available. The resulting set of linear equations can be solved using a linear solver for $\bar{S}_{I,i}$ and EGP_{0-G}. Whereas $S_I(t)$ is defined as a piecewise, time-variant step function over a data set (Equation 3.32 and Figure 3.19), EGP_{0-G} is defined as a constant value by appropriate adjustment of the coefficient of EGP_{0-G} in the expression for $\bar{A}$.

Integral-based parameter identification, as described, is a single step, computationally convex and fast method that only requires linearly interpolated data. By constraining the linear least squares estimation to non-zero values and smoothing the estimated S_I to remove the effects of noise, the resulting profile is physiologically accurate, and the effects caused by noisy data are reduced [Hann et al., 2005b].

$$S_I(t) = \sum_{i=1}^{N} \bar{S}_{I,i}\big(H(t - t_{i-1}) - H(t - t_i)\big) \tag{3.32}$$

Insulin-dependent clearance, determined by S_I, can be well identified, as the model is rich in information in this respect. By forcing the most variability into S_I (the only time-variant parameter) with the remainder of the parameters *a priori* identified from clinical literature, unique identification of S_I is assured. As such, $S_I(t)$ is the driving parameter behind the identified patient data.

The value of CNS is derived from results of studies by Del Prato and col-

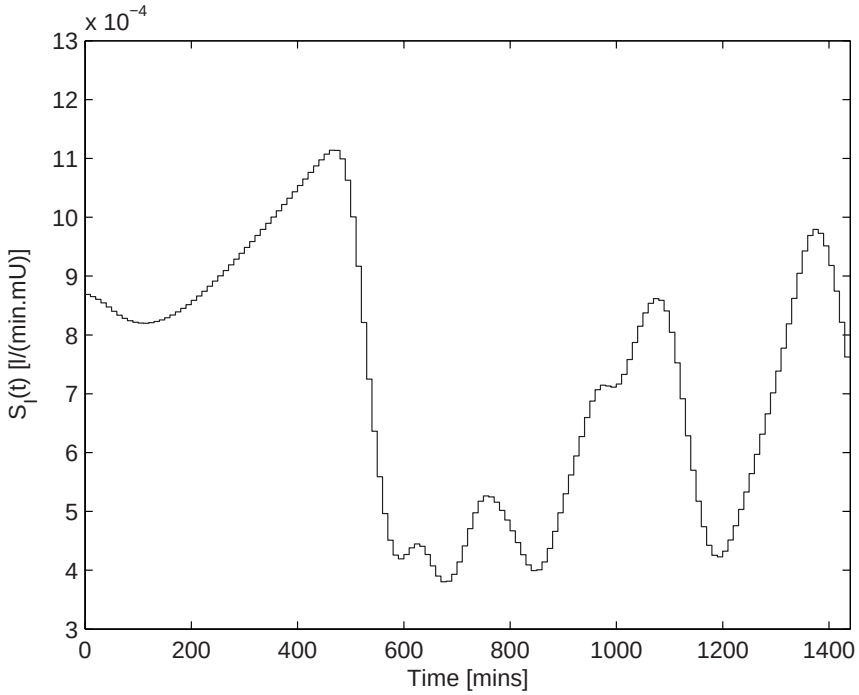

Figure 3.19 Sample patient $S_I(t)$ profile as obtained from model fit. Note the 10min interval for fitting the stepwise, time-variant $S_I(t)$.

leagues [Del Prato et al., 1997, 1995] as discussed in Subsection 3.3.2.2. Insulin-independent clearance, p_G, is difficult to estimate accurately without specialised experimental protocols to suppress endogenous insulin response [Best et al., 1996; Del Prato et al., 1997; Quon et al., 1994]. In addition, p_G effectively scales S_I, and identifying *both* using integral-based identification may lead to non-unique identifiability of either parameter. By fixing this constant as a population value across cohorts, the bias introduced by this effect is only systematic and equal in magnitude across all individuals, thus not introducing added variability. Thus, p_G can be fixed *a priori* to a mean value from the literature. In this case, a value of $p_G = 0.006\text{min}^{-1}$ is chosen in accordance with Del Prato et al. [1997, 1995] as discussed in Subsection 3.3.2.2 as well as others [Quon et al., 1994; Regittnig et al., 1999].

3.5 Conclusions

The model structure chosen for this application is a mono-compartmental description, similar to the Minimal Model and the model used in previous glycaemic control research at the University of Canterbury [Chase et al., 2005b]. Many glucose-insulin pharmacodynamic (PD) system models have been presented in previous research, ranging from one- to three-compartments. Identification of glucose model parameters is difficult. A mono-compartment description with minimal parameters can be used with good performance if identified correctly. The derived glucose PD model contains insulin-independent and insulin-dependent glucose losses and accounts for endogenous and exogenous glucose input.

This knowledge, combined with the modelled peripheral insulin from Chapter 2 and the integral-based fitting method, allows for a robust and fast estimation of insulin sensitivity S_I, as shown schematically in Figure 3.12. The model and method is simple, requires minimal data, and is thus well suited for use in an *in silico* simulation or clinical setting. A figure of the entire model is shown in Figure 3.18 with the sc insulin model developed in Chapter 2.

The model enables a physiological and accurate description of the relevant metabolic dynamics of the hormone and is useful for application in a simulation setting. The estimation method developed employs *a priori* information, combined with a robust and convex integral-based estimation, for a fast and physiological identification of S_I. With the conclusion of the modelling segment, the necessary tools for *in silico* simulation of glycaemic control protocols are now ready. In the next chapter, a virtual patient cohort is identified and an *in silico* simulation tool is developed for testing glycaemic control protocols in simulation.

Chapter 4

In Silico Simulation of Glycaemic Control

This chapter reports the identification on a virtual patient cohort of the glucose-insulin pharmacodynamic system model developed in Chapter 3. This chapter also reports the development of a simple and practical, adaptive method for control of Type 1 diabetes, and subsequent *in silico* simulation on a virtual patient cohort. The *in silico* simulation method presented is an efficient, clinically validated way [Chase et al., 2007, 2008; Hovorka et al., 2004, 2005; Lonergan et al., 2006b; Wilinska et al., 2006] to develop and test control algorithms and methods.

4.1 Methods

4.1.1 Patient Cohort

The patient data used in this study is obtained from AIDA on-line^2, the web-based version of the AIDA educational diabetes program [Reed and Lehmann, 2005]. AIDA on-line^2 incorporates the physiological model developed by Lehmann and Deutsch [1992b] and can simulate glycaemic levels for any insulin or meal stimuli over a period of one day. The patient data (n=40) for this study are obtained from sample diabetes case scenarios available with AIDA on-line^2. Referring to Table 4.1 and 4.2, each patient case is unique in body weight, meal/carbohydrate consumed, and insulin treatment. Each patient also has unique clinical variables of hepatic and peripheral insulin sensitivity, glucose renal threshold, and glomerular filtration rate. Hence, the AIDA on-line^2 cohort represents a broad range of patients and possible clinical behaviour. To retrieve the blood glucose, plasma

insulin and meal glucose absorption rate from AIDA on-line[2], the 'Advanced' display is selected to output the data in text format. A sample of this data is shown in Figure 4.1.

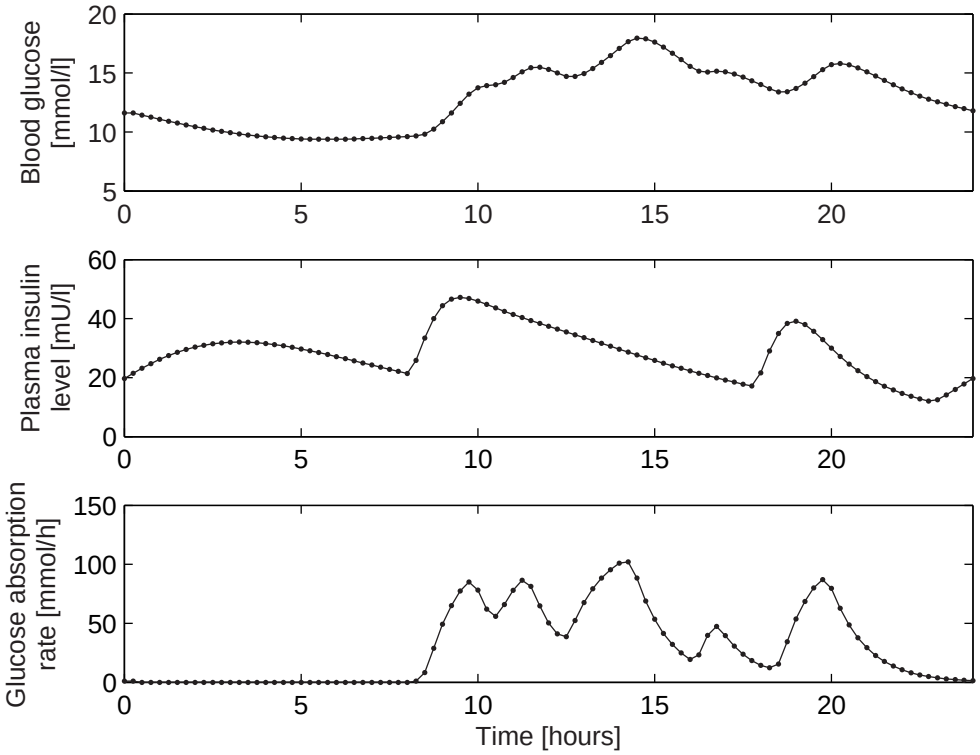

Figure 4.1 Sample raw blood glucose, plasma insulin level and glucose absorption rate data from AIDA on-line[2] [Reed and Lehmann, 2005].

4.1.2 Simulation Method

For *in silico* simulation, the virtual patient method is used [Chase et al., 2007, 2008; Lonergan et al., 2006b]. This method has been utilised to develop effective glycaemic control protocols by simulating the physiological glycaemic response to glucose and insulin stimuli [Chase et al., 2007, 2008; Lonergan et al., 2006b]. The glycaemic responses are generated with patient-specific $S_I(t)$ profiles derived from retrospective data. This clinically validated method [Chase et al., 2007] enables extensive simulations to be performed in a short time for rapid development and testing of any control methodology. The *in silico* simulation was performed using MATLAB® (The Mathworks, Natick, MA, USA) implemented on a PC notebook

(Pentium M 1.7Ghz).

To obtain the retrospective $S_I(t)$ patient data profiles, the model is first fitted to the glucose data from AIDA on-line^2 using the linear and convex, integral-based parameter identification method described in Chapter 3. AIDA on-line^2 uses a first-order Euler integration method with a 15mins step-size to solve its plasma glucose model equation [Lehmann and Deutsch, 1992b, 1993].

The AIDA on-line^2 data is a simulation of the patient steady-state response to fixed, daily insulin and dietary stimuli. To make the results of this study comparable, simulations are performed over a period of three days with the same, fixed insulin and dietary stimuli. Plasma glucose, insulin, and meal Ra profiles from the third day are considered steady-state (AIDA assumes the data from the second day are steady state [Lehmann and Deutsch, 1992b, 1993]) and are taken as the final result. A MATLAB® numerical ode solver is used to solve the model equations with a 1min time step. Biphasic insulin preparations are treated as in AIDA with the insulin response assumed to be a superposition of the individual components of the preparation [Lehmann and Deutsch, 1992b]. This is an acknowledged simplification considering the large variety and lack of data on such preparations.

4.1.3 Model Fit Error to Data from Patient Cohort

To gauge the model fit to data, the absolute and absolute percentage errors of the $G(t)$ model fit to the AIDA on-line^2 patient data cohort are shown in Table 4.3 to 4.5. In Table 4.3, per patient errors are shown while the total errors over the entire cohort are shown in Table 4.5. A sample $G(t)$ fit to data from Patient 1 is also shown in Figure 4.2.

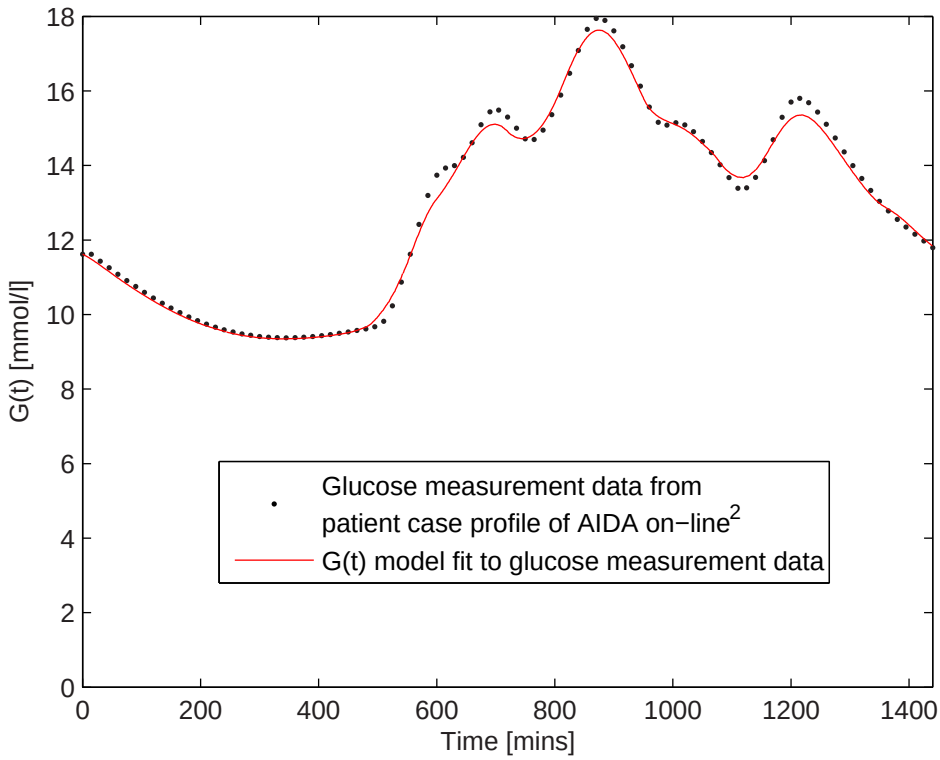

Figure 4.2 $G(t)$ model fit to glucose measurement data for Patient 1 shown with the glucose measurement data from AIDA on-line[2].

Table 4.1 Details of the patient cohort (n=40) from AIDA on-line[2] showing body weight, total carbohydrate consumed, total prandial insulin dose, total basal insulin dose, and the unique clinical variables of hepatic and peripheral insulin sensitivity, glucose renal threshold, and glomerular filtration rate

Case number	Body weight [kg]	Total carbohydrate consumed [g]	Total prandial insulin dose [U]	Total basal insulin dose [U]	Renal threshold	Renal function	Hepatic insulin sensitivity	Peripheral insulin sensitivity
1	70	130	7	30	Normal	Normal	Reduced	Reduced
2	68	180	13	10	High	Normal	Increased	Increased
3	70	120	9	13	Normal	Normal	Normal	Increased
4	60	180	13	12	Normal	Normal	Increased	Increased
5	98	180	12	12	Normal	Normal	Normal	Normal
6	76	120	8	28	Normal	Normal	Reduced	Increased
7	70	90	7	24	Normal	Normal	Increased	Reduced
8	70	120	10	20	Normal	Normal	Reduced	Increased
9	70	180	12	12	High	Normal	Normal	Increased
10	70	120	15	8	Normal	Normal	Normal	Increased
11	70	205	16	22	Normal	Normal	Normal	Increased
12	70	185	24	20	Normal	Normal	Reduced	Increased
13	76	100	8	26	Normal	Normal	Normal	Increased
14	65	70	5	20	Normal	Normal	Reduced	Normal
15	99	115	6	42	Normal	Normal	Reduced	Normal
16	70	180	9	32	Normal	Normal	Reduced	Increased
17	70	110	10	24	Normal	Normal	Reduced	Increased
18	60	165	18	36	High	Normal	Reduced	Increased
19	60	180	12	12	Normal	Normal	Normal	Increased
20	70	105	8	36	Normal	Normal	Normal	Increased
21	98	295	34	40	Normal	Normal	Reduced	Reduced
22	75	70	Biphasic 40		Normal	Normal	Reduced	Reduced
23	87	177	38	12	Normal	Normal	Reduced	Increased

Table 4.2 Details of the patient cohort (n=40) from AIDA on-line[2] showing body weight, total carbohydrate consumed, total prandial insulin dose, total basal insulin dose, and the unique clinical variables of hepatic and peripheral insulin sensitivity, glucose renal threshold, and glomerular filtration rate (continued)

Case number	Body weight [kg]	Total carbohydrate consumed [g]	Total prandial insulin dose [U]	Total basal insulin dose [U]	Renal threshold	Renal function	Hepatic insulin sensitivity	Peripheral insulin sensitivity
24	76	95	7	24	Normal	Normal	Normal	Increased
25	70	120	18	28	Normal	Normal	Reduced	Normal
26	80	170	Biphasic 20		Normal	Normal	Normal	Increased
27	70	120	9	13	Low	Normal	Normal	Normal
28	75	85	5	40	Normal	Normal	Normal	Increased
29	83	60	12	25	Normal	Normal	Reduced	Normal
30	80	165	16	36	Normal	Normal	Reduced	Increased
31	99	220	29	14	Low	Normal	Normal	Increased
32	90	70	0	28	Normal	Normal	Reduced	Reduced
33	98	180	0	18	Normal	Normal	Normal	Increased
34	60	175	17	13	High	Normal	Normal	Increased
35	60	170	22	10	Normal	Normal	Normal	Increased
36	70	100	8	32	Normal	Normal	Reduced	Increased
37	70	105	9	36	High	Normal	Reduced	Reduced
38	70	95	Biphasic 26		Normal	Normal	Normal	Reduced
39	70	110	12	35	High	Normal	Reduced	Increased
40	76	100	7	30	Normal	Normal	Normal	Normal

Table 4.3 Per patient absolute and absolute percentage $G(t)$ model fit error to the patient cohort data (n=40) from AIDA on-line[2]

Case number	Absolute % $G(t)$ fit error [%]			Absolute $G(t)$ fit error [mmol/l]		
	Median	5^{th} percentile	95^{th} percentile	Median	5^{th} percentile	95^{th} percentile
1	0.84	0.08	2.87	0.10	0.01	0.43
2	1.28	0.05	7.14	0.10	0.00	0.50
3	1.19	0.02	3.56	0.12	0.00	0.37
4	1.72	0.05	7.84	0.12	0.00	0.42
5	0.94	0.11	3.24	0.11	0.01	0.36
6	1.25	0.04	4.89	0.13	0.00	0.53
7	1.93	0.11	4.52	0.07	0.00	0.20
8	0.96	0.05	4.46	0.09	0.00	0.49
9	1.03	0.10	2.94	0.12	0.01	0.39
10	1.92	0.28	4.27	0.17	0.02	0.39
11	3.09	0.20	14.04	0.20	0.01	2.39
12	1.23	0.05	8.78	0.13	0.00	0.70
13	1.08	0.09	4.80	0.07	0.00	0.26
14	0.47	0.04	3.43	0.05	0.00	0.47
15	1.00	0.12	3.84	0.08	0.01	0.29
16	1.61	0.11	5.84	0.18	0.01	0.59
17	1.31	0.06	4.38	0.13	0.00	0.38
18	3.34	0.32	7.84	0.21	0.03	0.80
19	1.23	0.09	4.14	0.16	0.01	0.52
20	2.89	0.17	21.39	0.13	0.00	0.89
21	2.73	0.49	7.17	0.32	0.06	0.93
22	0.88	0.11	3.95	0.09	0.01	0.50
23	1.50	0.03	4.96	0.11	0.00	0.33
24	1.98	0.21	6.67	0.14	0.01	0.43
25	1.37	0.02	7.44	0.09	0.00	0.59
26	0.67	0.09	2.48	0.07	0.01	0.31
27	0.69	0.08	2.74	0.06	0.01	0.27
28	0.81	0.09	6.27	0.05	0.00	0.36
29	0.81	0.15	4.48	0.07	0.01	0.40
30	9.36	0.98	37.10	0.72	0.06	2.56
31	1.16	0.11	8.67	0.08	0.01	0.44
32	0.60	0.06	2.36	0.06	0.01	0.28
33	0.93	0.13	2.72	0.10	0.01	0.29
34	1.84	0.01	5.93	0.15	0.00	0.44
35	3.30	0.18	11.70	0.26	0.01	1.06

Table 4.4 Per patient absolute and absolute percentage $G(t)$ model fit error to the patient cohort data (n=40) from AIDA on-line[2] (continued)

Case number	Absolute % $G(t)$ fit error [%]			Absolute $G(t)$ fit error [mmol/l]		
	Median	5^{th} percentile	95^{th} percentile	Median	5^{th} percentile	95^{th} percentile
36	1.36	0.19	5.05	0.12	0.01	0.39
37	0.94	0.03	3.38	0.12	0.00	0.46
38	0.73	0.08	3.07	0.08	0.01	0.40
39	1.29	0.04	5.53	0.11	0.00	0.51
40	1.70	0.20	7.20	0.10	0.01	0.31
Median	1.24	0.09	4.85	0.11	0.01	0.43
Range	0.47-9.36	0.01-0.98	2.36-37.10	0.05-0.72	0.00-0.06	0.20-2.56

Table 4.5 Total absolute and absolute percentage $G(t)$ model fit error to the patient cohort data (n=40) from AIDA on-line[2]

Absolute % $G(t)$ fit error [%]			Absolute $G(t)$ fit error [mmol/l]		
Median	5^{th} percentile	95^{th} percentile	Median	5^{th} percentile	95^{th} percentile
1.33	0.08	7.20	0.12	0.01	0.56

From Table 4.3 and 4.4, the per patient median (95% range) absolute percentage error in $G(t)$ is 1.24% (0.09-4.85%), which translates into a per patient absolute error in $G(t)$ of 0.11mmol/l (0.01-0.43mmol/l). Over the entire cohort the figures are 1.33% (0.08-7.20%) and 0.12mmol/l (0.01-0.56mmol/l) as shown in Table 4.5, which are similar. The errors reported are extremely low and within the measurement errors of clinical methods of glucose measurement in current use. This shows that the model and S_I identification method are capable of capturing all patient $G(t)$ dynamics, which will produce a more physiologically accurate simulation.

4.1.4 Glucose measurement, insulin type and meals

The control protocols developed and tested in this study aim to treat the broad Type 1 diabetes population using conventional techniques, i.e., self-monitoring blood glucose (SMBG) measurement, and multiple daily injection (MDI) therapy. Hence, the control protocols may only receive discrete glucose data at sparse intervals characteristic of SMBG. Measurement frequencies of 2, 4, 6, 8 and 10/day are simulated in this study.

The AIDA on-line[2] virtual cohort is treated with a range of short-acting, older intermediate/long-acting, or biphasic insulin [Lehmann and Deutsch, 1992b, 1993; Reed and Lehmann, 2005]. In this study, only rapid-acting monomeric insulin (MI) analogues and the basal insulin analogue glargine are used. Insulin analogues have a more physiological and less variable pharmacokinetic profile than traditional insulin preparations [Guerci and Sauvanet, 2005] and allow more faithful basal-bolus insulin replacement [Stephens and Riddle, 2003].

Clinically, reduced hypoglycaemia and glycosylated haemoglobin (HbA_{1c}) have been associated with insulin glargine and MI [Distiller and Joffe, 2006; Gallen and Carter, 2003]. MI injected at the start of meals reduced postprandial glucose excursions compared to regular human insulin injected 30mins prior [Anderson et al., 1997]. In addition, only one daily insulin glargine injection is required for basal insulin replacement [Heinemann et al., 2000].

These are the key clinical reasons insulin analogues are chosen. While suboptimal glycaemic control is as much a symptom of poorly-adapted treatment

strategy [Samann et al., 2005] as insulin type, it is logical to begin with the least compromised insulin preparations. The insulin model used in this study is capable of modelling the pharmacokinetic profiles of both MI analogues and insulin glargine as shown in Chapter 2.

The meal carbohydrate content is assumed known to the patient through carbohydrate counting [Bruttomesso et al., 2001; Gregory and Davis, 1994; Warshaw and Kulkarni, 2004]. While the technique is only approximate and can be prone to inaccuracy [Kildegaard et al., 2007], it remains the key clinical strategy recommended by the ADA to estimate the glycaemic effect of meals for the purpose of adjusting insulin dosage [ADA, 2006b].

4.1.5 Control methodology

In this study, two prandial insulin treatment protocols, a conventional control protocol (CC) and the adaptive control protocol (AC) developed in this study, are simulated *in silico*. The controls protocol is an unpublished protocol used to treat the AIDA on-line^2 cohort and is not the AIDA [Lehmann and Deutsch, 1992a] or AIDA^2 [Lehmann and Deutsch, 1993] insulin dosage advisors. The controls group results are calculated from the AIDA on-line^2 patient data (the same data used to generate the virtual patient profiles for this *in silico* study). Hence, *in silico* simulation is not required for the controls group. For each tested protocol, SMBG frequencies of 2, 4, 6, 8 and 10/day are tested. In addition, a basal insulin titration regimen is used with both protocols to observe the outcome of optimal basal insulin replacement using insulin glargine compared to controls. The target blood glucose is 5mmol/l and a maximum bolus dose of 15U is assumed for both protocols.

Conventional control (CC)

The CC protocol is based on a published IIT [BD Diabetes Learning Centre, 2006; Hanas, 2005; Walsh and Roberts, 1994]. The protocol administers a bolus at the start of the meal, $t_{meal,i}$ (where $t_{meal,i}$ is the time of the ith meal). One glucose measurement at the start of the meal is required to calculate the bolus size. The CC protocol is not adaptive as it uses fixed, suboptimal, patient-specific

parameters determined from the original AIDA on-line[2] patient data. Referring to Figure 4.3, the Carbohydrate-to-Insulin (CIR) ratio is determined for each patient using the 450 Rule for regular insulin (37 out of the 40 patients in the cohort are treated with regular insulin) [Walsh and Roberts, 1994]. In contrast, the 500 Rule is used if the patient is treated with MI [Walsh and Roberts, 1994]. The CIR can also be calculated with the following equation:

$$\text{CIR [g of carb per U regular insulin]} = \frac{450}{\text{Total Daily Insulin Dose}} \tag{4.1}$$

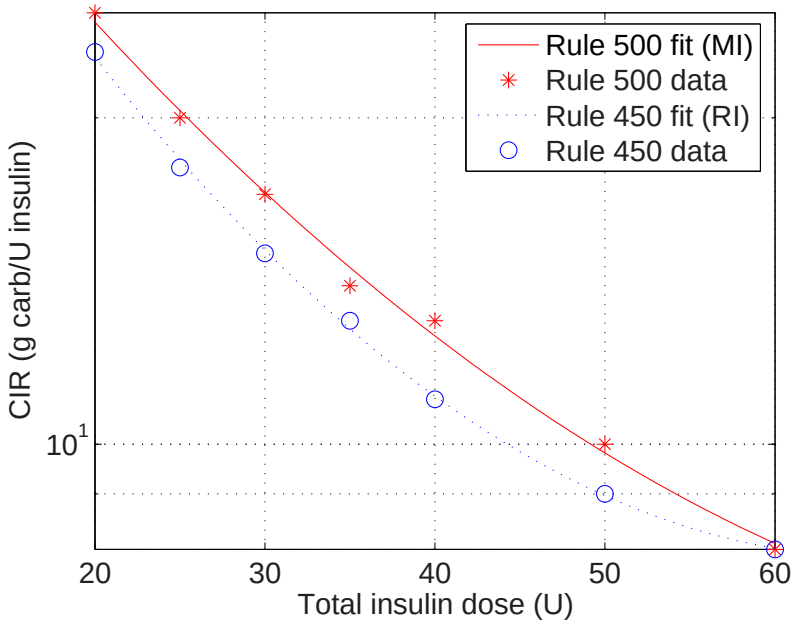

Figure 4.3 The carbohydrate-to-insulin (CIR) ratio is determined for each patient using the 450 Rule for regular insulin (37 out of the 40 patients in the cohort are treated with regular insulin with the rest on biphasic insulin). Data reproduced from Walsh and Roberts [1994].

Referring to Figure 4.4, an insulin sensitivity factor (ISF) is similarly determined for each patient using the 1500 Rule for regular insulin [Hanas, 2005]. As in the calculation of CIR, the 1800 Rule is used instead if the the patient is treated with MI [Hanas, 2005]. The ISF can also be calculated using the following equation:

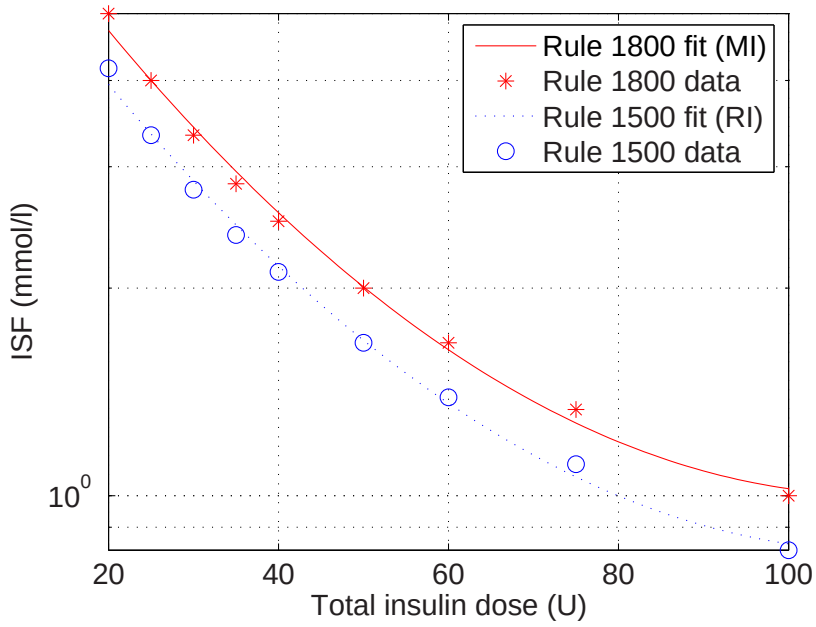

Figure 4.4 The insulin sensitivity factor (ISF) is determined for each patient using the 1500 Rule for regular insulin. Data reproduced from Hanas [2005].

$$\text{ISF [mmol/l per U regular insulin]} = \frac{1500}{18 \times \text{Total Daily Insulin Dose}} \tag{4.2}$$

Using the patient CIR and ISF parameters, the CC protocol then calculates the ith prandial insulin dose assuming that the ith meal carbohydrate count is known from carbohydrate counting.

$$\text{Prandial dose}_i\text{[U]} = \min(\text{Maximum bolus dose}, \text{Meal dose}_i + \text{Correction dose}_i) \tag{4.3}$$

where

$$\text{Meal dose}_i\text{[U]} = \left(\frac{\text{Meal carbohydrate count}_i}{\text{CIR}}\right)$$

$$\text{Correction dose}_i\text{[U]} = \left(\frac{\bar{G}^i_{meal} - \text{Target blood glucose}}{\text{ISF}}\right)$$

Adaptive control (AC)

The AC protocol utilises an adaptive method to determine the prandial insulin dose. The protocol comprises a twin bolus regimen per meal, with a conservative initial bolus, and an aggressive second bolus to accurately restore glycaemia to basal. The second bolus is administered 90mins after the start of the meal and, hence, the first bolus. The first bolus is dosed according to the CC protocol. As such, two glucose measurements are required per meal, $\bar{G}^i_{meal,1}$ and $\bar{G}^i_{meal,2}$ before each bolus, at $t_{meal,i}$ and $t_{meal,i}$+90 (where $t_{meal,i}$ is the time of the ith meal).

This time interval between boluses of 90mins is not arbitrary. In normal individuals, plasma glucose is restored to pre-meal basal levels in approximately 120mins [Dalla Man et al., 2004] for a normal meal (∼1g glucose/kg body weight) and up to 360mins [Korach-Andre et al., 2004] for a very large meal (∼4.5g glucose/kg body weight). The 90min time interval chosen ensures minimal postprandial hyperglycaemic exposure. In addition, the time to peak plasma concentration after MI injection ranges from 30-70mins [Lindholm et al., 1999], which ensures the second bolus is administered only after the plasma insulin concentration from the first bolus has peaked, and approximately 30mins to the peak pharmacodynamic effect of the first bolus [Woodworth et al., 1993]. Hence, the 90min time interval is a compromise, injecting the second bolus as late as possible for the first bolus to reach its pharmacodynamic peak for safety, while ensuring that the plasma insulin concentration does not wane, but is maintained and increased as necessary to minimise postprandial glycaemic excursion.

The AC protocol is adaptive by optimising the patient-specific model parameter S_I to glucose measurement data. Accurately identifying the current patient condition in S_I allows the safer administration of the aggressive insulin bolus. Referring to Equation 4.7, $G(t)$ for the identification of S_I is linearly interpolated from the glucose measurements $\bar{G}^i_{meal,1}$ and $\bar{G}^i_{meal,2}$. For the ith meal, the identified patient $\bar{S}_{I,i}$ between the measurements at $t_{meal,i}$ and $t_{meal,i}$+90 is used to predict the glycaemic response of the patient in the period $\geq t_{meal,i}$+90 to some prediction end point, t_{pred} as shown in Equation 4.8.

$$\begin{aligned}\int_{t_i}^{t_i+90}\dot{G}(t)\mathrm{d}t &= \int_{t_i}^{t_i+90}\big[EGP_{0-G} - p_G\cdot G(t) - \bar{S}_{I,i}\cdot G(t)\cdot Q(t)\\ &\quad - RGC(t) - CNS + P(t)\big]\mathrm{d}t\\ G(t_{meal,i}+90) - G(t_{meal,i}) &= \int_{t_i}^{t_i+90}\big[EGP_{0-G} - RGC(t) - CNS + P(t)\big]\mathrm{d}t\\ &\quad - p_G\int_{t_i}^{t_i+90}G(t)\mathrm{d}t\\ &\quad - \bar{S}_{I,i}\int_{t_i}^{t_i+90}G(t)\cdot Q(t)\mathrm{d}t \qquad (4.4)\end{aligned}$$

Rearranging

$$\begin{aligned}\bar{S}_{I,i}\int_{t_i}^{t_i+90}G(t)\cdot Q(t)\mathrm{d}t &= \int_{t_i}^{t_i+90}\big[EGP_{0-G} - RGC(t) - CNS + P(t)\big]\mathrm{d}t\\ &\quad - p_G\int_{t_i}^{t_i+90}G(t)\mathrm{d}t\\ &\quad - \big[G(t_{meal,i}+90) - G(t_{meal,i})\big] \qquad (4.5)\end{aligned}$$

Substituting the measurements, $\bar{G}^i_{meal,1}$ and $\bar{G}^i_{meal,2}$

$$\begin{aligned}\bar{S}_{I,i}\int_{t_i}^{t_i+90}G(t)\cdot Q(t)\mathrm{d}t &= \int_{t_i}^{t_i+90}\big[EGP_{0-G} - RGC(t) - CNS + P(t)\big]\mathrm{d}t\\ &\quad - p_G\int_{t_i}^{t_i+90}G(t)\mathrm{d}t\\ &\quad - \big[\bar{G}^i_{meal,2} - \bar{G}^i_{meal,2}\big] \qquad (4.6)\end{aligned}$$

where $G(t)$ in the time interval $[t_{meal,i}, t_{meal,i}+90]$ is approximated as:

$$\begin{aligned}G(t_{meal,i}\le t\le t_{meal,i}+90) &= G(t_{meal,i})\\ &\quad + \big[G(t_{meal,i}+90) - G(t_{meal,i})\big]\left(\frac{t-t_{meal,i}}{90}\right)\\ &= \bar{G}^i_{meal,1} + (\bar{G}^i_{meal,2} - \bar{G}^i_{meal,1})\left(\frac{t-t_{meal,i}}{90}\right) \qquad (4.7)\end{aligned}$$

Piecewise linear interpolation between discrete glucose measurement data is sufficient in longer term data [Hann et al., 2005b] or control trials [Wong et al., 2005]. Then, assuming S_I remains constant over the prediction horizon,

$$S_I(t_{meal,i} + 90 \leq t \leq t_{pred}) = \bar{S}_{I,i} \tag{4.8}$$

Once the patient $\bar{S}_{I,i}$ is known, the second bolus dose is determined iteratively. From Equation 4.8, a predicted glycaemic response is generated up to a prediction horizon of 2hrs ($t_{pred} = t_{meal,i}$+90+120). The objective of the iteration is to achieve the 5mmol/l target blood glucose level from the predicted glycaemic response within the 2hr prediction horizon. If $\bar{G}^{i}_{meal,3} \leq$ target blood glucose level of 5mmol/l, or if the iteration results in a zero dose (the predicted glucose response *without* an administered second bolus achieves the target blood glucose level within the prediction horizon), then no second bolus is administered. If the iteration results in a dose exceeding the 15U maximum bolus dose, then the full 15U is administered. In all iterations, using the model enables all incoming glucose and insulin from prior MI and insulin glargine doses to be accurately accounted for in determining the correction bolus.

4.1.6 Basal insulin titration regimen

To optimise basal insulin replacement, a protocol based on the forced-titration regimens of Fritsche et al. [2003] and Riddle et al. [2003] is used (see Table 4.6). Unlike other basal dosing schemes [DeWitt and Dugdale, 2003; Holman and Turner, 1985], this regimen has been shown to be clinically effective in a treat-to-target trial [Riddle et al., 2003]. The Fritsche et al. protocol does not specify a dose decrement if hypoglycaemia occurs, but the similar Riddle et al. protocol specifies a small dose decrement of 2-4U/day if the fasting plasma glucose (FPG) is below 3.0mmol/l. Hence, referring to Table 4.6, the protocol decreases the basal dose by 2U/day if FPG<3mmol/l and by 4U/day if FPG<2mmol/l.

As in Riddle et al. [2003], the FPG is assumed to be the pre-breakfast blood glucose level and is closest to the ADA definition for FPG of 'no caloric intake for at least 8hrs' [ADA, 2006b]. The single daily glargine dose is injected at the last meal of the day instead of bedtime (as in Riddle et al.) as it does not require

Table 4.6 The basal insulin dosing regimen used to optimise the single, daily insulin glargine dose based on the forced-titration regimens of Fritsche et al. [2003] and Riddle et al. [2003]. This regimen incorporates a dose decrement if hypoglycaemia occurs which the Riddle et al. protocol does not specify explicitly. The initial basal dose is chosen to be 80% of the total basal dose from original patient data, i.e., AIDA on-line[2]

Fasting plasma glucose (FPG) [mmol/l]	Initial dose equivalent to 80% of total basal dose	
	Increment in glargine dose [U/day]	Decrement in glargine dose [U/day]
≥10.0	8	-
≥7.8 and <10.0	6	-
≥6.7 and <7.8	4	-
≥5.6 and <6.7	2	-
≥3.0 and <5.6	-	-
≥2.0 and <3.0	-	2
<2	-	4

assumptions about bed times and is unlikely to affect the titration scheme. Unlike Riddle et al., the initial basal dose is chosen to be 80% of the total basal dose from the original patient data, which is recommended for patients changing over to insulin glargine from other basal insulin types [Sanofi-Aventis, 2007]. The Riddle et al. initial basal dose of 10U is recommended only for insulin naïve patients and is less suitable for this study [Sanofi-Aventis, 2007]. The maximum insulin glargine dose is limited to 80U (hence 80U/day) even though doses up to 100U can be clinically prescribed [Sanofi-Aventis, 2007]. In the case of suboptimal basal insulin replacement, the basal insulin therapy from the controls cohort (the AIDA on-line[2] patient data) is used.

4.1.7 Location of SMBG measurements

SMBG frequencies of 2, 4, 6, 8 and 10/day are examined. For both the CC and AC protocols, the first SMBG measurement is always located at the start of breakfast (the approximate FPG) to titrate the basal insulin dose. For the CC protocol, each subsequent SMBG measurement is located at the start of the meal in descending order of meal size. As the AC protocol requires 2 SMBG measurements per meal, the second SMBG measurement is always 90mins after breakfast. Each subsequent pair of SMBG measurements is located at the start and 90mins after the start of the meal in descending order of meal size. Thus, additional pairs of measurements occur at lunch/dinner followed by between-meal

snacks. Hence, for an equivalent SMBG frequency, the CC protocol covers double the number of meals.

4.1.8 HbA_{1c} calculation

Glycosylated haemoglobin, HbA_{1c}, is one of two clinical assessment techniques for glycaemic control recommended by the ADA [ADA, 2006b]. The test assesses glycaemic control over the preceding 2-3 months [Sacks et al., 2002]. To be comparable to the AIDA on-line[2] data [Lehmann and Deutsch, 1993], the simulations in this study are prepared for steady-state glucose and insulin stimuli (although the control protocols tested are not limited in this respect). The resulting steady-state glycaemic response can then be used to calculate an indicative and approximate HbA_{1c} value [Rohlfing et al., 2002], if the control is assumed to be relatively constant over a 2-3 month period. From Rohlfing et al. [2002], HbA_{1c} can be defined as a linear function of mean plasma glucose only. Referring to Figure 4.5 of data reproduced from Rohlfing et al., a HbA_{1c} regression equation can be estimated.

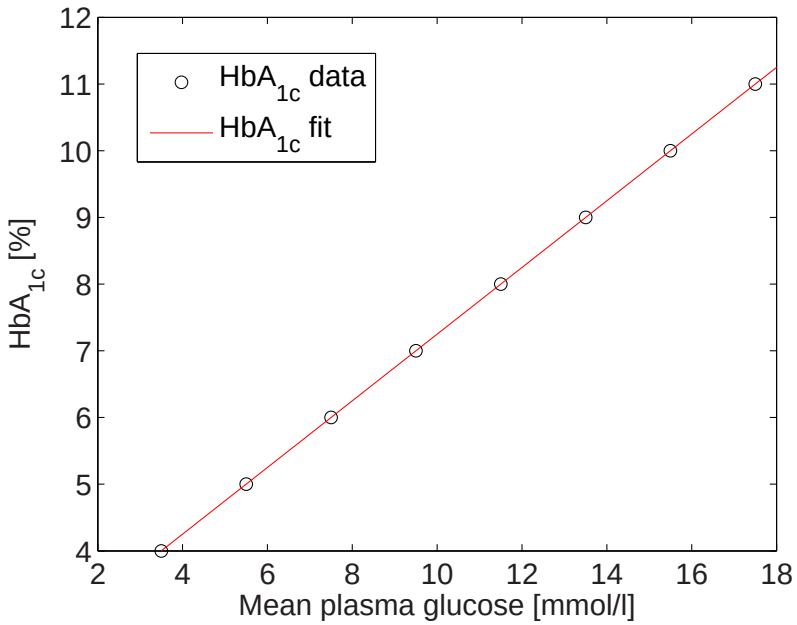

Figure 4.5 Estimating HbA_{1c} from mean plasma glucose with linear regression. Data reproduced from Rohlfing et al. [2002]

$$\mathrm{HbA}_{1c} = 0.5 \cdot \mathrm{MBG} + 2.25 \tag{4.9}$$

where

$$\mathrm{MBG} = \text{Mean blood glucose concentration [mmol/l]}$$

The MBG is calculated as the arithmetic mean of the 24h simulated glycaemic profile (1min time step). Compared to the HbA_{1c} regression equation in Equation 4.10 adapted from by AIDA on-line[2] [Lehmann, 2001], the Rohlfing et al. equation is more conservative.

$$\mathrm{HbA}_{1c} = 0.6 \cdot \mathrm{MBG} + 2.87 \tag{4.10}$$

The HbA_{1c} value calculated with Equation 4.9, while approximate and only if the control is assumed to persist for 2-3 months, provides a clinically significant performance metric to the results of this study. In particular, the DCCT [DCCT Research Group, 1993] and others have shown clinical outcomes as functions of HbA_{1c}, which is a reliable and accepted metric in large intervention trials.

4.1.9 Summary of simulations performed

4 controllers are simulated. These controllers are:

1. AC prandial insulin protocol - optimal basal insulin
2. AC prandial insulin protocol - suboptimal basal insulin
3. CC prandial insulin protocol - optimal basal insulin
4. CC prandial insulin protocol - suboptimal basal insulin

For each controller, SMBG frequencies of 2, 4, 6, 8 and 10/day are simulated, giving 20 simulations in total (5 SMBG frequencies simulated per controller type).

The controls cohort results are calculated from the AIDA on-line[2] patient data (the same data used to generate the virtual patient profiles for this *in silico* study). The results are not from the AIDA or AIDA[2] insulin dosage advisors [Lehmann and Deutsch, 1992a, 1993]. Hence, no *in silico* simulation is required for the controls group. Optimal basal insulin replacement is performed using the Fritsche-Riddle basal insulin forced-titration regimen. For suboptimal basal insulin replacement, the basal insulin dosing from the controls cohort (the AIDA on-line[2] patient data) is used.

HbA_{1c} distributions are compared using a non-parametric, two-tailed Wilcoxon signed-rank test. An asymptotic significance value of <0.05 is considered statistically significant. All calculations and analyses were performed using SPSS® (SPSS Inc., Chicago, IL, USA).

The hypoglycaemic level of 3.9mmol/l defined by the ADA is adopted in this study [ADA, 2005] as the mild hypoglycaemic threshold. The glucose level to define severe hypoglycaemia is assumed to be 3mmol/l. Cognitive function is impaired from ∼3mmol/l [Heller et al., 1987; Mitrakou et al., 1991], which matches the definition of the ADA for severe hypoglycaemia as 'an event requiring assistance of another person to actively administer [resuscitative actions]' [ADA, 2005]. While these definitions are used globally in this study, it is acknowledged that the hypoglycaemic level and response is complex and patient-specific [Cryer et al., 2003].

Protocol safety is evaluated by the time spent in mild ($\leq$3.9mmol/l) and severe ($\leq$3.0mmol/l) hypoglycaemia expressed as a percentage of total time.

4.2 Results and Discussion

The results of the *in silico* control simulation are as follows. A sample simulation is shown in Figure 4.6 of Patient 6 under control by the AC protocol with a SMBG frequency of 6/day. From this result, a patient-specific HbA_{1c} can be calculated for this patient and control scheme.

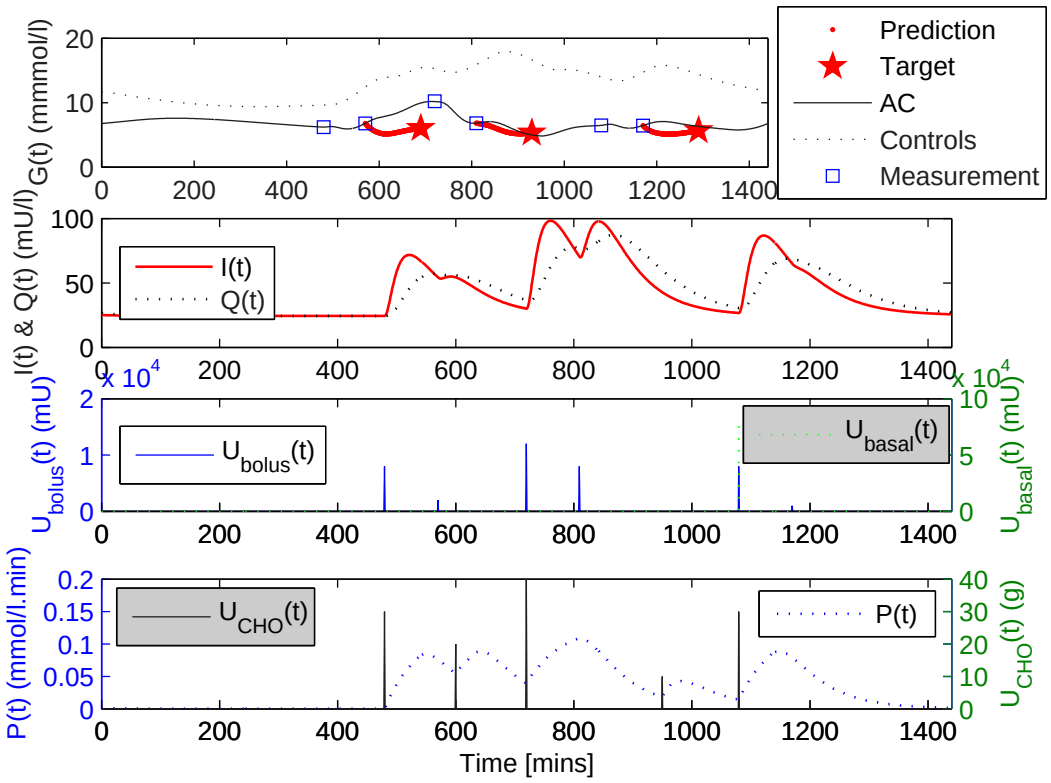

Figure 4.6 A sample *in silico* simulation of Patient 6 under control by the AC protocol with a SMBG frequency of 6/day

4.2.1 HbA_{1c}

Figures 4.7 to 4.10 show the empirical cumulative distribution function (CDF) of HbA_{1c} for the AC and CC protocols with the controls group for comparison, with and without optimal basal insulin replacement.

Referring to Figure 4.7 and Table 4.7, only 52.5% of the controls group cohort have an HbA_{1c}<7.0% while 40% had <6.5%. These thresholds are noteworthy as they are the HbA_{1c} glycaemic goals recommended by the ADA [ADA, 2006b] and AACE [AACE, 2002] respectively. Only 22.5% had HbA_{1c}<6% which is the normal range. The percentage of the controls cohort that meet the ADA recommended glycaemic goal of HbA_{1c}<7.0% is in agreement with the figure of 48.9% of the US adult diabetes population being 'in control' [Mainous et al., 2006], which supports the controls group as a realistic representation of the broad diabetes population and its treatment.

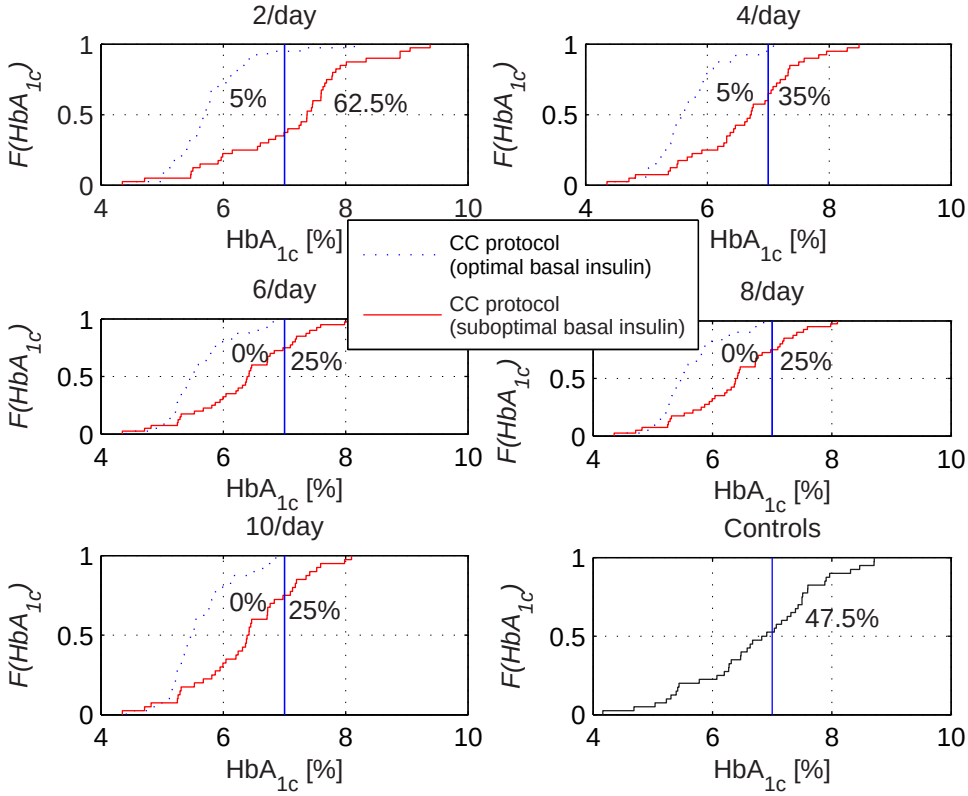

Figure 4.7 Empirical cumulative distribution function (CDF) of HbA_{1c} for the CC protocol with optimal and suboptimal basal insulin replacement compared to the controls group. The ADA recommended glycaemic control level as measured by HbA_{1c}=7% is shown with the percentage time spent above the threshold shown for each case.

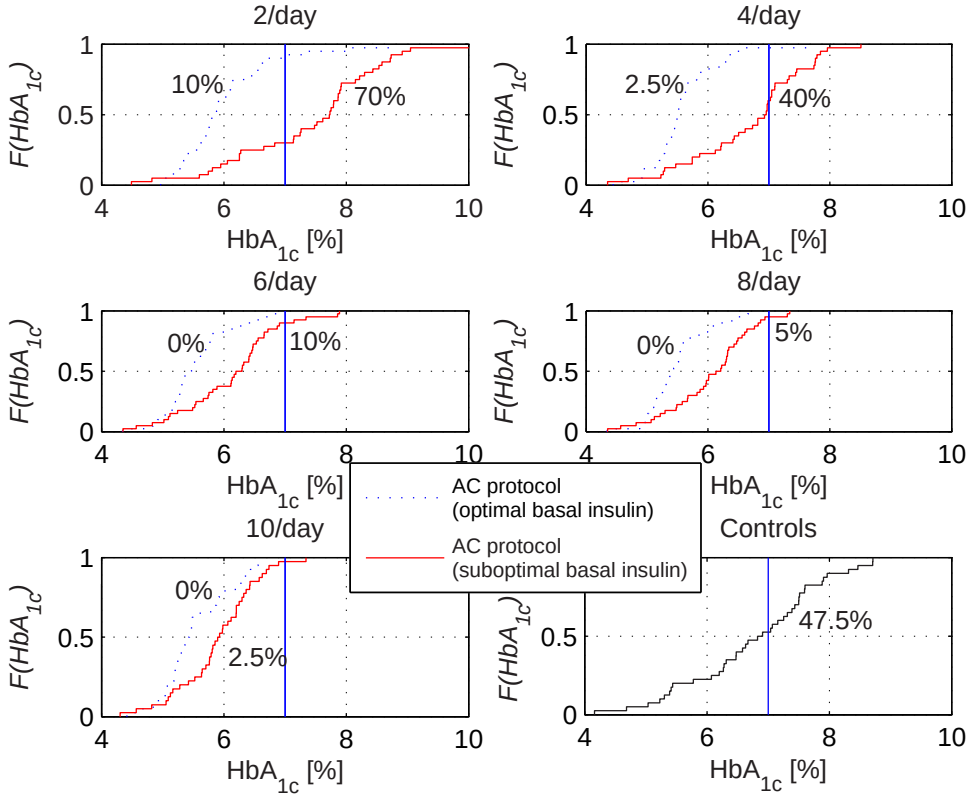

Figure 4.8 Empirical cumulative distribution function (CDF) of HbA_{1c} for the AC protocol with optimal and suboptimal basal insulin replacement compared to the controls group. The ADA recommended glycaemic control level as measured by HbA_{1c}=7% is shown with the percentage time spent above the threshold shown for each case.

Table 4.7 Percentage of the cohort controlled to ADA [ADA, 2006b] and AACE [AACE, 2002] glycaemic control recommendations, and to normal HbA_{1c} levels. The percentage of the controls group controlled to ADA recommended HbA_{1c} (52.5%) is in excellent agreement with the figure of 48.9% [Mainous et al., 2006] of the US adult diabetes population being 'in control'

Basal protocol type	Prandial protocol type	SMBG frequency [/day]	HbA_{1c}[%]		
			<6.0	<6.5	<7.0
Controls			22.5	40.0	52.5
Controls (suboptimal)	CC	2	22.5	25.0	37.5†
		4	25.0	42.5	60.0†
		6	32.5	60.0	75.0†
		8	32.5	60.0	75.0†
		10	32.5	60.0	75.0†
	AC	2	15.0	25.0	30.0†‡
		4	22.5	35.0	60.0
		6	37.5	72.5	90.0†‡
		8	42.5	77.5	95.0†‡
		10	57.5	85.0	97.5†‡
Forced-titration regimen (optimal)	CC	2	70.0	90.0	95.0†*
		4	80.0	92.5	95.0†*
		6	82.5	90.0	100.0†*
		8	82.5	90.0	100.0†*
		10	82.5	90.0	100.0†*
	AC	2	62.5	77.5	90.0†‡*
		4	82.5	95.0	97.5†*
		6	85.0	92.5	100.0†*
		8	85.0	95.0	100.0†‡*
		10	77.5	92.5	100.0†*

† Statistically significant difference compared to controls
‡ Statistically significant difference compared to CC protocol (for equivalent basal insulin protocol and SMBG frequency)
* Statistically significant difference compared to suboptimal basal insulin protocol (for equivalent prandial insulin protocol and SMBG frequency)

4.2.1.1 Suboptimal basal insulin

Compared to controls, both CC and AC protocols with suboptimal basal insulin replacement perform significantly better for SMBG frequencies ≥4/day and ≥6/day respectively. By design, the CC protocol covers twice as many meals as the AC protocol and this advantage is apparent at lower SMBG frequencies. At higher SMBG frequencies, the AC protocol is able to cover most meals in the day with increased accuracy, outperforming the CC protocol significantly for all SMBG frequencies ≥6/day. At a SMBG frequency of 6/day, 90% and 72.5% of the cohort meet ADA and AACE clinical recommendations respectively with the AC protocol compared to 75% and 60% for the CC protocol.

This result is in agreement with clinical results of long-term control using MI. It has been shown that optimal basal insulin replacement to the use of MI is required to achieve maximum benefit [Anderson et al., 1997; Home et al., 1998; Lindholm et al., 1999]. The pharmacokinetic profile of MI enables truer bolus insulin replacement than regular human insulin, and as such, requires a truer basal insulin regiment. Basal insulin regiments developed and optimised to regular insulin boluses will be suboptimal with MI boluses. This is evident for both AC and CC protocols with suboptimal basal insulin replacement, which have non-significant HbA_{1c} to controls for SMBG frequencies less than ∼3/day.

4.2.1.2 Optimal basal insulin

With optimal basal insulin replacement, glycaemic control is further enhanced. For a 6/day SMBG frequency, the AC protocol now results in 100% of the cohort controlled to ADA HbA_{1c} guidelines, 92.5% to AACE guidelines, and 85% to normal levels. However, the difference between CC and AC protocols with suboptimal basal insulin replacement (Figure 4.9) is much larger than with optimal basal insulin treatment (Figure 4.10). As expected, the AC protocol exceeds the CC protocol for all SMBG frequencies except 2/day. However, only the result from the 8/day SMBG frequency is statistically significant. For AACE and the normal HbA_{1c} thresholds given a 6/day SMBG frequency, the difference between the two protocols is just 2.5% of the cohort or 1 patient.

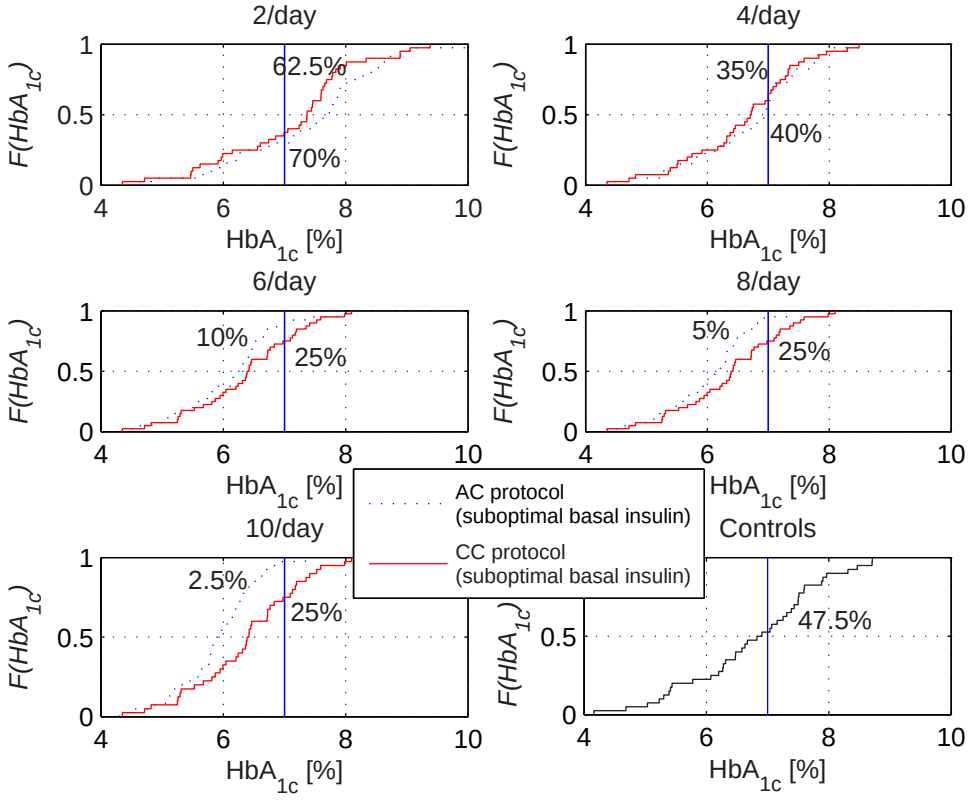

Figure 4.9 Empirical cumulative distribution function (CDF) of HbA_{1c} for both AC and CC protocols with suboptimal basal insulin replacement compared to the controls group. The ADA recommended glycaemic control level as measured by HbA_{1c}=7% is shown with the percentage time spent above the threshold shown for each case.

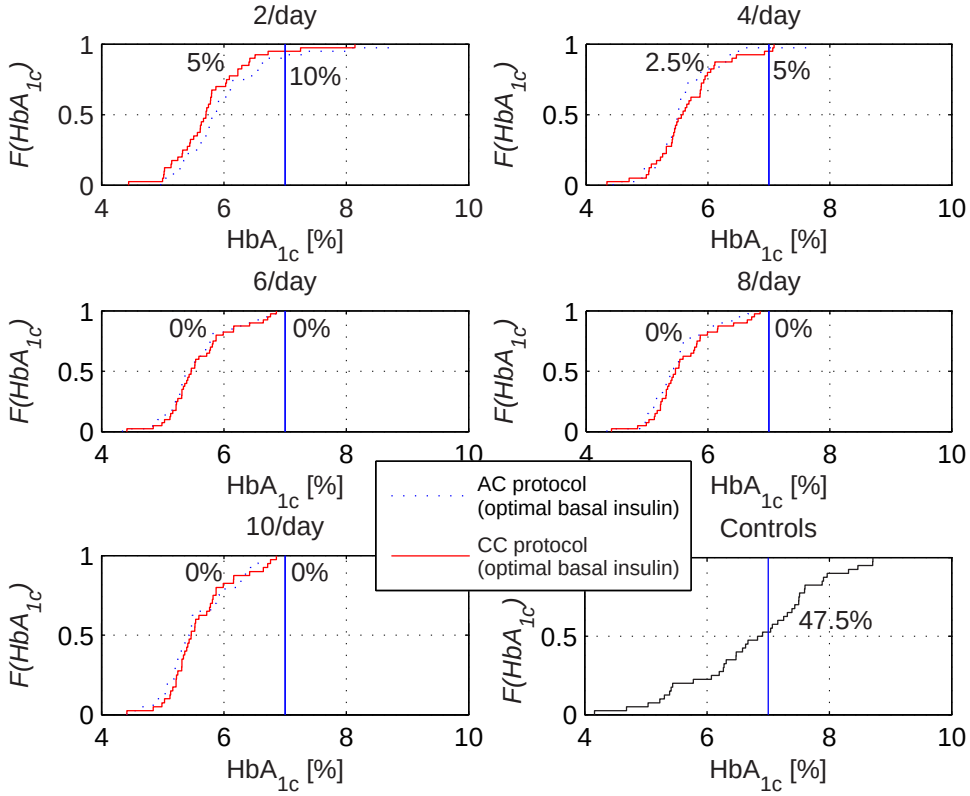

Figure 4.10 Empirical cumulative distribution function (CDF) of HbA_{1c} for both AC and CC protocols with optimal basal insulin replacement compared to the controls group. The ADA recommended glycaemic control level as measured by HbA_{1c}=7% is shown with the percentage time spent above the threshold shown for each case.

These results indicate that if basal insulin replacement is optimal, both prandial insulin protocols perform similarly. However, if basal insulin replacement is suboptimal and insulin requirements in the post-absorptive period are not met, then the AC protocol compensates more effectively than the CC protocol, especially at SMBG frequencies $\geq$6/day where sufficient measurements exist to cover most of the meals in the day. The HbA_{1c} results are summarised in Figure 4.11.

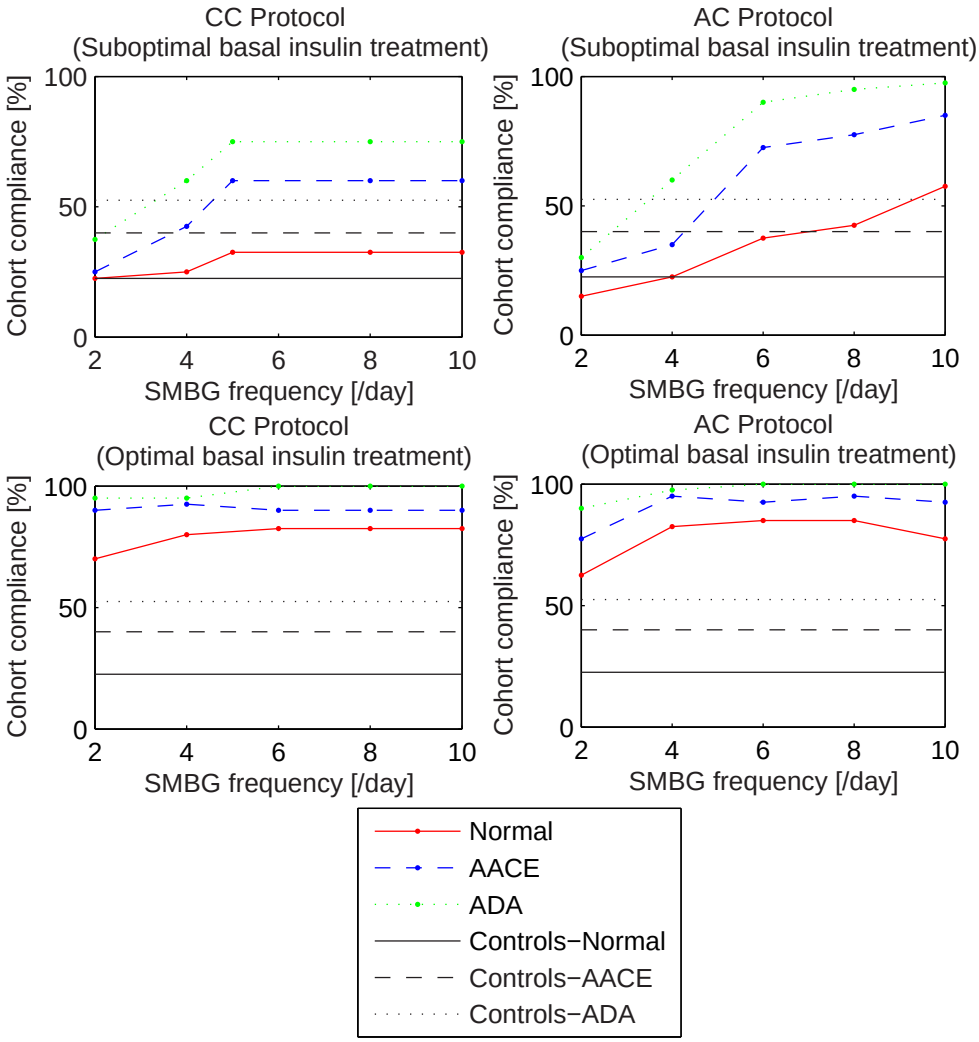

Figure 4.11 The cohort percentage controlled to clinically relevant HbA_{1c} levels (as recommended by the ADA [ADA, 2006b] and AACE [AACE, 2002]) compared to the controls group. The normal HbA_{1c} level of 6.0% is shown for comparison.

4.2.2 Hypoglycaemia

CC protocol

Referring to Figure 4.12 to 4.15, the total time spent by the cohort in mild ($t_{hypo,mild}$) and severe hypoglycaemia ($t_{hypo,sev}$) is shown as a percentage. For the controls group, $t_{hypo,mild}$ is 7.7%. From Figure 4.12 for the CC protocol with suboptimal basal insulin replacement, $t_{hypo,mild}$ is relatively constant over all SMBG frequencies at 4.2-4.9%.

For the CC protocol with optimal basal insulin replacement, $t_{hypo,mild}$ decreases with increasing SMBG frequency with the highest $t_{hypo,mild}$ of 8.5% occurring for a SMBG frequency of 2/day. This figure exceeds the controls group (7.7%) and the suboptimal basal insulin CC protocol (4.3%).

At a SMBG frequency of 4/day, $t_{hypo,mild}$ is 6.5% compared to 4.5% for the suboptimal basal insulin CC protocol. At a SMBG frequency of 6/day, $t_{hypo,mild}$ is comparable to the suboptimal basal insulin CC protocol (4.5% compared to 4.2%), dropping further to 2.9% compared to 4.9% for the suboptimal basal insulin CC protocol at a SMBG frequency of 10/day.

Similarly, $t_{hypo,sev}$ is relatively constant at $\sim$1.8% for the CC protocol with suboptimal basal insulin replacement. Like $t_{hypo,mild}$, $t_{hypo,sev}$ under the CC protocol with optimal basal insulin replacement is maximum at 1.2% for a SMBG frequency of 2/day and decreases to 0.6% for a SMBG frequency of 10/day. For the controls group, $t_{hypo,sev}$ is 3.5%.

In summary, across all SMBG frequencies, $t_{hypo,sev}$ under the optimal basal insulin CC protocol is reduced by 66-83% over controls and by 33-67% over the suboptimal basal insulin CC protocol. However, $t_{hypo,mild}$ is increased at least until a SMBG frequency of 4/day and is decreased for all SMBG frequencies >6/day. Under the CC protocol and with a low SMBG frequency, e.g., 2-4/day, the prandial glycaemic excursion especially for the last meal of the day is usually not completely restored to basal.

This failure to reach a basal level overnight is important because it affects the pre-breakfast glucose measurement used for the titration of the basal insulin

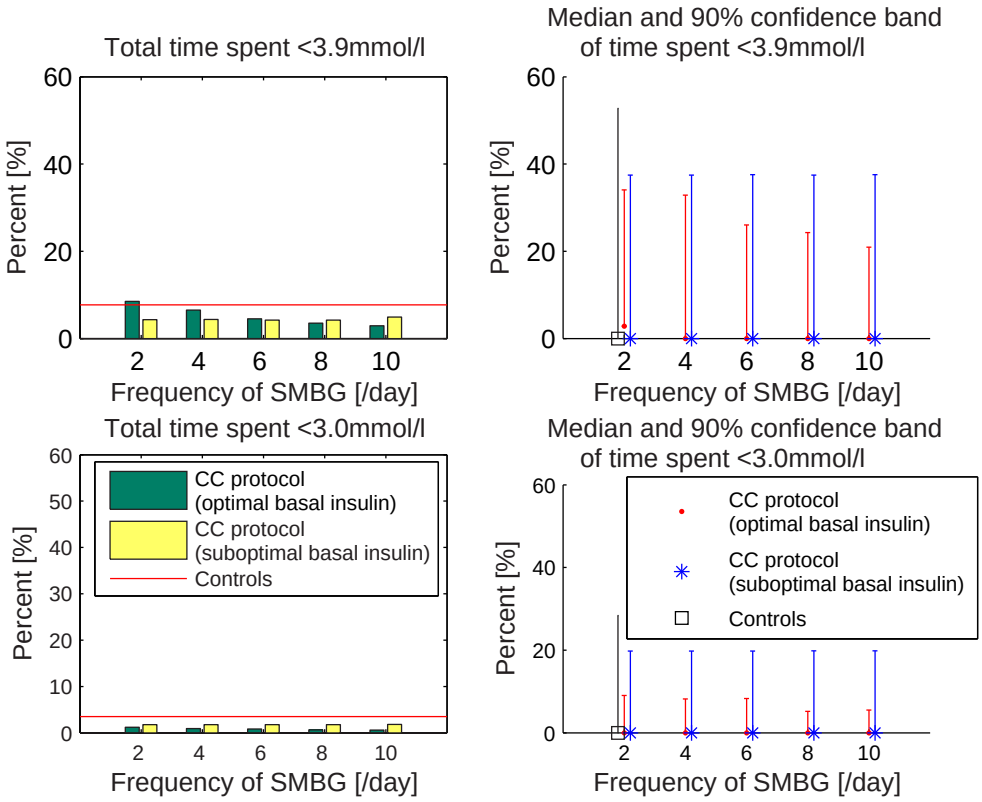

Figure 4.12 Total time spent by the cohort, and the cohort median and 90% confidence band for the time spent in mild and severe hypoglycaemia under the CC protocol in conditions of optimal and suboptimal basal insulin replacement.

dose, resulting in an aggressive dose increase and increased mild hypoglycaemia. Fortunately, this problem does not result in increased severe hypoglycaemia, and in fact, optimal basal insulin replacement with insulin glargine results in lower occurrences of severe hypoglycaemia across all SMBG frequencies. With SMBG frequencies of 6/day or more, occurrences of both mild and severe hypoglycaemia are reduced over controls and the suboptimal basal insulin CC protocol.

AC protocol

Referring to Figure 4.13 for the AC protocol with suboptimal basal insulin replacement, $t_{hypo,mild}$ is relatively constant over all SMBG frequencies at 4.2-4.4%. For the AC protocol with optimal basal insulin replacement, $t_{hypo,mild}$ decreases with increasing SMBG frequency with the highest $t_{hypo,mild}$ of 3.1% and 3.2% occurring for SMBG frequencies of 2/day and 4/day respectively. This figure is

60% less than the controls group (7.7%) and 28% less than the suboptimal basal insulin CC protocol (4.4%). At a SMBG frequency of 8/day, $t_{hypo,mild}$ reaches a nadir of 0.7% before increasing to 1.3% for a SMBG frequency of 10/day.

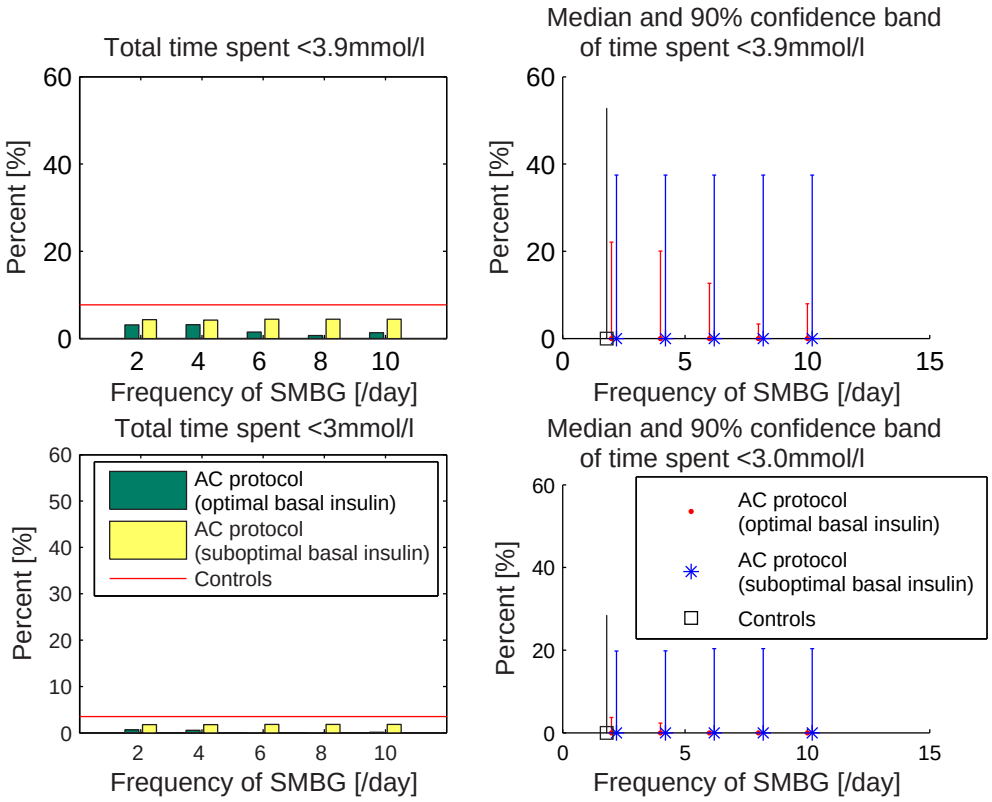

Figure 4.13 Total time spent by the cohort, and the cohort median and 90% confidence band for the time spent in, mild and severe hypoglycaemia under the AC protocol in conditions of optimal and suboptimal basal insulin replacement.

Similarly, $t_{hypo,sev}$ is relatively constant at ∼1.8% for the AC protocol with suboptimal basal insulin replacement. Like $t_{hypo,mild}$, $t_{hypo,sev}$ under the AC protocol with optimal basal insulin replacement is maximum at 0.6% for a SMBG frequencies of 2/day and 4/day but decreases to zero percent for SMBG frequencies ≥6/day.

In summary, across all SMBG frequencies, $t_{hypo,sev}$ under the AC protocol with optimal basal insulin replacement is reduced by 86-100% over controls and by 72-100% over the AC protocol with suboptimal basal insulin replacement. Across all SMBG frequencies, $t_{hypo,mild}$ under the AC protocol with optimal basal insulin replacement is reduced by 58-91% over controls and 27-84% over the AC protocol with suboptimal basal insulin replacement. Prandial glycaemic excursions are

more completely restored to basal under the AC protocol even with a low SMBG frequency. This results in a more accurate pre-breakfast glucose measurement for basal insulin titration with the forced-titration regimen, with lower resultant mild and severe hypoglycaemia.

Summary of hypoglycaemia results

Referring to Figure 4.14 for optimal basal insulin replacement, the AC protocol outperforms the CC protocol in hypoglycaemia occurrence over all SMBG frequencies. Given suboptimal basal insulin replacement, occurrence of hypoglycaemia, both mild and severe, is similar between the two protocols (see Figure 4.15). The results of this comparison are similar to that of HbA_{1c}, whereby the advantage of the AC protocol is most apparent in conditions of poor basal insulin replacement.

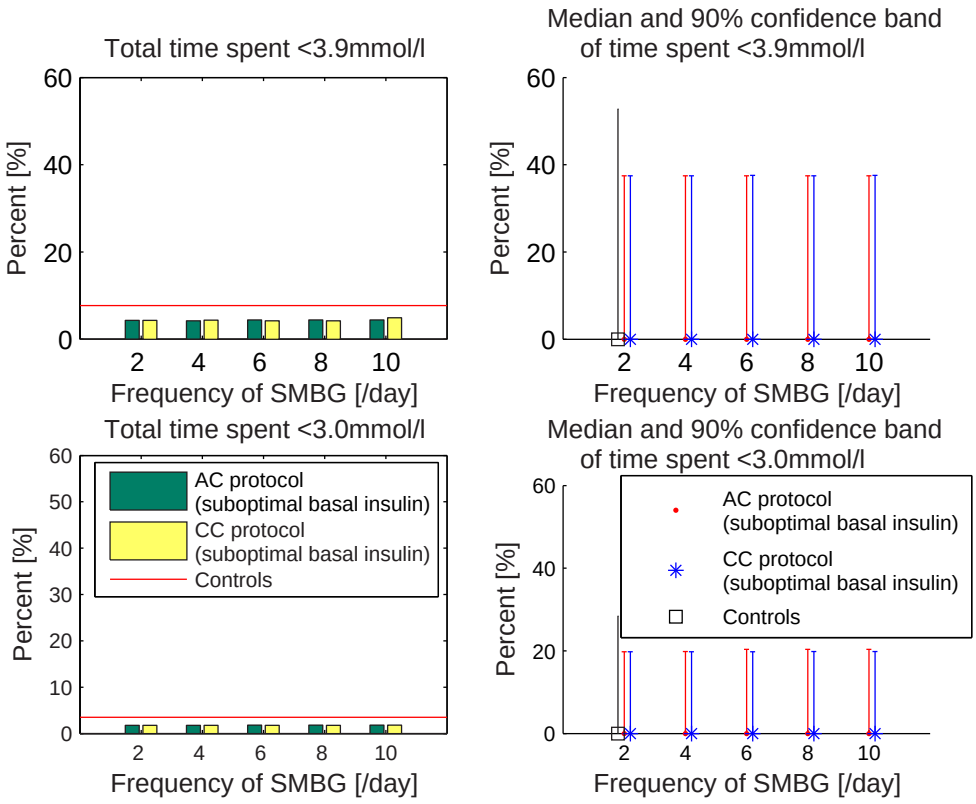

Figure 4.14 Total time spent by the cohort, and the cohort median and 90% confidence band for the time spent in mild and severe hypoglycaemia under AC and CC protocols and suboptimal basal insulin replacement.

Contrary to the DCCT [DCCT Research Group, 1993], hypoglycaemia did not increase under the conventional IIT (CC protocol) in this study. In both cases of suboptimal and optimal basal insulin replacement, severe hypoglycaemia is reduced for all SMBG frequencies compared to controls. This result is in excellent agreement with the study by Samann et al. [2005] where implementation of a flexible IIT protocol improved glycaemic control without increased risk of severe hypoglycaemia. The protocol in the Samann et al. study consists of a structured inpatient training course, implemented into routine care with continuous quality assurance on a national level. Hence, it is reasonable to assume high patient protocol adherence, and that the conditions in this particular study are comparable to that inherent of the *in silico* simulation, which assumes full patient adherence.

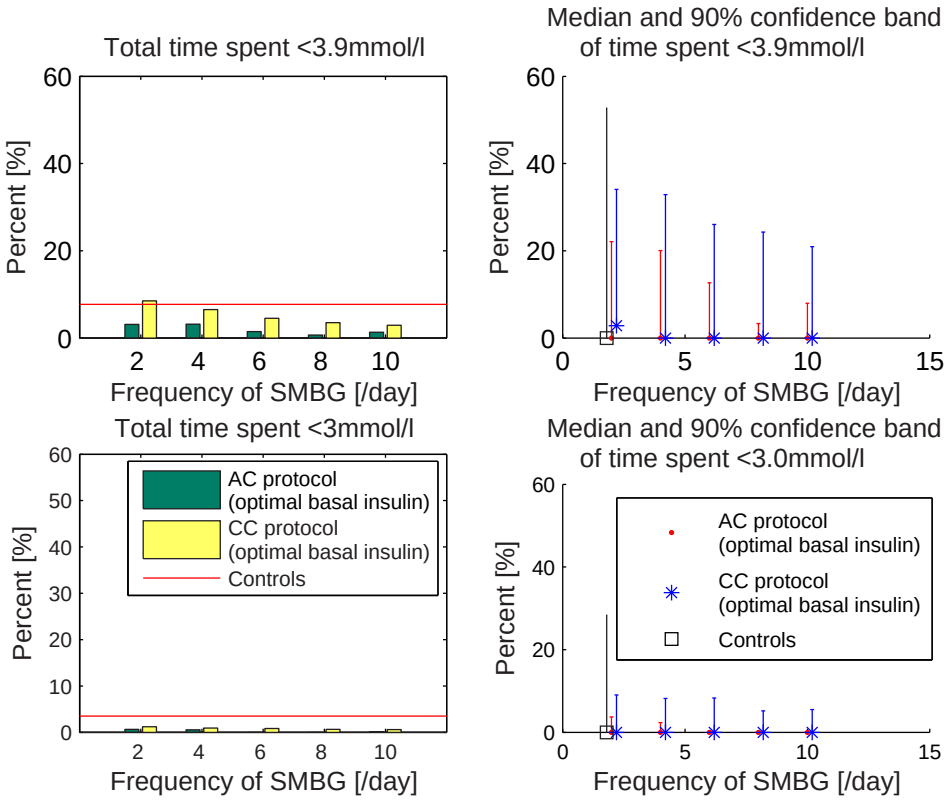

Figure 4.15 Total time spent by the cohort, and the cohort median and 90% confidence band for the time spent in mild and severe hypoglycaemia under AC and CC protocols and optimal basal insulin replacement.

Table 4.8 Summary of total hypoglycaemia over the cohort from *in silico* simulation of the AC and CC protocols in conditions of optimal and suboptimal basal insulin replacement

Basal protocol type	Prandial protocol type	SMBG frequency [/day]	Hypoglycaemia	
			$t_{hypo,mild}$	$t_{hypo,sev}$
Controls			7.7	3.5
Controls (suboptimal)	CC	2	4.3	1.8
		4	4.4	1.8
		6	4.2	1.8
		8	4.2	1.8
		10	4.9	1.8
	AC	2	4.3	1.8
		4	4.2	1.8
		6	4.4	1.8
		8	4.4	1.8
		10	4.4	1.8
Forced titration regimen (optimal)	CC	2	8.5	1.2
		4	6.5	0.9
		6	4.5	0.8
		8	3.5	0.6
		10	2.9	0.6
	AC	2	3.1	0.6
		4	3.2	0.6
		6	1.5	0.0
		8	0.7	0.0
		10	1.3	0.1

Table 4.9 Summary of hypoglycaemia per patient from *in silico* simulation of the AC and CC protocols in conditions of optimal and suboptimal basal insulin replacement

Basal protocol type	Prandial protocol type	SMBG frequency [/day]	Hypoglycaemia	
			$t_{hypo,mild}$	$t_{hypo,sev}$
Controls			0 (0-53)	0 (0-28)
Controls (suboptimal)	CC	2	0 (0-37)	0 (0-20)
		4	0 (0-37)	0 (0-20)
		6	0 (0-38)	0 (0-20)
		8	0 (0-37)	0 (0-20)
		10	0 (0-38)	0 (0-20)
	AC	2	0 (0-37)	0 (0-20)
		4	0 (0-37)	0 (0-20)
		6	0 (0-37)	0 (0-20)
		8	0 (0-37)	0 (0-20)
		10	0 (0-37)	0 (0-20)
Forced titration regimen (optimal)	CC	2	3 (0-31)	0 (0-9)
		4	0 (0-33)	0 (0-8)
		6	0 (0-26)	0 (0-8)
		8	0 (0-24)	0 (0-5)
		10	0 (0-21)	0 (0-6)
	AC	2	0 (0-22)	0 (0-4)
		4	0 (0-20)	0 (0-2)
		6	0 (0-13)	0 (0-0)
		8	0 (0-3)	0 (0-0)
		10	0 (0-8)	0 (0-0)

4.2.3 SMBG frequency

The frequency of SMBG has been known to affect glycaemic control, as reviewed by Blonde [2005]. For Type 1 diabetes, the ADA [ADA, 2006b] and AACE [AACE, 2002] both recommend SMBG frequencies ≥3/day and in a study by Monnier et al. [2004], even 5- to 8-point daily glucose monitoring is recommended. Davidson et al. [2004] has modelled HbA_{1c} and SMBG with Equation 4.11.

$$HbA_{1c} = 5.99 + \frac{5.32}{\text{tests per day} + 1.39} \tag{4.11}$$

Referring to Figure 4.16, the data from Davidson et al. is reproduced with the median cohort HbA_{1c} of this study for the various protocols and basal insulin replacement regimens.

The Davidson et al. curve follows closely the suboptimal basal insulin CC protocol. This result supports the validity of the *in silico* simulation, which produces a similar HbA_{1c} simulating a conventional IIT under suboptimal basal insulin replacement. With SMBG frequency >4/day, the suboptimal basal insulin AC protocol reduces the median HbA_{1c} over the CC protocol under the same basal insulin replacement. Both protocols with optimal basal insulin replacement result in a normal median HbA_{1c} even at a low SMBG frequency of 2/day although the AC protocol results in marginally lower HbA_{1c} for all SMBG frequencies ≥6/day. This result also implies that, clinically, poor glycaemic control largely results from suboptimal basal insulin replacement. Basal insulin replacement has a more significant effect on HbA_{1c} than the difference between AC and CC prandial insulin protocols.

The forced-titration regimen of basal insulin dosing has been found to be safe only if sufficient SMBG, and consequently prandial control, is applied in order for the assumed FPG value to be an accurate. The basal insulin forced-titration regimen relies on a single, pre-breakfast FPG value and if a patient is poorly controlled prandially, the assumed FPG value is likely to be influenced by the postprandial excursion from the previous night. From this study, this minimum SMBG frequency is approximately ∼6/day for a conventional IIT (CC

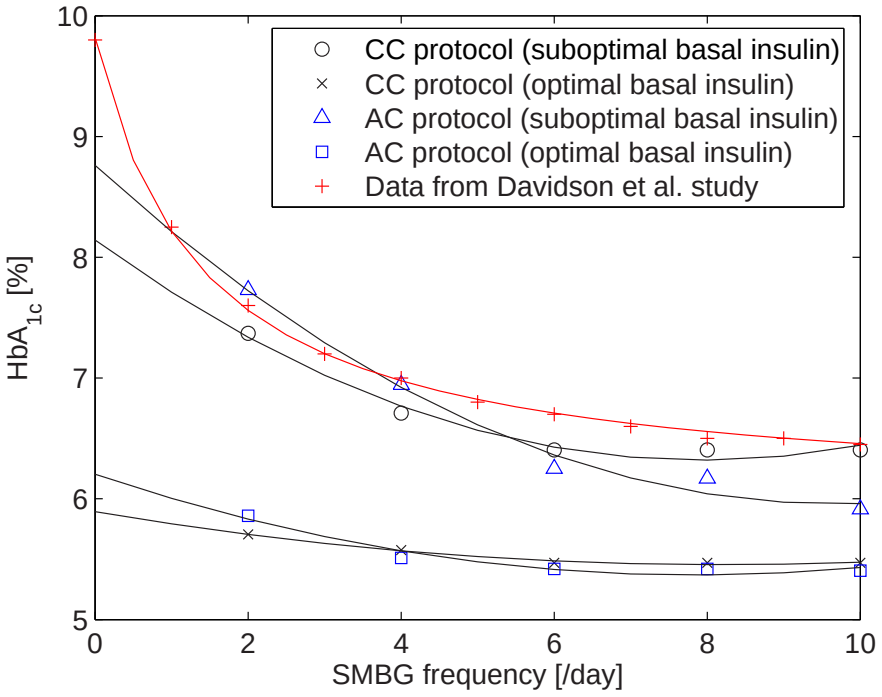

Figure 4.16 Predicted HbA_{1c} data from Davidson et al. [2004] and the median cohort HbA_{1c} of this study vs. SMBG frequency. The Davidson et al. curve follows approximately the suboptimal basal insulin CC protocol.

protocol). With the AC protocol, the SMBG frequency does not present a safety issue regardless of basal insulin replacement.

Referring to Table 4.7, the suboptimal basal insulin CC protocol (a conventional IIT) and a SMBG frequency of 4/day results in 60% of the cohort controlled to ADA guidelines, and 25% to normal HbA_{1c} levels. With 6- or 8-point daily glucose monitoring, these figures are 75.0% and 32.5% respectively. Hence, control with the minimum ADA recommended SMBG frequency, or even the Monnier et al. daily 8-point measurement, is unsatisfactory if the protocol implemented is a conventional IIT with suboptimal basal insulin replacement. From this study, glycaemic control with the suboptimal basal insulin CC protocol saturates at a SMBG frequency of 6/day with 75% of the cohort meeting ADA guidelines. Hence, a SMBG frequency of 6/day should be the minimum for a conventional IIT with a suboptimal basal insulin regimen.

With optimal basal insulin replacement, the adaptive AC protocol with a SMBG frequency of 4/day results in 97.5% of the cohort controlled to ADA

guidelines, and 82.5% to normal HbA_{1c} levels. In addition, mild hypoglycaemia is reduced by 27% and severe hypoglycaemia by 50% in comparison to the sub-optimal basal insulin CC protocol. With optimal basal insulin replacement, the CC protocol produces similarly excellent glycaemic control but mild hypoglycaemia is increased 103% compared to the AC protocol. Fear of hypoglycaemia is frequently cited for deliberate insulin under-dosing, both prandial and basal [Fritsche et al., 2003; Morris et al., 1997]. Hence, the adaptability of the AC protocol may represent the next evolution of IIT to deliver increased glycaemic control with increased safety.

4.2.4 Effect of optimal CIR and ISF parameters

In the *in silico* simulation performed in this study, the CC protocol is not adaptive as it uses fixed, suboptimal patient-specific parameters calculated using Equations 4.1 and 4.2 from the original AIDA on-line^2 patient data. This method calculates suboptimal parameters because there is an inherent assumption that the insulin treatment recorded the retrospective AIDA on-line^2 data is itself optimal. In clinical reality, retrospective patient data may be the only way to identify the CIR and ISF parameters for an individual patient, i.e., from retrospective records of prior insulin treatment.

However, in this section, the effect of optimal CIR and ISF parameters are explored. Clinically, this may be performed at regular monthly intervals for example, whereby the prior month's retrospective data of insulin treatment is used to reassess the Total Daily Insulin Dose using Equations 4.1 and 4.2, and recalculate the new CIR and ISF parameters. In this way, the Total Daily Insulin Dose may be optimised iteratively. In this section, the optimal CIR and ISF parameters are recalculated for each patient using the simulation results obtained for the AC protocol with optimal basal insulin replacement.

In Figure 4.17 and Table 4.10, the results are shown for the AC protocol with optimal basal insulin, with normal and optimal CIR and ISF parameter values. From Figure 4.17 and Table 4.10, the percentage of the cohort controlled to the ADA recommended $<7\%$ HbA_{1c} is identical for each measurement frequency. The cohort compliance to AACE and normal HbA_{1c} thresholds are similar as well up to SMBG frequency of 6/day. However, for SMBG frequencies 8/day to 10/day,

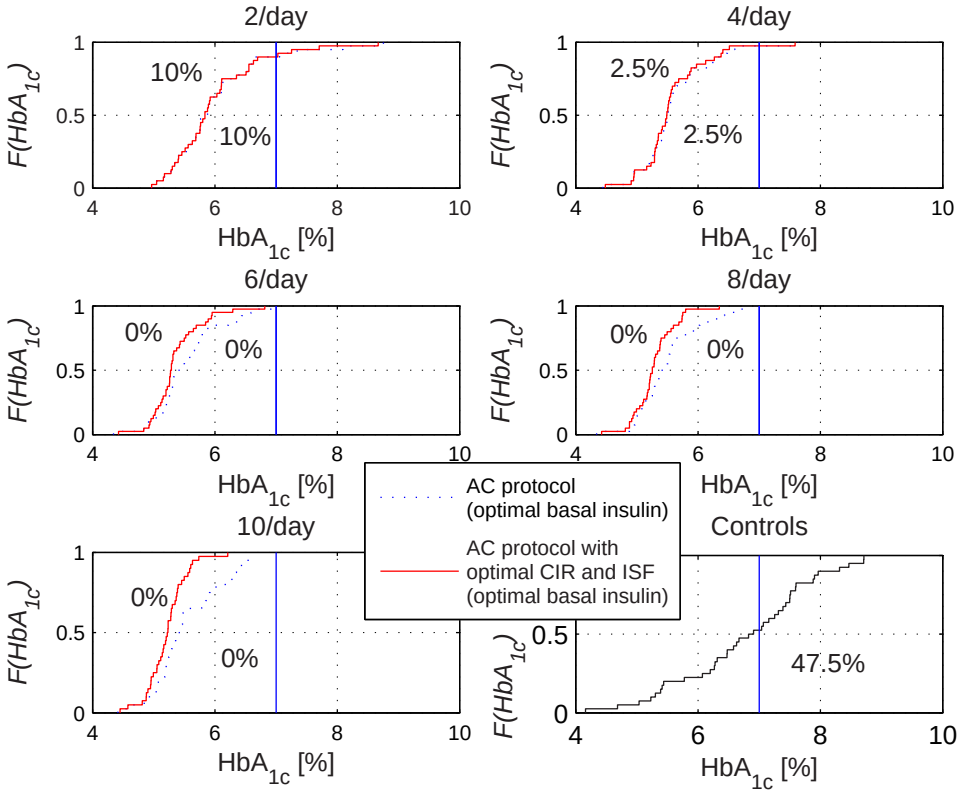

Figure 4.17 Empirical cumulative distribution function (CDF) of HbA_{1c} for the AC protocol with optimal basal insulin replacement with and without optimal CIR and ISF parameter values. The controls group is included for completeness. The ADA recommended glycaemic control level as measured by HbA_{1c}=7% is shown with the percentage time spent above the threshold shown for each case.

the cohort compliance to the AACE and normal thresholds increases dramatically for the optimal CIR and ISF parameter simulation as shown in Figure 4.17. For SMBG frequency of 8/day and 10/day, the cohort percentage controlled to normal HbA_{1c} of <6%, is 20% absolute higher for the optimal CIR and ISF simulation. With increasing SMBG frequency, the number of interventions calculated using the CIR and ISF parameters increases, and the effect of the optimal parameters become increasingly influential.

Referring to Figure 4.18 and Tables 4.11 and 4.12, the rate of mild hypoglycaemia especially is increased in the simulation with optimal CIR and ISF ratios. The initial prandial insulin intervention prescribed by the AC protocol is the only intervention affected by the CIR and ISF parameters. The initial prandial insulin bolus is, hence, not adaptive to real-time patient condition as is the second bolus calculated using S_I.

Table 4.10 The percentage of the cohort controlled to recommended HbA_{1c} thresholds (<7.0%, ADA [ADA, 2006b] and <6.5%, AACE [AACE, 2002]) and the normal HbA_{1c} level (<6.0%) under the AC protocol with optimal basal insulin replacement for the normal and optimal CIR and ISF parameter simulations. Note that the CIR and ISF parameters only affect the first bolus prescribed using the AC adaptive prandial protocol

Simulation type	SMBG frequency [/day]	HbA_{1c}[%]		
		<6.0	<6.5	<7.0
Controls		22.5	40.0	52.5
AC protocol with optimal CIR and ISF (optimal basal insulin)	2	62.6	75.5	90.0
	4	80.0	95.0	97.5
	6	87.5	97.5	100.0
	8	95.0	100.0	100.0
	10	97.5	100.0	100.0
AC protocol (optimal basal insulin)	2	62.5	77.5	90.0
	4	82.5	95.0	97.5
	6	85.0	92.5	100.0
	8	85.0	95.0	100.0
	10	77.5	92.5	100.0

The non-optimal CIR and ISF calculated from the AIDA on-line[2] patient data are conservative due to the generally low insulin doses prescribed in the original patient data. Once recalculated using the more optimal dosing provided by the AC protocol, the CIR and ISF parameters result in a more *aggressive* intervention resulting in the increased hypoglycaemia.

In summary, there is an advantage in iteratively optimising CIR and ISF parameters for more accurate first bolus insulin dosing with the AC protocol. The advantage to decreased HbA_{1c} is more apparent at higher SMBG frequencies $\geq$8/day. However, increased mild hypoglycaemia is apparent at SMBG frequencies $\geq$4/day. With further iterative optimisation of CIR and ISF, it is likely that both these clinical outcomes may be improved upon over the normal simulation. Even so, evidence reported in this section indicate that an aggressive CIR and ISF affects only higher SMBG frequencies, frequencies which are unlikely to be clinically achieved. In fact, the cohort compliance to the ADA HbA_{1c} threshold is identical for all SMBG frequencies between the two simulations while hypoglycaemia is increased even from an SMBG frequency of 4/day. Hence, optimising CIR and ISF parameters should be approached cautiously and may not be effective at the lower SMBG frequencies typical of most intensive insulin therapies.

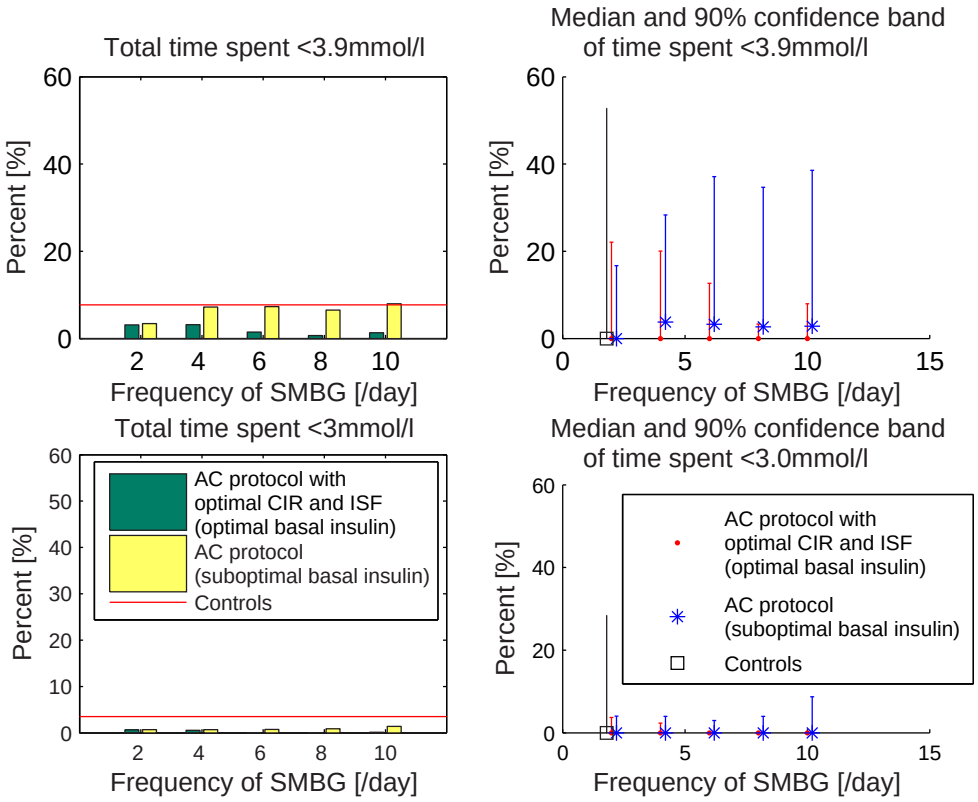

Figure 4.18 Total time spent by the cohort, and the cohort median and 90% confidence band, for the time spent in mild and severe hypoglycaemia under AC protocol with optimal basal insulin replacement with normal and optimal CIR and ISF parameters.

Table 4.11 Summary of total hypoglycaemia over the cohort from *in silico* simulation of the AC protocol in conditions of optimal basal insulin replacement with normal and optimal CIR and ISF parameters

Protocol type	SMBG frequency [/day]	Hypoglycaemia	
		$t_{hypo,mild}$	$t_{hypo,sev}$
Controls		7.7	3.5
AC with optimal CIR and ISF	2	3.4	0.7
	4	7.2	0.7
	6	7.3	0.7
	8	6.5	0.9
	10	8.0	1.4
AC	2	3.1	0.6
	4	3.2	0.6
	6	1.5	0.0
	8	0.7	0.0
	10	1.3	0.1

Table 4.12 Summary of hypoglycaemia per patient from *in silico* simulation of the AC protocol in conditions of optimal basal insulin replacement with normal and optimal CIR and ISF parameters

Protocol type	SMBG frequency [/day]	Hypoglycaemia	
		$t_{hypo,mild}$	$t_{hypo,sev}$
Controls		7.7	3.5
AC with optimal CIR and ISF	2	0 (0-17)	0 (0-4)
	4	4 (0-25)	0 (0-4)
	6	3 (0-34)	0 (0-3)
	8	3 (0-32)	0 (0-4)
	10	3 (0-36)	0 (0-9)
AC	2	0 (0-22)	0 (0-4)
	4	0 (0-20)	0 (0-2)
	6	0 (0-13)	0 (0-0)
	8	0 (0-3)	0 (0-0)
	10	0 (0-8)	0 (0-0)

4.3 Conclusions

An *in silico* simulation tool is presented that utilises an extended model of glucose kinetics, and the novel application of a subcutaneous insulin pharmacokinetic model. The virtual patient cohort and its default control protocol (the data of which is used for *in silico* simulation) can be considered an accurate representation of the broad diabetes population. The simulation tool is used to develop a robust, adaptive protocol for prandial insulin dosing.

In *in silico* simulation, results for the controls group and conventional IIT under suboptimal basal insulin match clinical expectations, with basal insulin replacement having the single, most significant effect on HbA_{1c}, much more so than the difference between prandial insulin protocols.

Specifically, the adaptive protocol significantly decreases HbA_{1c} in conditions of suboptimal basal insulin replacement for SMBG frequencies $\geq$6/day and reduces the occurrence of mild and severe hypoglycaemia by 86-100% over controls over all SMBG frequencies in conditions of optimal basal insulin. When a conventional IIT is employed in conditions of suboptimal basal insulin, the increase in cohort compliance to clinical control guidelines saturates at a SMBG frequency

of 6/day while to titrate the basal insulin dose optimally requires a minimum SMBG frequency of 6/day to adequately correct postprandial glycaemia from the previous night and obtain an accurate assumed FPG for basal dose titration.

With a SMBG frequency of 4/day and optimal basal insulin replacement, 97.5% of the cohort can be controlled to ADA clinical guidelines using the adaptive protocol, a result similar to a conventional IIT but which has 103% more mild hypoglycaemia. As fear of hypoglycaemia is a large psychological barrier to glycaemic control, the AC protocol may represent the next evolution of IIT that can deliver increased glycaemic control with increased safety.

The developed *in silico* simulation tool has been shown to produce results that match clinical expectations, a result that strongly supports the validity of the models and methods developed. With the completion of *in silico* simulation of the prandial and basal insulin protocols, the next step in this research is to determine the robustness of the adaptive protocol to uncertainties that may be encountered in clinical use. In the following chapter, a Monte Carlo analysis is performed by incorporating realistic errors and variability into the *in silico* simulation for this purpose.

Chapter 5

Monte Carlo Analysis

A model-based, adaptive AC protocol for the clinical control of Type 1 diabetes has been developed for use with SMBG and MDI, and simulated *in silico* on a virtual patient cohort in Chapter 4. To assess the robustness of the AC protocol to possible errors and variability in clinical application, an *in silico* Monte Carlo (MC) analysis is performed, taking into account all quantifiable errors and variability. These include: variability in subcutaneous insulin and meal glucose absorption, errors in SMBG measurements, carbohydrate counting, and dosing of insulin. The simulations are based on model-based 24hr insulin sensitivity profiles identified from a patient cohort (n=40) in Chapter 4, covering a broad range of possible clinical behaviour.

The Monte Carlo analysis evaluates effectiveness (HbA_{1c}) and safety (mild and severe hypoglycaemia) of the protocol in the presence of measurement, insulin dosing, and carbohydrate counting errors, as well as insulin absorption and meal glucose appearance variability from the modelled population parameters. The effects of all these uncertainties are not readily measured or estimated, and thus typically result in poor control seen in broader cohorts. Hence, any protocol must be robust to them and MC simulation can effectively quantify this robustness.

5.1 MC error definitions

Glucose measurement errors are assumed normally-distributed with precision (in coefficient of variation, CV) reported by Kimberly et al. [2006] for common SMBG monitors. In Kimberly et al., accuracy to reference glucose values is not tested.

Hence, to adapt these results for MC analysis, systematic bias is assumed zero with all error attributed only to the precision of the devices. Measurement biases of SMBG monitors have been studied and found to be generally small and inconsistent [Brunner et al., 1998], being attributed to sensor calibration, environmental, and/or operator/user factors, which are difficult to quantify.

The largest CV reported by Kimberly et al. is used in this MC study for a worst-case scenario. The precision is reported for 3 glycaemic ranges, 3.9-5.5mmol/l, 5.6-7.7mmol/l, and 7.8-11mmol/l with CV_{total} of 11.3%, 8.9% and 8.3% respectively. Note that even the precision of this monitor, and others [Brunner et al., 1998; Cohen et al., 2006], are insufficient to meet ADA recommendations for total error $\leq$5% [ADA, 1996; Goldstein et al., 2004].

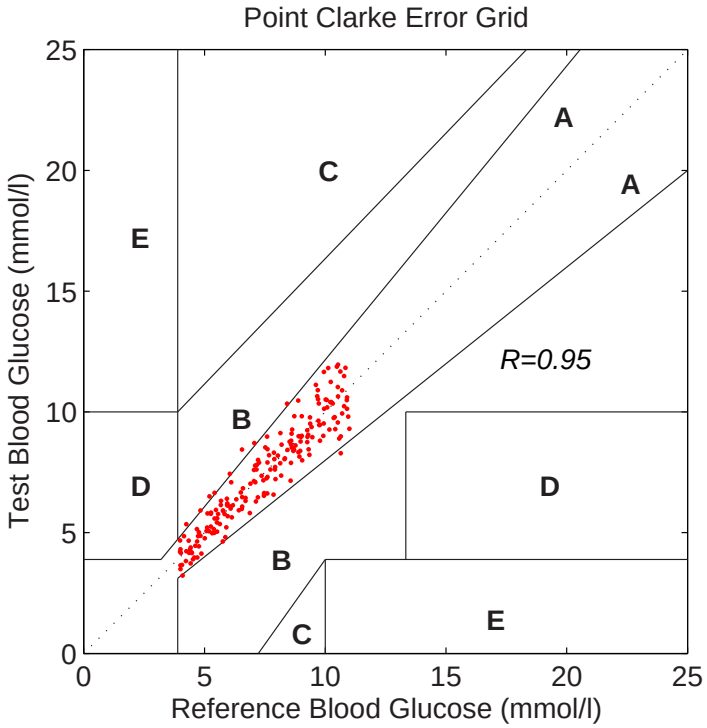

Figure 5.1 Clarke Error Grid analysis of the error distribution produced by the blood glucose monitor used in MC analysis. The error is partitioned into three glucose ranges (3.9-5.5mmol/l, 5.6-7.7mmol/l, and 7.8-11mmol/l) with individual coefficient of variation (CV_{total}=11.3%, 8.9% and 8.3% respectively). Error is shown for a uniformly distributed sample blood glucose reference data set (size 200) between 3.9mmol/l and 11mmol/l. A Spearman correlation coefficient of 0.95 is obtained with 96.5% of measurements within zone A with the rest in zone B.

An Error Grid analysis is shown in Figure 5.1 for the defined meter error distribution for this study. For a uniformly distributed sample blood glucose reference data set (size 200) between 3.9mmol/l and 11.0mmol/l, a Spearman

correlation coefficient of 0.95 is obtained with 96.5% of measurements within zone A with the rest in zone B.

Sources of error in insulin dosing include, but are not limited, to variations in the use of, or the inherent inaccuracy of, insulin injection apparatus, e.g., pens or syringes. Carbohydrate counting is a technique which is only approximate and can be prone to inaccuracy [Kildegaard et al., 2007]. In this MC analysis, both error types are assumed to be uniformly distributed between ±20%.

Variability in subcutaneous absorption has been widely studied [Guerci and Sauvanet, 2005; Heinemann, 2002; Heinemann et al., 1998; Heise et al., 2004; Lepore et al., 2000; Scholtz et al., 2005]. It is common to report variability of pharmacokinetic (PK) summary measures, such as time (after injection) to maximal plasma concentration, T_{max}, and maximal concentration, C_{max}, in CV. The use of CV implies a normal distribution of the summary measures, which is also assumed in this study. A summary of CV values from the literature is shown in Table 5.1. The reported inter- and intra-individual coefficients of variation (CV_{inter}, CV_{intra}) are used to calculate a total coefficient of variation, CV_{total} using Equation 5.1 for each MC virtual patient control trial.

$$\mathrm{CV}_{total} = \sqrt{\mathrm{CV}_{inter}^2 + \mathrm{CV}_{intra}^2} \tag{5.1}$$

Using this data of the PK profile, the MC simulation can now apply a realistic variability to the absorption profile of injected insulin. The process to convert the published CV values into a PK profile generated by the sc insulin absorption model in Chapter 2 is summarised below:

1. A sensitivity analysis is performed on the key model parameters identified in Chapter 2 and 3 and listed in Table 5.2 with their mean values.

2. Referring to Figure 5.2 and 5.3, the sensitivity analysis is used to determine the maximum variation in each individual parameter value from the mean (in percent), Δ, required for minimum 5% absolute change in both T_{max} and C_{max}. Thus, Δ is the step size to vary each parameter value from its mean.

3. A matrix of T_{max} and C_{max} values is obtained from the PK model simulation for each permutation of parameter values up to a $\pm 8\Delta$ range from the mean.

4. Finally, a CV of T_{max} and C_{max} is calculated for the normally distributed parameters with 3 standard deviation (SD) range ($\sim$100%) of $\pm\Delta$ up to $\pm 8\Delta$ from the mean. The variation resulting in a CV of T_{max} and C_{max} matching published values in Table 5.3 is then selected.

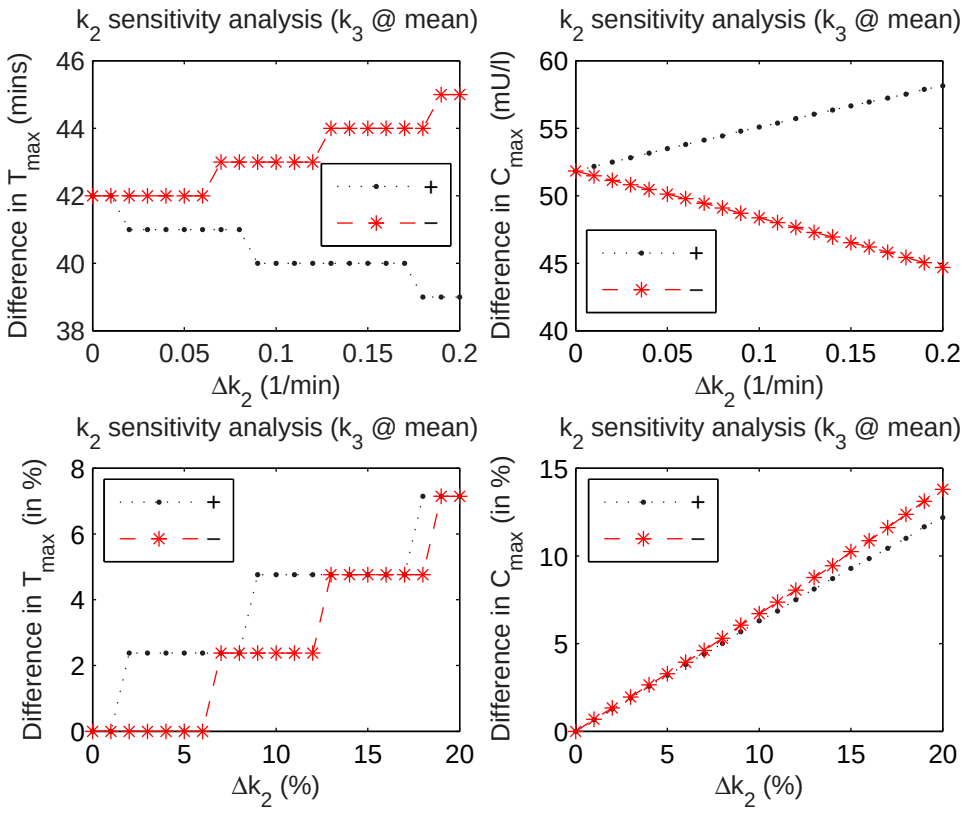

Figure 5.2 Sensitivity analysis of k_2 for the MI PK model. Δk_2 is selected for a minimum 5% absolute change in both T_{max} and C_{max}. Δk_2 is the step size to vary k_2 from the mean to calculate T_{max} and C_{max}.

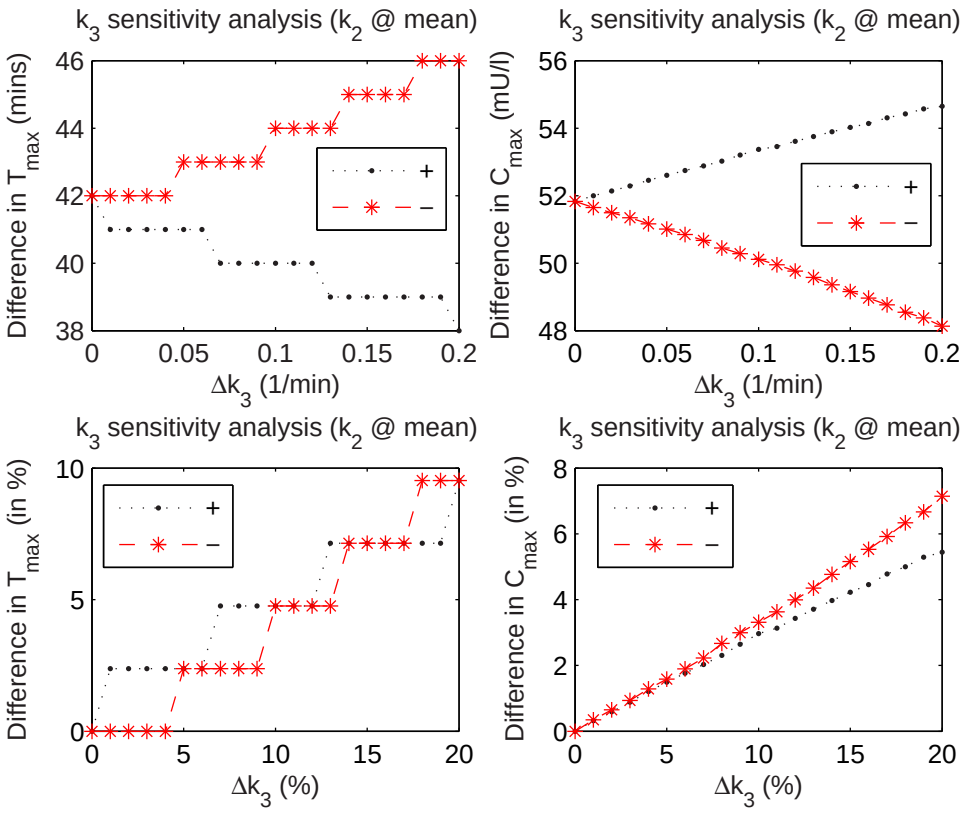

Figure 5.3 Sensitivity analysis of k_3 for the MI PK model. Δk_3 is selected for a minimum 5% absolute change in both T_{max} and C_{max}. Δk_3 is the step size to vary k_3 from the mean to calculate T_{max} and C_{max}.

Table 5.1 Variability in CV of pharmacokinetic summary measures T_{max} and C_{max} derived from literature. The use of CV implies a normal distribution of the summary measures, which is assumed in this study. The reported inter- and intra-batch coefficients of variation (CV_{inter}, CV_{intra}) are used to calculate a total coefficient of variation, CV_{total}

Insulin type	Study	PK summary measure	CV_{intra} [%]	CV_{inter} [%]	CV_{total} [%]
MI	1	T_{max}	15 ±6	18	23
		C_{max}	14 ±9	20	24
	2,3	T_{max}	15.2	-	-
		C_{max}	9.9	0	0
	4	T_{max}	-	24	-
		C_{max}	-	24	
Glargine	5	T_{max}	-	-	-
		C_{max}	-	-	33
	6	T_{max}	48 (26-69)†	-	36*/49**
		C_{max}	29 (16-41)†	-	25*/47**
	7	T_{max}	-	64	-
		C_{max}	-	33	

1. Heinemann et al. [1998]
2. Antsiferov et al. [1995]
3. Wilde and McTavish [1997]
4. Heise et al. [1998]
5. Heise et al. [2004]
6. Scholtz et al. [2005]
7. Heinemann et al. [2000]

† 95% CI

* 1st clamp study

** 2nd clamp study

Table 5.2 Key model parameters identified in Chapter 2 and 3 with mean values

Model type	Key parameters [unit]	Value
MI	k_2 [1/min]	0.0104
	k_3 [1/min]	0.0614
Glargine	$k_{prep,gla}$ [1/min]	0.0011
	$k_{1,gla}$ [1/min]	0.0078
	α_{gla} [unitless]	0.9192
Meal glucose appearance in plasma, $P(t)$	k_6 [1/min]	0.0388
	k_7 [1/min]	0.0097
	$GABS_{max}$ [g/min]	1.1

Table 5.3 CV of T_{max} and C_{max} chosen to match published values in Table 5.1 as closely as possible and which are used in the MC analysis

Model type	PK summary measure	CV_{total} [%]
MI	T_{max}	25
	C_{max}	25
Glargine	T_{max}	48
	C_{max}	33
Meal glucose	T_{max}	25
appearance in plasma, $P(t)$	C_{max}	25

As an example, the process is shown for MI. Referring to Figure 5.2 and 5.3, the sensitivity analysis is shown for parameters k_2 and k_3. The maximum variation from the mean ($\bar{k_2}$ and $\bar{k_3}$) resulting in an absolute 5% variation in T_{max} and C_{max} is set as the step size, Δk_2 and Δk_3. From Figure 5.4, T_{max} and C_{max} are derived from the PK model simulation for permutations of k_2 and k_3 where $k_2 = \left[\bar{k_2} - n\Delta k_2, \bar{k_2} - (n-1)\Delta k_2, ..., \bar{k_2} + (n-1)\Delta k_2, \bar{k_2} + n\Delta k_2\right]$ and $k_3 = \left[\bar{k_3} - n\Delta k_3, \bar{k_3} - (n-1)\Delta k_3, ..., \bar{k_3} + (n-1)\Delta k_3, \bar{k_3} + n\Delta k_3\right]$ and $2n+1$ is the arbitrary number of k_2 and k_3 values tested. Finally, a matrix of CV of T_{max} and C_{max} is calculated for a normally distributed k_2 and k_3. The normal distribution has a ± 3 SD range between $k_2 = \bar{k_2} \pm i\Delta k_2$ and $k_3 = \bar{k_3} \pm i\Delta k_3$, and is generated for all i, j where i=1,2,...,n and j=1,2,...,n. From Figure 5.5, appropriate i, j can then be selected to impart the required variation in the PK summary measures.

Meal carbohydrate amount and type are the main factors affecting meal glucose Ra [Korach-Andre et al., 2004; Wolever and Bolognesi, 1996a,b]. After errors in meal carbohydrate counting, variability in meal carbohydrate Ra in plasma is largely due to meal carbohydrate absorption of different carbohydrate types. In this MC analysis, meal glucose Ra is assumed to have a CV of T_{max} and C_{max} of 25% as values for this figure are not readily available in the literature. The variation in key parameters of the meal glucose Ra model in Table 5.2 is determined using the same technique applied to the MI model.

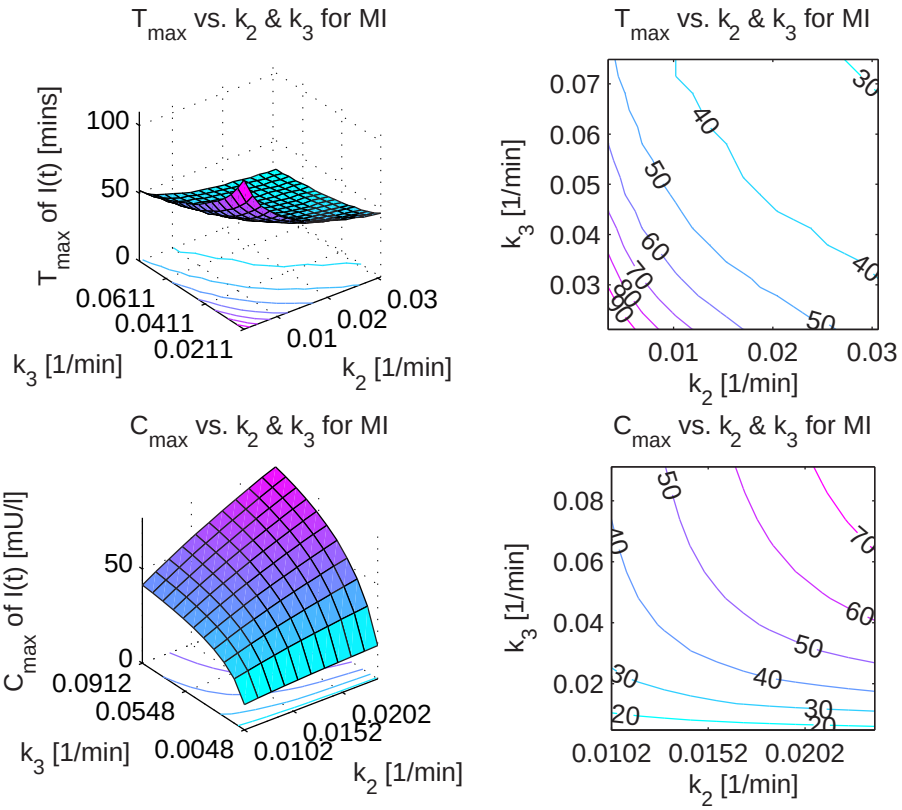

Figure 5.4 A grid of T_{max} and C_{max} are derived from the sc insulin PK model simulation for permutations of k_2 and k_3 where $k_2 = \left[\bar{k_2} - n\Delta k_2, \bar{k_2} - (n-1)\Delta k_2, ..., \bar{k_2} + (n-1)\Delta k_2, \bar{k_2} + n\Delta k_2\right]$ and $k_3 = \left[\bar{k_3} - n\Delta k_3, \bar{k_3} - (n-1)\Delta k_3, ..., \bar{k_3} + (n-1)\Delta k_3, \bar{k_3} + n\Delta k_3\right]$ and $2n+1$ is the arbitrary number of k_2 and k_3 values tested.

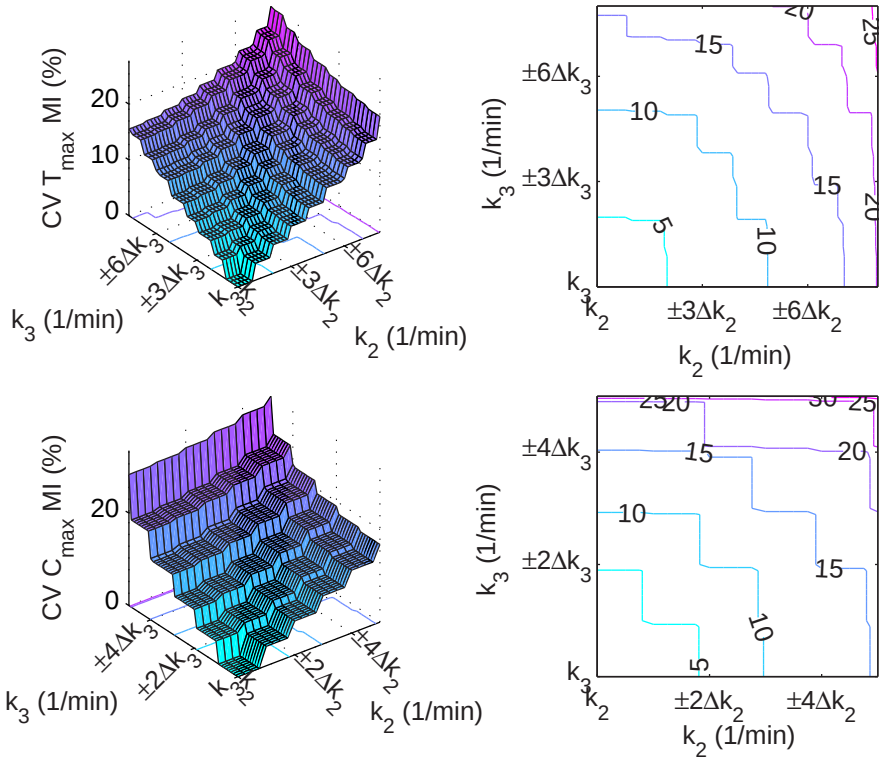

Figure 5.5 A matrix of CV of T_{max} and C_{max} calculated for a normally distributed k_2 and k_3. The normal distribution has a ±3 SD range between $k_2 = \bar{k_2} \pm i\Delta k_2$ and $k_3 = \bar{k_3} \pm i\Delta k_3$, and is generated for all i, j where i=1,2,...,n and j=1,2,...,n. An appropriate i, j can then be selected to impart the required variation in T_{max} and C_{max}.

5.2 Monte Carlo iterations

It is likely that the AC protocol will be in clinical use with optimal basal insulin replacement, and CIR and ISF parameters, which are simulated here. The required number of MC simulations is identified to be 300 per patient in a convergence test, as the variability in the patient blood glucose (SD) did not change significantly with additional runs. In total, 300 simulations per patient per SMBG frequency are performed for a cohort of 40 patients and 5 SMBG frequencies (2, 4, 6, 8 and 10) resulting in 60,000 (300 x 40 x 5) simulations. Each simulation is 24h in length, resulting in a total of 1,440,000 simulated patient hours. Figure 5.6 shows a single virtual control simulation trial with MC error in profiles of blood glucose, insulin concentration and meal glucose appearance as an example.

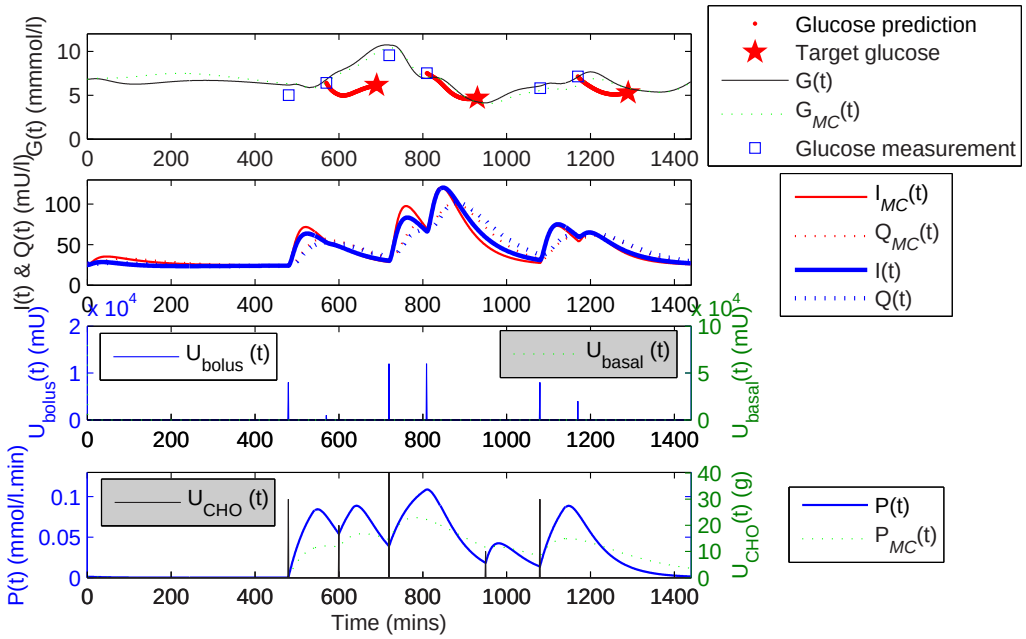

Figure 5.6 A sample virtual control simulation trial with MC error in profiles of blood glucose, insulin concentration and meal glucose appearance.

5.3 Results metrics

All calculations and analyses are performed using SPSS® (SPSS Inc., Chicago, IL, USA). Distributions are compared using a non-parametric, two-tailed Wilcoxon

signed-rank test. An asymptotic significance value of $\leq$0.05 is considered statistically significant. Protocol effectiveness is evaluated by HbA_{1c} as determined by the method of [Rohlfing et al., 2002] as described in Chapter 4. Protocol safety is evaluated by the time spent in mild ($\leq$3.9mmol/l) and severe ($\leq$3.0mmol/l) hypoglycaemia [ADA, 2005] expressed as a percentage of total time as also described in Chapter 4. Other indicators of effectiveness used are the time spent in clinically important bands, e.g., the normal 4-6mmol/l band and the wider normal 4-8mmol/l band.

5.4 Results

The results of the Monte Carlo *in silico* simulation of the AC protocol in conditions of optimal basal insulin replacement, and optimal CIR and ISF parameters, are as follows.

5.4.1 HbA_{1c}

Referring to Figure 5.7 and Table 5.4, the empirical cumulative distribution function (CDF) of HbA_{1c} under the AC control protocol is shown with the controls group for comparison, with and without applied MC error. Referring to Figure 5.7 and Table 5.4, only 52.5% of the controls group cohort have a HbA_{1c}<7.0% [ADA, 2006b] and only 40% have <6.5% [AACE, 2002]. Only 22.5% of the cohort have normal HbA_{1c} (<6.0%).

All MC HbA_{1c} distributions are significantly lower than the no error simulation for equivalent SMBG frequency. For a 6/day measurement frequency and no error, the control protocol results in 100% of the cohort controlled to ADA guidelines, 97.5% to AACE guidelines, and 87.5% to normal HbA_{1c} levels. With MC error, these figures are 100%, 97.5% and 92.5% respectively, which although statistically significant, is only a difference of one patient controlled to within normal HbA_{1c} level. All distributions decrease significantly with increasing SMBG frequency, as expected. Hence, the effectiveness of the protocol is robust to simulated MC error.

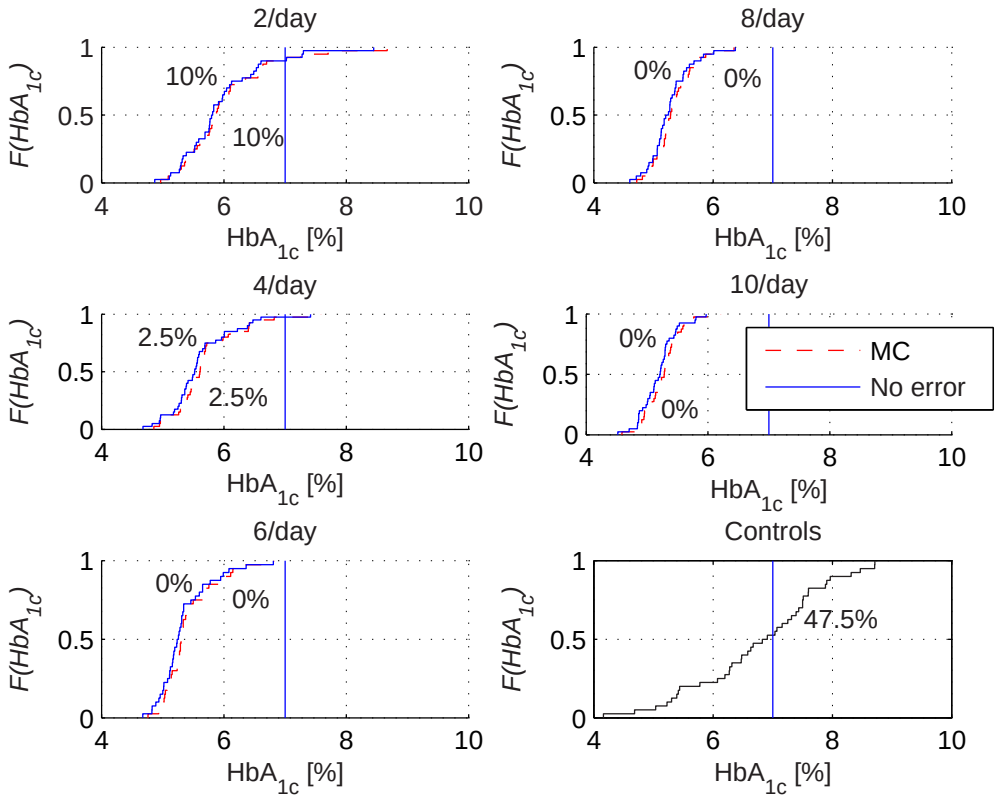

Figure 5.7 The empirical cumulative distribution function (CDF) of HbA_{1c} under the AC control protocol (with optimal basal insulin replacement, and CIR and ISF parameters) for the no error and MC simulations, with the controls group for comparison. The results of the no error simulation are adapted from Chapter 4.

5.4.2 Other metrics

Referring to Figure 5.8 and Table 5.5, the median and 95% confidence band of the time spent by the cohort in mild ($\leq$3.9mmol/l) and severe ($\leq$3.0mmol/l) hypoglycaemia, and in the 4-6mmol/l and 4-8mmol/l bands are shown as a percentage. In Figure 5.9, the asymtotic significance level calculated from the Wilcoxon signed-rank test for the distribution of the results metrics between MC and no error simulations are shown versus SMBG frequency.

Table 5.4 The percentage of the cohort controlled to recommended HbA_{1c} thresholds (<7.0%, ADA [ADA, 2006b] and <6.5%, AACE [AACE, 2002]) and the normal HbA_{1c} level (<6.0%) under the AC control protocol (with optimal basal insulin replacement, and CIR and ISF parameters) for the no error and MC simulations, with the controls group for comparison. The results of the no error simulation are adapted from Chapter 4.

Simulation type	SMBG frequency [/day]	HbA_{1c}[%]		
		<6.0	<6.5	<7.0
Controls		22.5	40.0	52.5
No error	2	62.6	75.5	90.0
	4	80.0	95.0	97.5
	6	87.5	97.5	100.0
	8	95.0	100.0	100.0
	10	97.5	100.0	100.0
MC	2	65.0	82.5	90.0
	4	80.0	95.0	97.5
	6	92.5	97.5	100.0
	8	95.0	100.0	100.0
	10	100.0	100.0	100.0

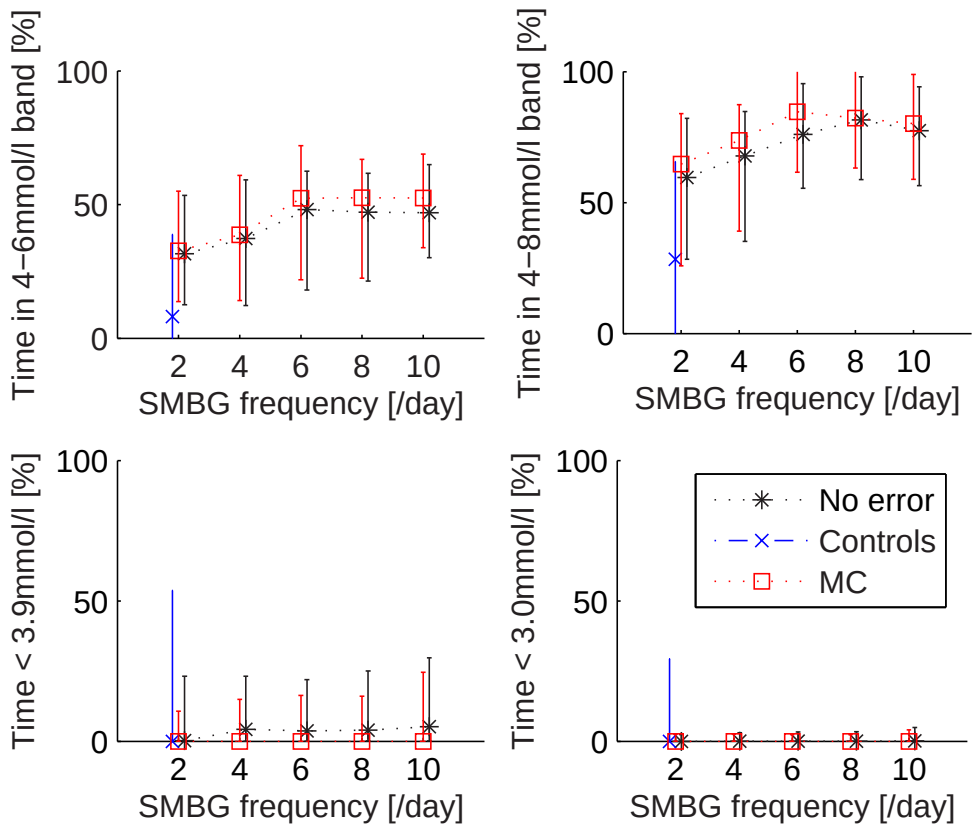

Figure 5.8 Median and 95% confidence bands of the time spent by the cohort in mild (≤3.9mmol/l) and severe (≤3.0mmol/l) hypoglycaemia, and in the 4-6mmol/l and 4-8mmol/l bands under the AC control protocol (with optimal basal insulin replacement, and CIR and ISF parameters) for the no error and MC simulations, with the controls group for comparison. The results of the no error simulation are adapted from Chapter 4.

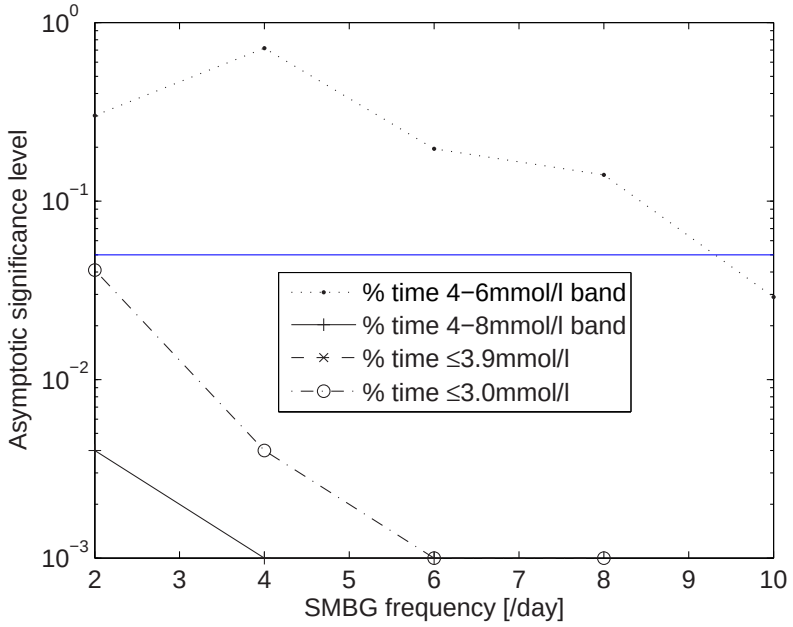

Figure 5.9 Asymtotic significance level calculated from the Wilcoxon signed-rank test for the distribution of the percent time spent in the 4-6mmol/l band, 4-8mmol/l band, $\leq$3.9mmol/l and $\leq$3.0mmol/l between MC and no error simulations versus SMBG frequency. The asymptotic significance value of $\leq$0.05 considered statistically significant is the horizontal line shown in the figure as a comparison.

Table 5.5 Median and 95% confidence bands of the time spent by the cohort in mild (≤3.9mmol/l) and severe (≤3.0mmol/l) hypoglycaemia, and in the 4-6mmol/l and 4-8mmol/l bands under the AC control protocol (with optimal basal insulin replacement, and CIR and ISF parameters) for the no error and MC simulations, with the controls group for comparison. The results of the no error simulation are adapted from Chapter 4.

Simulation type	SMBG frequency [/day]	Metrics [%]			
		Time spent ≤3.0mmol/l	Time spent ≤3.9mmol/l	Time spent 4-6 mmol/l	Time spent 4-8 mmol/l
Controls		0 (0-29.52)	0 (0-53.68)	8.08 (0-38.76)	28.38 (0-65.58)
MC	2	0† (0-2.37)	0.2† (0-23.18)	31.65 (12.52-53.46)	59.62† (28.38-82.21)
	4	0.03† (0-3.04)	4.22$^{\dagger *}$ (0-23.15)	37.30* (12.24-59.29)	67.82$^{\dagger *}$ (35.24-84.77)
	6	0.03† (0-3.34)	3.72† (0.02-21.92)	48.10* (18.02-62.46)	76.05$^{\dagger *}$ (55.50-95.43)
	8	0.07† (0-3.42)	3.95† (0.10-25.05)	47.17* (21.35-61.71)	81.57† (58.76-98.03)
	10	0.12$^{\dagger *}$ (0-4.87)	5.19$^{\dagger *}$ (0.19-29.71)	46.93† (30.10-64.99)	77.49$^{\dagger *}$ (56.50-94.20)
No error	2	0 (0-2.45)	0 (0-10.70)	32.69 (13.72-55.05)	64.68 (25.90-83.95)
	4	0 (0-2.57)	0* (0-14.92)	38.65* (14.16-60.90)	73.70* (39.07-87.40)
	6	0 (0-2.43)	0 (0-16.33)	52.39* (21.86-72.07)	84.73* (61.62-100.00)
	8	0 (0-2.43)	0 (0-16.05)	52.53 (22.50-66.95)	82.30 (63.22-100.00)
	10	0* (0-4.04)	0* (0-24.62)	52.46 (33.92-68.89)	80.15* (58.90-98.92)

† Distribution significantly different compared to equivalent SMBG frequency no error simulation

* Distribution significantly different compared to previous SMBG frequency

5.4.2.1 Hypoglycaemia

For the controls group, the 95% confidence band of time spent in mild and severe hypoglycaemia is 0-53.68% and 0-29.52% respectively, decreasing significantly under no error control to 0-16.33% and 0-2.43% for a SMBG frequency of 6/day. In MC simulation with the same SMBG frequency, the median rises to 3.72% and 0.03%, with a 95% confidence band of 0.02-21.92% and 0-3.34% respectively. While the increase in hypoglycaemia is small, the increase is significant over the no error simulation for equivalent SMBG frequency. However, the figures are still very much reduced compared to controls. This result shows that the safety of the protocol remains robust to simulated MC error with this protocol compared to an average cohort.

With SMBG frequency, MC severe hypoglycaemia is not significantly different until from 8 to 10/day, where it increases significantly. MC mild hypoglycaemia is significantly increased only from SMBG frequency 2 to 4/day, and from 8 to 10/day. Both trends are also apparent in the no error simulation, which implies an optimal SMBG frequency for safety from both mild and severe hypoglycaemia at 4 to 8/day.

5.4.2.2 Time in the 4-6mmol/l and 4-8mmol/l bands

Time spent in the 4-6mmol/l band increases significantly with increasing SMBG frequency except from 8 to 10/day, which is insignificant. In contrast, time spent in the 4-8mmol/l band increases with increasing SMBG frequency except from 8 to 10/day, where it *decreases* significantly.

While the distributions are increased, the no error simulation median time spent in the 4-8mmol/l band reaches a zenith (84.73%) at 6/day. With MC error, the zenith (81.57%) occurs at 8/day. With greater uncertainties within the system, a higher SMBG frequency can be expected to result in an increased level of control compared to the no error simulation, which has generally been the trend observed clinically [Davidson et al., 2004; Karter et al., 2001; Schutt et al., 2006]. The time spent in the normal 4-6mmol/l band for the MC simulation is not significantly different to no error simulation except for SMBG frequency of 10/day, where it is significantly less.

5.5 Discussion

In summary, there is a significant increase in mild and severe hypoglycaemia from SBMG frequency of 8 to 10/day. There is also a concurrent, insignificant increase in time spent in the 4-6mmol/l band and a significant decrease in time spent in the 4-8mmol/l band from SMBG frequency of 8 to 10/day. In addition, the MC time spent in the 4-6mmol/l band is significantly less than the no error simulation only for SMBG frequency of 10/day.

These results indicate a peak in overall control at SMBG frequency 8/day. The peak is followed by a small but significant decline in control effectiveness and safety after SMBG frequency of 8/day. As such, a SMBG frequency (or rather, a frequency of control intervention) of >8/day with the developed AC protocol cannot be recommended based on the results of this MC study. The time span of insulin effect (with its inherent variability) gets closer to or overlaps the next insulin intervention with increasing SMBG frequency. The model-based approach in this study should reduce this effect, clinically termed 'bolus stacking'. However, variability in S_I and the limitations in its prediction while determining the correction dose contribute to this effect.

Clinically, a SMBG frequency of ∼6/day is probably an acceptable compromise between control effectiveness and safety, and the patient effort required to perform the SMBG and control interventions using the adaptive protocol. Referring to Table 5.4, it is also the minimum SMBG frequency to result in 100% of the cohort controlled to the ADA clinical glycaemic control guideline.

It has been shown in Chapter 4 previously that an 8-point SMBG frequency may be insufficient if the protocol implemented is a conventional IIT with suboptimal basal insulin replacement. From Chapter 4, glycaemic control with the suboptimal basal insulin conventional protocol saturates at a SMBG frequency of 6/day with only 75% of the cohort meeting ADA guidelines. However in this MC analysis of the AC protocol in conditions of optimal basal insulin, 97.5% of the cohort meet the ADA recommended HbA_{1c} level even with a SMBG frequency of 4/day. Incidentally, this is also the minimum SMBG frequency recommended for calibration of CGMS devices [Medtronic Inc., 2004].

From another perspective, the percentage of the cohort meeting clinical guide-

lines is plotted as a function of the minimum SMBG frequency required in Figure 5.10. With MC error, 90% of the cohort meet the ADA guideline with just 2 measurements a day. A further 7.5% required only 4 measurements a day, and 2.5% (1 patient) required 6 measurements a day. Hence, different patients can be optimally controlled with different SMBG frequency, matching clinical results. Note that the lower the SMBG frequency, the lower the clinical effort or burden required to implement the protocol, and thus, patient protocol compliance is likely to be higher.

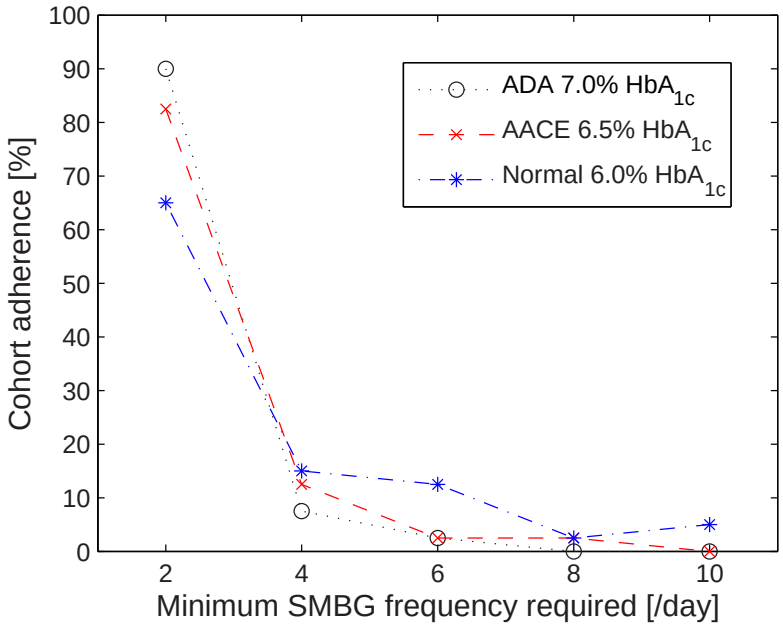

Figure 5.10 Percentage of cohort complying to ADA [ADA, 2006b], AACE [AACE, 2002] and normal HbA_{1c} levels as a function of minimum SMBG frequency required.

In safety, the protocol is also robust to the applied MC error. With a 6/day SMBG frequency, the 95% confidence bands of time spent in severe and mild hypoglycaemia are 3% and 22% compared to 30% and 54% for the controls group (a relative reduction of 90% and 59% respectively). Compared to the no error simulation, the figures are 2% and 16%, a statistically significant, but acceptable absolute difference of 1% and 6%. As fear of hypoglycaemia is a large psychological barrier to glycaemic control, the AC control protocol may represent the next evolution of ambulatory intensive insulin therapy to deliver increased glycaemic control with increased safety.

5.6 Conclusions

An *in silico* Monte Carlo simulation tool is presented that utilises an extended, validated model of glucose kinetics, and a novel subcutaneous insulin pharmacokinetic model. The virtual patient cohort and its default control protocol (the data of which is used for *in silico* simulation) is representative of the broad diabetes population. The developed Monte Carlo simulation tool is based on physiologic, and realistic error and variability from literature.

The simulation tool is used to test an adaptive protocol for prandial insulin dosing in conjunction with the Fritsche-Riddle basal insulin forced-titration regimen in long-term control. A MC analysis with simulated error in insulin and meal absorption, insulin dosing, meal carbohydrate counting and blood glucose measurements is performed.

In a MC simulation of over 1,400,000 patient hours, the control protocol controlled 100% of the cohort to the ADA recommended glycaemic control with a SMBG frequency of 6/day. A defined peak in control is achieved at SMBG frequency of 8/day with a small but significant decrease in the time spent in the 4-8mmol/l band, and consequent increase in mild and severe hypoglycaemia at SMBG frequency of 10/day. In addition, time spent in the 4-6mmol/l band is not significantly different to the no error simulation for all SMBG frequencies except for 10/day.

For all SMBG frequencies, the cohort HbA_{1c} distribution is reduced while hypoglycaemia is increased over the no error simulation, as can be expected. While statistically significant, the difference in 95% confidence band of time spent in severe and mild hypoglycaemia is an acceptable 1% and 6% respectively over the no error simulation for a 6/day SMBG frequency. Fear of hypoglycaemia is a large psychological barrier to effective glycaemic control and, hence, the AC control protocol may represent the next evolution of ambulatory intensive insulin therapy to deliver increased glycaemic control with increased safety.

The objective of the MC analysis is to test the robustness of the adaptive AC control protocol first developed in Chapter 4. The *in silico* simulation tool from Chapter 4 is expanded with physiologic, and realistic error and variability that would apply in a real-time clinical situation. From this analysis, results that

match clinical expectations are obtained, results that strongly support the performance of the proposed adaptive protocol. With the completion of the Monte Carlo analysis, the next step in this research is to explore possible areas for increasing performance, both in effectiveness and safety. This aspect is investigated in the following chapter in the identification and prediction of circadian rhythms in S_I.

Chapter 6

Modelling of Diurnal Variation in S_I

Circadian rhythmicity and sleep-wake phases have profound and independent effects on glucose tolerance, as reviewed by Van Cauter et al. [1997]. In normal man, insulin secretion controls the balance between hepatic glucose production and glucose uptake to achieve plasma glucose homeostasis with little variation across the day. While diurnal patterns in glucose tolerance exist in normal humans, they are more apparent in impaired glucose homeostasis, e.g., diabetes [Bolli, 1988; Bolli et al., 1993].

In insulin-dependent diabetes (IDDM), the dawn phenomenon is the main dynamic encountered in diurnal glucose tolerance. Circadian counter-regulatory hormone rhythmicity, as regulated by the suprachiasmatic nucleus, e.g., cortisol, glucagon, and epinephrine, has been shown to be less significant a driver for this behaviour than sleep-associated growth hormone (GH) secretion [Clore et al., 1989; Perriello et al., 1991]. Patients with well controlled glycaemia exhibit less GH secretion and consequently less overnight glucose increase, which matches experimental observation [Press et al., 1984]. The exact mechanism of diurnal glucose tolerance is still being debated, but has been attributed to reduced effective insulin sensitivity manifested in impaired suppression of hepatic glucose production and peripheral glucose clearance. However, the phenomenon is well documented in IDDM (80-100% of patients with Type 1 diabetes exhibit diurnal glucose tolerance), and is consistent and reproducible intra-subject (with CV <6%) [Bolli et al., 1993].

As such, identification and prediction of this rhythm is of utmost clinical relevance. Dietary and/or insulin management can be improved with precise, *a priori* knowledge of this rhythm. If patient-specific, model-based effective insulin

sensitivity (a surrogate measure of glucose tolerance) can be predicted with a probability distribution based on clinically observed diurnal variation, potentially safer and more effective glycaemic control can be attained with less frequent measurement.

This chapter reports the identification of diurnal cycles in the model-based, effective insulin sensitivity parameter, S_I, using the system model of Type 1 diabetes developed in Chapter 3. An autoregressive (AR) model is also implemented on the residuals to account for further variation in insulin sensitivity due to patient-specific conditions or variations. Hence, all major sources of potential patient variation are addressed. The overall goal is to better understand how an individual's ability to utilise insulin can vary over time.

From the control simulations performed in Chapter 4 and 5, the SMBG frequency and, hence, intervention frequency, can be considered a cost, both financial and in patient effort, and reduced measurement frequency while maintaining good control is desirable. The aim of this chapter is to increase predictive accuracy of the model via modelling variations in the driving parameter, i.e., effective insulin sensitivity.

6.1 Methods

6.1.1 Patient cohort

Table 6.1 outlines a retrospective cohort of Type 1 diabetes mellitus patients (n=21) from which data is collected. Of these, 19 data sets are obtained via a data donation request with informed consent, where 12 are from daily logs recorded by outpatient Type 1 diabetes patients and 7 are from postoperative, insulin-dependent diabetes (IDDM) patients admitted to the Cardiothoracic Ward (CTW) of Christchurch Hospital. The final 2 data sets are taken from studies published by Lehmann and colleagues [Lehmann and Deutsch, 1992a, 1993] for which age data is not available.

Median length of each data set is 90 hours (with 90% of sets between 35 and 184 hours in length). Sex is biased towards males (14 to 7). Insulin type

use is diverse, ranging from IV insulin to subcutaneous insulin including MI analogue, RI, NPH insulin and insulin glargine. Median (inter-quartile range) of time between measurements is 120mins (66-240mins) across the cohort with mean of 181mins. Excluding the data sets of Lehmann et al., the median age of the cohort is 26 with inter-quartile range 21 to 65 years old.

Table 6.1 Details of the Type 1 diabetes patient cohort (n=21) of which retrospective data is collected for this study. 19 data sets are obtained via a data donation request with informed consent. Of this, 12 data sets are from daily logs recorded by ambulatory Type 1 diabetes patients and 7 sets are from postoperative, insulin-dependent diabetic (IDDM) patients admitted to the Cardiothoracic Ward (CTW) of Christchurch Hospital. 2 data sets are taken from studies published by Lehmann and colleagues [Lehmann and Deutsch, 1992a, 1993] of which age data is not available.

Patient number	Length of data [hours]	Insulin type		Average CHO intake/day [g/day]	Average total insulin dose/day [U/day]	Age/Sex [years/ M or F]	Body weight [kg]
		Bolus	Basal				
1	36	MI	NPH	464	118.0	20M	77
2	70	MI	NPH	239	44.9	8F	35
5	37	CSII		307	84.0	33M	74
46	61	CSII		268	61.2	33M	74
48	39	RH	Lente	111	30.8	-M	70
49	40	RH	NPH	216	28.2	-F	60
50	159	CSII		162	21.7	26F	63
51	114	CSII		144	24.3	26F	63
52	112	CSII		149	24.0	26F	63
53	136	MI	Glargine	183	38.0	18M	48
54	181	MI	NPH	318	107.7	21M	72
55	98	MI/RH	IV	136	40.2	65M	74
56	100	RH	IV	188	68.9	73M	90
57	116	NPH		117	28.6	82M	110
58	54	Penmix 30		170	39.1	59M	92
59	90	IV		130	45.5	65F	79
60	188	MI	NPH/IV	100	35.1	66F	77
61	97	RH		51	12.4	76M	79
62	132	MI	Glargine	303	69.1	21M	72
63	33	MI	Glargine	397	66.2	21M	72
64	130	MI	Glargine	251	52.8	21M	72

6.1.2 Diurnal S_I modelling

Referring to Chapter 4, S_I prediction with the adaptive AC protocol can be said to be simplistic, assuming a constant S_I from the end of the S_I identification period up to the end of the prediction horizon at time, t_{pred}. In addition, the control algorithms of Chase et al. [2005b] and Wong et al. [2006a,b] administering intravenous insulin to critically ill cohorts use S_I from the previous hour, or a weighted average of prior $S_I(t)$ values to 'predict' $S_I(t)$ for hourly, patient-specific, blood glucose-targeted insulin interventions.

In these studies on critically ill patients, interventions are specified after half-hourly or hourly glucose measurements. Critically ill patients are highly variable and dynamic, as evidenced in Wong et al. [2006a]. With the availability of sufficient nursing effort, hourly interventions based on hourly glucose measurements and, hence, 1 hour prediction horizons can be considered the norm for consistent tight control.

In ambulatory or outpatient Type 1 diabetes, SMBG frequency is much lower and variable, and regular SMBG is uncommon. In studies by Evans et al. [1999] and Karter et al. [2001], only 20% to 67% of Type 1 diabetics measured on average once or more a day. In the study by Karter et al., only 34% of Type 1 diabetes adhered to the ADA recommended daily SMBG frequency of 3 or more [ADA, 2006b], while in a study by Schutt et al. [2006], the average SMBG frequency was 4.4/day.

Hence, these studies show quite a large variability in SMBG frequency performed clinically in Type 1 diabetes. What is known is that with reduced glucose measurement frequency compared to critical care, a more effective method is needed to predict the time evolution of S_I over longer prediction horizons between interventions to enable better prediction. A secondary objective would be to produce patient-specific S_I confidence bands. These bands would allow more confident estimation of S_I for any given insulin intervention or meal disturbance, leading to safer, more optimal diabetes management.

To achieve this goal, the patient $S_I(t)$ profile or signal is considered a time series with fixed-period, cyclical components of diurnal nature. As $S_I(t)$ is piecewise constant, for the purposes of this study it can be considered a discrete time

series $S_t = \{S_1, ..., S_N\}$. The *deterministic* diurnal cycle is first identified by performing a discrete Fourier transform (DFT) on the patient S_t signal obtained through model fit to patient data as described in Chapter 4. No filtering or smoothing is performed on the raw S_t signal. The assumption is that the cycle is a sinusoid or a superposition of sinusoids. An example of a patient S_t profile is shown in Figure 6.1.

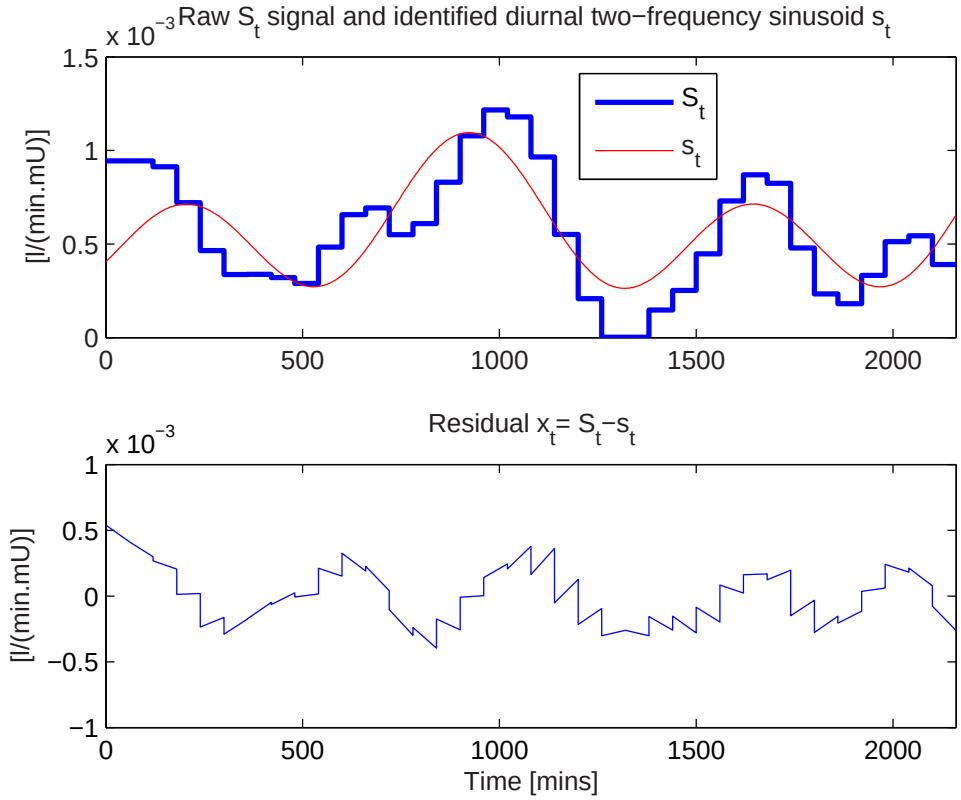

Figure 6.1 The discrete S_t signal of Patient 1 shown with the approximated discrete diurnal cycle s_t and the residuals $x_t = S_t - s_t$.

The DFT is computed with a fast Fourier transform (FFT) algorithm to derive the power spectrum with an example shown in Figure 6.2, from which the two strongest frequency components can be identified. Referring to Figure 6.3, a histogram of the two strongest identified frequencies for the cohort are shown. Only two frequencies are identified, which are also usually the lowest, following the principle of parsimony. Modelling further, usually higher, frequencies would likely *over-fit* the data. These frequencies can be attributed to signal noise, harmonics and/or leakage and not the underlying diurnal cycle.

It is also important to note also that S_I is a measure of effective insulin

sensitivity, a parameter that accounts for many, as yet unmodelled, dynamics such as exercise, stress, and hypoglycaemic counter-regulation. All of these other dynamics can be considered to be effectively superimposed on the true signal. The diurnal S_I dynamics of interest in this study have a much lower frequency than the Nyquist frequency (2 cycles per hour) and aliasing is thus not an issue. With a median (inter-quartile) data length of 98 (40-130) hours, the fundamental Fourier frequency is also much lower than the frequencies of interest.

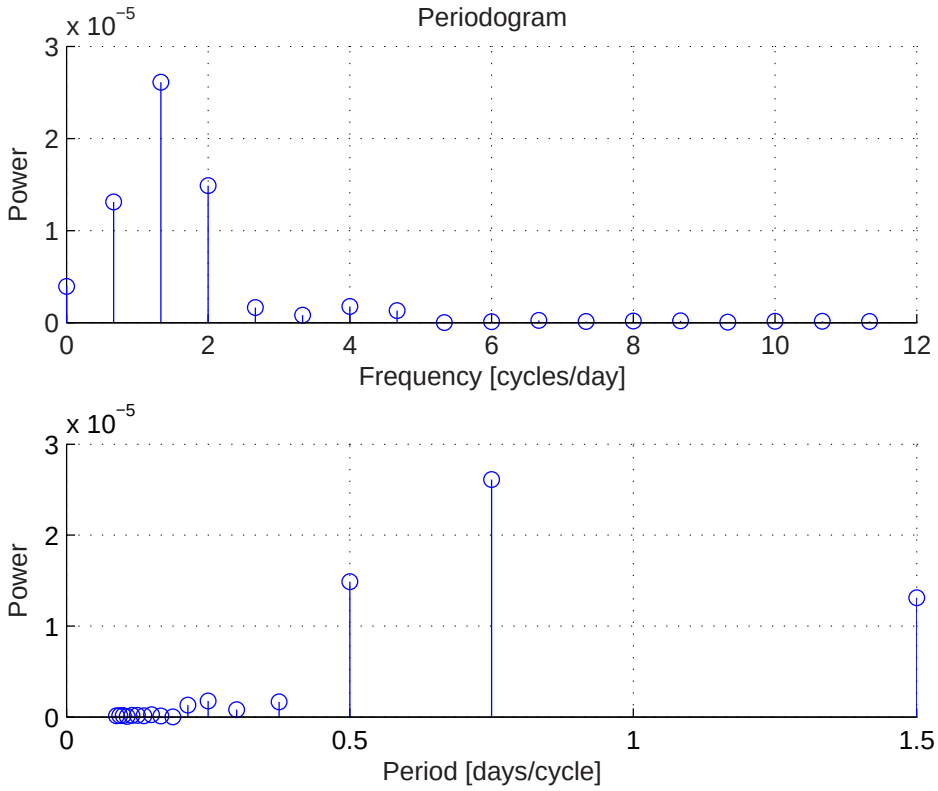

Figure 6.2 The DFT (shown here for Patient 1) is computed with a fast Fourier transform (FFT) algorithm to derive the power spectrum and identify the two strongest frequency components. Only two frequencies are identified (which are also usually the lowest) following the principle of parsimony. Modelling further, usually higher frequencies would likely over-fit the data, frequencies which can be attributed to signal noise, harmonics and/or leakage in the Fourier analysis and not the true, underlying diurnal cycle.

From Figure 6.3, it can be seen that there is a strong, primary frequency in S_I that is common to many patients in the cohort at approximately 0.75 cycles/day. The median (inter-quartile range) frequency is 0.8 (0.7-0.8) cycles/day. However, the secondary frequency is not as uniform across the cohort, with a 95th percentile range from 0.2 to 1.9 cycles/day. A five-parameter, sinusoidal diurnal cycle, s_t can thus be defined.

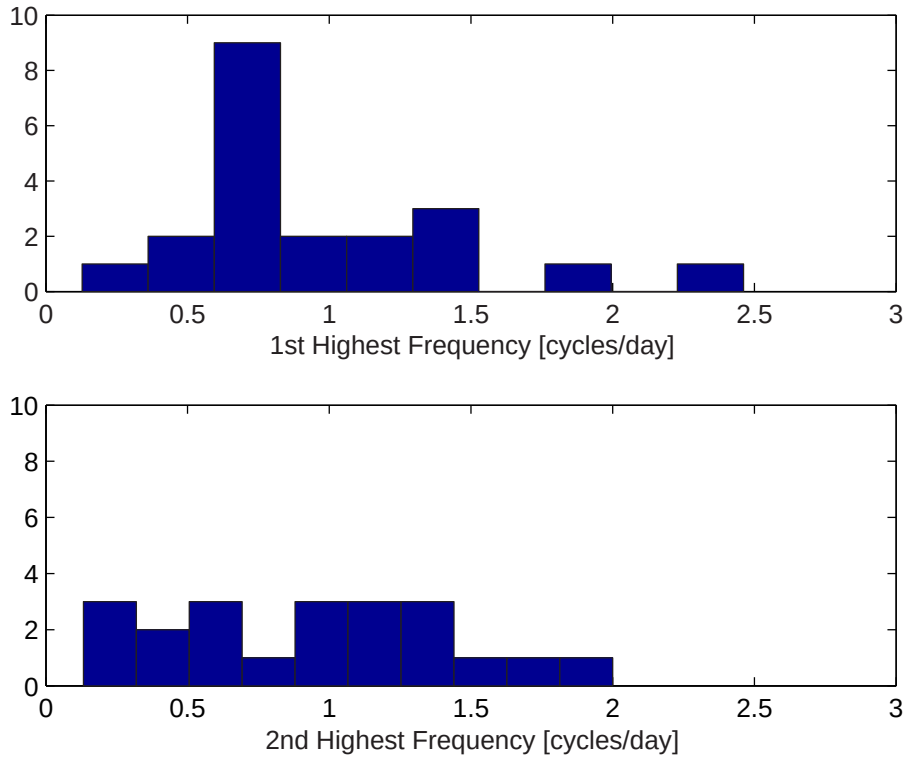

Figure 6.3 Histogram of the two strongest identified frequencies via DFT for the cohort. There is a strong, primary frequency in S_I which is common to many patients in the cohort at around 0.75 cycles/day. The median (inter-quartile range) frequency is 0.8 (0.7-0.8) cycles/day.

$$s_t = A_1 \sin(\omega_1 t) + B_1 \cos(\omega_1 t) + A_2 \sin(\omega_2 t) + B_2 \cos(\omega_2 t) + C \tag{6.1}$$

where ω_1 and ω_2 are the two frequencies of highest power, and A_1, A_2, B_1, B_2, C are unknown constants. This representation accounts for differences in phase of the two frequency cycles in the constants. A_1, A_2, B_1, B_2, C are solved by minimising the sum of squares objective function, S in Equation 6.2.

$$\begin{aligned} S(A_1, A_2, B_1, B_2, C) &= \sum_{t=1}^{N} (X_t)^2 \\ &= \sum_{t=1}^{N} (S_t - s_t)^2 \\ &= \sum_{t=1}^{N} \big[S_t - A_1 \sin(\omega_1 t) + B_1 \cos(\omega_1 t) \\ &\quad + A_2 \sin(\omega_2 t) + B_2 \cos(\omega_2 t) + C \big]^2 \end{aligned} \tag{6.2}$$

Once identified, s_t is subtracted from S_t, leaving the residuals x_t.

$$x_t = S_t - s_t$$

where $s_t = \{s_1, ..., s_N\}$ and $x_t = \{x_1, ..., x_N\}$ is the residual at t.

By observation, x_t is of stable variance with zero mean, has no trend or seasonal variation, and is normally distributed (Kolmogorov-Smirnov test, $p \leq 0.05$). As such, x_t requires no transformation and can be considered a stationary, discrete stochastic process.

By observation of an example of the sample autocorrelation function (ac.f.) in Figure 6.4, an autoregressive (AR) probability model is selected to best model x_t. From the cohort sample partial ac.f., the median AR model order (inter-quartile range) for the cohort is 3 (3-4). Thus, an AR(4) model is selected to model the residuals, x_t, across the cohort and is of the form in Equation 6.3.

$$x_t = \alpha_1 x_{t-1} + \alpha_2 x_{t-2} + \alpha_3 x_{t-3} + \alpha_4 x_{t-4} + a_t \tag{6.3}$$

where $\{a_t\}$ is a zero-mean, independent random process with common distribution function F_a, with $E[a^2] = \sigma_a^2 < \infty$, and α_1, α_2, α_3, α_4 are constants. The

parameters α_1, α_2, α_3, α_4 may be estimated as $\hat{\alpha}_1$, $\hat{\alpha}_2$, $\hat{\alpha}_3$, $\hat{\alpha}_4$ with least squares minimisation of the Yule-Walker equations:

$$\bar{A}\{\bar{\alpha}\}^T = \bar{b} \tag{6.4}$$

where $\{\hat{\alpha}\}^T = \{\hat{\alpha}_1, \hat{\alpha}_2, \hat{\alpha}_3, \hat{\alpha}_4\}$, , $\bar{A} = \begin{pmatrix} 1 & r_1 & r_2 & r_3 \\ r_1 & 1 & r_1 & r_2 \\ r_2 & r_1 & 1 & r_1 \\ r_3 & r_2 & r_1 & 1 \end{pmatrix}$, $\bar{b}^T = (r_1, r_2, r_3, r_4)$, $r_k = \frac{c_k}{c_0}$ is the estimator for the ac.f. at lag k, and c_k is the sample autocovariance function (acv.f.) at lag k which is defined as:

$$c_k = \frac{1}{N}\sum_{t=1}^{N-k}(x_t - \bar{x})(x_{t+k} - \bar{x})$$

The solution of Equation 6.4 is performed using Levinson-Durbin recursion. Further information on AR methods in this study can be found in Chatfield [2000, 2004] and Bloomfield [2000].

In summary, S_t is modelled *both* deterministically and stochastically. The main underlying diurnal cycle is modelled deterministically by Equation 6.1, while the rest of the complex, unmodelled metabolic variation is accounted for stochastically in Equation 6.3. With the removal of the cyclical diurnal variation in S_t, the residuals adhere reasonably to the required assumptions for a stationary, stochastic AR process and the model chosen can be sensibly employed in this situation. From the fitting of the sinusoidal diurnal cycle, and the identification of the AR model parameters from each individual data set, the method presented is patient-specific.

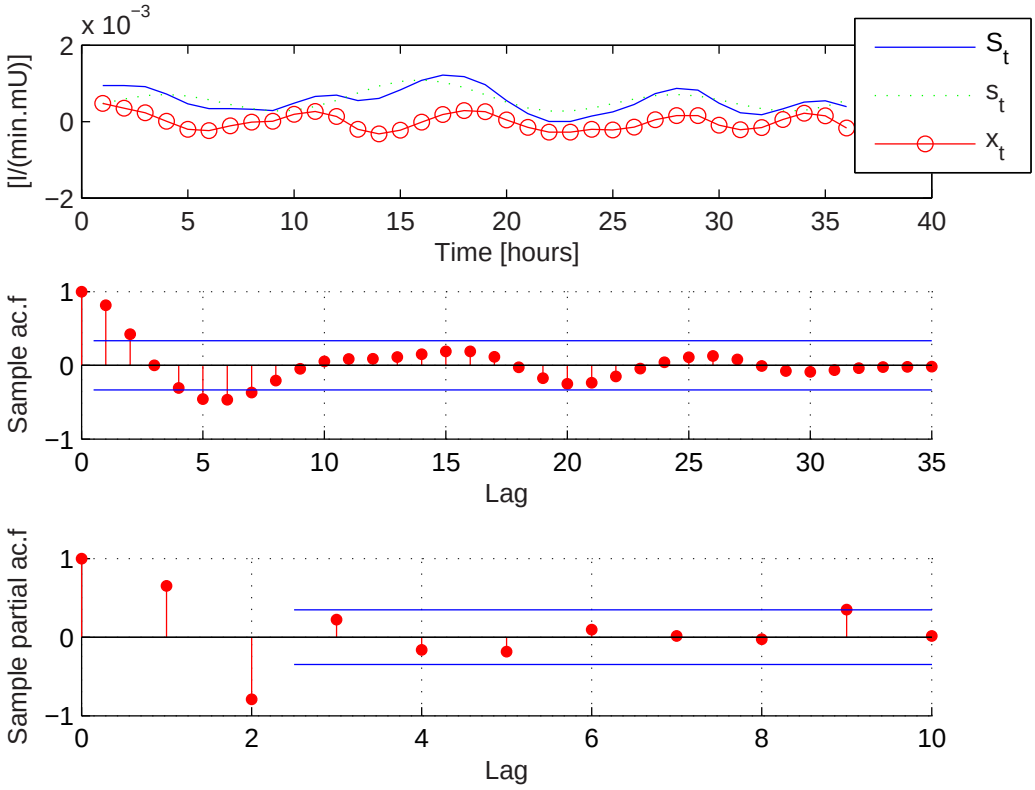

Figure 6.4 An autoregressive probability model is selected to best model x_t by observation of the sample autocorrelation function which is shown here for Patient 1. From the cohort sample partial autocorrelation function, the median AR model order (inter-quartile range) for the cohort is 3 (3-4). An AR(4) model is hence selected to model x_t across the cohort and is of the form in Equation 6.3.

6.1.3 S_I prediction

Predictions are performed for prediction horizons or leads ranging from 1 to 6 hours. 6 hours is the maximum lead that can reasonably be expected in outpatient Type 1 diabetes given the current knowledge of SMBG frequency in the population. For prediction bands, the AR bootstrap method of Thombs and Schucany [1990] is used in this study. While the model assumptions are reasonably qualified, the non-parametric bootstrap resampling method is chosen given that the parameter, S_I, is forced to account for many complex, non-random effects superimposed on the diurnal cycle.

The Thombs and Schucany [1990] method is outlined briefly here for clarity. Given a data set $x_t = \{x_1, ..., x_N\}$, the ith residual is defined in Equation 6.5.

$$\hat{a}_i = x_i - \hat{\alpha}_1 x_{i-1} + \hat{\alpha}_2 x_{i-2} + \hat{\alpha}_3 x_{i-3} + \hat{\alpha}_4 x_{i-4} \tag{6.5}$$

where $\hat{a}_i$ replaces the true errors a_i from the estimated distribution $\hat{F}_a$, $\hat{\alpha}_1$, $\hat{\alpha}_2$, $\hat{\alpha}_3$, $\hat{\alpha}_4$ are the least squares estimates of the AR model parameters and i=5,...,N.

Given the AR(4) process, 4 starting values are needed with the remainder of the bootstrap replicate generated using Equation 6.6.

$$x_j^* = \hat{\alpha}_1 x_{j-1}^* + \hat{\alpha}_2 x_{j-2}^* + \hat{\alpha}_3 x_{j-3}^* + \hat{\alpha}_4 x_{j-4}^* + \hat{a}_j^* \tag{6.6}$$

where $\hat{a}_j^*$ is a random draw from $\hat{F}_a$, and $\hat{F}_a$, $\hat{\alpha}_1$, $\hat{\alpha}_2$, $\hat{\alpha}_3$, $\hat{\alpha}_4$ are as in Equation 6.5 and j=5,...,N.

Given a data set with N observations $x_t = \{x_1, ..., x_N\}$ of the AR(4) process, let $x_t^* = \{x_1^*, ..., x_N^*\}$ be a typical bootstrap replicate. For a single replicate, the point prediction X_{t+k}^* for lead k is

$$X^*_{t+k} = \hat{\alpha}^*_1 x^*_{t+k-1} + \hat{\alpha}^*_2 x^*_{t+k-2} + \hat{\alpha}^*_3 x^*_{t+k-3} + \hat{\alpha}^*_4 x^*_{t+k-4} + \hat{a}^*_{t+k} \tag{6.7}$$

where $\hat{a}^*_{t+k}$ is a random draw from $\hat{F}_a$, and $\hat{\alpha}^*_1$, $\hat{\alpha}^*_2$, $\hat{\alpha}^*_3$, $\hat{\alpha}^*_4$ are the least squares estimates calculated from the bootstrap replicate of Equation 6.6 using Equation 6.4. Equation 6.7 is also used for calculating the point predictions.

Depending on lag k, x^*_{t+k-i} $(i = 1, ..., 4)$ will be one of the first 4 values of the bootstrap replicate or a bootstrap future value X^*_{t+k}. For k=1 hour, X^*_{t+k} is only dependent on $\hat{\alpha}^*_1$, $\hat{\alpha}^*_2$, $\hat{\alpha}^*_3$, $\hat{\alpha}^*_4$ and $\hat{a}^*$ which varies with each replicate. For subsequent k up to 6 hours, X^*_{t+k} must be calculated recursively. As x^*_{t+k-i} $(i = 1, ..., 4)$ in Equation 6.7 is now substituted by predicted future values X^*_{t+k-i} $(i = 1, ..., 4)$, the precision of the estimate can be expected to decrease as lag k increases. Having obtained B bootstrap future values from the B bootstrap replicates $(X^{*,1}_{t+k}, ..., X^{*,B}_{t+k})$ in Figure 6.5, the prediction bands are defined as quantiles of the bootstrap CDF. Hence, for a given β, a $100\beta\%$ prediction interval for X_{t+k} can be calculated from Equation 6.8.

$$\left[L^*_B(x), U^*_B(x)\right] = \left[Q^*_B\left(\frac{1-\beta}{2}\right), Q^*_B\left(\frac{1+\beta}{2}\right)\right] \tag{6.8}$$

A summary of the procedure is as follows.

1. Compute residuals from Equation 6.5. Let $\hat{F}_a$ be the empirical CDF of the residuals. No transformation or centering of mean is required.
2. Generate bootstrap replicate using Equation 6.6.
3. Compute AR model estimates $\hat{\alpha}^*_1$, $\hat{\alpha}^*_2$, $\hat{\alpha}^*_3$, $\hat{\alpha}^*_4$ from the bootstrap replicate as per Equation 6.4. Compute a bootstrap point prediction as in Equation 6.7 for lag k=1,...,6 using $\hat{a}^*_{t+k}$, a random draw from $\hat{F}_a$.
4. Repeat Step 2 to 3 for B bootstrap replicates.
5. Calculate the required prediction band from the quantiles of the bootstrap CDF as in Equation 6.8.

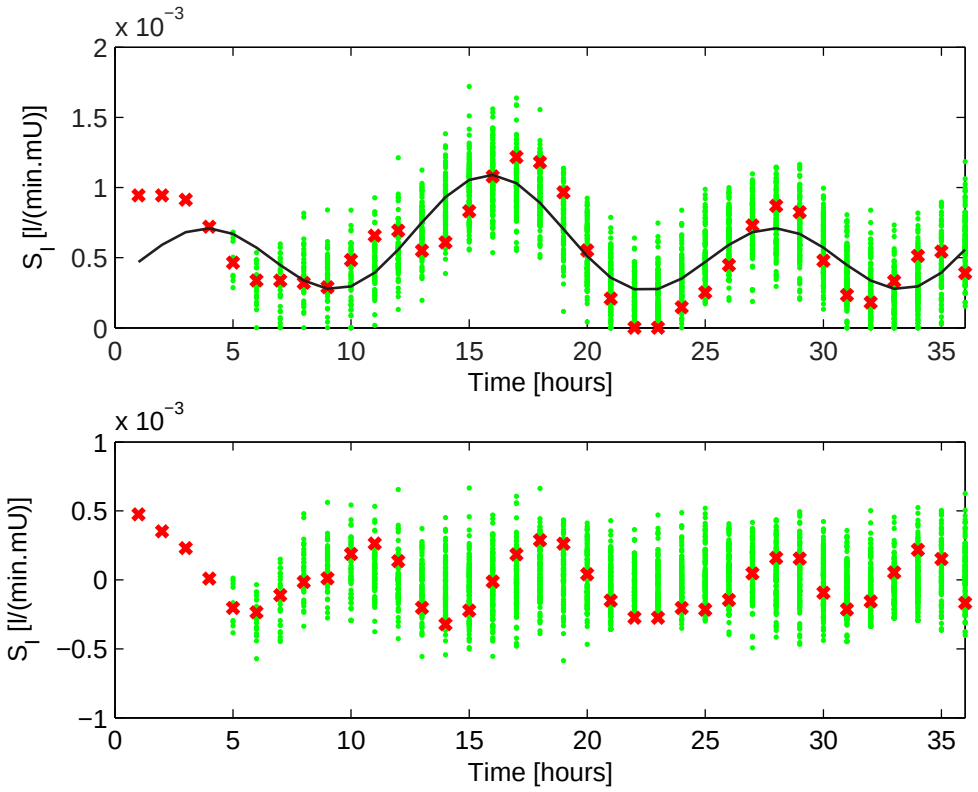

Figure 6.5 B bootstrap future values from the B bootstrap replicates $(X^{*,1}_{t+k}, ..., X^{*,B}_{t+k})$ shown for Patient 1. The prediction bands are defined as quantiles of the bootstrap CDF. The points (.) show the bootstrap future values, the crosses (x) indicate the original residuals $x_t = \{x_1, ..., x_N\}$ and the line (-) denotes the identified diurnal cycle plotted as a continuous curve.

6.1.4 Comparison prediction methods

The diurnal cycle and AR(4) prediction model developed in this study is compared to two previously published prediction methods.

6.1.4.1 Fixed parameter AR(3) method

The first is a weighted average point S_I prediction used by Chase et al. [2005b] and Wong et al. [2006a,b] for a k=1 prediction lead. Referring to Equation 6.9 to 6.11 and for $s_t = \{s_1, ..., s_N\}$, the k=1 prediction is defined for N=1, 2, and 3 or more.

$$S_{t+1} = \frac{1}{11}[8s_t + 2s_{t-1} + s_{t-2}] \qquad \text{if } N \geq 3 \tag{6.9}$$

$$S_{t+1} = \frac{1}{6}[4s_t + 2s_{t-1}] \qquad \text{if } N = 2 \tag{6.10}$$

$$S_{t+1} = s_t \qquad \text{if } N = 1 \tag{6.11}$$

For purposes of comparison in this study, the method of Chase et al. is extended to leads k=2,...,6 in Equation 6.12 to 6.14.

$$S_{t+k} = \frac{1}{11}[8s_t + 2s_{t-1} + s_{t-2}] \qquad \text{if } N \geq 3 \tag{6.12}$$

$$S_{t+k} = \frac{1}{6}[4s_t + 2s_{t-1}] \qquad \text{if } N = 2 \tag{6.13}$$

$$S_{t+k} = s_t \qquad \text{if } N = 1 \tag{6.14}$$

Like the AR model used in this study, for subsequent k=2,...,6 hours, S_{t+k} must be calculated recursively with s_{t-j} (j=0,1,2) in Equations 6.12 to 6.14 substituted by predicted future values S^*_{t-j} (j=0,1,2). This form of the Chase et al. prediction model is effectively a fixed parameter AR(3) model.

6.1.4.2 Markov stochastic method

The second prediction method compared is that of Lin and colleagues [Lin et al., 2006, 2008]. The Lin et al. stochastic S_I model assumes an AR(1) or Markov process, and uses a two-dimensional kernel density estimation method to calculate the conditional probability density function of S_{t+1} given S_t. The method is stochastic, and population or cohort based, requiring a cohort of S_{t+1} and S_t data to fit the model. More information on the models and methods can be found in Lin et al. [2006, 2008]. The conditional probability distribution function of S_{t+1} given S_t calculated for this study is shown in Figure 6.6 with the actual S_{t+1} and S_t data points used.

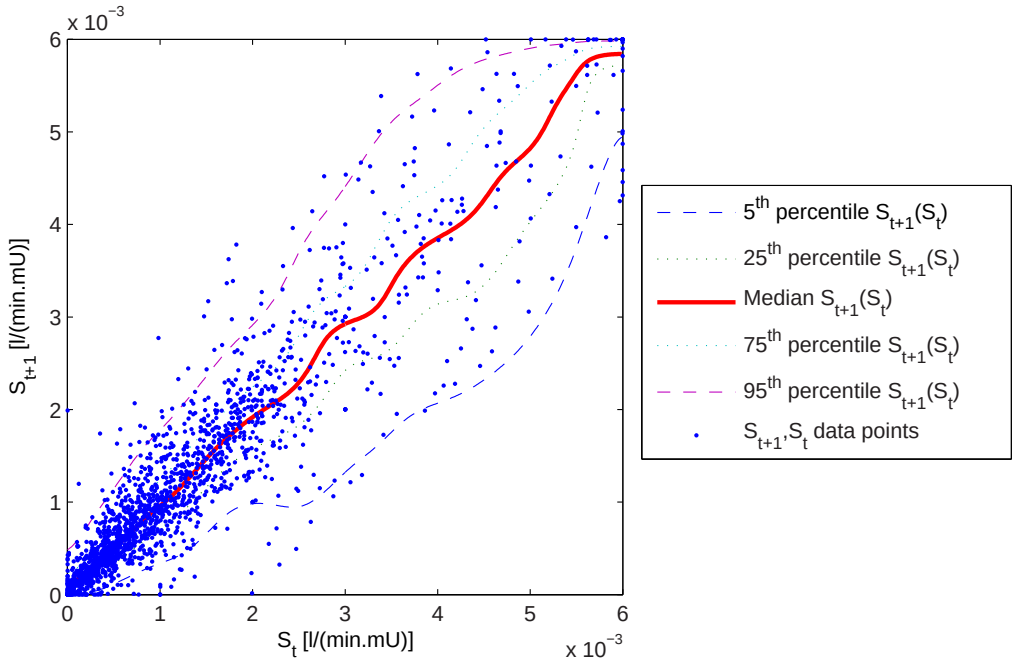

Figure 6.6 The Lin and colleagues [Lin et al., 2006, 2008] stochastic S_I model assumes an AR(1) or Markov process, and uses a two-dimensional kernel density estimation method to calculate the conditional probability density function of S_{t+1} given S_t. The conditional probability distribution function of S_{t+1} given S_t calculated for this study is shown here with the actual S_{t+1} and S_t data points used for building the model.

6.1.4.3 Summary of comparison methods

Both comparison methods were developed for and applied on critically ill cohorts with stress-induced hyperglycaemia. The Chase et al. and Wong et al. method has been shown to perform well for 1 hour prediction leads [Wong et al., 2006a,b], but this study extends this method to leads of 2 to 6 hours. Unlike the combined deterministic and stochastic model developed in this study, the Chase et al. and Lin et al. methods are stochastic only. The Chase et al. and Lin et al. prediction methods are fixed and population-based respectively, not patient-specific.

The Lin et al. model also assumes a Markov process. The justification for this model is that the cohort of interest is highly dynamic, and further compounded by drug and steroid therapy, which can be the case in critical illness [Wong et al., 2006b]. Compared to outpatient or ambulatory Type 1 diabetes, S_I diurnal cycles in these cohorts may be less well defined and not as useful for prediction purposes.

6.1.5 Results metrics

All prediction methods are assessed on two criteria:

1. Point $S_I(t)$ and $G(t)$ predictions
2. $G(t)$ prediction band widths

Leads of 1 to 6 hours are assessed. For leads >1 hour, only the Chase et al. and the developed prediction method are tested as the Lin et al. model cannot be easily made to predict leads exceeding 1 hour. For the Lin et al. [2006, 2008] model, the area under the conditional probability distribution function pd.f of S_{t+1} given S_t is scaled to 1.0. Point predictions are calculated by numerically integrating the conditional pd.f of S_{t+1} from either tail until an area of 0.5 is obtained. Similar to the calculation of the AR prediction bands, prediction bands for the Lin et al. model are defined as quantiles of the conditional pd.f. For a given β, a $100\beta\%$ prediction interval can be calculated by integrating the conditional pd.f from both tails individually until the area of $1/2\ 100\beta$ is obtained.

Using the fixed parameter AR(3) method of Chase et al., bootstrap prediction bounds are calculated as outlined in Subsection 6.1.3 for the developed prediction method. As an example, the S_t prediction bands for Patient 1 calculated from both the method developed here (top plot) and the Lin et al. method (bottom plot) is shown in Figure 6.7 for a 1-hour prediction lead.

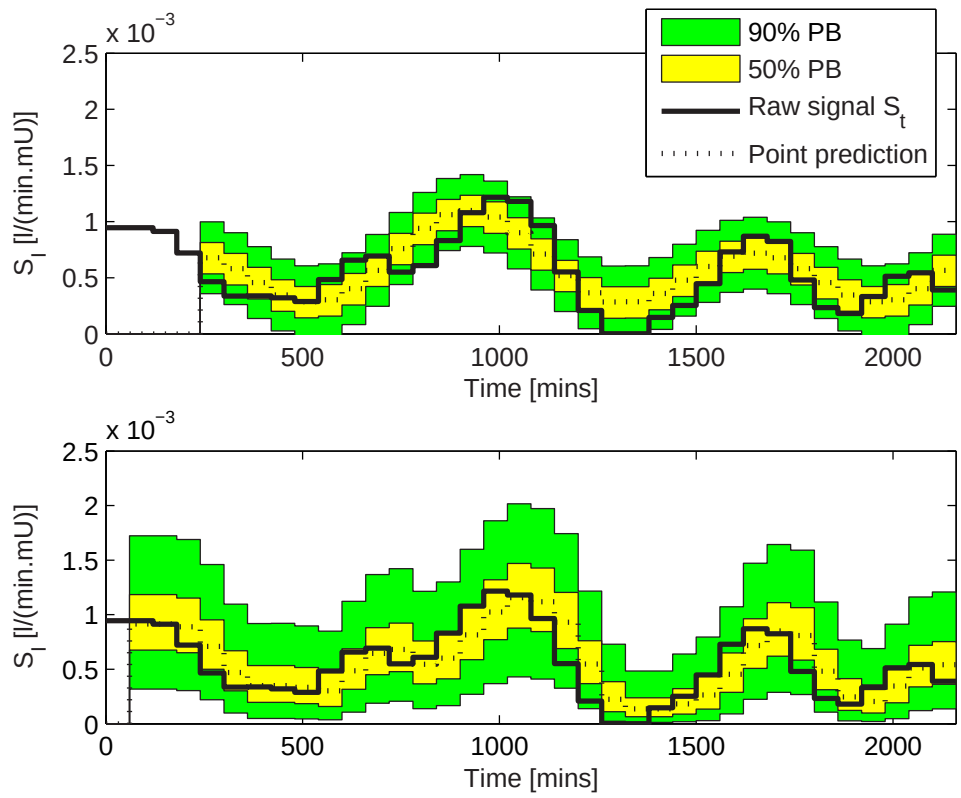

Figure 6.7 Bootstrap prediction bounds for Patient 1 are calculated using the method of Thombs and Schucany [Thombs and Schucany, 1990] for the diurnal cycle and AR(4) method (top plot) and the Lin et al. method (bottom plot) for a 1-hour prediction lead.

6.2 Results

6.2.1 Point predictions

6.2.1.1 Point S_I predictions

The absolute point S_I prediction errors are shown in Table 6.2 with the median values shown in Figure 6.8. The Lin et al. method is compared to the other methods for a 1 hour lead only. The diurnal cycle and AR(4) method results in lower point S_I prediction errors compared to all other methods. For a 1 hour lead, the median (inter-quartile range or IQR) absolute percentage prediction errors are 14.9% (5.6-31.2%) for the diurnal cycle prediction model vs. 20.6% (6.6-42.7%) for the Lin et al. stochastic model and 23.6% (0.7-48.5%) for the

fixed parameter AR(3) model. This result is an improvement of ∼28% from Lin et al. and ∼37% from the fixed parameter AR(3) model. With increasing lead, the diurnal cycle model reduces the absolute percentage prediction error from the fixed parameter AR(3) model by 22%-30% from lead 2 to 6 hours. While the point S_I forecast errors are large at longer leads, there is a marked reduction compared to the fixed parameter AR(3) method.

Figure 6.9 and Table 6.3 show the absolute point S_I prediction errors. For all leads, median absolute prediction errors are zero, and IQR is approximately symmetrical. These are good indicators that all tested methods are unbiased. The error IQR is smallest for the diurnal and AR(4) method, and saturates at 4 hours (leads 4 to 6 hours have the same prediction error IQR). The fixed parameter AR(3) model error IQR increases up until the prediction lead of 6 hours, following the more classical decrease in precision with increasing lead.

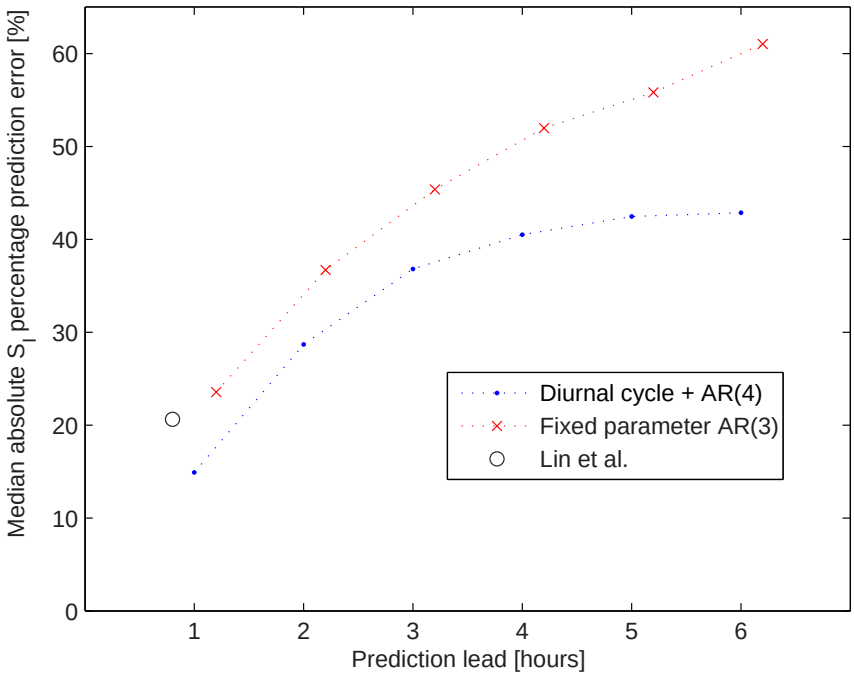

Figure 6.8 The median absolute point S_I prediction errors. The Lin et al. method is compared to the other methods for a 1 hour lead only.

Table 6.2 Absolute percentage S_I point prediction errors. The Lin et al. method is compared to the other methods for a 1 hour lead only. The diurnal cycle and AR(4) method results in lower point prediction errors compared to all other methods. For a 1 hour lead, the median (inter-quartile range or IQR) absolute percentage prediction errors are 14.9% (5.6-31.2%) for the diurnal cycle prediction model vs. 20.6% (6.6-42.7%) for the Lin et al. stochastic model and 23.6% (0.7-48.5%) for the fixed parameter AR(3) model.

Prediction lead [hours]	Absolute percentage S_I point prediction error [%]					
	1	2	3	4	5	6
Diurnal cycle	14.9	28.7	36.8	40.5	42.5	42.9
AR(4)	(5.6-31.2)	(11.0-55.4)	(14.6-67.5)	(15.5-71.3)	(16.6-73.1)	(16.2-74.0)
Fixed parameter	23.6	36.7	45.4	52.0	55.8	61.0
AR(3)	(0.7-48.5)	(12.3-76.7)	(14.8-92.5)	(18.6-99.2)	(20.7 99.9)	(21.9-106.5)
	20.6	-	-	-	-	-
Lin et al.	(6.6-42.7)					

Table 6.3 Absolute S_I point prediction errors. For all leads, median absolute prediction errors are zero, and IQR is approximately symmetrical. These are good indicators that all tested methods are unbiased. The error IQR is smallest for the diurnal and AR(4) method, and saturates at 4 hours (leads 4 to 6 hours have the same prediction error IQR). The fixed parameter AR(3) model error IQR increases up until the prediction lead of 6 hours, following the more classical decrease in precision with increasing lead.

Prediction lead [hours]	Absolute S_I point prediction error [l/(min.mU)]					
	1	2	3	4	5	6
Diurnal cycle	0	0	0	0	0	0
AR(4)	(-0.0001-0.0001)	(-0.0002-0.0002)	(-0.0003-0.0003)	(-0.0003-0.0004)	(-0.0003-0.0004)	(-0.0003-0.0004)
Fixed parameter	0	0	0	0	0	0
AR(3)	(-0.0001-0.0001)	(-0.0003-0.0003)	(-0.0004-0.0003)	(-0.0004-0.0004)	(-0.0005-0.0004)	(-0.0005-0.0005)
	0	-	-	-	-	-
Lin et al.	(-0.0002-0.0001)					

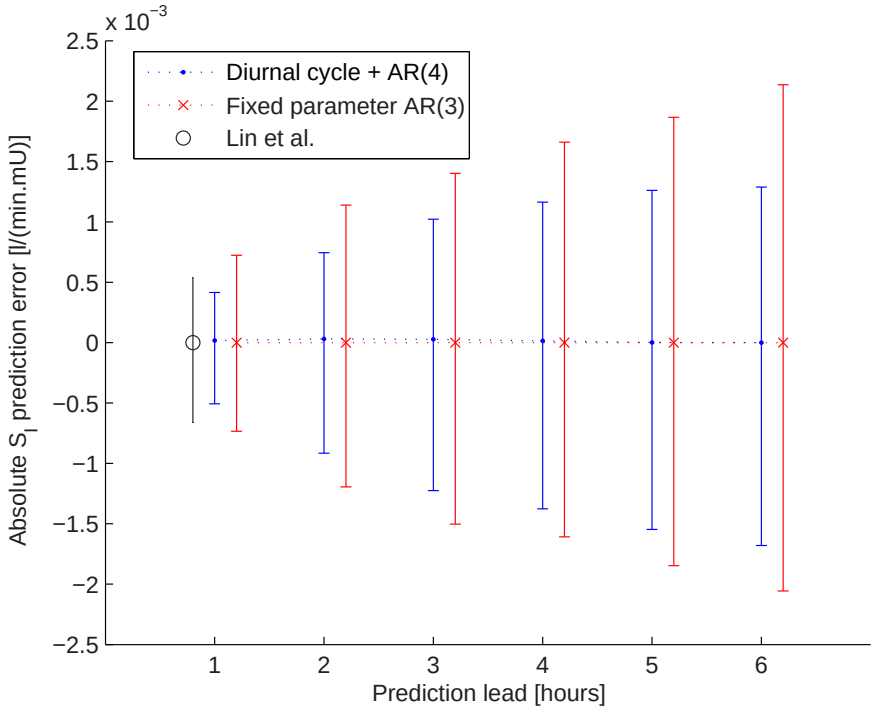

Figure 6.9 The absolute S_I point prediction error. For all leads, median absolute prediction errors are zero, and IQR is approximately symmetrical, good indicators that all tested methods are unbiased. The error IQR is smallest for the diurnal and AR(4) method, and saturates at 4 hours (leads 4 to 6 hours have the same prediction error IQR). The fixed parameter AR(3) model error IQR increases up until the prediction lead of 6 hours, following the more classical decrease in precision with increasing lead.

From Figure 6.10 to 6.12 and Table 6.4, the per patient correlation coefficients between the point S_I forecasts and the actual S_I values are shown for leads 1 to 6 hours. As expected, the correlation coefficient decreases with increasing prediction lead. With the fixed parameter AR(3) model, the median correlation coefficient drops from 0.87 to 0.10 from a 1 to 6 hour lead in Figure 6.10. With the diurnal cycle and AR(4) model, the median correlation coefficient drops from 0.96 to 0.63 for equivalent prediction lead in Figure 6.11. For all leads, the median correlation coefficients between point forecast S_I and actual S_I are higher for the diurnal cycle and AR(4) model compared to the fixed parameter AR(3) method, and for a lead of 1 hour, the Lin et al. method as well as shown in Figure 6.12. The reduction in correlation coefficient and correlation coefficient IQR reflects the more precise results obtained with the patient-specific, diurnal cycle and AR(4) model compared to the cohort based fixed parameter AR(3) and Lin et al. methods.

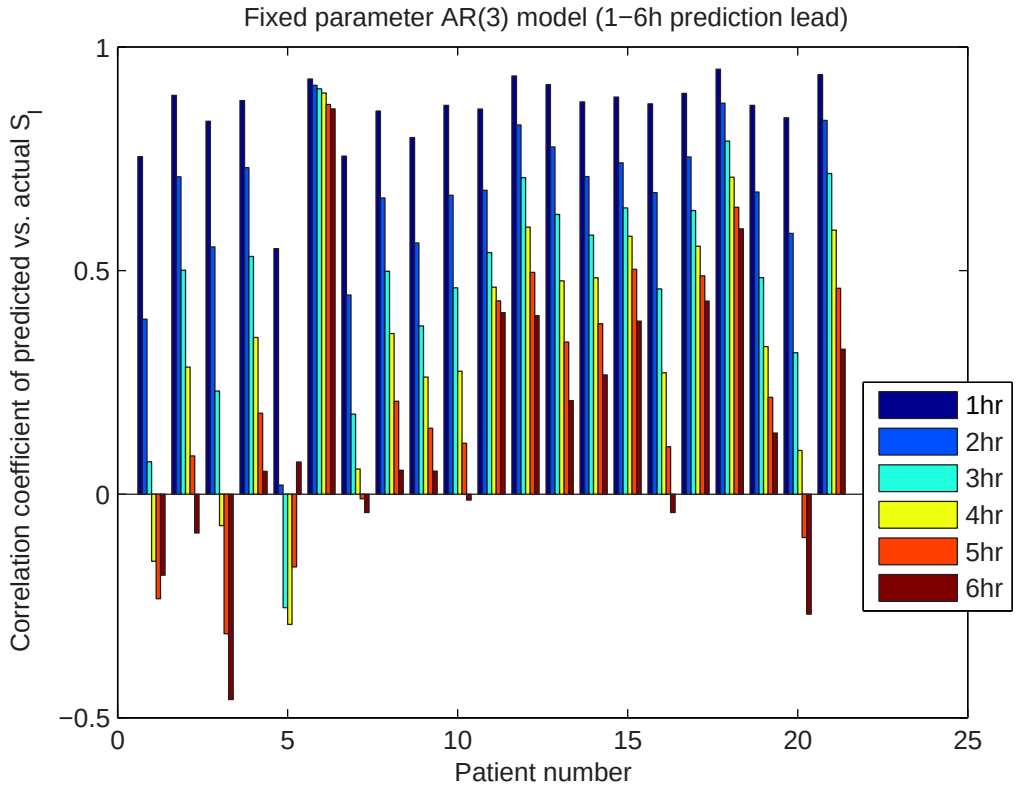

Figure 6.10 The correlation coefficients between the point S_I forecasts and the actual S_I values are shown for leads 1 to 6 hours for the fixed parameter AR(3) method. As expected, the correlation coefficient decreases with increasing the prediction lead with the median correlation coefficient dropping from 0.87 to 0.10 from a 1 to 6 hour lead.

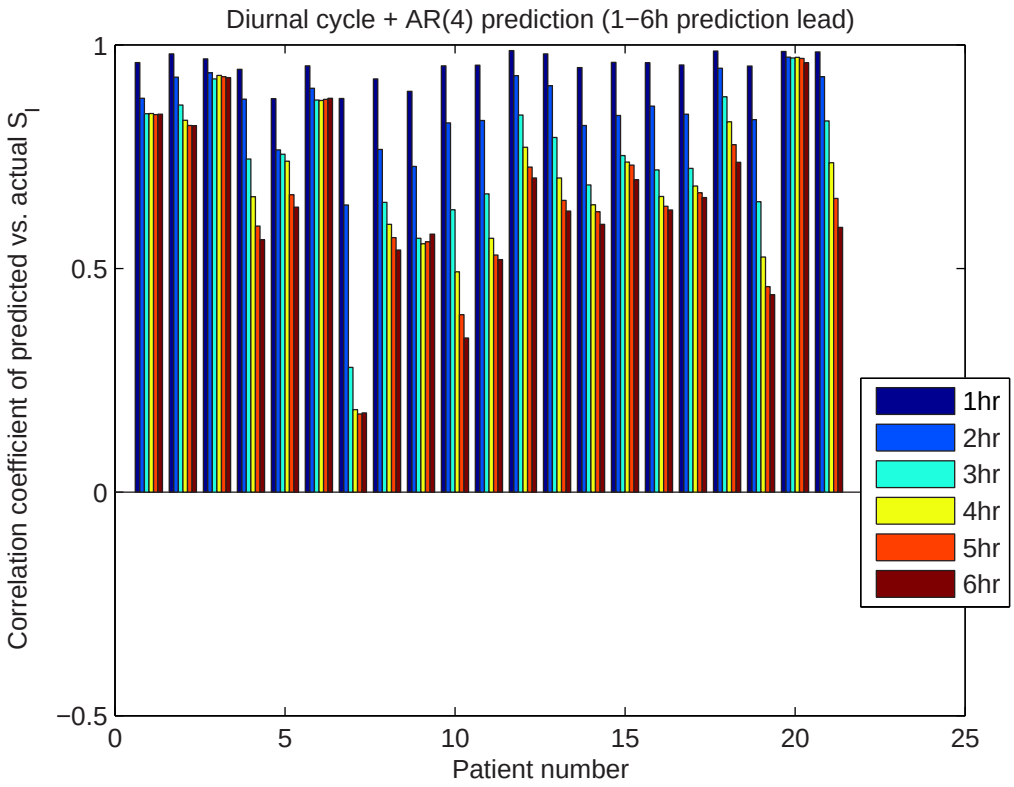

Figure 6.11 The correlation coefficients between the point S_I forecasts and the actual S_I values are shown for leads 1 to 6 hours for the diurnal cycle and AR(4) method. The median correlation coefficient drops from 0.96 to 0.63 from a 1 to 6 hour lead.

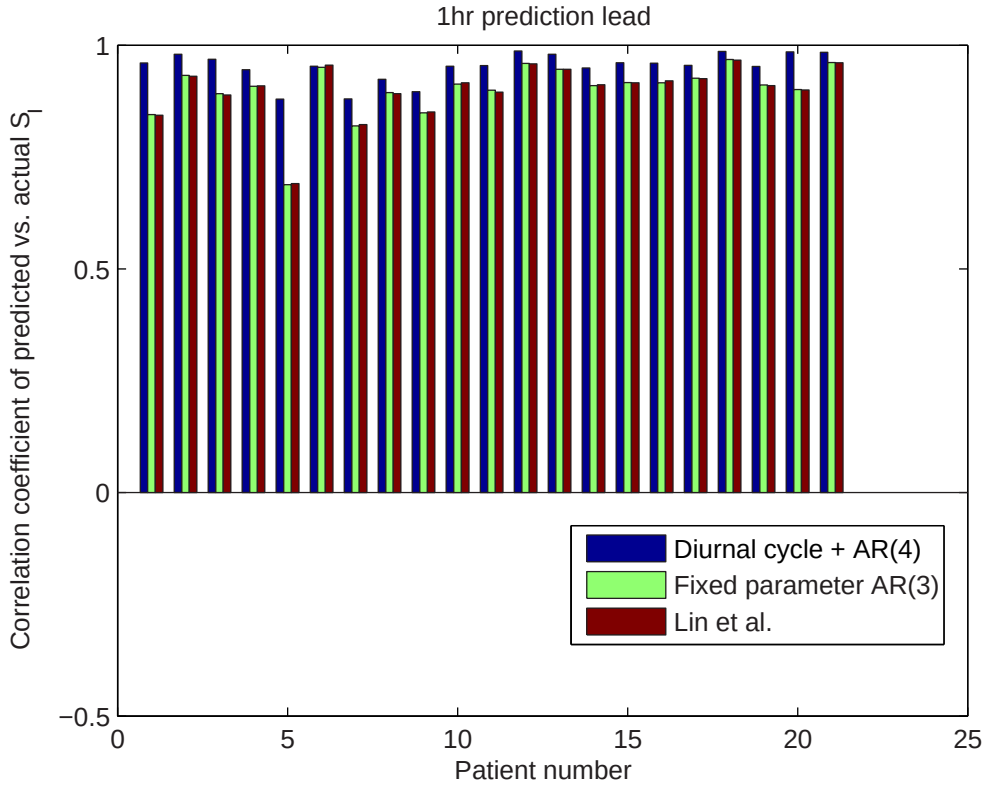

Figure 6.12 The correlation coefficients between the point S_I forecasts and the actual S_I values are shown for a 1 hour lead for the fixed parameter AR(3) method, diurnal cycle and AR(4) method, and the Lin et al. method. The median correlation coefficients between point forecast S_I and actual S_I are higher for the diurnal cycle and AR(4) model compared to both the fixed parameter AR(3) and Lin et al. methods.

Table 6.4 Correlation coefficients between the point S_I forecasts and the actual S_I values for leads 1 to 6 hours. As expected, the correlation coefficient decreases with increasing the prediction lead. With the fixed parameter AR(3) model, the median correlation coefficient drops from 0.87 to 0.10 from a 1 to 6 hour lead. With the diurnal cycle and AR(4) model, the median correlation coefficient drops from 0.96 to 0.63 for equivalent prediction lead. For all leads, the median correlation coefficients between point forecast S_I and actual S_I are higher for the diurnal cycle and AR(4) model compared to the fixed parameter AR(3), and for lead of 1 hour, the Lin et al. method.

Prediction lead [hours]	Correlation coefficient R between point S_I prediction and actual S_I					
	1	2	3	4	5	6
Diurnal cycle AR(4)	0.9576 (0.9490-0.9796)	0.8709 (0.8253-0.9289)	0.7541 (0.6667-0.8655)	0.7193 (0.5984-0.8312)	0.6607 (0.5691-0.8198)	0.6339 (0.5640-0.8189)
Fixed parameter AR(3)	0.8747 (0.8416-0.9155)	0.6945 (0.5832-0.7763)	0.5161 (0.3763-0.6339)	0.3545 (0.2615-0.5765)	0.2121 (0.0855-0.4882)	0.1043 (-0.0410-0.3988)
Lin et al.	0.9137 (0.8918-0.9464)	-	-	-	-	-

6.2.1.2 Point $G(t)$ predictions

For clinical use, the $S_I(t)$ forecasts are translated into forecasts of glucose excursion $G(t)$ over the prediction lead for a given insulin and/or nutrition input. Glucose predictions are performed by substituting the S_I forecasts into the $G(t)$ model equations from Chapter 3 and determining the $G(t)$ evolution over the prediction lead compared against the $G(t)$ excursion using the actual S_I (identified from patient data). For prediction bands, the equal-tailed prediction interval in $G(t)$ is calculated from the equal-tailed prediction intervals of $S_I(t)$, which is an acceptable approximation for clinical real-time use [Lin et al., 2008]. Using the diurnal cycle and AR(4) method, the $G(t)$ prediction bands for Patient 1 are shown in Figure 6.13 as calculated from the $S_I(t)$ prediction bands in Figure 6.5.

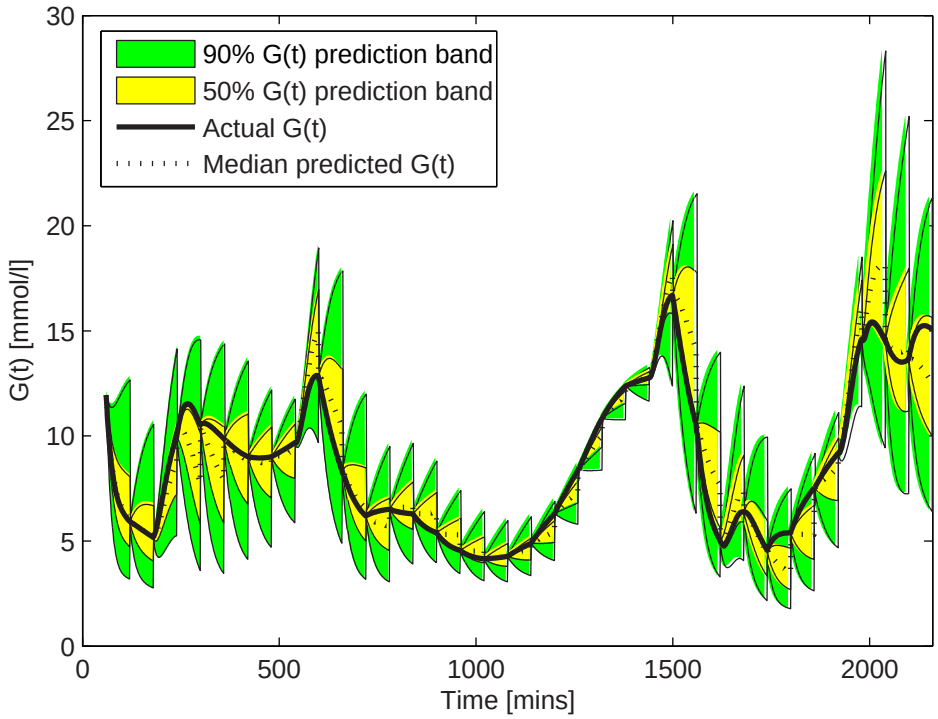

Figure 6.13 The $G(t)$ prediction bands for Patient 1 calculated using the $S_I(t)$ bootstrapped prediction bands and diurnal cycle and AR(4) method in Figure 6.5.

From Table 6.5 and Figure 6.14, the median (90% range) absolute percentage $G(t)$ prediction error per patient is shown. As for the $S_I(t)$ forecasts, the diurnal cycle and AR(4) model predicts $G(t)$ more accurately for all leads compared

to both fixed parameter AR(3) and Lin et al methods. At 1 hour, the $G(t)$ prediction error is 4.0%, compared to 7.2% and 5.6% for the fixed parameter AR(3) and Lin et al. methods respectively, reflecting the accuracy obtained with the $S_I(t)$ point forecasts. For a 1 hour lead, the 90% range of the $G(t)$ prediction error for the diurnal cycle and AR(4) model is 73% and 13% smaller than the fixed parameter AR(3) model and Lin et al. methods respectively. For leads 2-6 hours, the diurnal cycle and AR(4) method median point $G(t)$ prediction error is 48-73% smaller than the fixed parameter AR(3), while the 90% range of the $G(t)$ prediction error is smaller by 19-10%. Hence, the diurnal cycle and AR(4) method performs more accurately *and* more consistently across the tested cohort compared to both comparison methods.

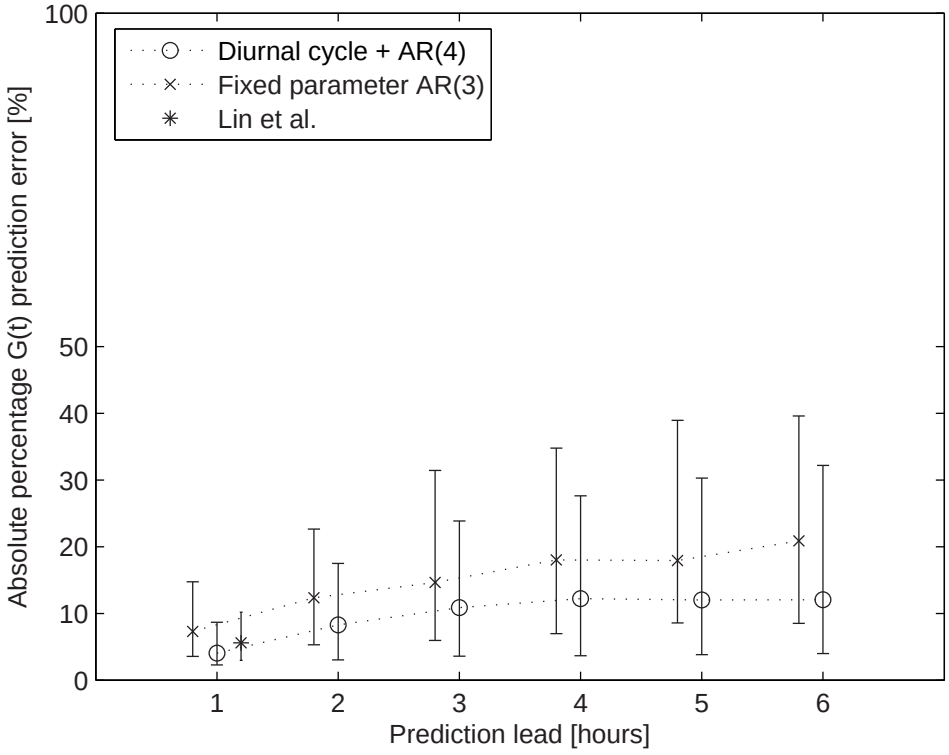

Figure 6.14 The median (90% range) absolute percentage $G(t)$ prediction error per patient is shown. As for the $S_I(t)$ forecasts, the diurnal cycle and AR(4) model predicts $G(t)$ more accurately and more consistently for all leads compared to both fixed parameter AR(3) and Lin et al methods.

Table 6.5 Median (90% range) absolute percentage $G(t)$ prediction error per patient. As for the $S_I(t)$ forecasts, the diurnal cycle and AR(4) model predicts $G(t)$ more accurately for all leads compared to both fixed parameter AR(3) and Lin et al methods. At 1 hour, the $G(t)$ prediction error is 4.0%, compared to 7.2% and 5.6% for the fixed parameter AR(3) and Lin et al. methods respectively, reflecting the accuracy obtained with the $S_I(t)$ point forecasts. For a 1 hour lead, the 90% range of the $G(t)$ prediction error for the diurnal cycle and AR(4) model is 73% and 13% smaller than the fixed parameter AR(3) model and Lin et al. methods respectively. For leads 2-6 hours, the diurnal cycle and AR(4) method median point $G(t)$ prediction error is 48-73% smaller than the fixed parameter AR(3) while the 90% range of the $G(t)$ prediction error is smaller by 19-10%. Hence, the diurnal cycle and AR(4) method performs more accurately and more consistently across the tested cohort compared to both comparison methods.

Prediction lead [hours]	Absolute percentage $G(t)$ (IQR) point prediction error [%]					
	1	2	3	4	5	6
Diurnal cycle AR(4)	4.0 (2.3-8.7)	8.3 (3.0-17.5)	10.9 (3.6-23.9)	12.2 (3.7-27.6)	12.0 (3.8-30.3)	12.1 (4.0-32.2)
Fixed parameter AR(3)	7.2 (3.6-14.7)	12.3 (5.3-22.6)	14.7 (6.0-31.5)	18.0 (7.0-34.8)	17.9 (8.6-13.4)	20.9 (8.5-39.6)
Lin et al.	5.6 (3.0-10.2)	-	-	-	-	-

6.2.2 Prediction bands

6.2.2.1 Percentage of actual $G(t)$ in the 90% and 50% G(t) prediction bands

The median (90% range) for the percentage of actual $G(t)$ within the 90% and 50% $G(t)$ prediction bands is shown in Table 6.6 and Figure 6.15. For the diurnal cycle and AR(4) model, the median percentage of actual $G(t)$ in the 90% and 50% prediction band have a 90% range from 88-90% and 44-49% respectively across all prediction leads. Compared to the fixed parameter AR(3) model, the figures are 96-97% and 61-68% respectively. For a 1 hour prediction lead, the Lin et al. model results in a median 92% and 61% of actual $G(t)$ within the 90% and 50% prediction bands, respectively.

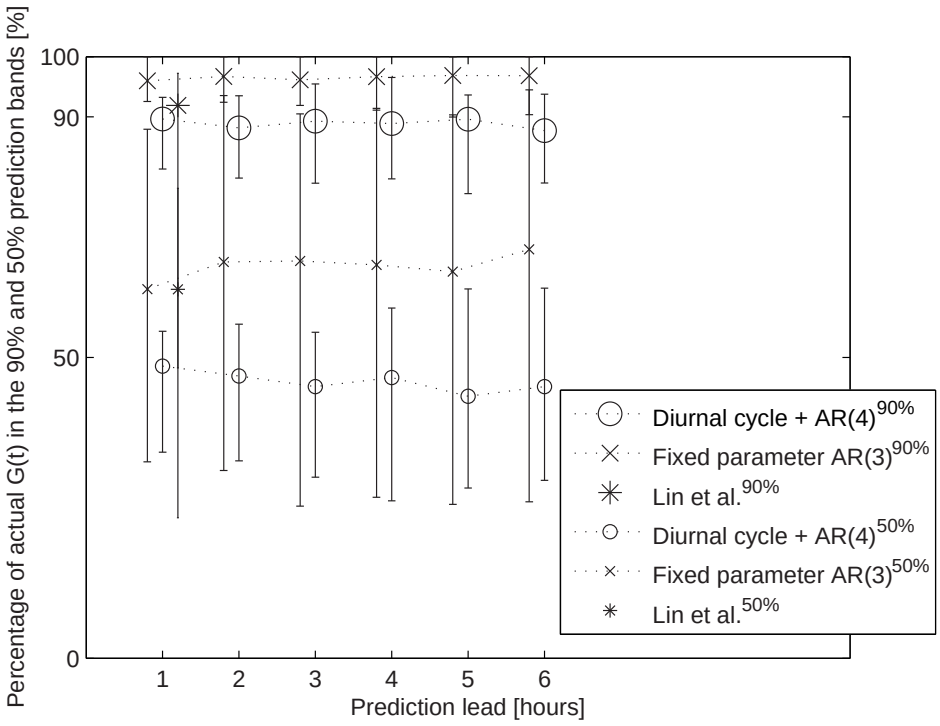

Figure 6.15 The median (90% range) for the percentage of actual $G(t)$ within the 90% and 50% $G(t)$ prediction bands. For the diurnal cycle and AR(4) model, the median percentage of actual $G(t)$ in the 90% and 50% prediction band have a 90% range from 88-90% and 44-49% respectively across all prediction leads. Compared to the fixed parameter AR(3) model, the figures are 96-97% and 61-68% respectively. For a 1 hour prediction lead, the Lin et al. model results in a median 92% and 61% of actual $G(t)$ within the 90% and 50% prediction bands respectively.

Table 6.6 Median (90% range) for the percentage of actual $G(t)$ within the 90% and 50% $G(t)$ prediction bands. For the diurnal cycle and AR(4) model, the median percentage of actual $G(t)$ in the 90% and 50% prediction band have a 90% range from 88-90% and 44-49% respectively across all prediction leads. Compared to the fixed parameter AR(3) model, the figures are 96-97% and 61-68% respectively. For a 1 hour prediction lead, the Lin et al. model results in a median 92% and 61% of actual $G(t)$ within the 90% and 50% prediction bands respectively.

	Median (90% confidence band) percentage of actual $G(t)$ within the 90% and 50% prediction bands [%]											
Prediction lead [hours]	1		2		3		4		5		6	
	90%	50%	90%	50%	90%	50%	90%	50%	90%	50%	90%	50%
Diurnal cycle +AR(4)	90 (81-93)	49 (34-54)	88 (80-94)	47 (33-56)	89 (79-95)	45 (30-54)	89 (80-97)	47 (26-58)	90 (77-94)	44 (28-61)	88 (79-94)	45 (30-62)
Fixed parameter AR(3)	96 (93-100)	61 (33-88)	97 (92-100)	66 (31-94)	96 (92-100)	66 (25-91)	97 (91-100)	65 (27-91)	97 (90-100)	64 (26-90)	97 (90-100)	68 (26-95)
Lin et al.	92 (48-97)	61 (23-78)	-	-	-	-	-	-	-	-	-	-

The median percentage of actual $G(t)$ in the respective prediction bands is only slightly overestimated by the diurnal cycle and AR(4) model, but underestimated by both fixed parameter AR(3) and Lin et al. methods. The patient-specific method also results in a more consistent percentage of actual $G(t)$ within the respective prediction bands. For the Lin et al. method, the percentage of actual $G(t)$ in the 90% and 50% prediction bands have a 90% range between 48-97% and 23-78% for a 1 hour lead. The same figures for the diurnal cycle and AR(4) method are 81-93% and 34-54% respectively, and for the fixed parameter AR(3) model, this figure is 93-100% and 33-88%. The patient-specific, diurnal cycle and AR(4) method has a 90% range that is only 12% wide across the entire cohort compared to the population-based Lin et al. method, which is 49% wide.

6.2.2.2 $S_I(t)$ and $G(t)$ prediction band width

The per patient median $S_I(t)$ and $G(t)$ prediction band widths are shown in Table 6.7 to 6.10. For a 1hr prediction lead, the diurnal cycle and AR(4) method produces a median 90% $G(t)$ prediction band width that is 0.8 times larger than the Lin et al. method, with a 90% range that is 0.4 times larger. This result can again be expected given that the patient-specific diurnal cycle and AR(4) method is patient-specific.

Naturally, the AR prediction bands will be narrow if the residuals x_t are small, which will be the case if the patient data set S_t is well approximated with the diurnal cycle s_t. Conversely, the AR prediction bands will be wide if the residuals x_t are large, which will be the case if patient S_t is poorly approximated by the diurnal cycle s_t, all of which results in a wider range in $G(t)$ prediction band width. This ensures that the percentage of actual $G(t)$ in the respective prediction bands (as shown in Table 6.6) remains as close as possible to the theoretical figure. The fixed parameter AR(3) method produces a median 90% G(t) prediction band width that is 0.3 times larger and with a 90% range 0.4 times larger than the diurnal cycle and AR(4) method.

Table 6.7 The per patient median $S_I(t)$ prediction band widths.

	Median (90% confidence band) of the 90% and 50% $S_I(t)$ prediction band widths [l/(min.mU)]					
Prediction lead [hours]	1		2		3	
	90%	50%	90%	50%	90%	50%
Diurnal cycle	0.0021	0.0008	0.0020	0.0008	0.0019	0.0008
+AR(4)	(0.0005-0.0061)	(0.0002-0.0033)	(0.0006-0.0060)	(0.0002-0.0029)	(0.0006-0.0060)	(0.0002-0.0027)
Fixed parameter	0.0026	0.0012	0.0026	0.0013	0.0027	0.0013
AR(3)	(0.0010-0.0071)	(0.0005-0.0045)	(0.0010-0.0072)	(0.0005-0.0041)	(0.0011-0.0072)	(0.0005-0.0040)
Lin et al.	0.0011	0.0004	-	-	-	-
	(0.0009-0.0017)	(0.0003-0.0006)				

Table 6.8 The per patient median $S_I(t)$ prediction band widths (continued).

Prediction lead [hours]	Median (90% confidence band) of the 90% and 50% $S_I(t)$ prediction band widths [l/(min.mU)]					
	4		5		6	
	90%	50%	90%	50%	90%	50%
Diurnal cycle +AR(4)	0.0019 (0.0006-0.0062)	0.0008 (0.0002-0.0027)	0.0020 (0.0005-0.0061)	0.0008 (0.0002-0.0026)	0.0020 (0.0006-0.0059)	0.0009 (0.0002-0.0026)
Fixed parameter AR(3)	0.0028 (0.0010-0.0076)	0.0012 (0.0006-0.0038)	0.0028 (0.0010-0.0076)	0.0013 (0.0005-0.0039)	0.0028 (0.0010-0.0077)	0.0014 (0.0005-0.0037)

Table 6.9 The per patient median $G(t)$ prediction band widths. For a 1hr prediction lead, the diurnal cycle and AR(4) method produces a median 90% $G(t)$ prediction band width that is 0.8 times larger than the Lin et al. method with a 90% range that is 0.4 times larger.

Prediction lead [hours]	Median (90% confidence band) of the 90% and 50% $G(t)$ prediction band widths [mmol/l]							
	1		2		3		4	
	90%	50%	90%	50%	90%	50%	90%	50%
Diurnal cycle +AR(4)	5.7 (1.7-9.1)	2.2 (0.7-3.9)	5.5 (1.8-9.0)	2.2 (0.8-3.6)	4.9 (1.9-8.7)	2.2 (0.7-3.4)	4.9 (1.8-8.1)	2.1 (0.7-3.3)
Fixed parameter AR(3)	7.4 (3.1-13.2)	4.2 (1.4-6.8)	7.7 (3.0-13.1)	4.2 (1.5-7.2)	7.4 (2.9-13.4)	3.9 (1.5-7.3)	7.4 (2.8-13.3)	3.6 (1.6-7.6)
Lin et al.	3.1 (2.1-7.5)	1.1 (0.8-2.9)	-	-	-	-	-	-

From Table 6.7 to 6.10, the prediction band widths of both $S_I(t)$ and $G(t)$ are very large for the fixed parameter AR(3) method compared to the diurnal cycle and AR(4) method. This result is expected given that a wider variation in $S_I(t)$ is modelled using the AR(3) model, rather than the residuals *after* removal of the patient-specific diurnal cycle as in the case of the diurnal cycle and AR(4) method. The resulting width of the bands may explain the underestimation of the percentage of actual $G(t)$ in the respective prediction bands.

Table 6.10 The per patient median $G(t)$ prediction band widths. For a 1hr prediction lead, the diurnal cycle and AR(4) method produces a median 90% $G(t)$ prediction band width that is 0.8 times larger than the Lin et al. method with a 90% range that is 0.4 times larger (continued).

	Median (90% confidence band) of the 90% and 50% $G(t)$ prediction band widths [mmol/l]			
Prediction lead [hours]	5		6	
	90%	50%	90%	50%
Diurnal cycle +AR(4)	4.6 (1.8-8.1)	2.0 (0.7-3.4)	4.6 (2.1-7.5)	2.0 (0.7-3.2)
Fixed parameter AR(3)	7.0 (2.7-13.4)	3.6 (1.6-7.7)	6.8 (2.8-13.5)	3.8 (1.4-7.8)

6.3 Discussion

From the results presented, the diurnal cycle and AR(4) method to predict S_I and, hence, $G(t)$, outperforms the fixed parameter AR(3) and Lin et al. methods for the cohort tested. Median per patient point prediction error is significantly reduced (4.0%) over both comparison methods (5.6% and 7.2%), and the percentage of actual $G(t)$ within the respective prediction bands match the theoretical figure more consistently over the entire cohort.

In a glycaemic control situation, insulin interventions are determined in order for the lower bound of the 0.90 probability prediction interval for $G(t)$ to be at a suitable minimum glucose level, e.g., 4.0mmol/l [Lin et al., 2008]. From a safety perspective, there is greater possibility of hypoglycaemia if the percentage of actual $G(t)$ within the 0.90 probability prediction interval is less than 90% for any normal glycaemic target. The diurnal cycle and AR(4) method results in 90%

of the cohort having a percentage of actual $G(t)$ in the 90% $G(t)$ prediction band of between 81-93%, compared to 48-97% of the Lin et al. method, an advantage of the patient-specific approach over a population-based method.

The 90% range of the $G(t)$ prediction band width by the diurnal cycle and AR(4) method is 0.4 times larger (1.7-9.1mmol/l) compared to the Lin et al. method (2.1-7.5mmol/l). While the frequencies of the diurnal cycle and AR model parameters are determined per patient, the AR model order is formulated for this cohort as a population. As a result, the widths of the prediction intervals reflect a more realistic *model uncertainty* for that particular patient. A poor match to the diurnal cycle model results in higher residuals and widening of the prediction band width, while an excellent match reduces the residuals and narrows the prediction band width. As 90% of patients have 81-93% of actual $G(t)$ within the 90% $G(t)$ prediction interval, this indicates that the prediction intervals are probably of acceptable width compared to the Lin et al. method.

In this study, the same data sets are used for model formulation and identification, as well as in-sample forecasting, due to the small data sets available per patient. Even with data splitting, a genuine test sample may be impossible to obtain. Unavoidably, this study is hence subject to model selection bias and model uncertainty. However, all models are identified and forecast on the same data set (except the fixed parameter AR(3) method), which provides a compatible comparison between methods.

The two frequency sinusoidal diurnal cycle and the AR(4) model chosen for this study is shown to result in smaller prediction error and reduced forecast variance in-sample compared to the other tested methods for all prediction leads. While model specification error or model uncertainty is ignored in this study, further application of the models and methods to longer data sets with data splitting will permit out-of-sample forecasting for true evaluation of the model predictions.

While parsimony of the diurnal cycle and AR(4) model is considered, it is less parsimonious than the comparison methods tested with 12 fitted parameters. This contributes to further model uncertainty and may result in wider forecast variance in a genuine out-of-sample forecast competition. In reality, the genuine out-of-sample prediction of all tested methods is likely to be worse than the in-

sample results presented. Further research with split data sets with both training and blinded test samples will permit true out-of-sample forecast comparison of each method.

6.4 Conclusions

Circadian rhythmicity and sleep-wake phases have profound and independent effects on effective insulin sensitivity. It is well documented in IDDM, and is consistent and reproducible intra-subject. Identification and prediction of this rhythm is thus of utmost clinical relevance, with potential for safer and more effective glycaemic control with less frequent measurement.

A method for identifying the diurnal cycle in $S_I(t)$ (a model-based index of effective insulin sensitivity), and modelling it in retrospective patient data is presented. The method consists of fitting a two-frequency sinusoid to $S_I(t)$ and an AR(4) model to the subsequent residuals. The aim of this study is to increase predictive accuracy of the previously published glucose kinetics model via modelling the driving parameter $S_I(t)$ over two comparison methods, a fixed parameter AR(3), and a Markov stochastic model of Lin and colleagues [Lin et al., 2006, 2008].

Median absolute percentage $G(t)$ prediction error per patient is significantly reduced (4.0%) over the fixed parameter AR(3) and Markov comparison methods (7.2% and 5.6% respectively), and the percentage of actual $G(t)$ within the respective prediction bands match the theoretical figure more consistently over the entire cohort. The diurnal cycle and AR(4) method results in 90% of the cohort having a percentage of actual $G(t)$ in the 90% $G(t)$ prediction band of between 81-93%, compared to 48-97% of the Lin et al. method.

For leads 2-6 hours, the diurnal cycle and AR(4) method median point $G(t)$ prediction error is 48-73% smaller than the fixed parameter AR(3), while the 90% range of the $G(t)$ prediction error is smaller by 19-10%. The median prediction band width produced by the diurnal cycle and AR(4) method is 0.8 times larger with a 0.4 times larger 90% band width range (1.7-9.1mmol/l) compared to the Lin et al. Markov method (2.1-7.5mmol/l). This demonstrates the characteristics of the patient-specific over the population-based method. The widths of the

prediction intervals reflect a more realistic model uncertainty for each individual patient. A poor match to the diurnal cycle model results in higher residuals, and a widening of the prediction band width, and vice versa.

This study shows that significant potential exists in the identification of a dual frequency, sinusoidal diurnal cycle in $S_I(t)$, and a residual autoregressive (AR) model to predict $S_I(t)$ evolution. With reduced prediction error compared to comparison methods for all prediction leads up to 6 hours, reduced SMBG frequency with no decline in glycaemic control effectiveness or safety is possible. Further research with split data sets with both training and blinded test samples will permit true out-of-sample forecast comparison of each method.

The objective of this chapter is to explore possible areas for further improving the performance of the adaptive protocol developed in Chapters 4 and 5. In this chapter, a method for identifying and predicting the circadian rhythm in S_I is presented. This ability to obtain accurate, long-range $G(t)$ prediction is valuable from a clinical aspect as reduced measurement frequency is then possible without the usually associated disadvantages. The method presented promises to increase the effectiveness of the adaptive protocol developed in this research, and will form the basis for future work in this area. With the completion of this chapter, this research is now concluded and the following chapters discuss the results that have been obtained thus far and the possible future path of this research area.

Chapter 7

Conclusions

Diabetes has reached epidemic proportions worldwide. Type 1 diabetes while less prevalent than Type 2 diabetes is also growing yearly along with insulin-dependent Type 2 diabetes, which is treated somewhat similarly. In particular, the total number of affected individuals and the level of associated complications is growing for this chronic disease. Thus, the increasing number of major complications, such as heart disease, renal failure, blindness and limb amputation, are beginning to consume a major and increasing portion of worldwide healthcare costs.

Scientific evidence has so far shown that intensive insulin therapy aimed at a HbA_{1c} of 7% or lower reduced the incidence of complications by up to 76% compared to conventional insulin therapy with an average HbA_{1c} of ∼9% [DCCT Research Group, 1993; DCCT/EDIC Research Group, 1999]. Moreover, the effects of intensive therapy over a 6.5y duration persists for at least 10y after, a so called *metabolic memory*. Thus, effective early intervention can slow the momentum of complications far more easily, and economically, than later intervention [DCCT/EDIC Research Group, 1999].

This thesis aimed at developing a clinical, adaptive glycaemic control protocol that is more *effective* and *safer* than current clinical protocols, while only requiring little additional clinical or computational effort in order to be accepted in a clinical setting. For similar reason, the protocol must use conventional SMBG measurement and the subcutaneous MDI therapy. The protocol design incorporates physiological modelling and engineering techniques to adapt to individual patient clinical requirements, and by doing so, produces accurate, patient-specific recommendations for insulin interventions.

7.1 General Outcomes

A simple, physiological compartmental model for the pharmacokinetics (PK) of subcutaneously injected insulin is first developed. While the absorption process itself is subject to much variability, such models enable a real-time *estimation* of plasma insulin concentration. This information would otherwise be lacking in the clinical environment of outpatient Type 1 diabetes management due to the inconvenience, cost, and laboratory turnaround for plasma insulin measurements.

The plasma insulin and glucose model structure developed for application in this study contains physiological insulin-independent and insulin-dependent glucose losses. It also accounts for endogenous and exogenous glucose inputs and appearance for accurate description of the relevant metabolic dynamics of glucose and insulin. Combined with the convex integral-based fitting method, the overall system model allows robust and fast estimation of effective insulin sensitivity, S_I, the driving parameter. All models developed are validated on clinical data. The models and methods are minimal, and are thus well suited for *in silico* simulation or a clinical decision support setting.

In this study, an *in silico* simulation tool is also developed. A virtual patient cohort is developed on patient data from a representative cohort of the broad diabetes population. The simulation tool is used to develop the adaptive protocol for prandial insulin dosing against a conventional intensive insulin therapy (IIT), as well as a controls group representative of the general diabetes population. The effect on glycaemic control of suboptimal and optimal, prandial and basal insulin therapies is also investigated with results matching clinical expectations. To gauge the robustness of the developed adaptive protocol, a Monte Carlo (MC) analysis incorporating realistic and physiological errors in insulin and meal absorption, insulin dosing, meal carbohydrate counting and blood glucose measurements is performed.

Due to the relatively infrequent glucose measurement in outpatient Type 1 diabetes, a method for identifying the diurnal cycle in S_I and modelling it in retrospective patient data is also presented. The method consists of identifying deterministic and stochastic components in the patient S_I profile. Circadian rhythmicity and sleep-wake phases have profound effects on effective insulin sensitivity. Identification and prediction of this rhythm is of utmost clinical relevance,

with potential for greater control *with* less frequent measurement.

7.2 Specific Outcomes

Subcutaneous insulin pharmacokinetic model

The model accounts for the concentration dependency of subcutaneous regular insulin injection, and the dose dependency of insulin glargine absorption. In particular, 13 patient-specific model parameters over all insulin types are identified using 37 sets of plasma insulin mean time course data from reported clinical studies. All fitted parameters have a coefficient of variation <100% (median 57%, 95th percentile 3.6 - 60.6%) and can be considered *a posteriori* identifiable.

The identified model is then validated using the PK summary measures t_{max} and C_{max}. Of the 37 model fits, 22 are validated on both measures reported by each study. An additional 6 model fits are partially validated on one summary measure. All partially validated model fits have errors not exceeding 12% of reported or estimated T_{max} or C_{max} ranges. No model fit failed the validation for *both* reported measures.

The results demonstrate the model's ability to capture the fundamental dynamics of insulin action for all clinically relevant insulin types, and is characterised by a unified and consistent, computationally-minimal, compartmental structure. No such model has been previously developed and as such, it is a foundation for future studies in this area.

Adaptive protocol and *in silico* simulation tool

The virtual patient cohort and its default control protocol (the data of which is used for *in silico* simulation) can be considered a good representation of the broad diabetes population. The simulation tool is used to develop a robust, adaptive protocol for prandial insulin dosing and assess the effects of optimal and suboptimal, basal and prandial insulin replacement.

In simulation, the adaptive protocol significantly decreased HbA_{1c} in conditions of suboptimal basal insulin replacement for SMBG frequencies $\geq$6/day. It also reduced mild and severe hypoglycaemia by 86-100% over controls across SMBG frequencies 2 to 10/day in conditions of optimal basal insulin. Basal insulin replacement has the single, most significant effect on HbA_{1c}, much more so than the difference between prandial insulin protocols.

With a conventional IIT in conditions of suboptimal basal insulin, the increase in cohort compliance to clinical control guidelines *saturates* at a SMBG frequency of 6/day. In addition, under conventional IIT, the basal insulin forced-titration regimen requires a minimum SMBG frequency of 6/day to safely titrate the basal dose without increased hypoglycaemia. Overaggressive basal dose titration with a conventional IIT at lower SMBG frequencies is likely to be caused by uncorrected postprandial hyperglycaemia from the previous night, resulting in an erroneous assumed FPG used for basal dose titration.

With a SMBG frequency of 4/day and optimal basal insulin replacement, 97.5% of the cohort can be controlled to ADA clinical guidelines using the adaptive protocol, a result similar to a conventional IIT but which has 103% more mild hypoglycaemia.

With regards to the validity of the *in silico* simulation tool, the HbA_{1c} simulation results for the conventional IIT is shown to be in excellent agreement with clinical results reported in literature, and the HbA_{1c} distribution of the controls cohort is also in agreement with published studies of the general diabetes population.

Overall these results:

1. Match clinical expectations

2. Exceed clinically reported safety from hypoglycaemia reported for conventional intensive insulin therapies

3. Utilise the simplest and lowest cost tools for diabetes management

Monte Carlo analysis of adaptive protocol

A Monte Carlo (MC) analysis is then performed on the adaptive protocol for prandial insulin dosing in conjunction with the Fritsche-Riddle basal insulin forced-titration regimen in long-term control. Errors in insulin and meal absorption, insulin dosing, meal carbohydrate counting, and blood glucose measurements are simulated.

In a MC simulation of over 1,400,000 patient hours, the adaptive protocol controlled 100% of the cohort to the ADA recommended threshold with a SMBG frequency of just 6/day. Unlike the no error simulation, a defined *peak* in control is observed at SMBG frequency of 8/day, with a small but significant decrease in the time spent in the 4-8mmol/l band and a consequent increase in mild and severe hypoglycaemia at SMBG frequency of 10/day. In addition, time spent in the 4-6mmol/l band is not significantly different to the no error simulation for all SMBG frequencies except 10/day.

For all SMBG frequencies, the cohort HbA_{1c} distribution is reduced while hypoglycaemia is increased over the no error simulation, as expected. While statistically significant, the difference in the 95% confidence band of the time spent in severe and mild hypoglycaemia is an acceptable 1% and 6% respectively over the no error simulation for a 6/day SMBG frequency.

Overall, the adaptive protocol developed is robust in both *effectiveness* and *safety* to the realistic and physiologic, simulated errors in Monte Carlo analysis. More importantly, the increase in mild hypoglycaemia is an absolute 1% over the no error simulation for a 6/day SMBG frequency, which can be considered an acceptable penalty with no reduction in effectiveness.

Diurnal S_I identification and S_I variation prediction

Median absolute percentage $G(t)$ prediction error per patient is significantly reduced (4.0%) over comparison methods, and the percentage of actual $G(t)$ within the respective prediction bands match the theoretical figure more consistently over the entire cohort. The dual frequency, diurnal cycle and stochastic AR(4) method results in 90% of the cohort having a percentage of actual $G(t)$ in the

90% $G(t)$ prediction band of between 81-93%.

For leads 2-6h, the diurnal cycle and AR(4) method median point $G(t)$ prediction error is 48-73% smaller than comparison methods, with a 90% range of the $G(t)$ prediction error smaller by 19-10% from leads 2 to 6h. The median prediction band width produced by the diurnal cycle and AR(4) method is 0.8 times larger, with a 0.4 times larger 90% band width range (1.7-9.1mmol/l) compared to the Lin et al. Markov method (2.1-7.5mmol/l).

This set of results demonstrates the advantages of the patient-specific method over the population-based method. The width of the prediction intervals reflects a more realistic model uncertainty for that particular patient. Finally, a poor match to the diurnal cycle model results in higher residuals and widening of the prediction band width, and vice versa.

This study shows that significant potential exists in the identification of a dual frequency, sinusoidal diurnal cycle in $S_I(t)$ and a residual autoregressive (AR) model to predict $S_I(t)$ evolution. With reduced prediction error compared to comparison methods for *all* prediction leads up to 6 hours, a reduction in SMBG frequency with no decline in glycaemic control effectiveness or safety is possible. Further research with split data sets with both training and blinded test samples will permit true out-of-sample forecast comparison of each method. However, overall these results would offer significant clinical advantages in treatment.

Overall Summary

Finally, this research presents an entire framework for the realistic, and rapid development and testing of clinical glycaemic control protocols for outpatient Type 1 diabetes. The models and methods developed within this framework allow rapid and physiological identification of time-variant, patient-specific, effective insulin sensitivity profiles. These profiles form the responses of the virtual patient and can be used to develop and test clinical glycaemic control protocols in a broad range of patients. These effective insulin sensitivity profiles are rich in dynamics, specifically those circadian in nature which can be identified, extracted and potentially used for safer and more effective control.

Chapter 8

Future Work

The models and methods presented in this thesis have been developed to explore the possibilities in the *in silico* simulation of clinical protocols for glycaemic control, and their effect on clinically relevant outcomes, e.g., HbA_{1c}. The subcutaneous insulin PK models have been initially validated using simple measures and there is a measure of self validation in the *in silico* approach to the simulation of long-term glycaemic outcomes from glycaemic control protocols.

Specifically, the results for the measurement frequency and HbA_{1c} outcome match clinical expectations. Additionally, the conventional IIT results match clinical reports as well as the trend in HbA_{1c}. Results overall reflect standard clinical expectations and experience as well. For example, the impact of optimising basal insulin delivery has a larger impact than optimising prandial control in its absence, a result that is reasonably well accepted in clinical studies. Hence, there is a sense of cross validation with clinical expectations and published results as traditional methods of validation may not be applicable or suitable due to the nature of this study.

Even so, research has to be continued, especially to a full clinical validation of the developed AC protocol, and its comparison against the CC protocol as well as other comparative methods on individual subgroups of the broad Type 1 diabetes population. Additional optimisation can also be implemented to improve the practical aspects of the protocols presented and further simplify their eventual use.

8.1 *In Silico* Validation with Real Patient Data

The *in silico* simulation in this thesis is performed with virtual patient profiles generated using the the AIDA model [Lehmann and Deutsch, 1992b]. As an additional validation *before* clinical validation, the *in silico* simulation should be performed on real patient data profiles obtained from a broad range of Type 1 diabetes patients. Some of that data (n=21) has already been collected in the study of diurnal variation modelling of S_I in Chapter 6. With further sets of data, a comparable *in silico* simulation can be performed to the one in this thesis on the S_I patient profiles of real Type 1 diabetes patient data.

8.2 Clinical Validation

Clinical validation is of vital importance to create confidence and credibility in the developed protocol. Additional protocol validation is also necessary to strengthen the results in repeatability and replicate the robustness of the protocol shown in the Monte Carlo analysis in this thesis. Particularly important aspects include:

Effect of insulin dosing: This aspect was simulated *in silico* in the Monte Carlo analysis presented in this thesis. In clinical validation, the effect of errors in insulin dosing should be tested with sufficient subject numbers for a significant result. In a controlled test environment, safety from hypoglycaemia can be assured while exploring this very fundamental source of variability and error in the day to day implementation of the protocol. Error and variability in insulin dosing is not specific to the AC protocol and existing methods of glycaemic control have evolved to become robust to this error. Only through clinical validation can this error be quantified and accounted for in future iterations of the AC protocol.

Effect of carbohydrate counting: As with insulin dosing, this source of error is simulated *in silico* in the Monte Carlo analysis presented in this thesis. In clinical validation, the effect of carbohydrate counting and its errors on the AC protocol effectiveness and safety can be safely explored in a controlled test environment.

Effect of CIR and ISF on the protocol effectiveness and safety: The effect of CIR and ISF are briefly explored in Chapter 4 and the potential to optimise the two parameters for the calculation of the initial bolus dose with the AC protocol has been shown. Methods for the systematic optimisation of these two parameters should be further explored and developed *in silico* before clinical validation with the aim of improving the effectiveness of the overall protocol with a little or no increase in rate of hypoglycaemia.

8.3 Practical and Clinical Issues

8.3.1 Per Patient Adaptation of SMBG Frequency

From Chapter 5, the AC protocol is capable of controlling 97.5% of the cohort to ADA recommendations with just 4 SMBG measurements/day (90% with just 2/day) in *in silico* simulation with Monte Carlo error. As such, there is a capability to determine the minimum SMBG frequency, or adapt the SMBG frequency to achieve a target HbA_{1c} level *per patient*. As different patients exhibit varying levels of brittleness [Gill and Lucas, 1999; Tattersall, 1997], this is a potentially tremendous capability for a glycaemic control protocol and should be further explored in clinical implementation. Also, the ability to adapt SMBG frequency may be seen as more attractive from a clinical implementation sense than a hard recommendation for a minimum SMBG frequency.

8.3.2 Clinical Implementation of the AC Protocol

From the outset, the modelling principle is to minimise computational requirement. For example, the compartmental sc insulin PK model is chosen, as opposed to the multiple coupled partial differential equations of similarly specified, more physiological models. In addition, the lumping of the effects of insulin sensitivity into one parameter, S_I and the fast, convex, integral-based parameter identification method used to identify the S_I in real-time, are decisions focused on the clinical implementation of the protocol.

In this thesis, the implementation of the AC protocol software and the *in silico* simulation on MATLAB® (The Mathworks, Natick, MA, USA) is performed on a PC notebook (Pentium M 1.7Ghz). This level of computing power is now readily available in the majority of homes. However, the protocol may be more suitably implemented on a hand held PDA device for portability.

The incorporation of the protocol into such devices can be seen as a first step towards clinical implementation and may even be used in the clinical validation itself. An ideal setting for clinical validation would be a general hospital ward where Type 1 diabetes patients are transitioned from intravenous insulin administration, and enteral and parenteral nutrition, to sc insulin administration and mixed meals. The controlled environment of a hospital ward would enable patient and protocol adherence to be maintained at a high level, and accurate carbohydrate counts and insulin dosing can be performed. This would enable the protocol to be trialled for possible issues in clinical implementation before being implemented in the target outpatient Type 1 diabetes population.

8.4 Potential Additional Applications

While designed for Type 1 diabetes, the AC protocol in its current form can also be applied to the glycaemic control of long-term, insulin-dependent Type 2 diabetes. Long-term Type 2 diabetes is characterised by the cessation of residual endogenous insulin secretion *ala* Type 1 diabetes. Possible differences between the protocols for Type 1 and Type 2 diabetes are a lower effective insulin sensitivity in Type 2 diabetes, which would increase the insulin dose demand proportionately.

As endogenous insulin secretion is not modelled currently and is not necessary for Type 1 diabetes or long-term Type 2 diabetes, insulin resistant or early Type 2 diabetes will not be modelled adequately due to assumptions made and further work is required if the model is to be made appropriate for this cohort. Even so, as the majority of Type 2 diabetes patients are not insulin treated, the applicability of the AC protocol for treatment in these individuals may be of questionable value.

8.4.1 Meal or Nutrition Control

Another aspect of glycaemic control that has been trialled successfully is meal or nutrition control *in addition* to intensive insulin therapy. This approach has been extremely effective in stress-induced, hyperglycaemic, critically ill patients in intensive care fed enterally [Lonergan et al., 2006a,b]. The control of meals (specifically timing of meals and meal sizes) to aid insulin therapy in reducing postprandial glycaemic excursion may be valuable if the individual is highly insulin resistant and may be more applicable in long-term Type 2 diabetes than the current target population of Type 1 diabetes.

8.4.2 Use of Diurnal S_I Cycles

A method for identifying the diurnal cycle in S_I and modelling it in retrospective patient data has been shown in this thesis. The identification and prediction of this rhythm is of utmost clinical relevance, potentially leading to safer and more effective glycaemic control *with* less frequent measurement up to a prediction lead of 6 hours.

The use of diurnal S_I cycles for effective glycaemic prediction with reduced SMBG frequency must be investigated further. Further research with split data sets with both training and blinded test samples will permit a true out-of-sample forecast comparison of the method developed in this thesis.

Additionally, the method of identifying and predicting the diurnal cycles in S_I may even be incorporated into the AC protocol for further safety and effectiveness. As with the AC protocol, clinical effectiveness or utility of this method must be proven first in a clinical setting.

8.4.3 Modelling of Exercise

The modelling of exercise for glycaemic control has been attempted in literature [Arleth, 2005] and it is necessarily a complicated and challenging process. There is considerable difficulty in quantifying the intensity of exercise and without

quantitative measurements, only subjective quantification of exercise is possible. However, exercise is part of daily life in outpatient Type 1 diabetes and insulin-dependent Type 2 diabetes, and for completeness, a method to account or manage its metabolic effects with respect to S_I and G must be investigated.

8.5 Summary

Finally, the protocol and methods developed in this thesis offer great potential for improved glycaemic control and treatment of Type 1 diabetes. In particular, the developed adaptive protocol, its *in silico* simulation and Monte Carlo analysis, as well as the modelling of S_I diurnal cycle form a framework for the realistic, and rapid development and testing of clinical glycaemic control protocols for outpatient Type 1 diabetes.

In silico simulation using virtual patient profiles must be followed by simulation using patient profiles identified from real patient data, and clinical validation against current, widely used methods will provide confidence in the performance of the protocol. From there, further work on the practical aspects of its clinical implementation will ensure that the clinical realisation of the protocol is sufficiently simple to prevent issues that affect clinical use and protocol adherence.

Additional potential applications of the protocol, such as in the control of meals, and the use of the diurnal cycle in S_I can further improve performance of the protocol with little or no disadvantage to rate of hypoglycaemia or clinical effort.

References

AACE (2002). Medical guidelines for the management of diabetes mellitus: The aace system of intensive diabetes self-management-2002 update. *Endocr Prac*, 8 (Suppl. 1):40–64.

ADA (1996). Self-monitoring of blood glucose. *Diabetes Care*, 19:S62–S66.

ADA (2005). Defining and reporting hypoglycemia in diabetes: a report from the american diabetes association workgroup on hypoglycemia. *Diabetes Care*, 28(5):1245–9.

ADA (2006a). Diagnosis and classification of diabetes mellitus. *Diabetes Care*, 29(S1):S43–8.

ADA (2006b). Standards of medical care in diabetes-2006. *Diabetes Care*, 29:S4–S42.

Ader, M., Ni, T. C., and Bergman, R. N. (1997). Glucose effectiveness assessed under dynamic and steady state conditions. comparability of uptake versus production components. *J Clin Invest*, 99(6):1187–99.

Anderson, J. H., Brunelle, R. L., Koivisto, V. A., Pfutzner, A., Trautmann, M. E., Vignati, L., DiMarchi, R., Bowen, K. M., Cameron, D. P., Nankervis, A. J., Roberts, A. P., Zimmet, P., Borkenstein, M. H., Schernthaner, G., Waldhausl, W. K., DeLeeuw, I. H., Fery, F., Scheen, A., Somers, G., Fettes, I. M., Tildesley, H. D., Toth, E. L., Viikari, J., Altman, J. J., Bougneres, P. F., Drouin, P., Fossati, P., Guillausseau, P. J., Marechaud, E., Riou, J. P., Selam, J. L., Vialettes, P. B., Beyer, J., Federlin, K., Fussganger, R. D., Gries, F. A., Jastram, H. U., Koop, I., Landgraf, R., Rosak, C., Schatz, H., SchulzeSchleppinghoff, B., Seif, F. J., Stoeckmann, F., Karasik, A., Weitzman, S., Andreani, D., Bompiani, G., Crepaldi, G., Giorgino, R., Greco, A. V., Lauro, R., Maingay, D., Mancini, M., Menzinger, G., Muggeo, M., Pagano, G., Sacca, L., Tiengo,

A., Vigneri, R., Erkelens, D. W., Janssens, E. N., Lekkerkerker, J. F., Spijker, A. J., Daniels, A. R., Folling, I., Bonnici, F. B., Mollentze, W. F., Moore, R., Omar, M. A., Robertson, L. I., Astorga, R., deLeiva, A., Jara, A., Vazquez, J. A., Villardell, E., Agardh, C. D., Alexander, W. D., Barnett, A. H., Cassar, J., Hitman, G. A., Kesson, C. M., OHare, J. P., Shaw, K. M., Wales, J. K., Arslanian, S., Bastyr, E. J., Blevins, T. C., Boyce, P. A., Brink, S. J., Clarke, D. H., DeClue, T., Garber, A. J., Guthrie, R. A., Johnson, D. G., Krosnick, A., Linarelli, L. G., McCulloch, D. K., Mezitis, N. H., Raskin, P., Reeves, M. L., Rosenblatt, S., Schimel, D., Skyler, J. S., Sonnenberg, G. E., Whitehouse, F. W., and Zimmerman, B. (1997). Reduction of postprandial hyperglycemia and frequency of hypoglycemia in iddm patients on insulin-analog treatment. *Diabetes*, 46(2):265–270.

Andreassen, S., Benn, J. J., Hovorka, R., Olesen, K. G., and Carson, E. R. (1994). A probabilistic approach to glucose prediction and insulin dose adjustment: description of metabolic model and pilot evaluation study. *Comput Methods Programs Biomed*, 41(3-4):153–65.

Antsiferov, M., Woodworth, J. R., Mayorov, A., Ristic, S., and Dedov, I. (1995). Within patient variability in postprandial glucose excursion with lispro insulin analog compared with regular insulin. *Diabetologia*, 38:A190–A190.

Arleth, T. (2005). *Optimisation and Test of a Diabetes Insulin Advisory System*. PhD thesis, Centre for Model-based Medical Decision Support, Aalborg University.

Arleth, T., Andreassen, S., Federici, M. O., and Benedetti, M. M. (2000). A model of the endogenous glucose balance incorporating the characteristics of glucose transporters. *Comput Methods Programs Biomed*, 62(3):219–34.

Banting, F., Best, C., Collip, J., Campbell, W., and Fletcher, A. (1922). Pancreatic extracts in the treatment of diabetes mellitus. *Canadian Medical Association Journal*, 12:141–46.

Baron, A. D., Brechtel, G., Wallace, P., and Edelman, S. V. (1988). Rates and tissue sites of non-insulin- and insulin-mediated glucose uptake in humans. *Am J Physiol*, 255(6 Pt 1):E769–74.

BD Diabetes Learning Centre (2006). Insulin therapies: Managing diabetes with insulin.

Bellazzi, R., Nucci, G., and Cobelli, C. (2001). The subcutaneous route to insulin-dependent diabetes therapy. *Ieee Engineering in Medicine and Biology Magazine*, 20(1):54–64.

Bequette, B. W. (2005). A critical assessment of algorithms and challenges in the development of a closed-loop artificial pancreas. *Diabetes Technol Ther*, 7(1):28–47.

Berger, M., Cuppers, H. J., Hegner, H., Jorgens, V., and Berchtold, P. (1982). Absorption kinetics and biologic effects of subcutaneously injected insulin preparations. *Diabetes Care*, 5(2):77–91.

Berger, M. and Rodbard, D. (1989). Computer simulation of plasma insulin and glucose dynamics after subcutaneous insulin injection. *Diabetes Care*, 12(10):725–36.

Bergman, R. N., Finegood, D. T., and Ader, M. (1985). Assessment of insulin sensitivity in vivo. *Endocr Rev*, 6(1):45–86.

Bergman, R. N., Ider, Y. Z., Bowden, C. R., and Cobelli, C. (1979). Quantitative estimation of insulin sensitivity. *Am J Physiol*, 236(6):E667–77.

Bergman, R. N., Phillips, L. S., and Cobelli, C. (1981). Physiologic evaluation of factors controlling glucose tolerance in man: measurement of insulin sensitivity and beta-cell glucose sensitivity from the response to intravenous glucose. *J Clin Invest*, 68(6):1456–1467.

Best, J. D., Kahn, S. E., Ader, M., Watanabe, R. M., Ni, T. C., and Bergman, R. N. (1996). Role of glucose effectiveness in the determination of glucose tolerance. *Diabetes Care*, 19(9):1018–30.

Best, J. D., Taborsky, G. J., J., Halter, J. B., and Porte, D., J. (1981). Glucose disposal is not proportional to plasma glucose level in man. *Diabetes*, 30(10):847–50.

Binder, C. (1969). Absorption of injected insulin - a clinical-pharmacological study. *Acta Pharmacologica Et Toxicologica*, S 27:1–&.

Binder, C., Lauritzen, T., Faber, O., and Pramming, S. (1984). Insulin pharmacokinetics. *Diabetes Care*, 7(2):188–199.

Blonde, L.and Karter, A. J. (2005). Current evidence regarding the value of self-monitored blood glucose testing. *American Journal of Medicine*, 118:20s–26s.

Bloomfield, P. (2000). *Fourier analysis of time series: An introduction*. Wiley Series in Probability and Statistics. John Wiley & Sons, New York, 2nd edition.

Bolli, G. B. (1988). The dawn phenomenon - its origin and contribution to early morning hyperglycemia in diabetes-mellitus. *Diabetes and Metabolism*, 14(6):675–686.

Bolli, G. B., Di Marchi, R. D., Park, G. D., Pramming, S., and Koivisto, V. A. (1999). Insulin analogues and their potential in the management of diabetes mellitus. *Diabetologia*, 42 (10):1151–1167.

Bolli, G. B., Fanelli, C. G., Perriello, G., and Defeo, P. (1993). Nocturnal blood-glucose control in type-i diabetes-mellitus. *Diabetes Care*, 16:71–89.

Boroujerdi, M. A., Williams, C. D., Piwernetz, K., Carson, E. R., Hepp, K. D., and Sonksen, P. H. (1987). Simulation approach for planning insulin regimes. pages 41–46, New York. International Symposium on Advanced Models for Therapy of Insulin-Dependent Diabetes, Serona Symposium No. 37, Raven Press.

Bottermann, P., Gyaram, H., Wahl, K., Ermler, R., and Lebender, A. (1982). Insulin concentrations and time-action profiles of 3 different intermediate-acting insulin preparations in non-diabetic volunteers under glucose-controlled glucose-infusion technique. *Diabetes Care*, 5:43–52.

Boyle, P. J., Scott, J. C., Krentz, A. J., Nagy, R. J., Comstock, E., and Hoffman, C. (1994). Diminished brain glucose metabolism is a significant determinant for falling rates of systemic glucose utilization during sleep in normal humans. *J Clin Invest*, 93(2):529–35.

Brange, J., Owens, D. R., Kang, E. S., and Volund, A. (1988). Monomeric insulins obtained by protein engineering and their medical implications. *Nature*, 333(6174):679–682.

Brange, J., Owens, D. R., Kang, S., and Volund, A. (1990). Monomeric insulins and their experimental and clinical implications. *Diabetes Care*, 13(9):923–954.

Brange, J. and Volund, A. (1999). Insulin analogs with improved pharmacokinetic profiles. *Advanced Drug Delivery Reviews*, 35(2-3):307–335.

Brunner, G. A., Ellmerer, M., Sendlhofer, G., Wutte, A., Trajanoski, Z., Schaupp, L., Quehenberger, F., Wach, P., Krejs, G. J., and Pieber, T. R. (1998). Validation of home blood glucose meters with respect to clinical and analytical approaches. *Diabetes Care*, 21(4):585–90.

Bruttomesso, D., Pianta, A., Crazzolara, D., Capparotto, C., Dainese, E., Zurlo, C., Minicuci, N., Briani, G., and Tiengo, A. (2001). Teaching and training programme on carbohydrate counting in type 1 diabetic patients. *Diabetes Nutrition & Metabolism*, 14(5):259–267.

Camastra, S., Manco, M., Mari, A., Baldi, S., Gastaldelli, A., Greco, A. V., Mingrone, G., and Ferrannini, E. (2005). beta-cell function in morbidly obese subjects during free living: long-term effects of weight loss. *Diabetes*, 54(8):2382–9.

Campbell, R. K., White, J. R., Levien, T., and Baker, D. (2001). Insulin glargine. *Clinical Therapeutics*, 23(12):1938–1957.

Capaldo, B., Gastaldelli, A., Antoniello, S., Auletta, M., Pardo, F., Ciociaro, D., Guida, R., Ferrannini, E., and Sacca, L. (1999). Splanchnic and leg substrate exchange after ingestion of a natural mixed meal in humans. *Diabetes*, 48(5):958–66.

Carson, E. R. and Cobelli, C. (2001). *Modelling methodology for physiology and medicine*. Academic Press Series in Biomedical Engineering. Academic Press, San Diego.

Castillo, C., Bogardus, C., Bergman, R., Thuillez, P., and Lillioja, S. (1994). Interstitial insulin concentrations determine glucose uptake rates but not insulin resistance in lean and obese men. *J Clin Invest*, 93(1):10–6.

Caumo, A. and Cobelli, C. (1993). Hepatic glucose production during the labeled ivgtt: estimation by deconvolution with a new minimal model. *Am J Physiol*, 264(5 Pt 1):E829–41.

Caumo, A., Vicini, P., and Cobelli, C. (1996). Is the minimal model too minimal? *Diabetologia*, 39(8):997–1000.

Caumo, A., Vicini, P., Zachwieja, J. J., Avogaro, A., Yarasheski, K., Bier, D. M., and Cobelli, C. (1999). Undermodeling affects minimal model indexes: insights from a two-compartment model. *Am J Physiol*, 276(6 Pt 1):E1171–1193.

CDC (2005). National diabetes fact sheet: General information and national estimates on diabetes in the united states, 2005. Technical report, Centers for Disease Control and Prevention.

Cernea, S., Kidron, M., Wohlgelernter, J., Modi, P., and Raz, I. (2004). Comparison of pharmacokinetic and pharmacodynamic properties of single-dose oral insulin spray and subcutaneous insulin injection in healthy subjects using the euglycemic clamp technique. *Clinical Therapeutics*, 26(12):2084–2091.

Chapman, T. and Perry, C. (2004). Insulin detemir - a review of its use in the management of type 1 and 2 diabetes mellitus. *Drugs*, 64(22):2577–2595.

Chase, J., Shaw, G. M., Wong, X. W., Lotz, T., Lin, J., and Hann, C. E. (2006). Model-based glycaemic control in critical care - a review of the state of the possible. *Biomedical Signal Processing and Control*, 1(1):3–21.

Chase, J. G., Shaw, G. M., Lin, J., Doran, C. V., Bloomfield, M., Wake, G. C., Broughton, B., Hann, C., and Lotz, T. (2004). Impact of insulin-stimulated glucose removal saturation on dynamic modelling and control of hyperglycaemia. *International Journal of Intelligent Systems Technologies and Applications (IJISTA)*, 1(1/2):79–94.

Chase, J. G., Shaw, G. M., Lin, J., Doran, C. V., Hann, C., Lotz, T., Wake, G. C., and Broughton, B. (2005a). Targeted glycemic reduction in critical care using closed-loop control. *Diabetes Technol Ther*, 7(2):274–82.

Chase, J. G., Shaw, G. M., Lin, J., Doran, C. V., Hann, C., Robertson, M. B., Browne, P. M., Lotz, T., Wake, G. C., and Broughton, B. (2005b). Adaptive bolus-based targeted glucose regulation of hyperglycaemia in critical care. *Med Eng Phys*, 27(1):1–11.

Chase, J. G., Shaw, G. M., Lotz, T., LeCompte, A., Wong, J., Lin, J., Lonergan, T., Willacy, M., and Hann, C. E. (2007). Model-based insulin and nutrition administration for tight glycaemic control in critical care. *Curr Drug Deliv*, 4(4):283–96.

Chase, J. G., Wong, X.-W., Singh-Levett, I., Hollingsworth, L. J., Hann, C. E., Shaw, G. M., Lotz, T., and Lin, J. (2008). Simulation and initial proof-of-concept validation of a glycaemic regulation algorithm in critical care. *Control Engineering Practice*, 16(3):271–285.

Chatfield, C. (2000). *Time-series forecasting*. Chapman & Hall/CRC, Boca Raton, 1st edition.

Chatfield, C. (2004). *The analysis of time series - An introduction*. Statistical Science. Chapman & Hall/CRC, Boca Raton, 6th edition.

Chee, F., Fernando, T. L., Savkin, A. V., and van Heeden, V. (2003). Expert pid control system for blood glucose control in critically ill patients. *IEEE Trans Inf Technol Biomed*, 7(4):419–25.

Cherrington, A. D. (1999). Banting lecture 1997. control of glucose uptake and release by the liver in vivo. *Diabetes*, 48(5):1198–214.

Clausen, W. H., De Gaetano, A., and Volund, A. (2006). Within-patient variation of the pharmacokinetics of subcutaneously injected biphasic insulin aspart as assessed by compartmental modelling. *Diabetologia*, 49(9):2030–2038.

Clore, J. N., Nestler, J. E., and Blackard, W. G. (1989). Sleep-associated fall in glucose disposal and hepatic glucose output in normal humans - putative signaling mechanism linking peripheral and hepatic events. *Diabetes*, 38(3):285–290.

Cobelli, C., Toffolo, G., and Ferrannini, E. (1984). A model of glucose kinetics and their control by insulin, compartmental and noncompartmental approaches. *Mathematical Biosciences*, 72(2):291–315.

Cohen, M., Boyle, E., Delaney, C., and Shaw, J. (2006). A comparison of blood glucose meters in australia. *Diabetes Research and Clinical Practice*, 71(2):113–118.

Conn, P. M. and Goodman, H. M. (1998). *The endocrine system*. Published for the American Physiological Society by Oxford University Press, New York ; Oxford.

Cryer, P. E., Davis, S. N., and Shamoon, H. (2003). Hypoglycemia in diabetes. *Diabetes Care*, 26(6):1902–12.

Cudworth, A. G., Wolf, E., Gorsuch, A. N., and Festenstein, H. (1979). A new look at hla genetics with particular reference to type-1 diabetes. *Lancet*, 2:389–391.

Dahlquist, G. and Mustonen, L. (1994). Childhood onset diabetes–time trends and climatological factors. *Int J Epidemiol*, 23(6):1234–41.

Dalla Man, C., Camilleri, M., and Cobelli, C. (2006). A system model of oral glucose absorption: validation on gold standard data. *IEEE Trans Biomed Eng*, 53(12 Pt 1):2472–8.

Dalla Man, C., Caumo, A., Basu, R., Rizza, R., Toffolo, G., and Cobelli, C. (2004). Minimal model estimation of glucose absorption and insulin sensitivity from oral test: validation with a tracer method. *American Journal of Physiology-Endocrinology and Metabolism*, 287(4):E637–E643.

Dandona, P., Chaudhuri, A., Ghanim, H., and Mohanty, P. (2006). Anti-inflammatory effects of insulin and pro-inflammatory effects of glucose: relevance to the management of acute myocardial infarction and other acute coronary syndromes. *Rev Cardiovasc Med*, 7 Suppl 2:S25–34.

Davidson, P. C., Hebblewhite, H. R., Bode, B. W., Steed, R. D., and Steffes, P. G. (2004). Statistically fitted curve for a1c as a function of the smbg tests per day. In *64th Scientific Sessions of the American Diabetes Association*, volume 430-P, Orlando, Florida.

Davis, S. N., Thompson, C. J., Brown, M. D., Home, P. D., and Alberti, K. (1991). A comparison of the pharmacokinetics and metabolic effects of human regular and nph insulin mixtures. *Diabetes Research and Clinical Practice*, 13(1-2):107–117.

DCCT Research Group (1993). The effect of intensive treatment of diabetes on the development and progression of long-term complications in insulin-dependent diabetes mellitus. *N Engl J Med*, 329(14):977–86.

DCCT/EDIC Research Group (1999). Epidemiology of diabetes interventions and complications (edic). design, implementation, and preliminary results of a long-term follow-up of the diabetes control and complications trial cohort. *Diabetes Care*, 22(1):99–111.

Del Prato, S., Matsuda, M., Simonson, D. C., Groop, L. C., Sheehan, P., Leonetti, F., Bonadonna, R. C., and DeFronzo, R. A. (1997). Studies on the mass action effect of glucose in niddm and iddm: evidence for glucose resistance. *Diabetologia*, 40(6):687–97.

Del Prato, S., Riccio, A., Vigili de Kreutzenberg, S., Dorella, M., Tiengo, A., and DeFronzo, R. A. (1995). Basal plasma insulin levels exert a qualitative but not

quantitative effect on glucose-mediated glucose uptake. *Am J Physiol*, 268(6 Pt 1):E1089–95.

Demeijer, P. H. E. M., Lutterman, J. A., Vanlier, H. J. J., and Vantlaar, A. (1990). The variability of the absorption of subcutaneously injected insulin - effect of injection technique and relation with brittleness. *Diabetic Medicine*, 7(6):499–505.

Despopoulos, A. and Silbernagl, S. (2003). *Color atlas of physiology*. Thieme flexibook. G. Thieme Thieme Medical Publishers, Stuttgart New York, 5th edition.

DeWitt, D. E. and Dugdale, D. C. (2003). Using new insulin strategies in the outpatient treatment of diabetes - clinical applications. *Jama-Journal of the American Medical Association*, 289(17):2265–2269.

DiabetesUK (accessed 8 August 2007). Position statement on insulin pump therapy. Technical report.

Distiller, L. A. and Joffe, B. I. (2006). From the coalface: does glargine insulin improve hypoglycaemic episodes, glycaemic control or affect body mass in type 1 diabetic subjects who are attending a 'routine' diabetes clinic? *Diabetologia*, 49(11):2793–4.

Dobson, M. (1776). Nature of the urine in diabetes. *Med Obs Inqu*, 5:298–310.

Duckworth, W. C., Bennett, R. G., and Hamel, F. G. (1998). Insulin degradation: progress and potential. *Endocr Rev*, 19(5):608–24.

Duckworth, W. C., Hamel, F. G., and Peavy, D. E. (1988). Hepatic metabolism of insulin. *Am J Med*, 85(5A):71–6.

Duncan, G. E., Perri, M. G., Theriaque, D. W., Hutson, A. D., Eckel, R. H., and Stacpoole, P. W. (2003). Exercise training, without weight loss, increases insulin sensitivity and postheparin plasma lipase activity in previously sedentary adults. *Diabetes Care*, 26(3):557–562.

Elashoff, J. D., Reedy, T. J., and Meyer, J. H. (1982). Analysis of gastric emptying data. *Gastroenterology*, 83:1306–12.

Emdin, S. O., Dodson, G. G., Cutfield, J. M., and Cutfield, S. M. (1980). Role of zinc in insulin-biosynthesis - some possible zinc-insulin interactions in the pancreatic b-cell. *Diabetologia*, 19(3):174–182.

Evans, J. M. M., Newton, R. W., Ruta, D. A., MacDonald, T. M., Stevenson, R. J., and Morris, A. D. (1999). Frequency of blood glucose monitoring in relation to glycaemic control: observational study with diabetes database. *British Medical Journal*, 319(7202):83–86.

Ferrannini, E. (1997). Insulin resistance is central to the burden of diabetes. *Diabetes Metab Rev*, 13(2):81–6.

Ferrannini, E., Bjorkman, O., Reichard, G. A., Pilo, A., Olsson, M., Wahren, J., and Defronzo, R. A. (1985). The disposal of an oral glucose-load in healthy-subjects - a quantitative study. *Diabetes*, 34(6):580–588.

Ferrannini, E. and Cobelli, C. (1987a). The kinetics of insulin in man. i. general aspects. *Diabetes Metab Rev*, 3(2):335–63.

Ferrannini, E. and Cobelli, C. (1987b). The kinetics of insulin in man. ii. role of the liver. *Diabetes Metab Rev*, 3(2):365–97.

Ferrannini, E., Gastaldelli, A., Miyazaki, Y., Matsuda, M., Mari, A., and DeFronzo, R. A. (2005). beta-cell function in subjects spanning the range from normal glucose tolerance to overt diabetes: a new analysis. *J Clin Endocrinol Metab*, 90(1):493–500.

Ferrannini, E. and Mari, A. (2004). Beta cell function and its relation to insulin action in humans: a critical appraisal. *Diabetologia*, 47(5):943–56.

Ferrannini, E., Natali, A., Bell, P., Cavallo-Perin, P., Lalic, N., and Mingrone, G. (1997). Insulin resistance and hypersecretion in obesity. european group for the study of insulin resistance (egir). *J Clin Invest*, 100(5):1166–73.

Ferrannini, E., Wahren, J., Faber, O. K., Felig, P., Binder, C., and DeFronzo, R. A. (1983). Splanchnic and renal metabolism of insulin in human subjects: a dose-response study. *Am J Physiol*, 244(6):E517–27.

Fisher, M. E. (1991). A semiclosed-loop algorithm for the control of blood glucose levels in diabetics. *IEEE Trans Biomed Eng*, 38(1):57–61.

Flint, A., Moller, B. K., Raben, A., Pedersen, D., Tetens, I., Holst, J. J., and Astrup, A. (2004). The use of glycaemic index tables to predict glycaemic index of composite breakfast meals. *British Journal of Nutrition*, 91(6):979–989.

Fritsche, A., Schweitzer, M. A., and Haring, H. U. (2003). Glimepiride combined with morning insulin glargine, bedtime neutral protamine hagedorn insulin, or bedtime insulin glargine in patients with type 2 diabetes. a randomized, controlled trial. *Ann Intern Med*, 138(12):952–9.

Frost, D. P., Srivastava, M. C., Jones, R. H., Nabarro, J. D., and Sonksen, P. H. (1973). The kinetics of insulin metabolism in diabetes mellitus. *Postgrad Med J*, 49:Suppl 7:949–54.

Furler, S. M. and Kraegen, E. W. (1989). Quantitative aspects of subcutaneous insulin absorption. *Diabetic Medicine*, 6(8):657–665.

Gallen, I. W. and Carter, C. (2003). Prospective audit of the introduction of insulin glargine (lantus) into clinical practice in type 1 diabetic patients. *Diabetes Care*, 26(12):3352–3353.

Galloway, J. A., Spradlin, C. T., Nelson, R. L., Wentworth, S. M., Davidson, J. A., and Swarner, J. L. (1981). Factors influencing the absorption, serum-insulin concentration, and blood-glucose responses after injections of regular insulin and various insulin mixtures. *Diabetes Care*, 4(3):366–376.

Gerich, J. E. (2002). Novel insulins: Expanding options in diabetes management. *American Journal of Medicine*, 113(4):308–316.

Gerich, J. E. (2004). Insulin glargine: long-acting basal insulin analog for improved metabolic control. *Current Medical Research and Opinion*, 20(1):31–37.

Gill, G. and Lucas, S. (1999). Brittle diabetes characterised by recurrent hypoglycaemia. *Diabetes & Metabolism*, 25 (4):308–311.

Gin, H. and Hanaire-Broutin, H. (2005). Reproducibility and variability in the action of injected insulin. *Diabetes & Metabolism*, 31(1):7–13.

Goldstein, D. E., Little, R. R., Lorenz, R. A., Malone, J. I., Nathan, D., Peterson, C. M., and Sacks, D. B. (2004). Tests of glycemia in diabetes. *Diabetes Care*, 27(7):1761–73.

Gray, H. and Lewis, W. H. (1918). *Anatomy of the Human Body*. Lea & Febiger, Philadelphia.

Gregory, R. P. and Davis, D. L. (1994). Use of carbohydrate counting for meal planning in type-i diabetes. *Diabetes Educator*, 20(5):406–409.

Gudbjornsdottir, S., Sjostrand, M., Strindberg, L., Wahren, J., and Lonnroth, P. (2003). Direct measurements of the permeability surface area for insulin and glucose in human skeletal muscle. *J Clin Endocrinol Metab*, 88(10):4559–64.

Guerci, B., Floriot, M., Bohme, P., Durain, D., Benichou, M., Jellimann, S., and Drouin, P. (2003). Clinical performance of cgms in type 1 diabetic patients treated by continuous subcutaneous insulin infusion using insulin analogs. *Diabetes care*, 26(3):582–9.

Guerci, B. and Sauvanet, J. P. (2005). Subcutaneous insulin: pharmacokinetic variability and glycemic variability. *Diabetes & Metabolism*, 31(4):S7–S24.

Guyton, A. C. and Hall, J. E. (2000). *Textbook of medical physiology*. Saunders, Philadelphia ; London, 10th edition.

Hanas, R. (2005). *Type 1 Diabetes - a Guide for Children, Adolescents, Young Adults and Their Caregivers*. Marlowe & Company, NY.

Hann, C., Chase, J., Andreassen, S., Smith, B., and Shaw, G. (2005a). Diagnosis using a minimal cardiac model including reflex actions. *Intensive Care Med*, 31(S1):S18.

Hann, C., Chase, J., and Shaw, G. (2006). Integral-based identification of patient specific parameters for a minimal cardiac model. *Computer Methods and Programs in Biomedicine*, 81(2):181–192.

Hann, C. E., Chase, J. G., Lin, J., Lotz, T., Doran, C. V., and Shaw, G. M. (2005b). Integral-based parameter identification for long-term dynamic verification of a glucose-insulin system model. *Comput Methods Programs Biomed*, 77(3):259–270.

Hansen, T. K., Thiel, S., Wouters, P. J., Christiansen, J. S., and Van den Berghe, G. (2003). Intensive insulin therapy exerts antiinflammatory effects in critically ill patients and counteracts the adverse effect of low mannose-binding lectin levels. *The Journal of clinical endocrinology and metabolism*, 88(3):1082–8.

Hedman, C. A., Lindstrom, T., and Arnqvist, H. J. (2001). Direct comparison of insulin lispro and aspart shows small differences in plasma insulin profiles after subcutaneous injection in type 1 diabetes. *Diabetes Care*, 24(6):1120–1.

Heinemann, L. (2002). Variability of insulin absorption and insulin action. *Diabetes Technol Ther*, 4(5):673–82.

Heinemann, L. and Anderson, J. H., J. (2004). Measurement of insulin absorption and insulin action. *Diabetes Technol Ther*, 6(5):698–718.

Heinemann, L., Linkeschova, R., Rave, K., Hompesch, B., Sedlak, M., and Heise, T. (2000). Time-action profile of the long-acting insulin analog insulin glargine (hoe901) in comparison with those of nph insulin and placebo. *Diabetes Care*, 23(5):644–649.

Heinemann, L. and Richter, B. (1993). Clinical-pharmacology of human insulin. *Diabetes Care*, 16:90–100.

Heinemann, L., Weyer, C., Rauhaus, M., Heinrichs, S., and Heise, T. (1998). Variability of the metabolic effect of soluble insulin and the rapid-acting insulin analog insulin aspart. *Diabetes Care*, 21(11):1910–4.

Heise, T., Nosek, L., Ronn, B. B., Endahl, L., Heinemann, L., Kapitza, C., and Draeger, E. (2004). Lower within-subject variability of insulin detemir in comparison to nph insulin and insulin glargine in people with type 1 diabetes. *Diabetes*, 53(6):1614–1620.

Heise, T., Weyer, C., Serwas, A., Heinrichs, S., Osinga, J., Roach, P., Woodworth, J., Gudat, U., and Heinemann, L. (1998). Time-action profiles of novel premixed preparations of insulin lispro and npl insulin. *Diabetes Care*, 21(5):800–3.

Heller, S. R., Macdonald, I. A., Herbert, M., and Tattersall, R. B. (1987). Influence of sympathetic nervous system on hypoglycaemic warning symptoms. *Lancet*, 2(8555):359–63.

Hildebrandt, P. (1991). Subcutaneous absorption of insulin in insulin-dependent diabetic-patients - influence of species, physicochemical properties of insulin and physiological factors. *Danish Medical Bulletin*, 38(4):337–346.

Hildebrandt, P., Sestoft, L., and Nielsen, S. L. (1983). The absorption of subcutaneously injected short-acting soluble insulin - influence of injection technique and concentration. *Diabetes Care*, 6(5):459–462.

Hogan, P., Dall, T., and Nikolov, P. (2003). Economic costs of diabetes in the us in 2002. *Diabetes Care*, 26(3):917–32.

Holman, R. R. and Turner, R. C. (1985). A practical guide to basal and prandial insulin therapy. *Diabet Med*, 2(1):45–53.

Home, P. and Alberti, K. (1992). *International Textbook of Diabetes Mellitus: Insulin Therapy*. John Wiley & Sons, Chichester.

Home, P. and Ashwell, S. (2002). An overview of insulin glargine. *Diabetes-Metabolism Research and Reviews*, 18:S57–S63.

Home, P. D., Lindholm, A., Hylleberg, B., and Round, P. (1998). Improved glycemic control with insulin aspart: a multicenter randomized double-blind crossover trial in type 1 diabetic patients. uk insulin aspart study group. *Diabetes Care*, 21(11):1904–9.

Hordern, S. and Russell-Jones, D. (2005). Insulin detemir, does a new century bring a better basal insulin? *International Journal of Clinical Practice*, 59(6):730–739.

Hossain, P., Kawar, B., and El Nahas, M. (2007). Obesity and diabetes in the developing world–a growing challenge. *N Engl J Med*, 356(3):213–5.

Hovorka, R., Canonico, V., Chassin, L. J., Haueter, U., Massi-Benedetti, M., Federici, M. O., Pieber, T. R., Schaller, H. C., Schaupp, L., Vering, T., and Wilinska, M. E. (2004). Nonlinear model predictive control of glucose concentration in subjects with type 1 diabetes. *Physiological Measurement*, 25(4):905–920.

Hovorka, R., Powrie, J. K., Smith, G. D., Sonksen, P. H., Carson, E. R., and Jones, R. H. (1993). Five-compartment model of insulin kinetics and its use to investigate action of chloroquine in niddm. *Am J Physiol*, 265(1 Pt 1):E162–75.

Hovorka, R., Shojaee-Moradie, F., Carroll, P. V., Chassin, L. J., Gowrie, I. J., Jackson, N. C., Tudor, R. S., Umpleby, A. M., and Jones, R. H. (2002). Partitioning glucose distribution/transport, disposal, and endogenous production during ivgtt. *Am J Physiol Endocrinol Metab*, 282(5):E992–1007.

Hovorka, R., Wilinska, M. E., and Chassin, L. J. (2005). In silico simulation environment and glucose control in critically ill subjects: Strategic considerations. In *3rd European Medical & Biological Engineering Conference*, Prague, Czech Republic. IFMBE.

Hubinger, A., Weber, W., Jung, W., Wehmeyer, K., and Gries, F. A. (1992). The pharmacokinetics of 2 different concentrations of short-acting insulin, intermediate-acting insulin, and an insulin mixture following subcutaneous injection. *Clinical Investigator*, 70(7):621–626.

Insel, P. A., Kramer, K. J., Sherwin, R. S., Liljenquist, J. E., Tobin, J. D., Andres, R., and Berman, M. (1974). Modeling the insulin-glucose system in man. *Fed Proc*, 33(7):1865–8.

Jacquez, J. A. (1992). Theory of production rate calculations in steady and non-steady states and its application to glucose metabolism. *Am J Physiol*, 262(6 Pt 1):E779–90.

Jefferson, L. S. and Cherrington, A. (2001). *The endocrine pancreas and regulation of metabolism*, volume 2 of *Handbook of physiology - The endocrine system*. Oxford University Press, Oxford.

Johansen, K., Svendsen, P. A., and Lorup, B. (1984). Variations in renal threshold for glucose in type-1 (insulin-dependent) diabetes-mellitus. *Diabetologia*, 26(3):180–182.

Jones, R. H., Sonksen, P. H., Boroujerdi, M. A., and Carson, E. R. (1984). Number and affinity of insulin receptors in intact human subjects. *Diabetologia*, 27(2):207–11.

Kahn, S. E., Haffner, S. M., Heise, M. A., Herman, W. H., Holman, R. R., Jones, N. P., Kravitz, B. G., Lachin, J. M., O'Neill, M. C., Zinman, B., and Viberti, G. (2006a). Glycemic durability of rosiglitazone, metformin, or glyburide monotherapy. *N Engl J Med*, 355(23):2427–43.

Kahn, S. E., Hull, R. L., and Utzschneider, K. M. (2006b). Mechanisms linking obesity to insulin resistance and type 2 diabetes. *Nature*, 444(7121):840–6.

Kaku, K., Matsuda, M., Urae, A., and Irie, S. (2000). Pharmacokinetics and pharmacodynamics of insulin aspart, a rapid-acting analog of human insulin, in healthy japanese volunteers. *Diabetes Research and Clinical Practice*, 49(2-3):119–126.

Kang, S., Brange, J., Burch, A., Volund, A., and Owens, D. R. (1991a). Subcutaneous insulin absorption explained by insulin's physicochemical properties. evidence from absorption studies of soluble human insulin and insulin analogues in humans. *Diabetes Care*, 14(11):942–8.

Kang, S., Creagh, F. M., Peters, J. R., Brange, J., Volund, A., and Owens, D. R. (1991b). Comparison of subcutaneous soluble human insulin and insulin analogs (aspb9,glub27-aspb10-aspb28) on meal-related plasma-glucose excursions in type-i diabetic subjects. *Diabetes Care*, 14(7):571–577.

Karter, A. J., Ackerson, L. M., Darbinian, J. A., D'Agostino, R. B., Ferrara, A., Liu, J., and Selby, J. V. (2001). Self-monitoring of blood glucose levels and glycemic control: The northern california kaiser permanente diabetes registry. *American Journal of Medicine*, 111(1):1–9.

Karvonen, M. (2006). Incidence and trends of childhood type 1 diabetes worldwide 1990-1999. the diamond project group. *Diabet Med*, 23(8):857–66.

Karvonen, M., Tuomilehto, J., Libman, I., and LaPorte, F. B. (1993). A review of the recent epidemiological data on the worldwide incidence of type 1 (insulin-dependent) diabetes mellitus. world health organization diamond project group. *Diabetologia*, 36(10):883–92.

Kildegaard, J., Randlov, J., Poulsen, J. U., and Hejlesen, O. K. (2007). The impact of non-model-related variability on blood glucose prediction. *Diabetes Technology & Therapeutics*, 9(4):363–371.

Kimberly, M. M., Vesper, H. W., Caudill, S. P., Ethridge, S. F., Archibold, E., Porter, K. H., and Myers, G. L. (2006). Variability among five over-the-counter blood glucose monitors. *Clin Chim Acta*, 364(1-2):292–7.

Kleinfield, N. R. (2006). Diabetes and its awful toll quietly emerge as a crisis.

Klemp, P., Staberg, B., Madsbad, S., and Kolendorf, K. (1982a). The insulin absorption from subcutaneous tissue in smoking diabetics. *Acta Endocrinologica*, 100:37–37.

Klemp, P., Staberg, B., Madsbad, S., and Kolendorf, K. (1982b). Smoking reduces insulin absorption from subcutaneous tissue. *British Medical Journal*, 284(6311):237–237.

Klonoff, D. C. (2005). Continuous glucose monitoring: Roadmap for 21st century diabetes therapy. *Diabetes Care*, 28(5):1231–9.

Kobayashi, T., Sawano, S., Itoh, T., Kosaka, K., Hirayama, H., and Kasuya, Y. (1983). The pharmacokinetics of insulin after continuous subcutaneous infusion or bolus subcutaneous injection in diabetic patients. *Diabetes*, 32(4):331–6.

Koivisto, V. A. and Felig, P. (1978). Effects of leg exercise on insulin absorption in diabetic-patients. *New England Journal of Medicine*, 298(2):79–83.

Koivisto, V. A., Fortney, S., Hendler, R., and Felig, P. (1981). A rise in ambient-temperature augments insulin absorption in diabetic-patients. *Metabolism-Clinical and Experimental*, 30(4):402–405.

Kolendorf, K., Bojsen, J., and Nielsen, S. L. (1979). Adipose-tissue blood-flow and insulin disappearance from subcutaneous tissue. *Clinical Pharmacology & Therapeutics*, 25(5):598–604.

Korach-Andre, M., Roth, H., Barnoud, D., Pean, M., Peronnet, F., and Leverve, X. (2004). Glucose appearance in the peripheral circulation and liver glucose output in men after a large c-13 starch meal. *American Journal of Clinical Nutrition*, 80(4):881–886.

Kraegen, E. W. and Chisholm, D. J. (1984). Insulin responses to varying profiles of subcutaneous insulin infusion: kinetic modelling studies. *Diabetologia*, 26(3):208–213.

Lehmann, E. D. (1998). Aida - a computer-based interactive educational diabetes simulator. *Diabetes Educator*, 24(3):341–+.

Lehmann, E. D. (2001). Simulating glycosylated hemoglobin (hba1c) levels in diabetes using an interactive educational virtual diabetes patient simulator. *Diabetes Technol Ther*, 3(3):517–24.

Lehmann, E. D. and Deutsch, T. (1992a). Insulin dosage adjustment in diabetes. *J Biomech Eng*, 14(3):243–249.

Lehmann, E. D. and Deutsch, T. (1992b). A physiological model of glucose-insulin interaction in type 1 diabetes mellitus. *J Biomed Eng*, 14(3):235–42.

Lehmann, E. D. and Deutsch, T. (1993). Aida2: A mk. ii automated insulin dosage advisor. *J Biomed Eng*, 15:201–211.

Lepore, M., Pampanelli, S., Fanelli, C., Porcellati, F., Bartocci, L., Di Vincenzo, A., Cordoni, C., Costa, E., Brunetti, P., and Bolli, G. B. (2000). Pharmacokinetics and pharmacodynamics of subcutaneous injection of long-acting human insulin analog glargine, nph insulin, and ultralente human insulin and continuous subcutaneous infusion of insulin lispro. *Diabetes*, 49(12):2142–2148.

Lin, J., Lee, D., Chase, J., Hann, C., Lotz, T., and Wong, X. (2006). Stochastic modelling of insulin sensitivity variability in critical care. *Biomedical Signal Processing & Control*, 1:229–242.

Lin, J., Lee, D., Chase, J. G., Shaw, G. M., Le Compte, A., Lotz, T., Wong, J., Lonergan, T., and Hann, C. E. (2008). Stochastic modelling of insulin sensitivity and adaptive glycemic control for critical care. *Comput Methods Programs Biomed*, 89(2):141–152.

Lindholm, A., McEwen, J., and Riis, A. P. (1999). Improved postprandial glycemic control with insulin aspart. a randomized double-blind cross-over trial in type 1 diabetes. *Diabetes Care*, 22(5):801–5.

Livesey, G., Wilson, P. D. G., Dainty, J. R., Brown, J. C., Faulks, R. M., Roe, M. A., Newman, T. A., Eagles, J., Mellon, F. A., and Greenwood, R. H. (1998). Simultaneous time-varying systemic appearance of oral and hepatic glucose in adults monitored with stable isotopes. *American Journal of Physiology-Endocrinology and Metabolism*, 38(4):E717–E728.

Lonergan, T., Compte, A. L., Willacy, M., Chase, J. G., Shaw, G. M., Hann, C. E., Lotz, T., Lin, J., and Wong, X. W. (2006a). A pilot study of the sprint protocol for tight glycemic control in critically ill patients. *Diabetes Technol Ther*, 8(4):449–62.

Lonergan, T., LeCompte, A., Willacy, M., Chase, J. G., Shaw, G. M., Wong, X. W., Lotz, T., Lin, J., and Hann, C. E. (2006b). A simple insulin-nutrition protocol for tight glycemic control in critical illness: Development and protocol comparison. *Diabetes Technol Ther*, 8(2):191–206.

Lotz, T., Chase, J. G., Lin, J., Wong, X. W., Hann, C. E., McAuley, K. A., and Andreassen, S. (2006a). Integral-based identification of a physiological insulin and glucose model on euglycaemic clamp trials. In *14th IFAC Symposium on System Identification (SYSID 2006)*, pages 463–8, Newcastle, Australia. IFAC.

Lotz, T. F., Chase, J. G., McAuley, K. A., Lee, D. S., Lin, J., Hann, C. E., and Mann, J. I. (2006b). Transient and steady-state euglycemic clamp validation of a model for glycemic control and insulin sensitivity testing. *Diabetes Technol Ther*, 8(3):338–46.

Mainous, A. G., Diaz, V. A., Saxena, S., Baker, R., Everett, C. J., Koopman, R. J., and Majeed, A. (2006). Diabetes management in the usa and england: comparative analysis of national surveys. *Journal of the Royal Society of Medicine*, 99(9):463–469.

Mari, A. (1998). Assessment of insulin sensitivity and secretion with the labelled intravenous glucose tolerance test: improved modelling analysis. *Diabetologia*, 41(9):1029–39.

Mari, A., Wahren, J., Defronzo, R. A., and Ferrannini, E. (1994). Glucose-absorption and production following oral glucose - comparison of compartmental and arteriovenous-difference methods. *Metabolism-Clinical and Experimental*, 43(11):1419–1425.

McAuley, K. A., Williams, S. M., Mann, J. I., Goulding, A., Chisholm, A., Wilson, N., Story, G., McLay, R. T., Harper, M. J., and Jones, I. E. (2002). Intensive lifestyle changes are necessary to improve insulin sensitivity: a randomized controlled trial. *Diabetes Care*, 25(3):445–52.

McGuire, E. A., Tobin, J. D., Berman, M., and Andres, R. (1979). Kinetics of native insulin in diabetic, obese, and aged men. *Diabetes*, 28(2):110–20.

Medtronic Inc. (2004). Cgms system gold, continuous glucose monitoring overview.

Mitrakou, A., Ryan, C., Veneman, T., Mokan, M., Jenssen, T., Kiss, I., Durrant, J., Cryer, P., and Gerich, J. (1991). Hierarchy of glycemic thresholds for counterregulatory hormone secretion, symptoms, and cerebral dysfunction. *Am J Physiol*, 260(1 Pt 1):E67–74.

Monnier, L., Colette, C., Lapinski, H., and Boniface, H. (2004). Self-monitoring of blood glucose in diabetic patients: from the least common denominator to the greatest common multiple. *Diabetes Metab*, 30(2):113–9.

Morris, A. D., Boyle, D. I., McMahon, A. D., Greene, S. A., MacDonald, T. M., and Newton, R. W. (1997). Adherence to insulin treatment, glycaemic control, and ketoacidosis in insulin-dependent diabetes mellitus. the darts/memo collaboration. diabetes audit and research in tayside scotland. medicines monitoring unit. *Lancet*, 350(9090):1505–10.

Mosekilde, E., Jensen, K. S., Binder, C., Pramming, S., and Thorsteinsson, B. (1989). Modeling absorption kinetics of subcutaneous injected soluble insulin. *J Pharmacokinet Biopharm*, 17(1):67–87.

NICE (2003). Guidance on the use of continuous subcutaneous insulin infusion for diabetes. technology appraisal guidance no. 57. Technical report, National Institute for Clinical Excellence.

Nishida, Y., Tokuyama, K., Nagasaka, S., Higaki, Y., Fujimi, K., Kiyonaga, A., Shindo, M., Kusaka, I., Nakamura, T., Ishikawa, S. E., Saito, T., Nakamura, O., Sato, Y., and Tanaka, H. (2002). S(g), s(i), and egp of exercise-trained middle-aged men estimated by a two-compartment labeled minimal model. *Am J Physiol Endocrinol Metab*, 283(4):E809–16.

Noah, L., Krempf, M., Lecannu, G., Maugere, P., and Champ, M. (2000). Bioavailability of starch and postprandial changes in splanchnic glucose metabolism in pigs. *Am J Physiol Endocrinol Metab*, 278:E181–8.

Nucci, G. and Cobelli, C. (2000). Models of subcutaneous insulin kinetics. a critical review. *Computer Methods and Programs in Biomedicine*, 62(3):249–257.

O'Gorman D, J., Karlsson, H. K., McQuaid, S., Yousif, O., Rahman, Y., Gasparro, D., Glund, S., Chibalin, A. V., Zierath, J. R., and Nolan, J. J. (2006). Exercise training increases insulin-stimulated glucose disposal and glut4 (slc2a4) protein content in patients with type 2 diabetes. *Diabetologia*.

Onkamo, P., Vaananen, S., Karvonen, M., and Tuomilehto, J. (1999). Worldwide increase in incidence of type i diabetes–the analysis of the data on published incidence trends. *Diabetologia*, 42(12):1395–403.

Overkamp, D., Gautier, J. F., Renn, W., Pickert, A., Scheen, A. J., Schmulling, R. M., Eggstein, M., and Lefebvre, P. J. (1997). Glucose turnover in humans in the basal state and after intravenous glucose: a comparison of two models. *Am J Physiol*, 273(2 Pt 1):E284–96.

Owens, D. R., Coates, P. A., Luzio, S. D., Tinbergen, J. P., and Kurzhals, R. (2000). Pharmacokinetics of i-125-labeled insulin glargine (hoe 901) in healthy men - comparison with nph insulin and the influence of different subcutaneous injection sites. *Diabetes Care*, 23(6):813–819.

Owens, D. R., Vora, J. P., Heding, L. G., Luzio, S., Ryder, R. E. J., Atiea, J., and Hayes, T. M. (1986). Human, porcine and bovine ultralente insulin - subcutaneous administration in normal man. *Diabetic Medicine*, 3(4):326–329.

Owens, D. R., ZInman, B., and Bolli, G. B. (2001). Insulins today and beyond. *Lancet*, 358:739–46.

Parker, R. S., Doyle, F. J., Ward, J. H., and Peppas, N. A. (2000). Robust h-infinity glucose control in diabetes using a physiological model. *Aiche Journal*, 46:2537–2549.

Perriello, G., Defeo, P., Torlone, E., Fanelli, C., Santeusanio, F., Brunetti, P., and Bolli, G. B. (1991). The dawn phenomenon in type-1 (insulin-dependent) diabetes-mellitus - magnitude, frequency, variability, and dependency on glucose counterregulation and insulin sensitivity. *Diabetologia*, 34(1):21–28.

Petersen, K. F. and Shulman, G. I. (2006). Etiology of insulin resistance. *Am J Med*, 119(5 Suppl 1):S10–6.

Pham, M. (2005). Diabetes: Proprietary survey on insulin pumps and continuous blood glucose monitoring. Technical report, HSBC Securities (USA) Inc.

Pillonetto, G., Sparacino, G., Magni, P., Bellazzi, R., and Cobelli, C. (2002). Minimal model s(i)=0 problem in niddm subjects: nonzero bayesian estimates with credible confidence intervals. *Am J Physiol Endocrinol Metab*, 282(3):E564–573.

Plank, J., Wutte, A., Goerzer, E., Siebenhofer, A., Semlitsch, B., Sommer, R., Hirschberger, S., and Pieber, T. R. (2002). A direct comparison of insulin analogs aspart and lispro in type 1 diabetic patients. *Diabetes*, 51:A52–A52.

Polonsky, K. S., Given, B. D., Pugh, W., Licinio-Paixao, J., Thompson, J. E., Karrison, T., and Rubenstein, A. H. (1986). Calculation of the systemic delivery rate of insulin in normal man. *J Clin Endocrinol Metab*, 63(1):113–8.

Press, M., Tamborlane, W. V., and Sherwin, R. S. (1984). Importance of raised growth-hormone levels in mediating the metabolic derangements of diabetes. *New England Journal of Medicine*, 310 (13):810–815.

PriceWaterhouseCoopers (2001). Type 2 diabetes, managing for better health outcomes. Technical report, Diabetes New Zealand Inc.

Prigeon, R. L., Roder, M. E., Porte, D., J., and Kahn, S. E. (1996). The effect of insulin dose on the measurement of insulin sensitivity by the minimal model technique. evidence for saturable insulin transport in humans. *J Clin Invest*, 97(2):501–7.

Puckett, W. R. and Lightfoot, E. N. (1995). A model for multiple subcutaneous insulin injections developed from individual diabetic patient data. *American Journal of Physiology-Endocrinology and Metabolism*, 32(6):E1115–E1124.

Quon, M. J., Cochran, C., Taylor, S. I., and Eastman, R. C. (1994). Non-insulin-mediated glucose disappearance in subjects with iddm. discordance between experimental results and minimal model analysis. *Diabetes*, 43(7):890–6.

Radziuk, J. (2000). Insulin sensitivity and its measurement: structural commonalities among the methods. *J Clin Endocrinol Metab*, 85(12):4426–33.

Radziuk, J., Norwich, K. H., and Vranic, M. (1978). Experimental validation of measurements of glucose turnover in nonsteady state. *Am J Physiol*, 234(1):E84–93.

Rasio, E. A., Hampers, C. L., Soeldner, J. S., and Cahill, G. F., J. (1967). Diffusion of glucose, insulin, inulin, and evans blue protein into thoracic duct lymph of man. *J Clin Invest*, 46(6):903–10.

Rave, K., Nosek, L., Posner, J., Heise, T., Roggen, K., and van Hoogdalem, E. J. (2006). Renal glucose excretion as a function of blood glucose concentration in subjects with type 2 diabetes–results of a hyperglycaemic glucose clamp study. *Nephrol Dial Transplant*, 21(8):2166–71.

Reed, K. and Lehmann, E. D. (2005). Diabetes website review: www.2aida.org. *Diabetes Technol Ther*, 7(5):741–54.

Regittnig, W., Ellmerer, M., Fauler, G., Sendlhofer, G., Trajanoski, Z., Leis, H. J., Schaupp, L., Wach, P., and Pieber, T. R. (2003). Assessment of transcapillary glucose exchange in human skeletal muscle and adipose tissue. *Am J Physiol Endocrinol Metab*, 285(2):E241–51.

Regittnig, W., Trajanoski, Z., Leis, H. J., Ellmerer, M., Wutte, A., Sendlhofer, G., Schaupp, L., Brunner, G. A., Wach, P., and Pieber, T. R. (1999). Plasma and interstitial glucose dynamics after intravenous glucose injection: evaluation of the single-compartment glucose distribution assumption in the minimal models. *Diabetes*, 48(5):1070–81.

Riddle, M. C., Rosenstock, J., and Gerich, J. (2003). The treat-to-target trial - randomized addition of glargine or human nph insulin to oral therapy of type 2 diabetic patients. *Diabetes Care*, 26(11):3080–3086.

Rohlfing, C. L., Wiedmeyer, H. M., Little, R. R., England, J. D., Tennill, A., and Goldstein, D. E. (2002). Defining the relationship between plasma glucose and hba(1c): analysis of glucose profiles and hba(1c) in the diabetes control and complications trial. *Diabetes Care*, 25(2):275–8.

Sacks, D. B., Bruns, D. E., Goldstein, D. E., Maclaren, N. K., McDonald, J. M., and Parrott, M. (2002). Guidelines and recommendations for laboratory analysis in the diagnosis and management of diabetes mellitus. *Clin Chem*, 48(3):436–72.

Samann, A., Muhlhauser, I., Bender, R., Kloos, C., and Muller, U. A. (2005). Glycaemic control and severe hypoglycaemia following training in flexible, intensive insulin therapy to enable dietary freedom in people with type 1 diabetes: a prospective implementation study. *Diabetologia*.

Sanofi-Aventis (2007). Lantus (insulin glargine [rdna origin] injection) prescribing information.

Scheinberg, P. (1965). Observations on cerebral carbohydrate metabolism in man. *Annals of Internal Medicine*, 62(2):367–71.

Schinner, S., Scherbaum, W. A., Bornstein, S. R., and Barthel, A. (2005). Molecular mechanisms of insulin resistance. *Diabet Med*, 22(6):674–82.

Scholtz, H. E., Pretorius, S. G., Wessels, D. H., and Becker, R. H. A. (2005). Pharmacokinetic and glucodynamic variability: assessment of insulin glargine, nph insulin and insulin ultralente in healthy volunteers using a euglycaemic clamp technique. *Diabetologia*, 48(10):1988–1995.

Schutt, M., Kern, W., Krause, U., Busch, P., Dapp, A., Grziwotz, R., Mayer, I., Rosenbauer, J., Wagner, C., Zimmermann, A., Kerner, W., Holl, R. W., and initiative, D. (2006). Is the frequency of self-monitoring of blood glucose related to long-term metabolic control? multicenter analysis including 24,500 patients from 191 centers in germany and austria. *Experimental and Clinical Endocrinology & Diabetes*, 114(7):384–388.

Sherwin, R. S., Kramer, K. J., Tobin, J. D., Insel, P. A., Liljenquist, J. E., Berman, M., and Andres, R. (1974). A model of the kinetics of insulin in man. *J Clin Invest*, 53(5):1481–92.

Shimoda, S., Nishida, K., Sakakida, M., Konno, Y., Ichinose, K., Uehara, M., Nowak, T., and Shichiri, M. (1997). Closed-loop subcutaneous insulin infusion algorithm with a short-acting insulin analog for long-term clinical application of a wearable artificial endocrine pancreas. *Front Med Biol Eng*, 8(3):197–211.

Siesjo, B. K. (1988). Hypoglycemia, brain metabolism, and brain-damage. *Diabetes-Metabolism Reviews*, 4(2):113–144.

Silvers, A., Swenson, R. S., Farquhar, J. W., and Reaven, G. M. (1969). Derivation of a three compartment model describing disappearance of plasma insulin-131-i in man. *J Clin Invest*, 48(8):1461–9.

Sjostrand, M., Holmang, A., and Lonnroth, P. (1999). Measurement of interstitial insulin in human muscle. *Am J Physiol*, 276(1 Pt 1):E151–4.

Steil, G. M., Ader, M., Moore, D. M., Rebrin, K., and Bergman, R. N. (1996). Transendothelial insulin transport is not saturable in vivo. no evidence for a receptor-mediated process. *J Clin Invest*, 97(6):1497–503.

Steil, G. M., Panteleon, A. E., and Rebrin, K. (2004). Closed-loop insulin delivery-the path to physiological glucose control. *Adv Drug Deliv Rev*, 56(2):125–44.

Steil, G. M., Rebrin, K., Darwin, C., Hariri, F., and Saad, M. F. (2006). Feasibility of automating insulin delivery for the treatment of type 1 diabetes. *Diabetes*, 55(12):3344–50.

Stephens, E. and Riddle, M. (2003). Evolving approaches to intensive insulin therapy in type 1 diabetes: Multiple daily injections, insulin pumps and new methods of monitoring. *Reviews in Endocrine & Metabolic Disorders*, 4(4):325–334.

Tarin, C., Teufel, E., Pico, J., Bondia, J., and Pfleiderer, H. J. (2005). Comprehensive pharmacokinetic model of insulin glargine and other insulin formulations. *IEEE transactions on bio-medical engineering*, 52(12):1994–2005.

Tattersall, R. B. (1997). Brittle diabetes revisited: the third arnold bloom memorial lecture. *Diabet Med*, 14(2):99–110.

Thombs, L. A. and Schucany, W. R. (1990). Bootstrap prediction intervals for autoregression. *Journal of the American Statistical Association*, 85(410):486–492.

Thorsteinsson, B. (1990). Kinetic models for insulin disappearance from plasma in man. *Dan Med Bull*, 37(2):143–53.

Thorsteinsson, B., Fugleberg, S., Feldt-Rasmussen, B., Ellemann, K., and Binder, C. (1987). Kinetics models for insulin disappearance from plasma in type 1 diabetic patients. *Pharmacol Toxicol*, 60(2):90–95.

Toffolo, G., Campioni, M., Basu, R., Rizza, R. A., and Cobelli, C. (2006). A minimal model of insulin secretion and kinetics to assess hepatic insulin extraction. *Am J Physiol Endocrinol Metab*, 290(1):E169–76.

Toffolo, G., De Grandi, F., and Cobelli, C. (1995). Estimation of beta-cell sensitivity from intravenous glucose tolerance test c-peptide data. knowledge of the kinetics avoids errors in modeling the secretion. *Diabetes*, 44(7):845–54.

Trajanoski, Z., Wach, P., Kotanko, P., Ott, A., and Skraba, F. (1993). Pharmacokinetic model for the absorption of subcutaneously injected soluble insulin and monomeric insulin analogs. *Biomedizinische Technik*, 38(9):224–231.

Tranberg, K. G. and Dencker, H. (1978). Modeling of plasma disappearance of unlabeled insulin in man. *Am J Physiol*, 235(6):E577–85.

Tuomilehto, J., Lindstrom, J., Eriksson, J. G., Valle, T. T., Hamalainen, H., Ilanne-Parikka, P., Keinanen-Kiukaanniemi, S., Laakso, M., Louheranta, A., Rastas, M., Salminen, V., and Uusitupa, M. (2001). Prevention of type 2 diabetes mellitus by changes in lifestyle among subjects with impaired glucose tolerance. *N Engl J Med*, 344(18):1343–50.

Turnheim, K. and Waldhausl, W. K. (1988). Essentials of insulin pharmacokinetics. *Wien Klin Wochenschr*, 100(3):65–72.

Van Cauter, E., Polonsky, K. S., and Scheen, A. J. (1997). Roles of circadian rhythmicity and sleep in human glucose regulation. *Endocr Rev*, 18(5):716–38.

von Mach, M. A., Brinkmann, C., Hansen, T., Weilemann, L. S., and Beyer, J. (2002). Differences in pharmacokinetics and pharmacodynamics of insulin lispro and aspart in healthy volunteers. *Experimental and Clinical Endocrinology & Diabetes*, 110(8):416–419.

Walsh, J. and Roberts, R. (1994). *The Pocket Pancreas: Your Diabetes Guide for Improved Blood Sugars*. Diabetes Services Inc.

Warshaw, H. S. and Kulkarni, K. (2004). *Complete Guide to Carb Counting: How to take the mystery out of carb counting and unlock the secrets to blood glucose control.* American Diabetes Association, Virginia, 2nd edition.

Wild, S., Roglic, G., Green, A., Sicree, R., and King, H. (2004). Global prevalence of diabetes: estimates for the year 2000 and projections for 2030. *Diabetes Care*, 27(5):1047–53.

Wilde, M. I. and McTavish, D. (1997). Insulin lispro: a review of its pharmacological properties and therapeutic use in the management of diabetes mellitus. *Drugs*, 54(4):597–614.

Wilinska, M. E., Chassin, L. J., and Hovorka, R. (2006). Automated glucose control in the icu: Effect of nutritional protocol and measurement error. *Conf Proc IEEE Eng Med Biol Soc*, 1:67–70.

Wilinska, M. E., Chassin, L. J., Schaller, H. C., Schaupp, L., Pieber, T. R., and Hovorka, R. (2005). Insulin kinetics in type-1 diabetes: Continuous and bolus delivery of rapid acting insulin. *IEEE Transactions on Biomedical Engineering*, 52(1):3–12.

Windhager, E. (1992). *Renal physiology.* Handbook of Physiology. Oxford University Press, New York.

Wolever, T. M. S. and Bolognesi, C. (1996a). Prediction of glucose and insulin responses of normal subjects after consuming mixed meals varying in energy, protein, fat, carbohydrate and glycemic index. *Journal of Nutrition*, 126(11):2807–2812.

Wolever, T. M. S. and Bolognesi, C. (1996b). Source and amount of carbohydrate affect postprandial glucose and insulin in normal subjects. *Journal of Nutrition*, 126(11):2798–2806.

Wong, X. W., Chase, J. G., Shaw, G. M., Hann, C. E., Lotz, T., Lin, J., Singh-Levett, I., Hollingsworth, L. J., Wong, O. S., and Andreassen, S. (2006a). Model predictive glycaemic regulation in critical illness using insulin and nutrition input: a pilot study. *Med Eng Phys*, 28(7):665–81.

Wong, X. W., Chase, J. G., Shaw, G. M., Lin, J., Lotz, T., and Hann, C. E. (2005). Clinical trials of active and adaptive insulin and nutrition control to control hyperglycaemia in critically ill patients. In *Canterbury Health Research Conference*, pages 1–page, Christchurch.

Wong, X. W., Singh-Levett, I., Hollingsworth, L. J., Shaw, G. M., Hann, C. E., Lotz, T., Lin, J., Wong, O. S., and Chase, J. G. (2006b). A novel, model-based insulin and nutrition delivery controller for glycemic regulation in critically ill patients. *Diabetes Technol Ther*, 8(2):174–90.

Woodworth, J., Howey, D., Bowsher, R., Lutz, S., Santa, P., and Brady, P. (1993). [lys(b28), pro(b29)] human insulin (k) - dose-ranging vs humulin r (h). *Diabetes*, 42:A54–A54.

Worthington, D. R. L. (1997). Minimal model of food absorption in the gut. *Medical Informatics*, 22(1):35–45.

Yang, Y. J., Hope, I. D., Ader, M., and Bergman, R. N. (1989). Insulin transport across capillaries is rate limiting for insulin action in dogs. *J Clin Invest*, 84(5):1620–8.

Yates, T. L. and Fletcher, L. R. (2000). Prediction of a glucose appearance function from foods using deconvolution. *Ima Journal of Mathematics Applied in Medicine and Biology*, 17(2):169–184.

Zierler, K. (1999). Whole body glucose metabolism. *Am J Physiol*, 276(3 Pt 1):E409–426.